The role of tau and tau-associated protein networks in memory circuits and processes

By

Emmanuel Prikas

BSc(Adv)(Hons 1), MRes

Thesis
Submitted to Flinders University
for the degree of

Doctor of Philosophy in Neuroscience

College of Medicine and Public Health

16th of June 2023

TABLE OF CONTENTS

Table of Contents ..... *i*

Thesis Abstract ..... *iii*

Declaration ..... *v*

Acknowledgements ..... *vi*

List of Figures ..... *vii*

Publications ..... *ix*

Hypotheses ..... **x**

Rationale ..... **x**

Overarching Aims ..... **x**

CHAPTER ONE *1*

MEMORY-ASSOCIATED PROCESSES AND THE CONTRIBUTING ROLE OF TAU PROTEIN INTERACTIONS *1*

Thinking about thought: A brief history of learning, behaviour, and the mind **2**

Considerations for studying learning and memory in laboratory settings **3**

What is a memory? **4**

Categories of Memory **5**

Functional anatomy of the hippocampus **10**

Neuroplasticity: structural, functional, and synaptic plasticity **16**

Molecular mechanisms of learning and memory **18**

Neurological disorders of synaptic dysfunction **19**

Microtubule-binding protein tau: critical factor in healthy and disease brain **25**

The MAPT gene and physiological functions of tau **26**

CHAPTER TWO *31*

PROXIMITY-LABELLING IDENTIFIES TARGETS OF TAU IN GLUTAMATE RECEPTOR TRAFFICKING AND MEMORY FORMATION *31*

Introduction **32**

Results **34**

Discussion **51**

Supplementary Figures **55**

Materials and Methods **62**

CHAPTER THREE ***77***

TAU-ASSOCIATED PROTEIN-PROTEIN INTERACTION NETWORKS IN NEURONAL ENSEMBLES OF MEMORY ***77***

Introduction **78**

Results **83**

Supplementary Figures **106**

Discussion **99**

Materials and Methods **116**

Bibliography ***125***

Appendices ***142***

THESIS ABSTRACT

Neuroplasticity is a fundamental permissive feature of our brain that allows for processes of learning and memory. Our ability to think, adapt, and flourish in our environment across the lifespan depends on the dynamic connectivity and communication between neurons, known as synaptic plasticity.

The first chapter of this thesis begins with a comprehensive overview of our evolving conceptualisations of learning and memory. Ancient western philosophical notions on the nature of thoughts-in-mind as either pre-existing (idealism) or gathered from interaction with the environment (empiricism), provided the epistemological framework for how we understand contemporary neuroscientific research. To this end, we gather information using quantifiable behaviourist approaches and remain aware of ethological notions of inherited species-specific characteristics to understand and interpret our results. In describing memory research, I arrive at the 'engram': a latent but enduring physical-chemical change in the brain that was provoked through learning; a neural correlate or representation of a memory. Categorical and formal definitions of memory are then linked to their molecular mechanistic underpinnings in long-term potentiation and depression. These molecular memory mechanisms can impair as we age, and independently become dysfunctional in neurodegenerative disorders such as Alzheimer's Disease (AD). Alzheimer's Disease is characterised by brain tissue lesions from depositions of the aggregated microtubule-associated protein tau. Impaired memory is an early clinical symptom of AD and has been linked to synaptic dysfunction and pathologic redistribution of axonal tau to synapses and the cell soma. The tau protein is a central factor in AD and other tauopathies. I hypothesised that by identifying tau protein-protein interactions (PPIs) in physiologic conditions, we can gain a better understanding of the role of tau in neurodegenerative diseases.

This hypothesis was addressed in chapter 2, presenting published research on our proximity labelling proteomics approach to charting functional tau interactomes in primary neurons and mouse brain. I fused a modified biotin ligase, BioID2, to the N-terminus of full-length human tau protein (BioID2-tau), which biotinylated stable and transient tau interactors when expressed in biotin-enriched brain tissue. Tau interactors mapped onto pathways of cytoskeletal, post-synaptic receptor, and synaptic vesicle regulation and showed enrichment for Alzheimer's and Parkinson's diseases. Tau interacts with and inhibits the activity of vesicular ATPase N-ethylmaleimide sensitive fusion protein (NSF), which is essential for trafficking of glutamate receptor (AMPAR). *Tau*-deficient ($tau^{-/-}$) neurons showed aberrant localization of NSF and synaptic AMPAR surface levels, reversible through tau expression or NSF inhibition. Consequently, enhanced associative and object recognition memory, mediated by AMPAR, is suppressed in $tau^{-/-}$ mice by both hippocampal tau and infusion with an NSF-inhibiting peptide. Pathologic tau from AD mouse models and human AD samples enhances inhibition of NSF. Our

results map neuronal tau interactomes and delineate a physiologic and pathologic functional link of tau with NSF that regulates plasticity associated AMPAR shuttling and memory performance.

Tau-associated interactions in neurons may be mediating memory (engram) cell function within neural networks. Whether there are tau interactions that mediate specific engram function of a cell ensemble supporting learning/memory of a specific task is unknown. My aim in chapter 3 was to identify tau and tau-associated protein-protein interactions (PPIs) in engrams by harnessing the necessarily activity-dependent functions in memory engram cells. To address this, I fused an enhanced biotin ligase, MiniTurboID, to tau, under the expressional control of a modified neuronal activity-dependent promoter. I mapped the interactome of tau by labelling proteins in two spatial memory-associated engrams in hippocampus of *tau*$^{-/-}$ mice during a spatial memory paradigm. Among these were five central tau interactors, Sh3gl2, CamK2a, MeCP2, Ppp3ca, and Lin7c that occur in specific engram states when compared to general tau interactomes, in memory non-specific neurons. This suggests that these PPIs underlie memory processes and may be defined by engram-specific tau interactions at temporally significant points across persistent engram function, including learning, consolidation, maintenance, and retrieval from latency.

DECLARATION

I certify that this thesis does not incorporate without acknowledgment any material previously submitted for a degree or diploma in any university; and that to the best of my knowledge and belief it does not contain any material previously published or written by another person except where due reference is made in the text.

Name: Emmanuel Prikas

Signed: EP

Date: 26/02/2023

ACKNOWLEDGEMENTS

First and foremost, I would like to thank my supervisor Dr. Arne Ittner, who I have been with for over 5 years, since prior to commencing my Honours. Thank you for your patience, expertise, guidance, and generosity.

I am grateful to my immediate family for their financial and/or emotional support throughout this extended period of living modestly and researching intensively. Also, to my closest friends for your reciprocal altruism.

To all the members of the aiLab, thank you for putting up with my moods and personalities and for your support in the lab - day in, and day out.

To the staff (Flinders U and otherwise) and researchers at Flinders Medical Centre, thank you for welcoming us and for the positive and friendly environment you maintain.

To colleagues I've met along the way, mostly at Macquarie U, it was awesome to meet you all and I look forward to seeing you at conferences etc in future.

The research presented in this PhD thesis was supported by the Australian Government Research Training Program Scholarship (AGRTP), National Health and Medical Research Council (NHMRC), Australian Research Council (ARC), Dementia Australia Research Foundation (DARF), by the Flinders Foundation, and by Flinders University.

LIST OF FIGURES

Figure 1.1. Categories of memory……6

Figure 1.2 Non-associative learning in Aplysia californica……8

Figure 1.3. Overview summary of two forms of associative conditioning……9

Figure 1.4. Anatomy and function of the human and mouse hippocampus……11

Figure 1.5 Afferent (Input) and efferent (output) pathways of the hippocampus……12

Figure 1.6 The hippocampus in the centre of an auto-association network……13

Figure 1.7. Recreated schematic of single cell place and grid cell firing……15

Figure 1.8. Neuroplasticity. Structural, functional, synaptic plasticity as neuroplasticity……16

Figure 1.9. Synaptic plasticity. The flow diagram shows various forms of synaptic plasticity……18

Figure 1.10. Homosynaptic depression and facilitation……19

Figure 1.11. Schematic of Hebbian plasticity. ……20

Figure 1.12. Long-term potentiation and depression in the hippocampal CA3-CA1 synapse……22

Figure 1.13. The MAPT gene, tau transcript, and tau protein……25

Figure 1.14. Binding of tau to microtubules. ……26

Figure 2.1. Novel associations of microtubule-associated protein tau with synaptic vesicle cycle in proximity labelled interactomes……28

Figure 2.2. Proximity labelling links tau with synaptic vesicle regulation in mouse brain in vivo……29

Figure 2.3. Neuronal tau interactome maps onto processes of cytoskeletal, synaptic vesicle, and post-synaptic regulation. ……32

Figure 2.4. Direct interaction with tau regulates activity of essential synaptic vesicular ATPase NSF. ……35

Figure 2.5. Tau regulates NSF localization and GluA2 trafficking in chemically induced plasticity….38

Figure 2.6. Tau limits NSF-dependent associative learning and mediates pathologic inhibition of NSF in tau-transgenic mouse models and in AD brain lysates. ……40

Figure 3.1. Theoretical and experimental strategy for proximity labelling of tau interactions in active engram cells. ……78

Figure 3.2. Temporally controlled and activity-dependent expression for proximity labelling in mouse spatial memory. ……..……..…….80

Figure 3.3. Habituation and performance cut-offs ensured robust spatial learning and memory in the MWM task. ……..……...81

Figure 3.4: Tau interactomes in spatial learning and memory engrams. ……..…..88

Figure 3.5. A subset of functional MiniTurboID fusion proteins are confirmed as tau protein interactors…..……...…….……...90

Figure 3.6. Tau interactions in expanded engram networks. …….……..96

PUBLICATIONS

List of sole or co-authored publications that have been submitted, accepted, or published during my HDR candidature.

1. **Prikas**, **E**. et al (2023). Tau-associated protein-protein interaction networks in neuronal ensembles of memory. *Manuscript in preparation*.

2. **Prikas**, **E**., Paric, E., Asih, P. R., Stefanoska, K., Stefen, H., Fath, T., Poljak, A., & Ittner, A. (2022). Tau target identification reveals NSF-dependent effects on AMPA receptor trafficking and memory formation. The EMBO Journal, 41(18). https://doi.org/10.15252/embj.2021110242

3. **Prikas**, **E**., Ahel, H., Stefanoska, K., Asih, P., Volkerling A., Ittner L., Ittner A. (2021). Interaction between the guanylate kinase domain of PSD-95 and the proline-rich region and microtubule binding repeats 2 and 3 of tau. Biochemistry and Cell Biology. doi: 10.1139/bcb-2020-0604

4. **Prikas**, **E**., Poljak, A., & Ittner, A. (2020). Mapping p38α mitogen-activated protein kinase signaling by proximity-dependent labeling. Protein Science, 29(5), 1196-1210. doi: 10.1002/pro.3854

5. Asih, P., **Prikas**, **E**., Stefanoska, K., Tan, A., Ahel, H., & Ittner, A. (2020). Functions of p38 MAP Kinases in the Central Nervous System. Frontiers In Molecular Neuroscience, 13. doi: 10.3389/fnmol.2020.570586.

6. Asih, P. R., Stefanoska, K., **Prikas**, **E**., & Ittner, A. (2022). High level forebrain expression of active tau kinase p38γ exacerbates cognitive dysfunction in aged APP-transgenic Alzheimer's mice. Neuroscience, 484, 53–65. https://doi.org/10.1016/j.neuroscience.2022.01.005

7. Ittner, A., Asih, P., Tan, A., **Prikas**, **E**., Bertz, J., Stefanoska, K. ... & Ittner, LM. (2020). Reduction of advanced tau-mediated memory deficits by the MAP kinase p38γ. Acta Neuropathologica, 140(3), 279-294. doi: 10.1007/s00401-020-02191-1

8. Przybyla, M., van Eersel, J., van Hummel, A., van der Hoven, J., Sabale, M., & Harasta, A., Müller, J., Gajwani, M., **Prikas**, **E**., ... Ittner, A. & Ittner, L. (2020). Onset of hippocampal network aberration and memory deficits in P301S tau mice are associated with an early gene signature. Brain, 143(6), 1889-1904. doi: 10.1093/brain/awaa133

Hypotheses

There are two central hypotheses driving the body of work presented in this thesis. The first addresses the need for – and implications of – a reliable approach to labelling tau interactions. The second relates to a specific contribution of tau-associated interactions in memory processes.

(**1**) **Robust labelling of stable and transient tau interactions** in physiologically relevant conditions would generate a more complete tau interactome. This extensive interaction network would provide further insights into the role of tau in physiology and neurodegenerative diseases.

(**2**) **Tau and tau-associated protein interactors play a key role in the molecular mechanisms supporting memory** formation, consolidation, and/or retrieval. Specifically, tau PPI networks are critical for the circuit communication of cells associated with memory processes (engram cells).

Rationale

Tau protein contributes to the regulated transport of cell cargo through axons [2-4] but also localises to pre- and post-synapses [5-8], where its role is less well-defined. Mouse models of Alzheimer's disease (AD) have shown tau-dependent memory impairment and loss of synapses [9, 10]. Despite a growing literature, the tau protein-protein interactions (PPIs) currently known do not support a complete functional understanding of tau.

Traditional PPI identification techniques are limited by reliance on affinity purification and protein complex stability after tissue lysis [5, 11]. The proximity labelling technique of BioID bypasses these limitations and allows for generation of entire interaction networks with minimal necessary prior knowledge of interactors, eliminating significant technical and experimenter bias. Comparing differences between PPI networks that are representative of various states cellular states, e.g., physiological steady-state, during learning or memory, will aid in identifying state-dependent protein interaction clusters. Targeted functional assays based on state-associated protein clusters will characterise their putative role in supporting state function.

Overarching Aims

Testing the described hypotheses will require a feasible experimental strategy for identifying extensive PPI networks in relevant neurons or ensembles of neurons during dynamic biological states. This includes labelling of tau PPIs in cell culture and in memory-associated neurons of mice during behavioural/memory testing paradigms. The central overarching aim of this work is to determine and describe a potential link between tau protein interactions in resting state physiology and in memory function. This will be achieved by completion of the following intermediate aims:

(**1**) Evaluate the existing record of memory research literature to analyse and describe contemporary conceptions of molecular and cellular memory. (Ch #1)

(**2**) Discriminate tau-specific proximity labelling from background labelling, in different experimental neuronal systems such as cultured neurons and in mouse brain. (Ch #2)

(**3**) Confirm a putative tau interactor and characterise the interaction to gain novel mechanistic insights. (Ch #2)

(**4**) Generate engram interactomes that represent tau interactions during specific phases of spatiotemporal learning and memory in behaving mice. (Ch #3)

(**5**) Confirm tau engram interactions and bioinformatically analyse their role in the context of task-dependent and memory process-specific conditions. (Ch #3)

CHAPTER ONE

MEMORY-ASSOCIATED PROCESSES AND THE CONTRIBUTING ROLE OF TAU PROTEIN INTERACTIONS

Thinking about thought: A brief history of learning, behaviour, and the mind

Since Plato and Aristotle, two conflicting views have guided our understanding of the mind and on the origins of its content. Idealism claims that thoughts pre-exist and emerge from within an organism as it develops [12]. In contrast, an empiricist would postulate that thoughts are entirely the product of organismal senses, from interactions with the environment [13]. By the second half of the 19th century, these two philosophies would provide the intellectual framework for two experimental approaches in modern animal behavioural science. Consistent with the essentialist epistemology of idealism, ethology maintains that animal behaviours are evolutionarily adaptive traits that must be interpreted by observing animals in the wild; to 'interview an animal in its own language' [14]. Contrary to ethology, the empirical, laboratory-based approach of behaviourism, suggests that behaviours are learned through interactions with the (controllable) environment [15], with a focus on observable and quantifiable outcomes. The success and influence of both approaches has been profound.

Ethology contributed to our understanding of language by articulating the notion of critical periods: temporary developmental phases of high organismal sensitivity to informational stimuli [16]. Ethology also explained 'attachment', where primate infants display innate signalling behaviours that attach themselves to their parents [17]. One limitation of ethology is the difficulty in testing hypotheses, because of its inherently non-interventionist approach. Another criticism is that the central message of inherited and manifested traits can seem biologically deterministic and regressive.

Behaviourism has been crucial for the development of action-based behavioural therapies such as exposure therapy for phobias. This focuses on disassociating and overcoming fear or anxiety from objects or situations. For Alcohol Use Disorder, Aversion Therapy pairs an aversive stimulus (drug Antabuse), a hangover symptom amplifier, with a negative behaviour (consuming alcohol). More broadly, from companies rewarding work accomplishments, to governments punishing antisocial or criminal behaviour, the behaviourist framework pervades society. An early criticism levelled at behaviourism was that it did not account for mental processes, internal states, or feelings, which spawned the 'cognitive revolution' [18]. Developments in computer science generated entire new parallels between information processing in computers and human brain function.

Yet, despite their success and prominence, both theories fail to explain brain functions. Regardless of the form or origin of information constituting thought, the information is expressed in physical properties of the brain, neuronal interconnectivity, synaptic and network communication. Hence, behaviours must be explained in terms of neurophysiologic functions. The explanatory power offered by this approach is a multilevel integration of analyses, from the molecular to the behavioural [19].

Considerations for studying learning and memory in laboratory settings

Learning from experience is crucial to the survival strategies of all animals. Different ecological niches are home to a range of animal species with varying behaviours and sensorimotor features. Their nervous systems also vary; accordingly, they can be more or less centralised, with relatively stronger and weaker individual senses. A combination of lifespan, behaviours, neuroanatomy, and physiology together contribute to whether any particular species would make for a good animal model. But practical considerations alone are not enough to justify selection of an animal for study when the aim is to identify general and species-specific adaptations of learning and memory. This includes how an animal navigates through an environment, scanning and selecting the relevant information to store in a stable form, that can be retrieved to inform some better-adapted future behaviour. Between-species comparative studies are one way to determine adaptive generalities and specificities.

From ritualised movements in communicating bees, to tool making and use in feeding chimpanzees [20] – observing animals in the wild prompt research questions about unravelling general survival strategies and novel problem-solving in an ever-changing environment.

Yet the transition from natural habitat to a laboratory setting is an inevitable step towards hypothesis-driven behavioural research. Laboratories allow for monitoring the history of an animal's experience and setting up the appropriate control experiments. The inescapable trade-off is that the laboratory settings for data collection are a long way removed from natural conditions. The conditions for interfering experimentally in lab settings is presumably less impactful for invertebrates such as the mollusc *Aplysia* or the fly *Drosophila* relative to mammals. But the impact of a clash between ethology and behaviourism remains. Artificial light, human noises, and constrained living space stress animals and lead to poor psychological outcomes [21]. Aggression can manifest in inappropriate maternal behaviour in mice, or stress and anxiety in primates engaged in prolonged pacing (excessive stereotypic behaviours). A well-documented phenomenon is contagious anxiety, indicated by raised systemic cortisol in monkeys watching other monkeys restrained during blood collection, or blood pressure and heart rate elevations in rats seeing other rats being decapitated [21].

Limiting the stress response has stabilising effects on behavioural and physiological parameters, removing inconsistent confounding factors, and improving the consistency and accuracy of results [22, 23]. Acknowledging the outlined limitations should lead to better animal housing and handling practices, and to integrating complementary experimental models such as cell culture.

Many questions about learning and memory, such as primate communication and bird navigation, cannot be answered in the laboratory. For cognition-based questions that can be answered, interpretation of results can often be contentious. The neural basis of memory storage clearly exists in mice: mice can store memories. But how different is the content of the 'same' episodic memory

between a human and a mouse? [24] Considering the case of food-storing birds, who store up to 10,000 items per year in almost as many storage sites [25], the essential features of ‘what, when, where’ exist in mice albeit to a different level of complexity relative to humans. Behaviours can be ‘anxiety-like’ and memories can be ‘episodic-like’, which also acknowledges a spectrum, rather than a categorical distinction between ourselves and other mammals [26].

What is a memory?

An impressive feature of the human brain is its ability to learn complex information or a skill and be able to recall or replicate it later. This ability may be intentional or implicit. The information of a particular experience is processed, and if triggering significant enough emotion, will integrate sensory information to create a picture. A culmination of senses and a general ‘meaning’ of the experience can create a ‘mood’, allowing us to feel the effects of existing in a particular setting. Additionally, single images, sights, sounds, or ideas related to an experience can bring back the memory and feeling of that experience. In such cases, we are making simple associations at a later date and re-living the physical experience of the past.

Rather than recording information ‘about’ something we perceive, the brain records all available responses evoked by the interaction. These reactions include the visual patterns mapping an image in the brain; and all the sensorimotor patterns associated with viewing, touch, emotions, and feelings it may have sparked, and finally the memories it may have inspired us to recall. A memory is a recording of stimulus perturbations on our senses, other memories, emotions, and feelings that define the experience of an event. The more we engage in an experience, that is, an increased amount of interaction, the more likely we are to remember it – with a preference for contexts over specific event details [27].

In general terms, most higher order functions, whether consciously arising or not, are a form of memory. The formation of memories is one consequence of a fundamental feature of the brain: plasticity. Hence, storage of memories is intimately tied to ongoing information processing and adaptation in the brain. Memories in this case are experience/event-induced changes in neuronal firing propensity; we are the net effect of our experiences on our inherited physiology.

The persisting nature of memory suggests that experiences are sets of stimuli that induce state changes in the central nervous system (CNS), which are re-accessible. These physiological correlates of experience are thought to be memory representations These representations were defined by Richard Semon as enduring yet dormant modifications to the stimulus-perturbed substance and termed ‘engrams’ [28]. Thus, engrams are not memories; instead, they refer to the necessary physiology that allows a memory to be stored and to emerge from retrieval [29]. Semon proposed that

coincident activations become connected and act ‘engraphically’ (leave behind a unified engram complex) [30]. Therefore, the engram could be conceptualised as a ‘memory trace’.

By the 1930’s, Karl Lashley began searching for the engram in the brain of rats trained to find the route to reward in mazes [31]. Lashley postulated that maze route memory would localise in the cortex and so proceeded to lesion cortical tissue while testing maze performance. The extent – but not location – of lesions was predictive of impaired memory. Lashley deemed the engram ‘elusive’, as he ultimately failed in his attempts to find it.

In 1949, a student of Lashley, Donald Hebb, proposed the cell assembly theory, reminiscent of Semon’s engram complex [32]. Hebb stated that coactivation of interconnected cells forms a cell assembly, inducing intracellular changes that further strengthen these connections [33]. A functional implication of strengthened connections is a more robust cell assembly: reactivation of some cells leads to complete reactivation of the cell assembly, while fractional destruction of assembly cells only degrades the representation [32]. This cell assembly functionality is mirrored in contemporary computer-simulated neural networks of pattern recognition software [34].

Memory theorists like Semon, Lashley, and Hebb operated against a backdrop of landmark discoveries supporting the idea of brain regional specificity of mental functions. In 1855, post-mortem observations of brains from blind stroke patients led Bartolomeo Panizza to the discovery of the primary visual cortex [35]. In 1861, Pierre Paul Broca discovered that posterior left frontal lobe damage affected speech production [36]. In 1870, Gustav Fritz and Edvard Hitzig produced the first experimental evidence for cortical control of motor function in what is now known as the motor cortex [37]. This led to the futile pursuits of discrete neural memory systems and a potential ‘memory centre’ in the brain.

A difficulty arising with the aim of ‘finding a memory’ is that memory has multisensory qualitative features, exists in fundamentally different forms, and is thus differentially distributed in specific regions of the brain. Memory thus reflects the multitude of functional systems in which the brain is organised and should be conceived of as a property of navigating and ongoing processing of brain systems based on prior experience. The next section attempts to clarify various forms of memory and their associated features.

Categories of Memory

Learning and memory are integral to navigating through everyday life. This is because learning refers to a change in brain and/or behaviour that results from acquiring knowledge about the world through experiences. Memory defines the temporal dimension of mental organisation – the process by which knowledge or experience is acquired/encoded, stored/consolidated, and later recalled/retrieved [38].

The image (**Fig 1.1**) and definitions below intend to provide an overview of existing memory categories, with the caveat that formed memories in the brain are almost never composed of one single form of memory.

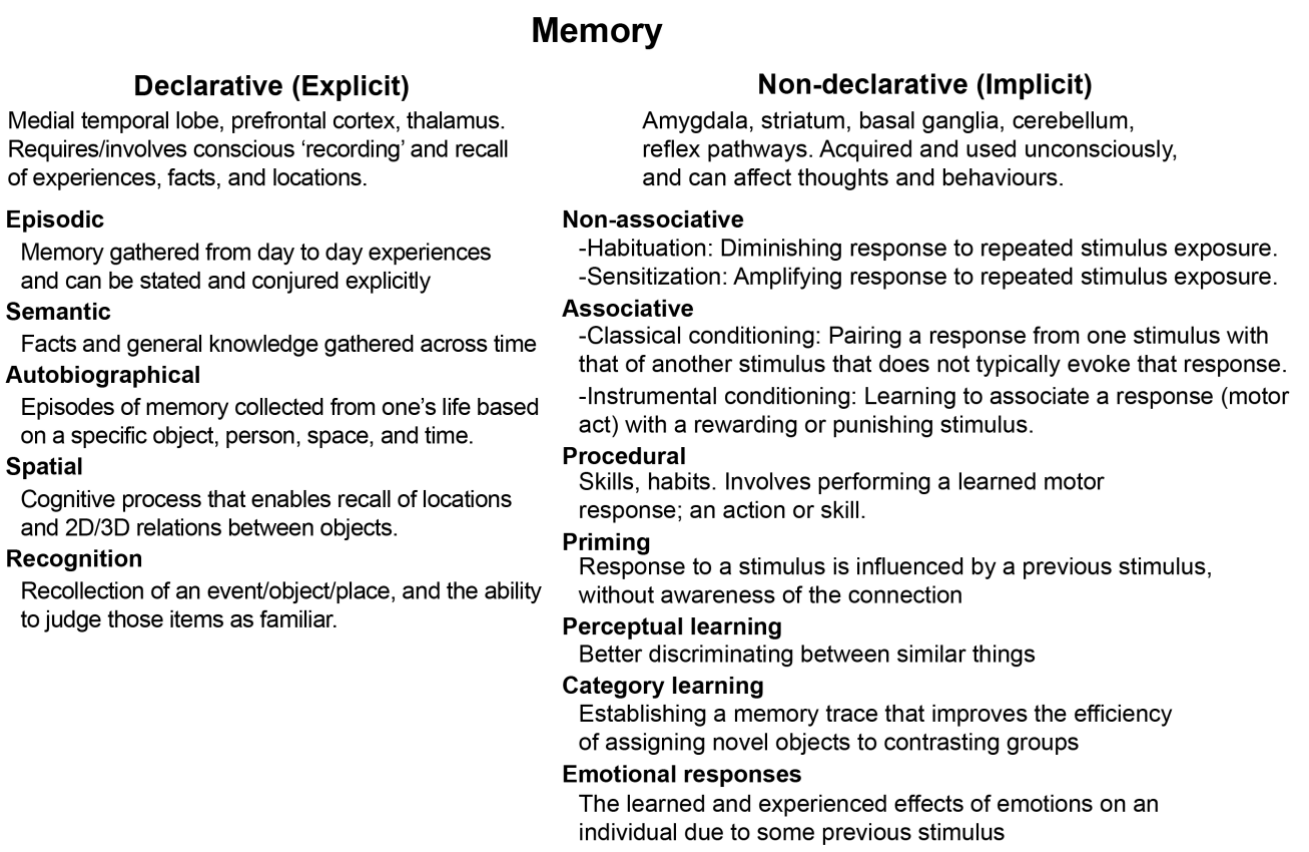

Figure 1.1. ***Categories of memory***. This is a summary diagram of declarative and non-declarative memory categories and their respective sub-categories.

Note*: Unless explicitly stated, 'memory' refers to long-term memory. Short-term memory is not simply a relatively transitory storage of the same information content as long-term memory. Rather, it is qualitatively different, and overlaps with working memory [39]. Some reports suggest a complete overlap. Briefly, short-term memory is the temporary maintenance of events in mind (1,3,4,6,2), while working memory is the temporary maintenance of events in mind as they are being manipulated (2x[4+3]/4^2=?) [39].*

1) Declarative (Explicit) memory: Brain regions associated with declarative memories are the medial temporal lobe structures and structures comprising the diencephalon [40-42]. Declarative memories require conscious involvement in the recording of experiences, facts, and locations. Conscious effort is required to recall information from declarative memory, as it must intentionally be brought to mind. Declarative memories can be divided into five broad categories, listed below.

(i) ***Episodic*** memory refers to memory of everyday events that can be explicitly stated. This includes times, places, the associated feelings, and context that make up that experience [43]. An example

would be: getting into an accident in traffic. The term was first coined by Endel Tulving in 1972 when he articulated the distinction between remembering (episodic; a feeling located in the past) and knowing (semantic; a factual recollection) [44]. Episodic memories are associated with the medial temporal lobe [40].

(ii) ***Semantic*** memory refers to general knowledge gathered throughout life. It involves the recall of concepts, ideas, meanings of words, and facts [45]. A semantic memory is knowing what a plane is – an engine with wings one boards to travel long distances. The inferior parietal cortex is associated with representational aspects of semantic memories [41].

(iii) ***Autobiographical*** memory refers to memories collected throughout one's life. It consists of a combination of episodic memories and semantic memories as they pertain to one's own life. This personal knowledge is categorised into lifetime periods, general events, and event-specific knowledge [46]. Autobiographical memory content is diffusely associated with regions throughout the brain [47].

(iv) ***Spatial*** memory refers to the recording and recalling of information representing spatial arrangement of an individual relative to the surroundings (orientation). Spatial memory allows one to plan and execute a route to a location (navigation) [48]. It forms a basic cognitive map: a mental representation of relative locations and associated attributes [49]. The hippocampus and medial entorhinal cortex are key areas for spatial memory [42]. Using a behavioural and memory neuroscience example, the Morris Water Maze (MWM) tests mouse spatial and reference memory by allowing mice to swim in a water tank where the 'escape' is to find a platform hidden 1 cm below the opaque, dyed-white water [50]. Four navigation cues are above the tank and the mouse must learn where the platform is by referring to the cues.

(v) ***Recognition*** memory refers to the ability to recollect/remember something in addition to being familiar/knowing that something. It is the recollection of event-related details and the feeling of having previously experienced that event [51]. The hippocampus is predominately linked to recognition memory [52], although regions can vary and depend on what is being recognised. Using a behavioural and memory neuroscience example [53], novel objected recognition (NOR) memory in mice can be tested by placing mice into a large box with two objects A and B for ~10 min and record the time the mouse has spent exploring each object. After 8-24 hrs, reintroduce the mouse with two object A and C, and repeat the measure of exploration time. Mice are naturally exploratory and an ability to recognise is indicated by more relative time spent exploring novel object C [53].

2) Non-declarative (Implicit) memory: Brain regions associated with non-declarative memory include the basal ganglia, cerebellum, amygdala, striatum, (cortical) reflex pathways. It refers to

unconsciously attained and unconsciously utilised memories that affect thoughts and behaviours [54]. Non-declarative memory can be subdivided into at least the seven categories listed below.

(i) ***Non-associative*** memory is the simplest yet most fundamental form of memory, as it requires no stimuli association or pairing – animal species alter responses from a single stimulus exposure [55].

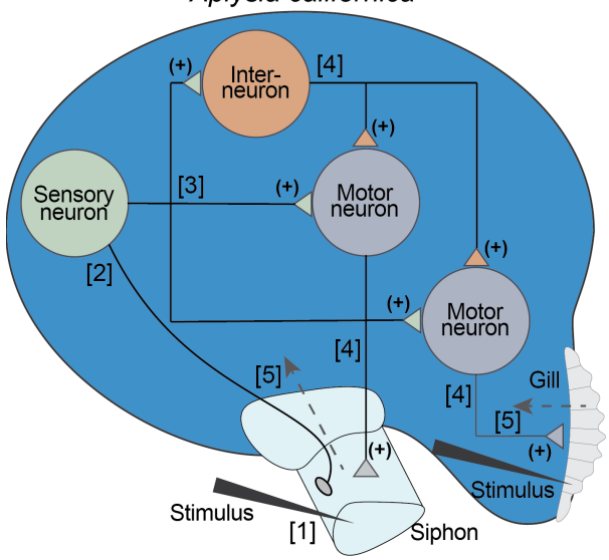

Figure 1.2. ***Non-associative learning in Aplysia californica***. Stimuli activate sensory neurons and withdrawal reflexes (grey arrows). Reflex sensitized by interneuron facilitation of motor firing. Repeat stimulation habituates response from depressed firing [1].

Two major forms are sensitization and habituation. Sensitization is learning that leads to increased responsiveness to a stimulus – most often noxious, e.g., pain and inflammation, or heightened senses when walking through a dark alley. Habituation is the decline in behavioural responsiveness to the continual presentation of a stimulus, e.g., from prolonged exposure to an odour/sound; and may be deliberate, to accelerate learning in mice (see **Chapters 2** and **3**). Non-associative learning came to prominence through the pioneering work of Eric Kandel in the 1960's, studying the gill and siphon withdrawal reflexes of the sea slug *Aplysia californica* (**Fig 1.2**) [1]. With their giant individual neurons and observable responses, it was the first demonstrated link between neuronal circuits and behaviour. Stimuli activate the terminals leaving the mechanosensory neurons in the central ganglia. The sensory neurons make excitatory synaptic connections with motor neurons and interneurons. A parallel excitatory pathway is provided by interneurons for motor neuron excitation (sensitization). Motor neuron action potentials are triggered by sensory neuron and interneuron inputs to activate muscle cells and the withdrawal reflex. Repeating the stimulus eventually leads to a reduced reflex response (habituation).

(ii) ***Associative*** memory is the unconscious learned pairing of two stimuli, or the formation of a link between two events (**Fig 1.3**) [56]. The two forms of associative learning, classical and instrumental, formed the foundation of behaviourism, which was dominant in the mid-20th century. These are still influential today, forming the behavioural component of research into addiction, post-traumatic stress, and neurodegeneration research into memory.

Redacted due to copyright restrictions

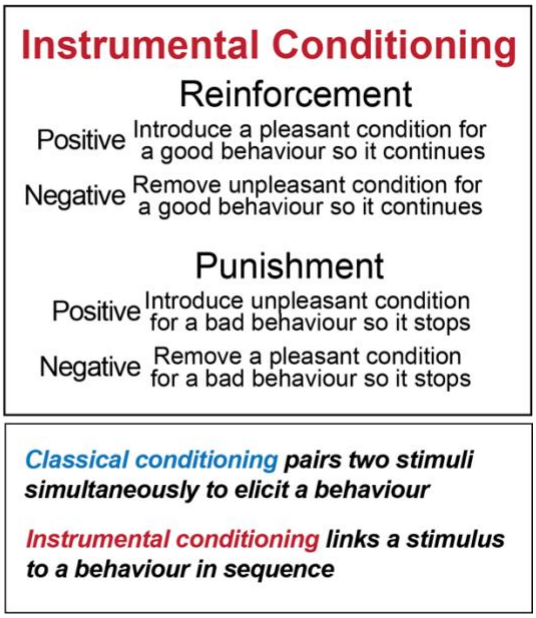

Figure 1.3. ***Overview summary of two forms of associative conditioning***.

(ii-1) ***Classical conditioning***: Using a behavioural neuroscience example, an association forms when a neutral stimulus cue (sound) becomes predictive of an unconditioned stimulus (electric shock) due to multiple occasions of context-shock co-exposures, or 'pairings' [57]. The indicator of an acquired association (pairing, into memory) would be a mouse freeze response upon hearing the sound (the cue), in expectation of a shock. This is 'cued fear conditioning', or CFC.

(ii-2) ***Instrumental conditioning*** is based on two forms of consequence, known as reinforcement (pleasant) and punishment (unpleasant). Note that 'positive' and 'negative' refer to adding or removing something (the reinforcement or the punishment), not to whether what is being added is itself good or bad. 'Pleasant' could be adding (positive) something good or removing (negative) something bad. 'Unpleasant' could be adding (positive) something bad or removing (negative) something good.

(iii) ***Procedural*** memory refers to a skill attained from learning to perform a task involving the integration of cognitive and motor skills [58]. Procedural memory generally refers to the point from which the task can be performed without conscious involvement. This includes learning to ride a bike or learning to read.

(iv) ***Priming*** refers to a subconsciously generated secondary stimulus following a primary stimulus [59]. It occurs when exposure to one stimulus influences the response to a subsequent stimulus, without awareness of any connection. It can be conceptual, associative, emotional, or perceptual. It works best in the same modality stimulus. For example, a semantic prime for 'grape' is 'cherry', and is theorised to be the case because of 'spreading activation' within associative networks [60].

(v) ***Perceptual*** learning and memory is the improvement in ability to discriminate between two similar things [61]. It forms the basis of complex cognitive processes such as language and relies on

underlying neural circuitry. Somebody with expertise in a field, with years of practice, would likely have refined perceptual skills pertaining to that field.

(vi) ***Category*** learning and memory (concept learning) refers to the attainment of concept, or the ability to segregate and clarify phenomena accordingly. It allows a learner to make subjective divisions, then comparisons, for better understanding. The two key components of a concept are the (1) attributes of data and the (2) conjunction of constraints on data, together determining a positive or negative instance of the concept [62].

(vii) ***Emotional*** learning and memory refer to the effect of emotions on an individual. Regulating one's own emotions is one example of engaging with them. Emotions have attentional and executive control on attention, to focus on what appears to be most relevant [63]. Associated brain regions include the prefrontal cortex, amygdala, and hippocampus. Emotional components to a memory can, in the right amounts, enhance the memory [63].

Together, these listed descriptions of categories of learning and memory demonstrate a range of aspects to the information content being learned and stored. They additionally make clear that no single region of the brain is responsible for memory [64]. Acknowledging this, the research described in chapters 2 and 3 related to memory categories of associative-classical learning (cued fear conditioning), recognition memory (novel object recognition), and spatial learning (Morris Water Maze), which all elicit regional engagement of the hippocampus [50, 65, 66]. Therefore, the next section presents an overview of hippocampal anatomical structure and associated function.

Functional anatomy of the hippocampus

The relatively simple structure of the hippocampus (HC) (**Fig 1.4**) makes it an ideal place to study mammalian synaptic neurotransmission. A slice can be kept alive in artificial cerebrospinal fluid for hours while fibre tracts are electrically stimulated, and synaptic responses are recorded. The ability to observe these cells greatly facilitated the study of the molecular correlate of learning: long term potentiation.

Information from primary sensory processing regions converge into the HC through perirhinal and entorhinal cortices (**Figs 1.4-1.6**). It is thought that these cortical inputs, once decorrelated, form the basis of discrete memory representations [67, 68].

Redacted due to copyright restrictions

Figure 1.4. ***Anatomy and function of the human and mouse hippocampus***. (**A**) *Human hippocampus in temporal lobe*. Hippocampus (HC) consists of two thin sheets of neurons folded onto each other - the dentate gyrus and Ammon's horn (division CA1-CA4). Focus here is on the CA3 and CA1 divisions. The subiculum mediates HC-cortex interactions (**B**) *Hippocampal trisynaptic microcircuit*. (1) Entorhinal cortex information flows through the perforant path and dentate gyrus (2) Granule cells of dentate gyrus project mossy fibre axons onto CA3 pyramidal neurons (3) Schaffer collateral axons of CA3 neurons synapse onto CA1 pyramidal neurons. *Adapted from Nolte's The Human Brain* [69], *and Neuroscience: Exploring the Brain* [70]

Entorhinal cortex → Dentate gyrus. Entorhinal cortical (EC) layer 2 projections reach dentate gyrus granule cells (GC) via the perforant pathway [71]. GCs project to CA3 neurons via mossy fibres (mf), which provide a sparse but powerful connection to CA3 pyramidal cells. Most synapses on CA3 pyramidal dendrites come from recurrent axon collaterals (Rc) of CA3 cells themselves [72]. This distribution of CA3 Rc effectively contributes relatively few of the total connections within the CA3 network in the rat HC [73, 74]. The CA3-CA3 Rc system is even more extensive in macaques than in rodents [75]. In humans, each hemisphere may have separate CA3 networks, because the left HC system is dedicated to memories based in language and the right HC system specializes in spatial memory [76]. The computational reason for this is that language does not work by spatial locations (no use/need for word-place episodic memory). Neurons comprising CA3 project to CA1 via the Schaffer collaterals, and projections that terminate in CA1 originate in EC layer 3.

Dentate gyrus → CA3. It is theorised that the dentate GC stage of HC processing preceding the CA3 stage acts in multiple ways to produce sparse yet efficient (i.e., nonredundant) representation in CA3 neurons that is necessary for the auto-association implemented by CA3 during learning by pattern separation [77]. Pattern separation here means the reduction in correlations between different memory patterns represented by a population of neurons in the neurons within the CA3 region [78]. The perforant path-dentate GC system, with its Hebb-like modifiability, may act as a competitive learning network to remove redundancy from inputs, producing a sparser and more categorized set of outputs [77]. The nonlinearity of NMDA-R activation may contribute to competitive network operations by ensuring that only the most active neurons remaining post-competitive feedback

inhibition have synapses that become modified, and thus learn to respond to that input [77]. Feedback inhibition may lead to a stabilised number of strongly active dentate neurons (projecting into CA3) relatively independent of total perforant path inputs to GCs. Another suggested way that the dentate GC stage of HC processing produces sparse yet efficient representation in CA3 is that the dentate GC–mf input to CA3 cells may be strong, and learning-dependent activation would efficiently force a new firing pattern onto CA3 cells [79]. Finally, dentate gyrus neurogenesis may perform a computational role in new pattern separation by providing new random connections to CA3 neurons via new dentate GCs [80]. In mice with impaired adult neurogenesis in the dentate gyrus, radial maze spatial learning was impaired for arms presented with little separation, but not when the arms were presented farther apart [81]. These same mice also had a deficit in small spatial separation in an objects-in-space task [81].

Redacted due to copyright restrictions

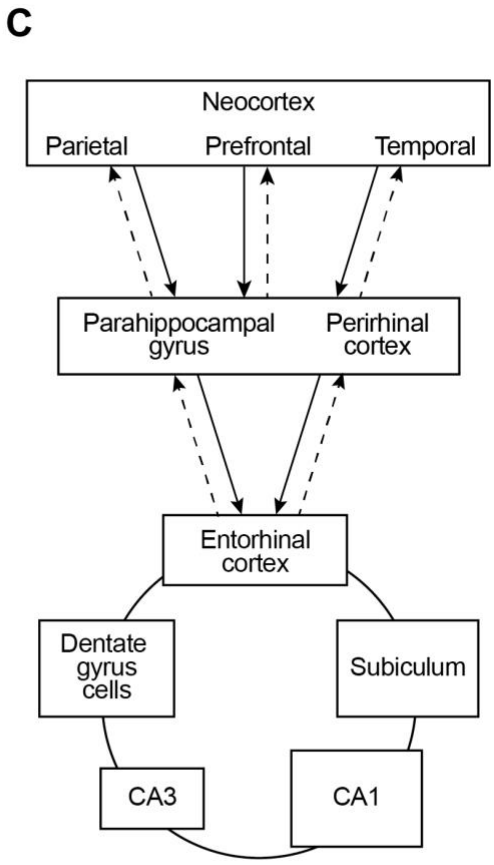

Figure 1.5. ***Afferent (Input) and efferent (output) pathways of the hippocampus***.

(**A**) *Hippocampus inputs*. The entorhinal cortex (EC) collects inputs from association areas and the olfactory bulb and is the major source of input to the hippocampus. The EC projects to dentate gyrus (DG), and from here to the hippocampus (CA). Other Direct inputs arrive from the amygdala (Am) and from the septal nuclei (S) through the fornix (also, not shown, other mandatory inputs such as from the contralateral HC or locus coeruleus). Neocortical inputs are shown projecting only to EC for simplicity, but some project directly into HC. All Am inputs show direct inputs to CA, whereas some synapse onto EC.

(**B**) *Hippocampus outputs*. Fibres reach anterior forebrain structures through the fornix, including to the anterior thalamic nucleus (A), mammillary body (MB), hypothalamus (Hy), septal nuclei (S), and ventral striatum (VS). Some pre-commissural fornix fibres spread beyond the S and VS, reaching anterior cingulate and orbital cortices. Many fibres pass from the subiculum to the EC, amygdala (Am), or to the posterior cingulate gyrus through the cingulum. The subiculum and EC are drawn together, despite overlapping and distinct connections (A) and (B) *Adapted from Nolte's The Human Brain* [69]

(**C**) *Simplified input/out block diagram of afferent and efferent HC pathways*. Forward connections (solid lines) go from neocortical association areas through to the hippocampus via the parahippocampal gyrus/perirhinal cortex, and entorhinal cortex. Back-projections (dashed lines) from CA1 pyramidal cells in the HC project through the subiculum, parahippocampal gyrus, out neocortical regions. The convergence and divergence are roughly proportional to box size e.g., HC CA3 cells are a single fairly isolated network from where back-projections diverge greatly as they approach higher areas. *Recreated from Learning and Memory – A Comprehensive Reference* [79, 82].

CA3 as an auto-association memory. Many HC synapses involved in learning show associative modification (e.g., long-term potentiation) [83]). Information processing at the CA3 stage may act as an auto-association memory to enable episodic memory formation and storage in the CA3 network [84]. The retrieval of a whole representation can thus be initiated by activating a cue that constitutes a small part of the same representation (due to extensive recurrent collateral connections). The recurrent collateral (Rc) synapses are the crucial modification for this [84]. The architecture of an auto-association network is shown in (**Fig 1.6**).

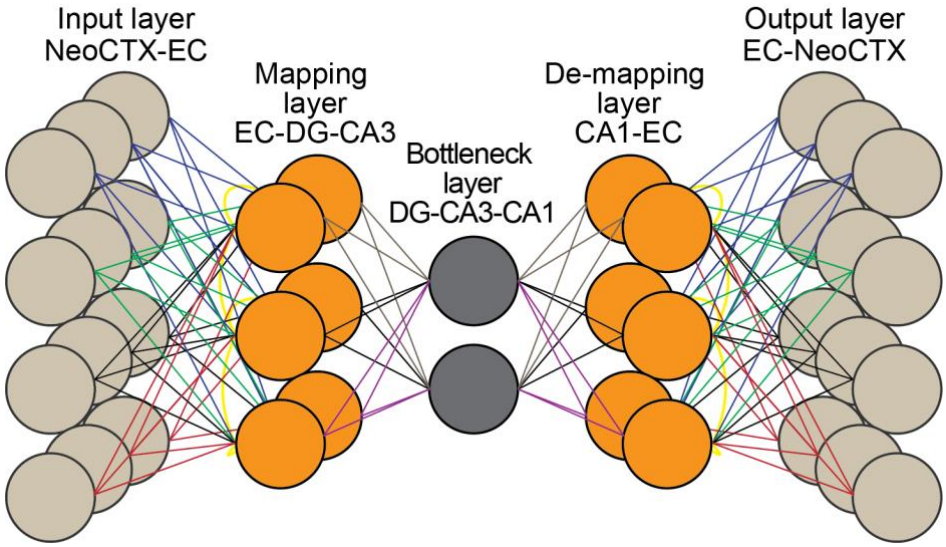

Figure 1.6. **The hippocampus in the centre of an auto-association network**. A schematised analogy of hippocampal information processing in the brain. An input layer is followed by a hidden mapping layer containing recurrent collaterals (yellow lines) and a bottleneck layer. Input data compression and feature extraction occurs at the bottleneck layer, followed by de-mapping and final output layer. The right-side network works opposite to the first, de-compressing information to regenerate and represent original input measures. *This is routed information through hippocampal circuitry allowing processing and transfer of information (contextual, spatial, semantic) to neocortical areas*. NeoCTX, neocortex; EC, entorhinal cortex; DG, dentate gyrus; CA1/3, *cornu ammonis* 1/3 [85-87]

Because CA3 operates effectively as a single network, it allows arbitrary associations between disparate inputs from throughout the cerebral cortex to be formed [88, 89]. Associations might be between information from the visual cortex (existence of an object), and information from parietal cortex (where object is in space) [75]. It is unknown if the auto-association hypothesis can account for/allows for a realistic number of 'total memories' to be stored and whether system operations are compatible with (continuous) spatial representations (nature of space is continuous) [90].

Given that hippocampal CA3 system capacity for memory is limited, some form of forgetting mechanism must ensure capacity for storage is not exceeded. Heterosynaptic LTD could enabling 'overwriting' of old memories [91]. A limited CA3 storage capacity is also consistent with the utility of the apparent HC-CTX information transfer; that the HC might be a useful storing information over days to months, and that this time would be dependent on the rate of episodic memory acquisition.

Processing of spatial patterns implies that there are continuous representations of space in the HC and has led to applications of continuous attractor models to help understand hippocampal function [90]. Moving through (inherently continuous) space correlates to single approximately Gaussian firing rates of individual cells (e.g., place cells) because of spatially overlapping fields; and because the auto-association theory states that these cells in CA3 are connected by Hebb-modifiable synapses [79]. A "Continuous Attractor" neural network (CANN) uses excitatory Rc connections between the neurons (as in CA3) to reflect inter-neuronal distance in the animal state space (e.g., place or head direction) [80]. CANN properties include maintaining a network of prolonged constant neural activity while global inhibition keeps the constant firing contained to a subset of neurons within a broader network (e.g., place and grid cells) [80]. The computational neuroscience-centred analogy of the HC as an auto-association centre is based on the functional anatomy of inputs to the HC and innumerable studies of HC damage, activity recordings, and declarative memory performance [78]. In fact, it is consistent with a prominent contemporary view of the HC as a centre for integrating and processing convergent sensory inputs that provide the information that forms declarative memories.

Neurons in the HC associated with spatial navigation are known as place cells [92]. Single cell recording in behaving rats showed that individual cells would fire as the rat approached a cue, in a box, linking firing rate to a location in the enclosure (**Fig 1.7**, *left*). Yet when the cue was moved, the place cell continued to fire relative to the cue. This suggested that the response was in reference to a visual input rather than the space itself. Single cell recordings also led to the discovery of grid cells in the entorhinal cortex, that responded to multiple locations forming a hexagonal grid (**Fig 1.7**, *right*) [93]. Since grid cells coordinate and overlap, these spatially modulated cells with periodic hexagonally spaced fields provide the spatial map input to hippocampal place cells. Both cell types fire in their corresponding locations in the dark, suggesting that beyond sensory receptive fields, responses are based on where mice 'think' they are. These discoveries formed not just the basis for navigation, but for a cognitive map: an internal representation of the environment with an integrated self [92]. The polysynaptic and direct pathways passing through the HC are important for spatial navigation, declarative learning, and memory processing [94-96]. The outputs can be conceptualised as feedback pathways from the HC, through the fornix (to the thalamus-retrosplenial cortex) and through the entorhinal cortex which project to the prefrontal cortex and the amygdala (**Figs 1.4, 1.5**). These feedback pathways allow higher cortical structures to engage in meaningful contextual representations of information encoded in and retrieved from the HC (**Fig 1.5C, 1.6**) [97]. The HC is not a 'centre' for processing/accessing memory in the same sense that the amygdala is for processing fear, or auditory A1 is for sound. Rather, it can be thought of as a catalyst for long-term memory, but the memory trace itself is distributed [31, 64].

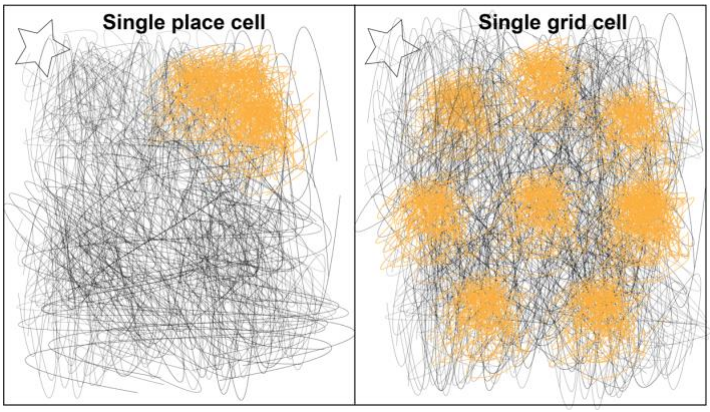

Figure 1.7. ***Recreated schematic of single cell place and grid cell firing.*** Black lines represent mouse walk path in an enclosure. Orange lines are locations where firing frequency of a single place or grid cell was highest. Star, orienting cue.

Neurons in the HC associated with memory are known as engram cells. An engram, or a memory trace, refers to the physical and/or chemical changes occurring in a network of cells as a result of learning [28, 98]. While these cells have been identified throughout CA1-4, the changes they undergo to remain part of a representative memory ensemble remains unknown. The activation of any cells in a cross section of the HC (i.e., **Fig 1.4B**) could be navigation- or memory-dependent [99]. Tracing the directed flow of 'information' into the HC from the major inputs pathways reveals axonal terminals forming synaptic contacts with neuronal dendrites or somas in sequence. These synaptic contacts are not permanent; rather, they are 'plastic'; and neuroplasticity is a fundamental feature of the brain, necessary for adapting to a dynamic external environment.

Neuroplasticity: structural, functional, and synaptic plasticity

The ability of the brain to adapt underlies its ability to learn complex information or a skill and be able to recall or execute it later. This property is neuroplasticity and refers to changes in neural network connectivity [100]. Besides learning, this property underlies nervous system changes during growth and development, ageing, recovering from brain injury, and in adapting to enriching social settings [100]. There are three general ways to describe neuroplasticity: structural, functional, and synaptic plasticity (**Fig 1.8**).

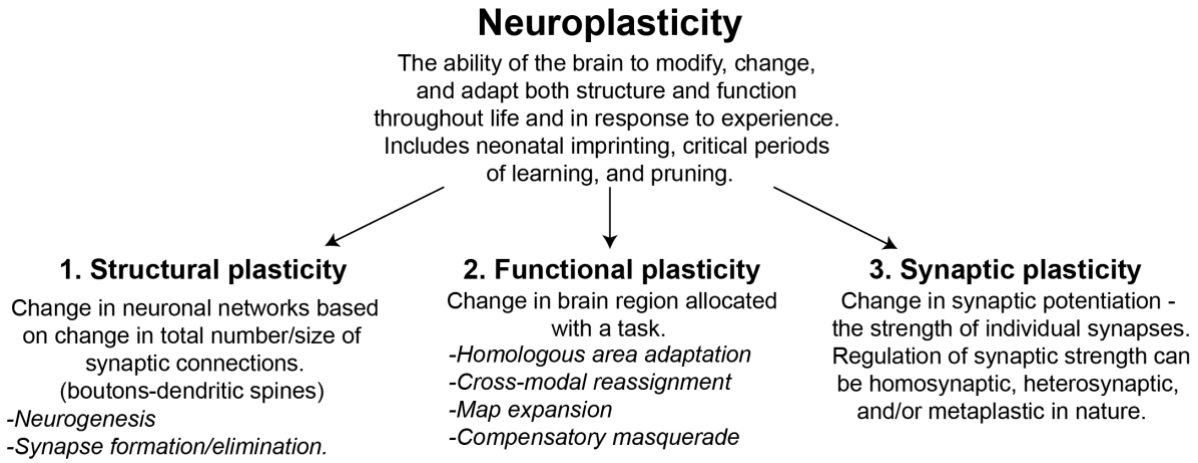

Figure 1.8. ***Neuroplasticity***. Structural, functional, and synaptic plasticity as forms of neuroplasticity.

1) ***Structural plasticity***: Describes the brains ability to change the total number, size, shape, and location of connections. Precise connectivity between neurons at sites of specialised communication (synapses) underlie efficient nervous system function.

One way to refine structural connectivity is by synapse elimination. Activity-dependent competition regulates at least two forms of structural plasticity. During input elimination, entire axon terminals and presynapses are being eliminated, for instance, when excess synapses are pruned in development to strengthen and refine remaining synapses into maturity [101]. The second activity-dependent form is terminal elimination, where individual contacts are eliminated during learning and memory [102]. Dendritic spine-colocalising major histocompatibility complex I (MHC-I) molecules released from neurons and possibly glial cells mediate spine disassembly [103]. Microglia selectively eliminate spines during development (pruning) by complement-mediated engulfment and elimination [104].

Structural changes can occur through synapse formation, whereby trans-synaptic cell adhesion molecules (CAMs) orchestrate synaptogenesis – as well as restructuring and elimination of synapses – in a bidirectional manner [105]. This process of synapse formation is most prominent during embryonic and post-natal development but does persist throughout life, in an activity-dependent manner [106].

Finally, structural plasticity can be achieved by increasing the total number of cells in the brain: neural stem cell differentiation into neurons at either of the two classic adult neurogenic niches: the subgranular zone of the hippocampal dentate gyrus [107], and the subventricular zone [108], but possibly also in the prefrontal cortex, amygdala, striatum, and substantia nigra [109]. Appreciation for the implications of adult neurogenesis is only gradually increasing. Nascent hippocampal neurons are particularly responsive to spatial learning-dependent plasticity [110] and have a low threshold for long-term potentiation (LTP) [111].

2) ***Functional plasticity***: Describes the brains ability to change the functional properties of neurons, believed to follow from – and is dependent on – structural plasticity [112]. This occurs in any of four known ways: cross-modal reassignment, homologous area adaptation, compensatory masquerade, and map expansion [113]. Cross-modal reassignment involves a novel signal input redirected into a region that has lost its native inputs, such as blindness that spares occipital area V1. Functional magnetic resonance and positron emission tomography with adults who became blind when young showed V1 activation from (Braille) somatosensory redirect [114]. Map expansion refers to becoming exceedingly proficient at a task using the devoted brain region, followed by an increase in cortical processing area into adjacent areas. Learning a visuomotor sequence led to increases in the cortical sensorimotor map [115]. In homologous area adaptation, in children with brain damage more than in adults, compromised brain tissue leads to a regional shift and associated cognitive task to a homologous region that becomes burdened with distinct cognitive processes and representations. The shifted module functions operate at sub-maximal capacity, as was the case in adolescents with severe right parietal damage [116]. They exhibited compromised arithmetic abilities in the native region but had relatively unaffected visuospatial skills (shifted cognition from right parietal) [116]. Damage was attained prior to school age and authors posited that the region was ‘claimed’ by visuospatial skills easier than if the region had already been specialised. Compensatory masquerade as functional plasticity involves novel use of an established cognitive process to perform a cognitive task from a now damaged region, for example, using verbal coordinates to navigate instead of spatial coordinates because spatial has been compromised [113].

Functional plasticity can be activity-dependent due to learning or compensatory following brain damage. It is believe that the degree to which the brain can transfer functions successfully depends on cognitive reserve [117].

3) ***Synaptic plasticity***: Describes the brains ability to changes the strength of any given synapse in response to changes in activity [118]. Synaptic strength is also known as ‘synaptic weight’ and is a function of presynaptic neurotransmitter release and binding to surface neurotransmitter receptors at the post-synapse [119]. Strength of a synapse ultimately depends on the extent of postsynaptic receptor activation following neurotransmitter binding.

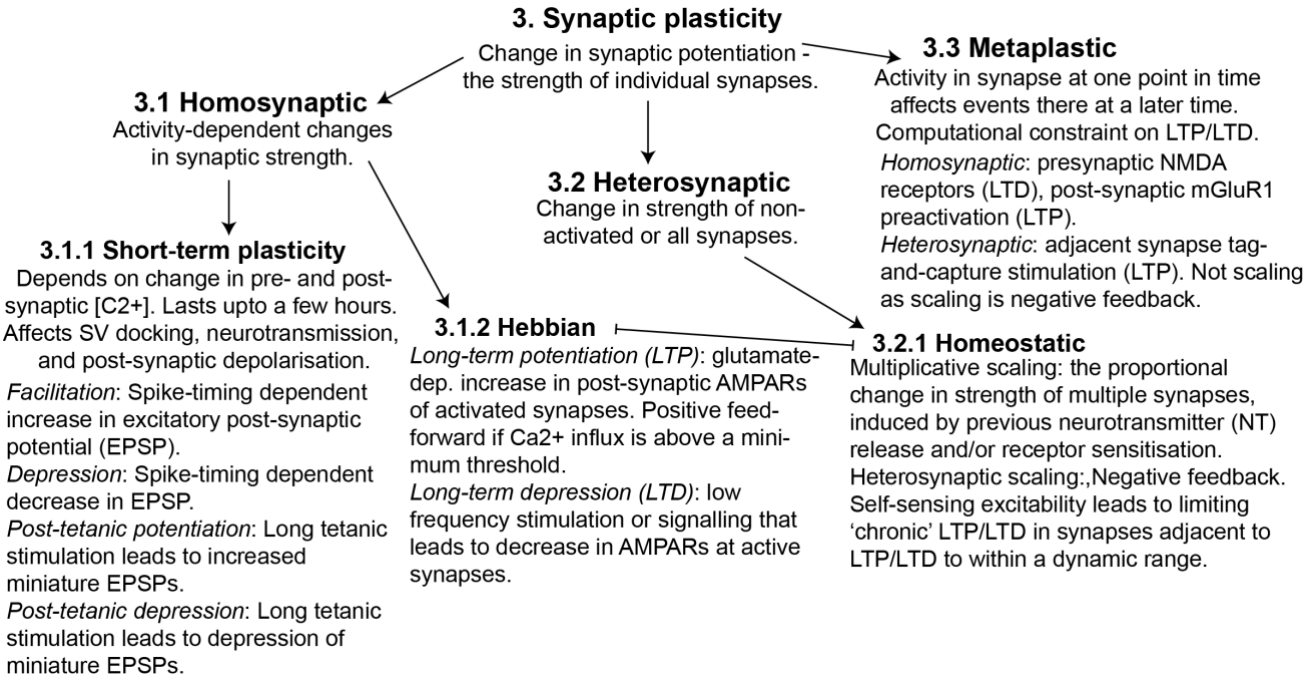

Figure 1.9. ***Synaptic plasticity***. The flow diagram shows various forms of synaptic plasticity.

3.1) ***Homosynaptic plasticity***: Homosynaptic plasticity is input-specific and refers to the postsynaptic changes in strength only occurring when specifically stimulated by a presynaptic target [120]. Therefore, the presynaptic signal spread is localised.

3.1.1) ***Short term plasticity***: Many synapses show a mixture of an increase or decrease in efficacy of neurotransmission at the synapse, knows as facilitation and depression respectively, that ranges from seconds to minutes. Depression can function to reduce noise, dynamic range of synapses, wave oscillations in neural networks, and contribute to habituation, by making synapses responsive to select stimuli or to broader changes in the level of activity [121]. Short-term homosynaptic depression can be caused by depletion of vesicles from the readily releasable pool, inhibitory auto-receptors of released neurotransmitters, inactivated calcium ion (Ca^{2+}) channels, or sodium ion (Na^{+}) channel-based refractory periods [122]. Short-term heterosynaptic depression can be a result of regulating conductance of ions, temporarily enhanced efficiency in first-stimulus release of vesicle pool by protein machinery, and/or depotentiated Ca^{2+} channel influx [122].

Residual Ca^{2+} in axon terminals increase second-stimulus release of neurotransmitters during frequency-dependent enhancement of firing at synapses [121]. Separate from endogenous ion buffer saturation at synapses, local action of Ca^{2+} is partially mediated by non-local targets for augmenting neurotransmission [122]. Potentiation following prolonged stimulus (post-tetanic potentiation, PTP) is prolonged because after tetanus, machinery for the removal of locally elevated Ca^{2+} are overloaded. Frequency-dependent increases in the efficacy of synapses allow conduction from signals of higher frequency (above a cut-off, akin to high-pass filters), allowing synapses to respond to certain activity

patterns and to discriminate signal from noise, which optimizes the information being transmitted through chemical synapses [122]. Short-term heterosynaptic facilitation (consistent with depression) can be a result of regulating conductance of ions, temporarily enhanced efficiency in the release pool protein machinery, and/or potentiated Ca^{2+} channel influx, although the effect on excitatory post-synaptic potentials is facilitation and not depression [121]. Subcellular locales of Ca^{2+}-dependent processes or Ca^{2+} influx are common sites for regulation by both homosynaptic and heterosynaptic forms of plasticity. This is consistent with the critical contribution of Ca^{2+} in the release of neurotransmitters.

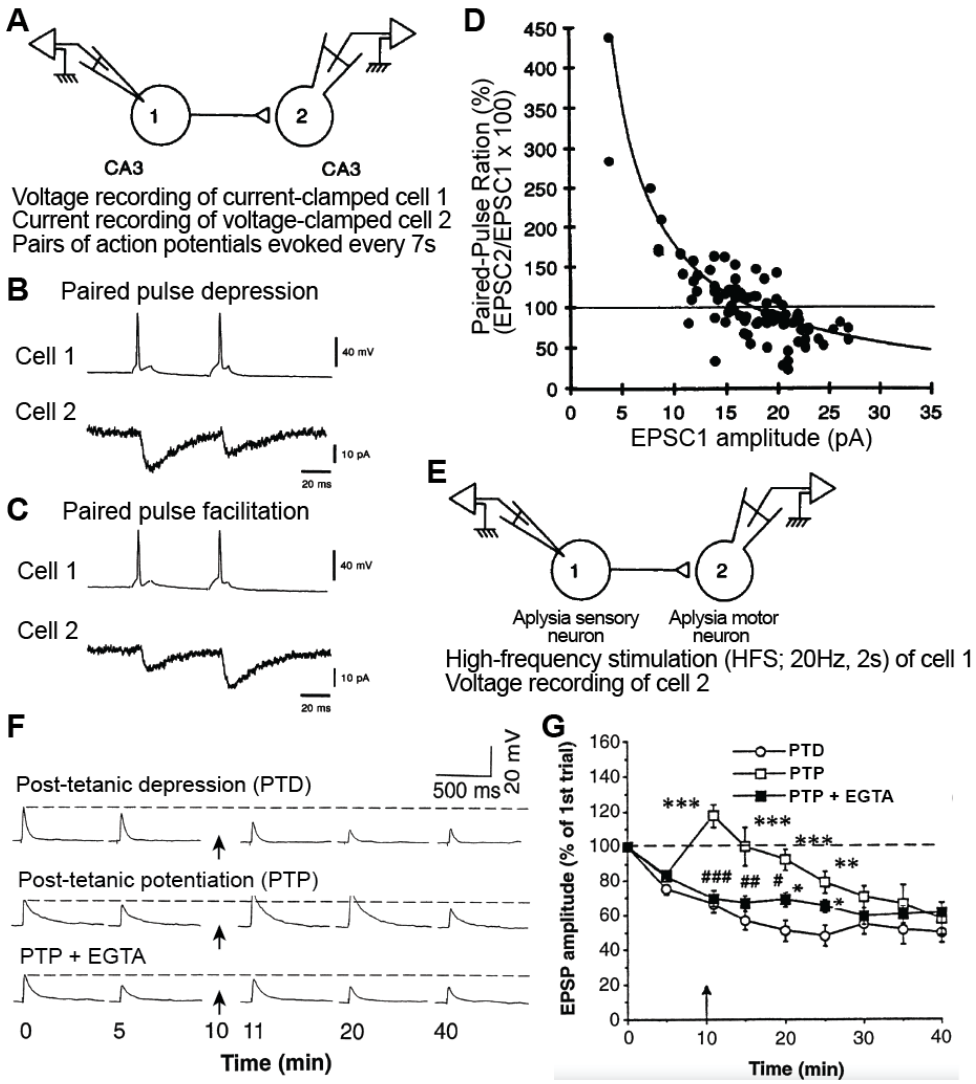

Figure 1.10. ***Homosynaptic depression and facilitation***. (**A**) Hippocampal slice culture schematic of intracellular voltage and current recordings. (**B**) Paired Pulse → ***Depression***: When the first excitatory postsynaptic current (EPSC1) amplitude from the first action potential (AP1) in cell 1 was large, EPSC2 from AP2 was small. (**C**) Paired Pulse → ***Facilitation***: When EPSC1 amplitude from AP1 was small, EPSC2 from AP2 was large. (**D**) Dot plot of paired-pulse ratios showing (i) EPSC2 > EPSC1 when EPSC1 < 10 pA, (ii) EPSC2 < EPSC1 when EPSC1 > 20 pA. (**E**) *Aplysia* sensory-motor synapse schematic of sensory neuron stimulation and excited motor neuron recording. (**F**) ***Post-Tetanic Depression/Potentiation***: Representative excitatory post-synaptic potentials (EPSPs) before and after HFS (20 Hz, 2s) of presynaptic sensory neurons at 10 min. PTD occurs when cytosolic Ca^{2+} is low. PTP occurs when cytosolic Ca^{2+} is high and is prevented when Ca^{2+}-chelating agent EGTA is injected into the presynaptic neuron. (**G**) Line graph showing motor EPSPs

following sensory neuron stimulation every 5 min, before and after HFS at 10 min. *Panels adapted and modified for illustrative purposes from Debanne et al (1996) and Bao et al (1997) [123, 124].*

3.1.2) ***Hebbian plasticity***: This form of plasticity is currently the most broadly accepted for cellular mechanisms of memory; stating that strengthening or weakening of synaptic units depends on their respective coincident or misaligned activity [32]. Strengthening connections in an assembly of firing neurons increases the probability of them firing together again [32] (**Fig 1.11**). For the probability of coincident firing to increase, a link must be created and endure between neurons that are likely to fire together again, even at times when they are not activated. The molecular underpinnings of Hebbian plasticity are described in section "**Molecular mechanisms of learning and memory**" [125, 126]

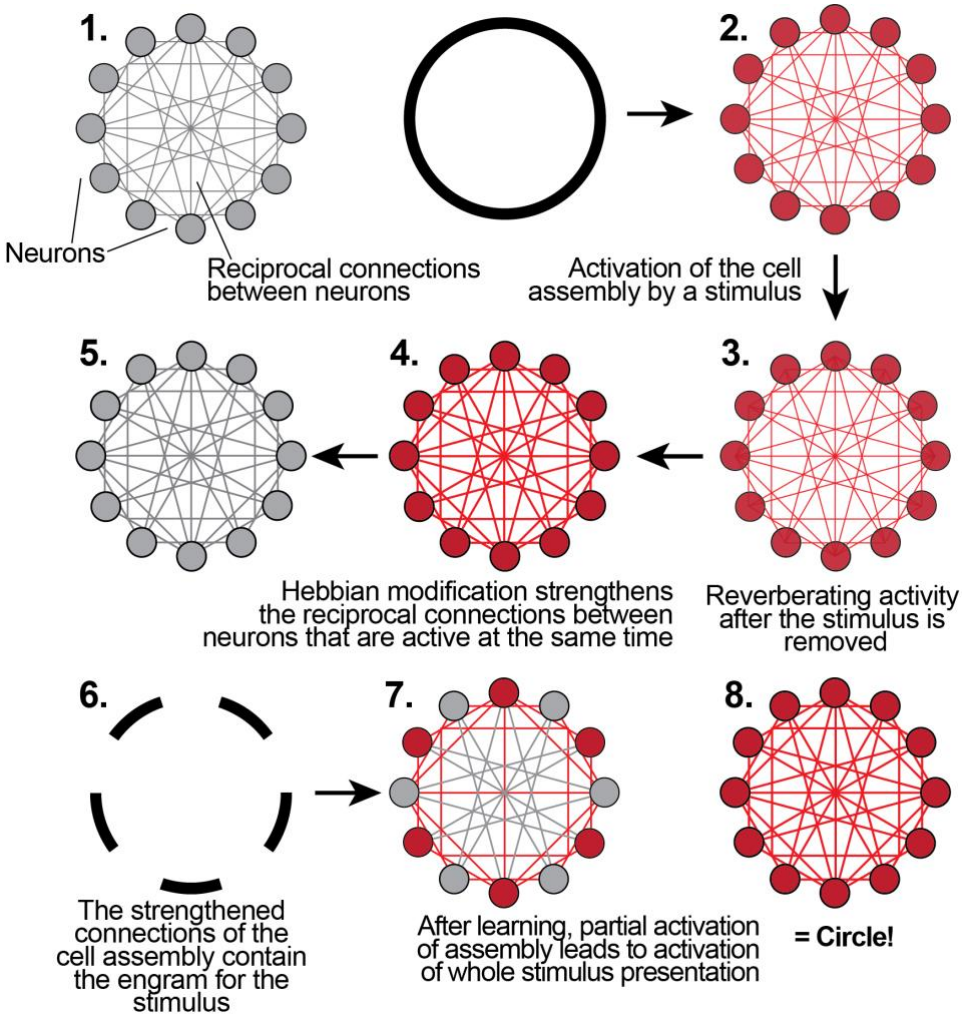

Figure 1.11. ***Schematic of Hebbian plasticity***. If cells fire together, the strength of their connection should increase. (1) Resting state neurons are stimulated by presentation of an image and they (2) activate. Stimulus is removed and activity causes changes in the (3) 'reverberating' neurons until connections are (4) reciprocally strengthened, (5) Neurons at resting state have modified and strengthened enough connections than only (6) part of the image (7) activates part of the cell and but due to the new associations, neurons activate to represent a circle [126, 127].

3.2) ***Heterosynaptic plasticity***: Induced by episodes of strong activity at the postsynapse but also at different synapses unrelated to the induction. This makes any synapse a target for heterosynaptic changes.

3.2.1) ***Homeostatic plasticity***. Synaptic scaling is the proportional adjustment to changes in synaptic weight across neurons in order to preserve weight distributions and therefore also firing patterns [126, 127]. Denervation super-sensitivity is the phenomenon of cutting a muscle-innervating neuron leading to increased electrical excitability of the muscle of the neuromuscular junction (NMJ) and to the neurotransmitter acetylcholine (ACh); shown to be a neuronal response to loss of synaptic input. Super-sensitivity can be induced by pharmacologically blocking neurotransmitter receptors or neuron/muscle electrical silencing by tetrodotoxin (TTX). This is likely a homeostatic response to loss of input. After electrical silencing of cortical neurons by manipulating synaptic input, excitability and synapses impinging on these neurons both increase [126, 127].

Do changes in synaptic strength affect tuned synaptic weight patterns? While absolute synaptic weights may change up or down, the multiplied/divided values are the same for all, and so relative difference in weights do not change, preserving relative distribution of synaptic weights (scaling) [125, 126]. Mechanisms for synaptic scaling may include somatic Ca^{2+} influx by voltage-gated ion channels (VGCC) and activation of Ca^{2+}-calmodulin-dependent kinase IV (CaMKIV) to regulate gene expression [128]. A period of activity leads to increased CaMKIV-dependent gene expression & vice versa [128]. This ultimately results in cell-wide insertion or removal of N-methyl-D-aspartic acid (NMDA-) and α-amino-3-hydroxy-5-methyl-4-isoxazolepropionic acid (AMPA-) receptors, over hours-days which is a longer time period than induction of LTP/LTD (sec-min) [126, 127]. This is likely due to the time necessary for synthesis or degradation of proteins required to adjust strengths of neuron-impinging synapses [129, 130].

3.3) ***Metaplasticity***: The history of synaptic or cellular activity influences the homeostatic ranges of synaptic processes, and plasticity takes place when outside of these homeostatic ranges of activation. Strong & weak NMDA receptor activation cause long-term potentiation (LTP) and long-term depression (LTD) respectively. 'Intermediate' activation, i.e., not many or few enough to cause a net change is the synaptic modification threshold. The BCM (experience-dependent changes in synaptic unit) states that the values of this minimum (activity required to induce LTP) threshold is dynamic, depending on integrated activity of postsynaptic neurons (↑↑LTP = ↑activity = ↑threshold necessary to continue to induce LTP; ↑↑LTD = ↓activity = ↓threshold of firing necessary to induce LTP) [129-131]. Computer simulations have shown that these threshold values change to preserve stimulus selectivity and memory. The subunit composition of NMDA (NR1-NR2B) is also a contributing factor to changes in the threshold value [125, 126].

Memory Storage: The storage of acquired episodic memory to long-term memory (LTM) requires the transfer of information from the HC to the neocortex [132]. Spatial memory transfer and storage occurs during sleep or non-attentive states in the HC & entorhinal cortex (EC). EEG firing patterns have been recorded during navigation. These are temporally compressed and replayed; and known as 'sharp-wave ripples' [133]. Just as spike timing-dependent plasticity might be a mechanism for storing millisecond-scale sequence information [134], so too might sharp-wave ripples store second-scale neural circuit firing patterns, believed to underlie episodic memories.

In the next section, the mechanisms of early and late LTP and LTD describe our current (Hebbian) understanding of learning and memory at a molecular level (**Fig 1.12**).

Molecular mechanisms of learning and memory

Coordinated activity of a presynaptic axon terminal and a post-synaptic dendritic spine strengthen the synaptic connection between them (spike-timing dependent plasticity, STDP). Uncoordinated activity between pre-/post-synaptic partners weakens this synaptic connection (STDP). Through synaptic vesicle processing/release and changes in surface receptor expression levels, LTP and LTD mediate changes in the strength of synapses, which in turn produce changes in the wiring patterns of neural circuits [126]. These synaptic changes accumulate throughout a network of interconnected neurons. Understanding changes in synaptic strength at the molecular level is critical because the net effect of neurons firing or misfiring together can be the wholesale change in structure and function of network properties that underlie learning and memory.

At the excitatory glutamatergic axodendritic synapse, the most common chemical synapse in the central nervous system [135], fusion of vesicles to the plasma membrane of pre-synaptic axon terminals leads to the release of glutamate neurotransmitter into the synaptic cleft (**Fig 1.12**, *top left*). Glutamate can bind to at least three types of integral membrane receptors at the dendritic spine, triggering synaptic activity: (i) Metabotropic glutamate G-protein coupled receptors, which modulate excitability at the synapse by activating biochemical cascades to modify activity of enzymes, channels and membrane potential [136, 137]; (ii) AMPA receptor channels, which convey the most synaptic current at glutamatergic synapses upon opening, become mostly permeable to Na^+ and K^+ [126]; and (iii) NMDA receptor channels, which require membrane depolarisation for the relief of Mg^{2+}-blocked channel pores to become permeable to Ca^{2+} [126]. Regardless of which glutamate receptors are activated, the post-synaptic influx of Na^+ depolarises membranes to prime NMDA receptors and activate more voltage-gated ion channels, and the influx of Ca^{2+} activates calcium-dependent proteins [138]. The most critically determining factor for which form of activity-dependent synaptic plasticity will occur (LTP or LTD) is the concentration of cytosolic Ca^{2+}, from endoplasmic reticulum efflux or from

VGCC influx [138]. Based on the subset of proteins that are activated, moderately elevated post-synaptic Ca^{2+} induces LTD while highly elevated Ca^{2+} induces LTP [138].

When pre-synaptic action potentials and post-synaptic neuron activity fail to correlate, less Ca^{2+} enters dendritic spines, fewer NMDA receptors are activated, and synaptic strength is weakened. At a molecular level, LTD is characterised by a reduction in post-synaptic surface receptor density, and to a lesser extent, a reduction in pre-synaptic neurotransmitter release (**Fig 1.12**, *bottom left*).

When there is coincident pre-synaptic and post-synaptic firing and dendritic spine Ca^{2+} concentrations are high, synapses undergo early LTP (**Fig 1.12**, *bottom centre*). Transient activation of CaMKII and PKC mediate early changes in LTP, which include sequestration of proteins and AMPA receptors to the activated dendritic spine [139]. Early LTP is maintained by the persistent activation of CaMKII and PKC, and expression of the constitutively active PKMζ, which is necessary to maintain LTP at facilitated synapses [140]. The activity of these kinases together modify the synaptic cytoskeleton, and increase AMPA receptor exocytosis and lateral diffusion into existing post-synaptic scaffolds such as PSD95 [141]. The key difference between early LTP and late LTP is that late LTP requires activity-dependent gene expression and protein translation. Nascent synaptic proteins include cytoskeletal proteins to enlarge dendritic spines, glutamate receptors, and scaffold proteins for increased capacity to express surface receptors (**Fig 1.12**, *bottom right*) [139].

In summary, synaptic plasticity is crucial to cognitive functions such as learning and memory. Great progress has been made in clarifying some key molecular mechanisms of how the brain modulates synaptic connections between neurons, such as with LTP and LTD. Yet it is also clear that impaired synaptic plasticity leads to defects in synaptic function, to loss of neuronal connectivity and to neurodegeneration [142]. The ways in which the integrity of synaptic plasticity mechanisms deteriorate are less well known, but clues toward an accurate target of focus to address this may lie in evaluating reports on the molecular neuropathology of tissue from Alzheimer's Disease (AD) patients and from mouse models of AD [143-145]. Epidemiological studies suggest that synaptic loss is an early pathological manifestation of AD progression and correlates with cognitive decline in AD patients [146, 147]. Because the central AD protein tau is present in dysfunctional synapses of AD tissue, it is essential to better understand how physiological tau can become toxic, contribute to synaptic loss, and to processes of neurodegeneration [145].

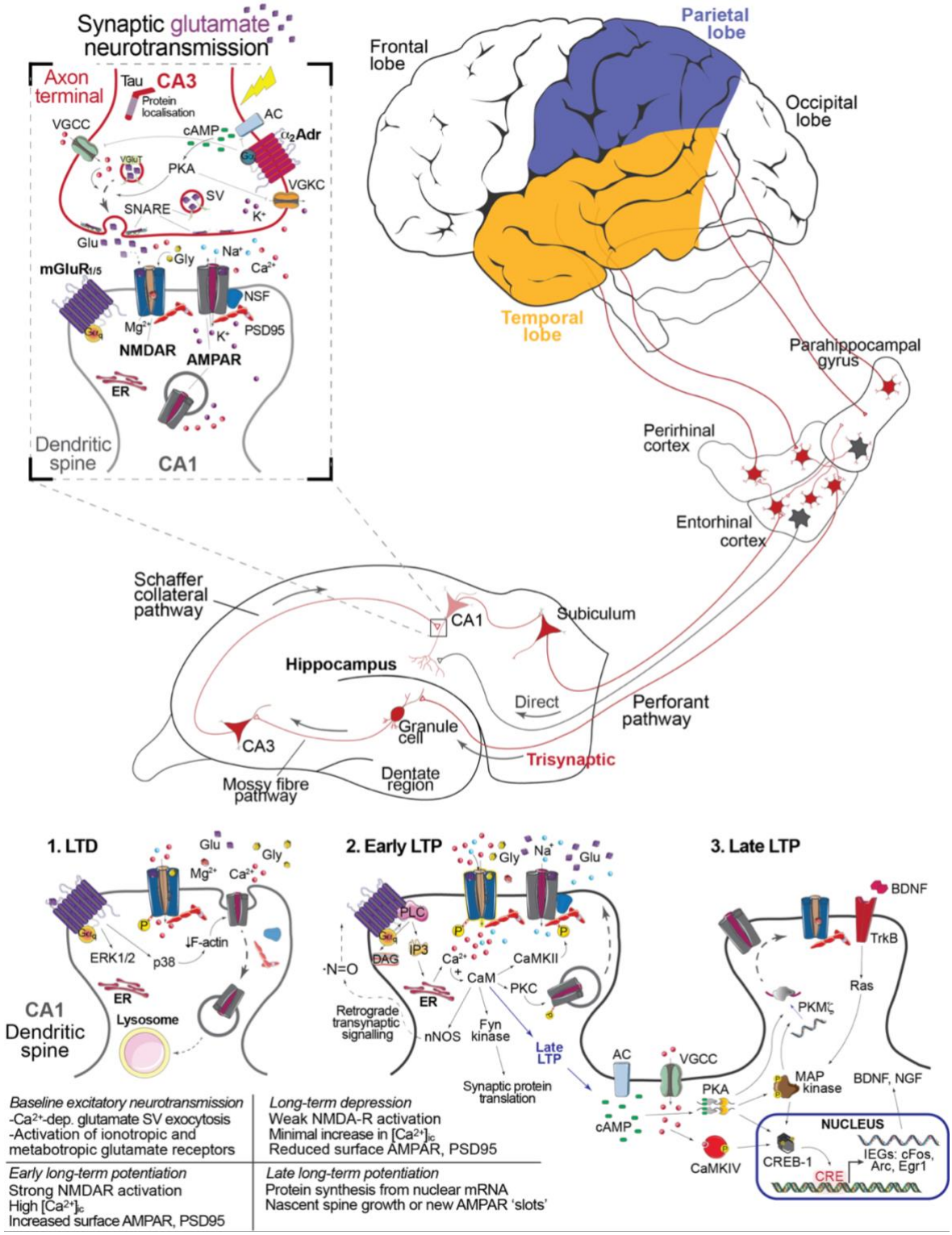

Figure 1.12. ***Long-term potentiation and depression in the hippocampal CA3-CA1 synapse***. Key events summary is shown on bottom left. *Top left*, Ca^{2+}-dependent vesicle fusion and neurotransmitter (NT) exocytosis from presynaptic CA3 axon terminal. Glutamate and glycine bind/activate ionotropic NMDA- and AMPA-receptors (-R). **1.** Activity-dependent LTD occurs when co-incident (membrane depolarisation + NT binding) detector NMDA-R opens but Ca^{2+} influx is low, activating phosphatases and receptor endocytosis. **2.** Activity-dependent early LTP if receptor activation is strong, to activate kinases for upregulated surface AMPA-R exocytosis and lateral diffusion trapping into scaffold PSD and stabilizer NSF. **3.** Late LTP – structural plasticity, (not synaptic P) shown for clarity. Protein synthesis-dependent event leading to increased baseline PSD scaffolds for AMPA-R docking. Synaptogenesis driven by expression of neurotrophin (Bdnf). [125, 126, 148]

Microtubule-binding protein tau: critical factor in healthy and disease brain

The known contribution of tau to the described synaptic processes of learning and memory is limited. The efforts described in the following two chapters attempt to broaden our understanding of the role of tau protein in synaptic plasticity by focusing on tau protein interactions. Well-documented tau functions include tau's role in neurodegenerative diseases. In healthy neurons, tau predominantly localises to axons [3] but is also present in synapses at lower levels [10]. Activity-dependent translocation of axonal tau to glutamatergic dendritic spines implicates tau in the regulation of physiological synaptic plasticity [149]. This synaptic relocalisation from the axon is disrupted by the presence of oligomeric amyloid beta (Aβ) [149]. Others have shown that hyperphosphorylated axonal tau has reduced tau-microtubule (MT) binding affinity, destabilising MTs and impairing axonal transport [150]. In AD patients, a high proportion of tau protein mislocalises to the postsynapse, which may be a direct consequence of this reduced MT-binding affinity [151]. High dendritic tau also leads to spastin-mediated destabilisation of MTs [152]. Furthermore, a causal link between accumulation of pathological tau and loss of synapses has been shown in AD mouse models, and a correlation between toxic tau and synaptic dysfunction observed in AD patients [145, 153, 154].

Synaptic impairment and loss are described as early changes in AD that directly involve tau [155], and this synaptic loss is accompanied by learning and memory deficits [147]. Somatodendritic redistribution of axonal tau is promoted by neurodegenerative disease and aberrant tau phosphorylation [151]. Limiting somatodendritic tau levels reduces memory impairments [10, 155], and interactions of tau with synaptic proteins are linked to this role of tau [8]. The interaction of pathologic tau with synaptogyrin-3 disrupts presynaptic function [156]. Presynaptic accumulating tau increases Ca^{2+} transients, temporarily increasing neurotransmitter release, then causing impairments in neurotransmitter exocytosis [157]. Dendritic spine infiltration of tau in post-synapses leads to reduced clustering of glutamate receptors (AMPA, NMDA), affecting transmission, and compromising memory performance [158, 159].

There may be a component of the axo-dendritic balance of tau that remains unclear. Loss of tau function, gain of toxic function, or mislocalisation may induce neurotoxicity or mediate Aβ-induced toxicity. Oligomeric Aβ inhibits activity-dependent movement of tau to the synapse, yet AD cases overwhelmingly report excessive tau in synapses. It could be activity-dependence that confers Aβ with an 'inhibitory' function. In the presence of Aβ, tau is thus pathogenic, independent of location.

The role of tau protein in memory is most often described in the context of neurodegenerative pathologies. While the neuropathological hallmarks of AD include extracellular Aβ plaques and intracellular neurofibrillary tau tangles, a whole subset of diseases called tauopathies are

characterised by intraneuronal depositions of aggregated tau, independent of Aβ. These include Frontotemporal Dementia (FTD), corticobasal degeneration, progressive supranuclear palsy, Pick disease, primary age-related tauopathy, and chronic traumatic encephalopathy (CTE) [160]. These tau depositions lead to cell death and to loss of functions associated with the affected brain regions. In many cases, these affected regions include the temporal lobe where hippocampal functions are compromised, and the ability to retrieve or store memories is lost [160]. It's uncertain whether some qualitative feature of memory or if some aspect of hippocampal neurophysiology, including tau functions, makes this region especially vulnerable to damage.

One attempt to address the possible effect of tau on hippocampal function is to modify levels of tau expression in mice and test memory performance. Yet characterisations of tau-deficient (*tau*$^{-/-}$) mouse phenotypes for attributing physiological roles to tau have been inconsistent. In some cases, *tau*$^{-/-}$ mice exhibited no behavioural deficits [161, 162]. This is likely due to compensatory adaptations by other microtubule-associated proteins (MAPs) during development [163]. One strategy to circumvent developmental compensations is to cross neuron specific inducible Cre transgenic mice with *Mapt*^{flox} mice. Another strategy is acute gene knock-down by AAV-mediated short hairpin RNA targeting the *Mapt* mRNA transcript. This was applied in HC of adult C57 wild-type mice and led to performance deficits in the MWM spatial memory paradigm, lower Bdnf levels, and reduced dendritic spine density [164]. Other reports involving *tau*$^{-/-}$ mice describe the presence of anxiety-related behaviours and/or impaired LTP and deficits in contextual/cued fear memory performance [165-167]. A selective deficit in LTD, necessary for clearing old memory representations, has also been seen in *tau*$^{-/-}$ mice; an effect replicated in HC slices by RNA interference of tau expression in the CA1 region [168]. In this case, phosphorylation of tau by GSK-3β was necessary for efficient NMDA receptor-mediated LTD [168]. Consistent with this report, through altered activity of PTEN, insulin-induced LTD was impaired in *tau*$^{-/-}$ mice [169]. Finally, HC dendrites of *tau*$^{-/-}$ mice were found to express fewer AMPA receptors under basal conditions, and showed impaired NMDA-induced or LTD-associated AMPA receptor internalisation [170, 171]. Taken together, the evidence suggests that physiological tau functions include molecular mechanisms that contribute to learning and memory, including both impaired LTP and LTD, but further investigations are needed – especially towards attempts at linking the extent of tau toxicity to impaired LTP, LTD, and to molecular hallmarks of neurodegeneration.

MAPT gene and physiological functions of tau

The MAPT gene encodes the microtubule-associated protein tau protein. It is located on human chromosome 17 and is comprised of 16 exons (**Fig 1.13**). While a large 758 amino acid (aa) length tau exists in the peripheral nervous system, expression in the mature brain includes six alternatively spliced isoforms [172, 173]. These six isoforms differ by amino-terminal inserts (0N/1N/2N),

determined by exclusion or inclusion of exons 2 and 3; and microtubule-binding domain (MTB) repeats (3R/4R), determined by exclusion or inclusion of exon 10 [172]. Between the projection domain and MTB repeats is a proline-rich region (PRR) with multiple phosphorylation sites. In mouse brain, the 0N isoforms mostly localise in the cell soma and axons, the 1N isoforms have the highest relative nuclear localisation, and the 2N isoforms predominate in axons, cell bodies, and to a lesser extend within dendrites, which may reflect differing functions between isoforms [174]. In the adult human brain, the proportion of 3R and 4R tau isoforms is approximately equal, but this changes in neurodegenerative diseases [175]. For instance, in FTD, splicing mutations in intron 10 result in overproduction of 4R tau isoforms, which are relatively more favourable hyperphosphorylation substrates that can lead to toxic gain of function and neurodegeneration [176]. Interestingly, mature mouse neurons do not express 3R tau isoforms, leading to an unusual phenomenon in DG and SVZ mouse brain regions of neurogenesis: the 3R tau isoform is (temporarily) present, but only in newly differentiated mouse brain neurons [177, 178].

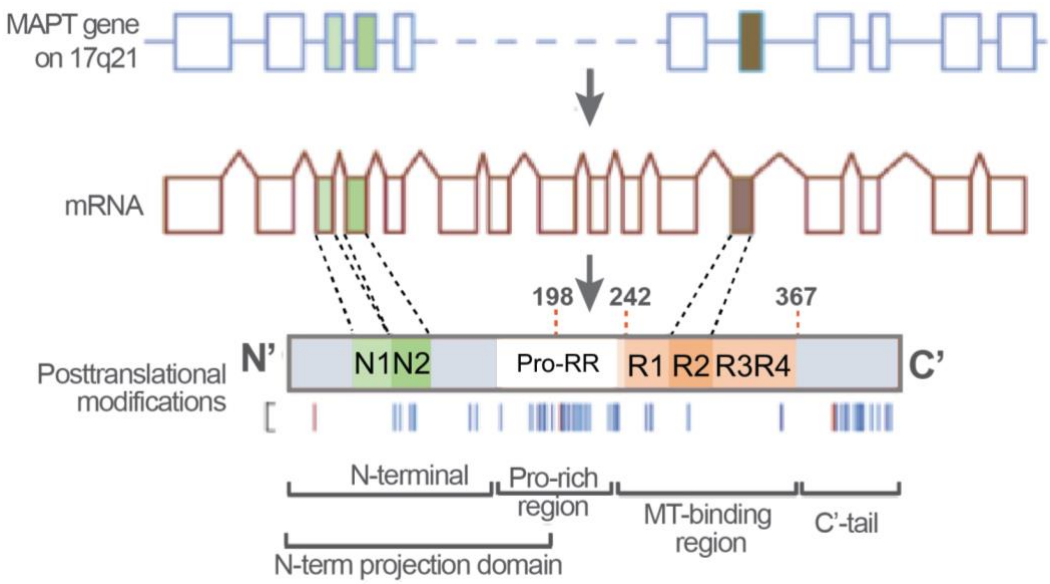

Figure 1.13. ***The MAPT gene, tau transcript, and tau protein***. Human *MAPT* gene (chromosome 17; 17q21.31). Sixteen exons encode 11 transcripts of RNA in the mature brain, and are alternatively spliced to create 6 isoforms. Projection domains of the N-terminal with 0N, 1N, or 2N acidic regions; C-terminal tails; sequences for a proline-rich region (Pro-RR; exons 5, 7, 9) that interact with SH3-domain containing proteins (Src-homology 3); microtubule binding repeat (MTB) domains (3R/4R). Isoforms vary from 352 to 441 amino acids in length (0N3R - 2N4R) [172]. *Adapted and modified from Ittner & Ittner (2018)* [151]

The N-terminal projection region interactions with synaptic vesicle associated proteins, either through direct PPIs or through membrane interactions [5, 8, 179]. This N-terminal region also interacts with membrane-associated annexin-2/5/6, that belong to a family of Ca^{2+}-regulated proteins involved in exocytosis and release of neurotransmitters [5, 6, 180], and with GSK-3β, the main tau kinase in mouse brain that is also associated with synaptic plasticity, memory, and AD pathology [181, 182]. The ~87aa length PRR contains 22 predicted phosphorylation sites (another 63 potential phospho-

sites exist in the remaining 354aa of full-length 441aa tau) [183]. This contributes to PRR as a module regulating signalling, with interactors including Src family non-receptor tyrosine kinase Fyn (PRR recognises SH3 domain of Fyn), phospholipase protein 2A, Pin1, and PKA [184]. Tau-tau interactions occur at the MTB region, and phosphorylation of residues within the MTB region reduces tau affinity for microtubules (MTs), influencing the extent of tau-tau interactions and by extension, possibly the formation of tau aggregates [184]. Finally, both N- and C-terminal regions participate in interactions to regulate the cytoskeleton and in regulation of axonal cargo transport by motor proteins when MTB regions interact with MTs [4, 184, 185]. Together the range of tau interactor functions support the idea that tau is not simply a MT-associated protein, but rather a multifunctional protein.

Tau predominately localises in axons and facilitates in the regulation of MT stability [186], a central cytoskeletal protein. These cylindrical protofilaments made of α-β tubulin heterodimers stack to form strong non-covalent interactions [187]. In relation to tau, MTs participate in maintaining the cytoskeleton, and thus, morphological integrity of the cell, as well as vesicle cargo transport throughout axons [188, 189]. Tau concentrations increase distally toward the terminal button, which promotes kinesin motor protein and cargo dissociation [4].

Multiple experimental approaches provide evidence for hydrophobic regions of tubulin monomers as binding targets for residues of tau amino acids in 3R or 4R regions [188, 190] (**Fig 1.14A**). The N-terminal projection domain of tau is believed to set the inter-MT distance and orientational uniformity of axonal tubulin polymers [191]. The presence of tau in axons increases proximo-distally with some presence also in dendritic spines (**Fig 1.14B**).

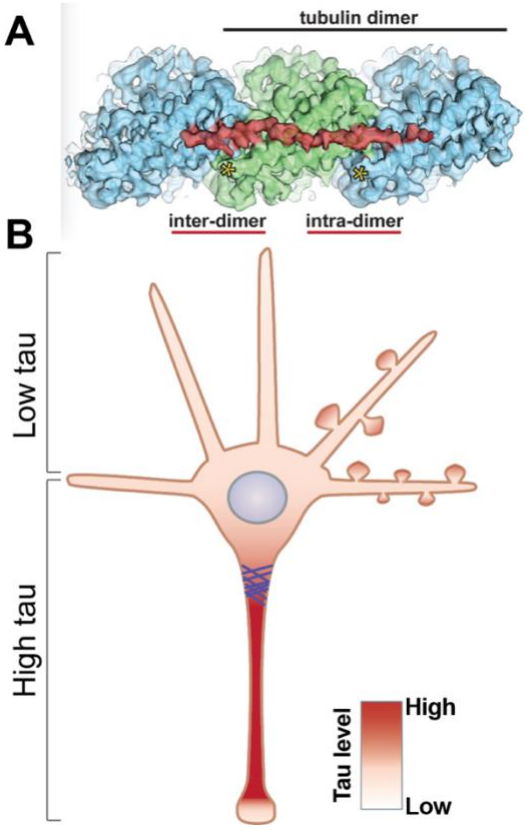

Figure 1.14. ***Tau binds microtubules***.

(**A**) Density map (cryo-EM, resolution 4.1 Å) displaying the 1R repeat of tau (in red) spanning across 3 monomers of tubulin from an MT (α-, green; β-, blue; C-term, * asterisks).

(**B**) Schematic displaying the subneuronal distribution of protein tau. Highest is in axon, then in dendritic spines.

Adapted from Kellogg et al (2018) [190] and Ittner & Ittner (2018) [151].

Tau localises predominately in the axon, with some in the post-synapse. There are small amounts in the soma and axon terminal. Axon initial segment (AIS) prevents retrograde movement of tau, increasing axon concentrations. The tau-MT interaction time is critical for regulating MT assembly and cargo transport. Monomers of tubulin bound to GTP associate with MTs during assembly, yet if GTP is dephosphorylated before GTP-bound tubulin monomers are being added [192-194], tubulin will dissociate from the assembling polymer. Using single molecule tracking, the tau-MT interaction time was calculated as ~40 msec [2] – balancing tubulin depolymerisation with non-interference of kinesin transport. Microtubules have been described as having two domains: a labile domain for MT assembly, and a stable domain identifiable from an excess of detyrosinated tubulin [195, 196]. With this ability to discriminate between regions, rat neuron cultures were *tau*-depleted and labile-to-stable mass was quantified to find loss in labile and increase in stable mass [197]. The authors concluded that tau may promote elongation rather than stability, which is inconsistent with the general description of tau as a MT stabiliser.

As tau functions continue to be disputed, its primary sequence is not. Tau is an intrinsically disordered protein (IDP) that shows no tendency for aggregation by itself [198, 199]. Over half of tau consists of just five amino acids (Gly, Pro, Lys, Thr, Ser). With comparatively more permissive regions for post-translational processing, IDP properties contrast those of globular proteins, particularly in functional regulation (more surface area access per time) and stability [200-202]. Proteins with such properties could be adaptive in the intracellular context – expressing proteins with IDP properties is desirable for

regulation of signalling pathways [203]. Furthermore, natively flexible protein interactors can fold onto/over binding partners [204]. The increased order increases specificity of binding but the entropic cost of folding is balanced by sacrificing affinity, and so interactions are on average weaker and more transient [205].

This chapter summarised general ideas surrounding learning and memory, the mechanisms that may underlie them, and tentatively introduced tau in the context of molecular mechanisms affecting memory in disease and non-disease states. In the next chapter, protein-protein interactions of tau are explored using an approach that notably identifies transient as well as stable interactions. The functional implications of these interactions are then explored further.

CHAPTER TWO

PROXIMITY-LABELLING IDENTIFIES TARGETS OF TAU IN GLUTAMATE RECEPTOR TRAFFICKING AND MEMORY FORMATION

This chapter is based entirely on the following publication:

Prikas E, Paric E, Asih PR, Stefanoska K, Stefen H, Fath T, Poljak A, & Ittner A. (2022). Tau target identification reveals NSF-dependent effects on AMPA receptor trafficking and memory formation. The EMBO Journal, 41(18). https://doi.org/10.15252/embj.2021110242.

See also **APPENDIX**

Author contributions:

Author	*Research design (%)*	*Data collection and analysis (%)*	*Writing and editing (%)*
Prikas, E	42	68	66
Paric, E	1	4	1
Asih, PR	1	3	1
Stefanoska, K	1	3	1
Stefen, H	1	1	1
Fath, T	1	1	1
Poljak, A	3	10	4
Ittner, A	50	10	25
Total	**100**	**100**	**100**

Introduction

The microtubule-associated protein tau is implicated in neurodegenerative disorders termed tauopathies, including Alzheimer's disease (AD), which are characterised by proteinaceous lesions due to aggregation and deposition of tau [206, 207]. Memory impairment is an early clinical feature of AD and correlates with synaptic impairment [208]. There are currently no effective treatments for the cognitive decline seen in AD and related dementias. Tau may contribute to AD-related cognitive deficits through gain-of-toxic functions or through loss of neuroprotective functions [151].

Molecular and morphological changes underlying learning and memory are described by synaptic plasticity – experience-dependent adaptations in synapse strength [141]. Synaptic plasticity has been studied in detail for hippocampal synapses, where changes in synaptic strength are governed by activation of N-methyl-D-aspartate receptors (NMDARs) and involve trafficking of AMPARs between synaptic and extra-synaptic regions of dendrites [209, 210]. Molecular processes controlling post-synaptic receptors, plasticity and learning are coordinated by protein-protein interactions (PPIs) [211].

In healthy neurons, tau predominantly localises to axons [3] but is also present in synapses, albeit at lower levels [10]. The way in which interactions of tau contribute to physiologic synaptic processes and healthy memory function remains unclear. Synaptic dysfunction and loss were described as early molecular and cellular changes in AD, preceding clinical onset of features by many years, and directly

involve tau [155]. Neurodegenerative disease and phosphorylation promote somatodendritic redistribution of axonal tau [151]. Limiting somatodendritic tau levels reduces memory impairments [10, 155], and interactions of tau with synaptic proteins are linked to this role of tau [8].

Despite a growing literature, the tau interactors currently known do not support a complete functional understanding of tau. In a physiologic state, verified tau interactor proteins include microtubules and annexins in the axon [6], vesicle-associated proteins such as synaptobrevin [8], postsynaptic proteins such as post-synaptic density protein-95 (PSD-95) [212], SynGAP [213] and filamentous actin in synapses [7]. A more complete tau interactome would provide insights into the role of tau in physiology. Traditional PPI affinity purification techniques are limited by reliance on affinity purification and protein complex stability after tissue lysis [5, 11]. In contrast, proximity labelling methods based on modified promiscuous BirA-related biotin ligases (BioID) covalently mark interacting proteins with biotin [214]. BioID labelling occurs in situ within living cells and tissue, avoiding tissue lysis or recovery of stable complexes or exposure to harsh chemicals, and additionally label transient PPIs [214]. Labelled proteins can then be identified by mass spectrometry (MS) and mapped into interactome networks [215]. BioID permits more complete charting of functional synaptic interactomes [216], localized protein networks [217] and entire signalling pathways [215, 218] through coverage of both stable and transient PPIs.

In this study, we mapped tau interactions using BioID, including cytoskeletal and novel interactions with synapse-associated proteins. We corroborate candidate tau interactor vesicular ATPase N-ethylmaleimide sensitive fusion protein (NSF), an enzyme essential for AMPA-type glutamate receptor (AMPAR) stabilisation by direct binding [219] and memory maintenance [220]. We show that tau regulates NSF activity and localization, linking tau with AMPAR surface expression and associative learning and memory. Thus, our study exemplifies how proximity labelling proteomics combined with targeted functional validation facilitates novel discovery. This delineates a physiologic role of tau mediated by the essential neuronal ATPase NSF.

Results

In vivo proximity labelling maps tau interactions in cultured neurons and mouse brain

To address tau interactions in primary neurons and mouse brain, we adapted proximity-dependent labelling with the optimized BirA enzyme BioID2 to biotinylate proteins interacting with tau [214]. Proximal proteins labelled by BioID2 fused to human tau (2N4R, 441 aa) were identified by mass spectrometry (MS) [215] (**Fig 2.1A**). Neuronal adeno-associated virus (AAV)-mediated expression of BioID2 fused to the N-terminus of tau (BioID2-tau) or background control BioID2 (BioID2), both with N-terminal myc tag, was driven by human Synapsin-1 minimal promoter and enhanced by a PHP.B capsid conferring neuronal tropism (**Fig 2.1B**).

To test expression and biotinylation by AAV-delivered BioID2-tau in isolated neurons, primary murine cortical neurons were transduced (DIV12) and treated with biotin-rich media (DIV19-20) (**Fig 2.1C**). Cells expressing soluble BioID2 served as control for non-specific biotinylation [215]. To visualise protein biotinylation and BioID transgene expression, neurons were labelled for tau and MYC tag with antibodies and for incorporated biotin with streptavidin. Signals for BioID2-tau and biotinylated protein overlapped in neurites of BioID2-tau-expressing cells (**Fig 2.1D**). Additional biotin incorporation non-congruent with tau was detected outside neurites, indicative of interactor biotinylation (**Fig 2.1D**). Perinuclear MYC signal in BioID2 control neurons overlayed with weak incorporation of biotin (**Fig 2.1D**). These results indicate subcellular locale-specific biotin incorporation with BioID2 fused to tau, partially overlapping with predominantly axonal localisation of tau in mature neurons [221].

We next identified putative interactors by mass spectrometry (MS). Tandem MS-MS from primary neurons identified 114 unique proteins from 544 biotin-labelled peptides, with 49 proteins exclusive to BioID2-tau (**Fig 2.1E**, **Appendix Tables 1**,**3**,**6**). Protein ontology (PO) analysis in BioID2-tau labelled proteins showed significant enrichment of synapse association and synaptic vesicle cycle, besides organelle and cytoskeletal organization (**Fig 2.1E**, **Appendix Table 4**). A non-redundant tau interactome was generated by comparing relative abundance of biotinylated proteins in BioID2-tau relative to control samples and mapped onto a network of novel and reported associations (PPI enrichment: $p = 3.33 \times 10^{-16}$; clustering coefficient = 0.510, average node degree = 3.35) (**Fig 2.1F**). Apart from clusters of microtubule-binding proteins, neuronal tau interactome was enriched for synapse associations and factors involved in synaptic vesicle cycle (**Fig 2.1G**). These results show that BioID2 can map tau interactomes in living neurons for discovery of novel functional associations.

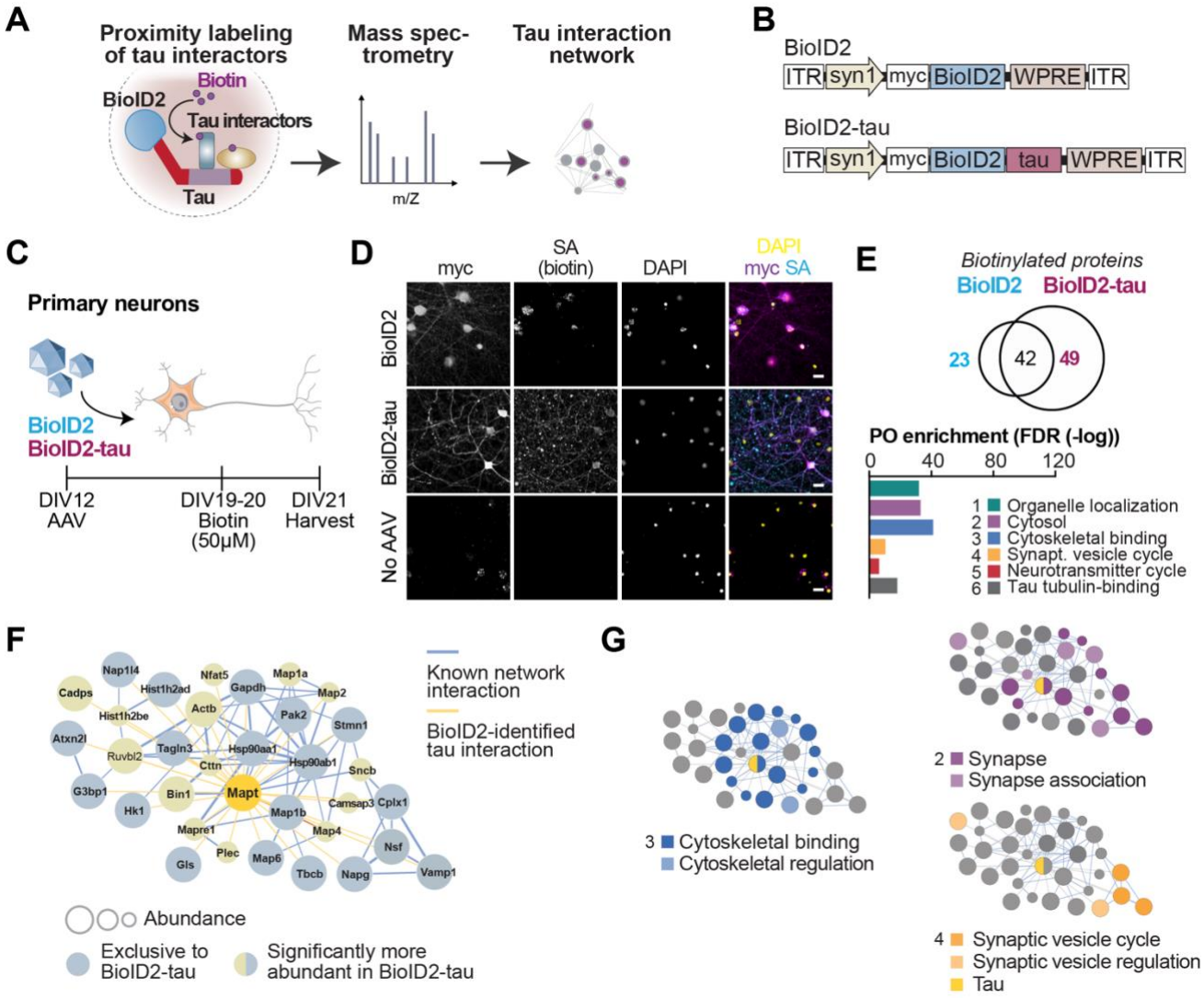

Figure 2.1. ***Novel associations of microtubule-associated protein tau with synaptic vesicle cycle in proximity labelled interactomes*.**

(**A**) Principle of proximity ligation catalysed by promiscuous biotin ligase BioID2 fused with human tau (441aa) (BioID2-tau) to map protein-protein interactions. Biotin supplementation enhances target biotinylation in BioID2-tau-expressing neurons. Labelled proteins are identified by LC-MS/MS after enrichment of biotinylated peptides.

(**B**) Adeno-associated virus (AAV) constructs for neuron-specific expression of BioID2-tau or BioID2 control. Syn-1, synapsin-1 minimal promoter; WPRE, Woodchuck Hepatitis Virus Posttranscriptional Regulatory Element

(**C**) Schematic of primary neuron transduction with AAVs expressing BioID2-tau or BioID2 control at day 12 in vitro (DIV12) followed by biotin-enriched media treatment (DIV19-20) and cell harvesting for proteomic analysis (DIV21).

(**D**) Immunofluorescence of neurons expressing BioID2-tau or BioID2 (myc) or non-transduced control cells. Cells were incubated in biotin medium (50 µM) or vehicle medium for 30 h prior to fixation and probed for biotin (streptavidin, SA) and cell nuclei (DAPI) (n = 3 biological replicates). BioID2-tau and incorporated biotin co-localise in axons and somata. Scale bar, 25 µm.

(**E**) Venn diagram of overlapping and unique interacting proteins identified by biotinylation in cultured cortical mouse neurons (DIV21) (n = 3 biological replicates). Protein ontology (PO) categories are: 1 biological processes, 2 cell component, 3 molecular function, 4 Kyoto encyclopaedia of genes and genomes (KEGG) pathway, 5 Reactome pathway, 6 PFAM protein domain. Note most enriched functional annotation clusters: 3 cytoskeletal binding and 4 synaptic vesicle cycle. FDR, false discovery rate

(**F**) Tau interactome network generated by BioID2 in cultured neurons (DIV21) (n = 3 biological replicates). Network of significantly abundant and exclusive interactors in BioID2-tau with network properties and PPI enrichment score (STRING v11.5).

(**G**) Functional ontology clusters for molecular function: cytoskeletal binding, cell component: synapse and KEGG: synaptic vesicle cycle mapped onto neuronal tau interactome network in (F). Additional associations with synaptic localization/function and synaptic vesicle regulation described in literature are mapped, respectively.

Having generated proof-of-principle interactomes for tau in isolated neurons, we next turned to identifying interactomes in neurons integrated in functional brain circuitry. We labelled intraneuronal tau interactions in mouse forebrain neurons by delivery of BioID2-tau at postnatal day 0 (P0), followed by biotin supplementation (P28-P35) (**Fig 2.2A**) as for previous brain BioID [216]. Immunoblot of brain lysates and histology confirmed comparable expression of BioID2-tau and BioID2 as well as biotin incorporation (**Fig 2.2B**). Tissue from non-injected biotin-treated controls was negative for both MYC and biotin incorporation (**Fig 2.2B-C, Appendix Fig S1**). Biotinylated peptide analysis and protein identification yielded 137 unique proteins from 935 biotinylated peptides (**Appendix Tables 1**,**3**,**7**). Notably, among biotinylated peptides from BioID2-tau samples were high-confidence peptides specific to murine tau (**Appendix Table 2**), suggesting reoccurring spatial proximity of bait tau and endogenous tau in mouse brain. Unique BioID2-tau proteins were functionally enriched for cytoskeletal/microtubule association, synapse localization, and synaptic vesicle cycle (**Fig 2.2D**, **Appendix Table 4**). Fifty-nine proteins exclusive to BioID2-tau were mapped onto a tau interactome (PPI enrichment: $p < 10^{-16}$; clustering coefficient = 0.51, average node degree = 5.83) (**Fig 2.2E**), which showed prominent node clusters for synaptic proteins and factors of synaptic vesicle cycle (**Fig 2.2F**).

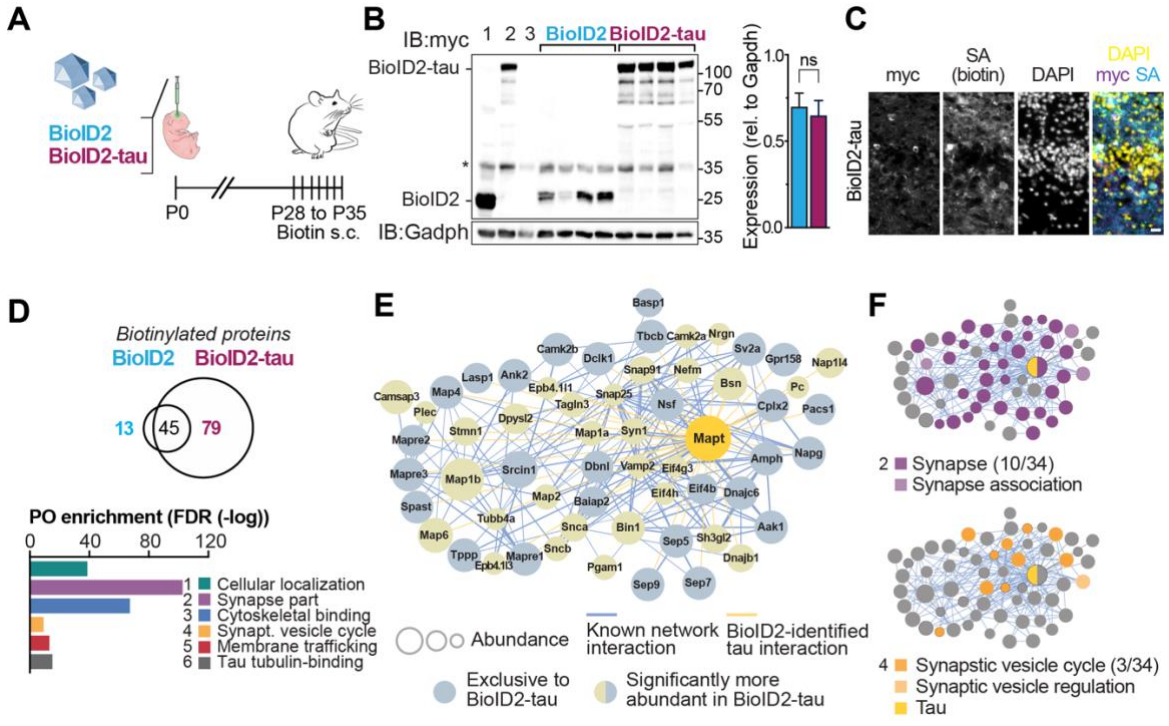

Figure 2.2. ***Proximity labelling links tau with synaptic vesicle regulation in mouse brain in vivo***

(**A**) Experimental schematic of post-natal interactome labelling of neuronal tau in vivo.

(**B**) Immunoblot of combined brain lysates from mice (P35) expressing BioID2-tau or BioID2 control (n = 4 biological replicates) probed for myc-tagged BioID2 and BioID2-tau. Controls: lysates from (1) BioID2- or (2) BioID2-tau-expressing and (3) non-transduced mouse brain. Loading, glyceraldehyde-3-phosphate dehydrogenase (Gapdh). *, unspecific band. Relative quantification confirmed similar expression levels of BioID2 and BioID2-tau. Means ± S.E.M. ns, not significant (Student's t-test)

(**C**) Immunofluorescence of P35 mouse brain expressing BioID2-tau. Hippocampal Cornu ammonis 1 (CA1) region was probed for BioID2-tau (myc), for incorporated biotin (streptavidin, SA) and for cell nuclei (DAPI) (n = 3-5 biological replicates). Scale bar, 50 µm.

(**D**) Tau interactome in mouse brain (P35) transduced at P0 to express BioID2-tau or BioID2 control (n = 12 biological replicates). Venn diagram shows overlapping and unique interacting proteins identified by biotinylation. Protein ontology (PO) enrichment (false discovery rate (FDR)) for highest ranking categories in 1 biological processes, 2 cell component, 3 molecular function, 4 KEGG pathway, 5 Reactome pathway, 6 PFAM protein domain are shown. Note most enriched functional annotation clusters: 2 synapse, 3 cytoskeletal binding, and 4 regulation of vesicle cycle.

(**E**) Tau interactome network generated by BioID2 in mouse brain (P35) (n = 12 biological replicates). Network of significantly abundant and exclusive interactors in BioID2-tau with network properties and PPI enrichment score (STRING v11.5).

(**F**) Functional ontology clusters mapped onto neuronal tau interactome network in (E) for cell component: synapse and for KEGG: synaptic vesicle cycle. Additional associations with synaptic localization/function and synaptic vesicle regulation described in literature are mapped, respectively.

Episomally expressed BioID2-tau may compete with endogenous tau for binding sites on interacting proteins in tau-competent (*tau*$^{+/+}$) mice [221]. To eliminate tau binding competition as done in previous tau expression studies [222, 223], we expressed BioID2-tau or BioID2 in the hippocampus of *tau*$^{-/-}$ mice (**SM Fig 2.1A-B**). BioID MS yielded 371 unique proteins from 2479 total biotinylated peptides (**SM Fig 2.1C**, **Appendix Tables 1**,**3**,**8**), resulting in a tau interactome of 93 non-redundant proteins with enrichment in neurite cytoskeletal binding, endocytosis, and synaptic vesicle association (**SM Fig 2.1C-E**, **Appendix Table 4**).

Tau interactors map onto pathways of synaptic vesicle cycling and postsynaptic receptor trafficking

To gain further insights into the functional tau interactome, we compared protein identities in the three networks (**Appendix Tables 3**,**5**) derived from proximity labelling with BioID2 tau in cultured neurons and brains of *tau*$^{+/+}$ (P35) and *tau*$^{-/-}$ (adult) mice (**Fig 2.3A**) and analysed combined enrichment in protein ontology (PO) terms (**Fig 2.3B**). From a total of 260 unique biotinylated proteins, 50 (19.2%) were common in all three systems and 99 (38%) were in at least two data sets (**Fig 2.3A**, **Appendix Table 3**). Thus, a significant proportion of neuronal tau interactors were consistently labelled by BioID2, independent of tissue-, age- and/or presence of endogenous tau. A total of 72 of 260 (28%) biotinylated proteins were previously reported to colocalise and/or interact with tau (**Appendix Table 5**), confirming the capacity of BioID2 to label bona fide interaction partners of tau [222, 224]. PO

enrichment mapped onto a network in strongly interconnected clusters of cytoskeletal binding, synapse association, and synaptic vesicle cycle (**Fig 2.3C**; **Appendix Fig S2, Table 4**). Enrichment of cytoskeletal protein binding and synaptic protein binding is consistent with established cytoskeletal and synaptic roles of tau [151, 225]. To identify disease associations among BioID2-labelled tau interaction, we mapped known disease association enrichment onto the network. Significantly enriched Parkinson's and Alzheimer's disease associations mapped across the network (**Fig 2.3B**). Other disease associations significantly overrepresented were prion disease and ALS (**Fig 2.3B**). This shows that physiologic tau interactomes disproportionately include factors involved in neurological disorders. Taken together, our BioID2 approach mapped an extensive tau interactome in living neurons that can be mined for discovery approaches of physiologic and pathologic tau mechanisms.

The combined interactome network from all three BioID2 expression systems was highly enriched for known interactions between nodes ($p < 10^{-16}$; clustering coefficient = 0.40, average node degree = 11.90) (**Fig 2.3C**). Independent of the expression system, tau candidate interactors included synaptic and vesicle-associated proteins as network hubs (**Appendix Fig S2**, **Table 4**). They included complexins, SNARE proteins Vamp1/2, Snap25, and synapsin-1, and N-ethylmaleimide sensitive fusion protein (NSF), which controls SNARE complex disassembly, vesicle cycle, and AMPAR stabilisation [219, 226]. To further highlight functional implication and proximity of candidate proteins to critical neuronal processes, we mapped tau interactions identified by BioID2 in all neuronal expression systems onto 3 main molecular pathways and processes enriched: (1) synaptic vesicle cycle (partially pertaining to both pre- and post-synaptic vesicles) (**Fig 2.3D**), organization of actin and microtubule cytoskeleton (**SM Fig 2.2A**-**B**), and post-synaptic receptor trafficking (**Fig 2.3E**). Thus, besides factors of cytoskeletal complexes and regulation, proteins involved in vesicular cycling, SNARE function, and AMPAR trafficking are integral to the neuronal tau interactome.

Direct protein-protein interaction of tau regulates the activity of vesicular ATPase NSF

To confirm a functional interaction of tau with vesicle trafficking, we focused on the putative interaction of tau with the exocytosis ATPase NSF, which was labelled in all three BioID2 tau interactomes (**Appendix Table 3**) and is a central component of synaptic processes (**Fig 2.3D**-**E**). Neuronal NSF is a synaptic ATPase associated with vesicle cycling and plasticity [227]. Interactome protein ontology (**Appendix Table 4**) and ex vivo interaction screens showed tau interacts with NSF-associated synaptic proteins [5, 11]. Yet, a direct and functional tau-NSF interaction has not been established.

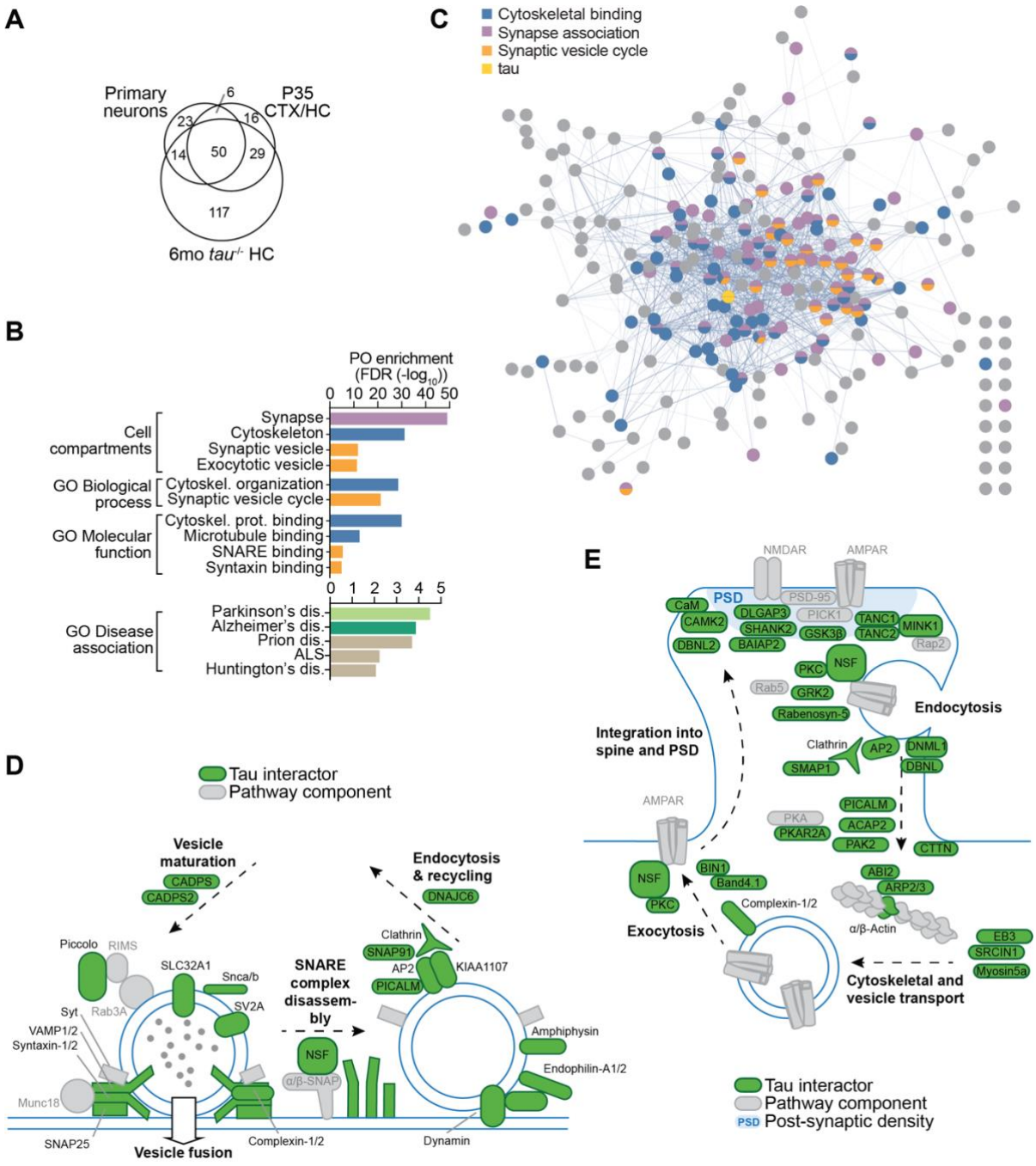

Figure 2.3. ***Neuronal tau interactome maps onto processes of cytoskeletal, synaptic vesicle, and post-synaptic regulation***.

(**A**) Venn diagram showing overlap and unique associations with tau in proximity labelled tau interactomes in 3 neuronal expression systems (primary murine neurons, P35 mouse cortex and hippocampus (P35 CTX/HC), and adult *tau*$^{-/-}$ hippocampus (6mo *tau*$^{-/-}$ HC).

(**B**) Selected highly significant GO term enrichment in combined proximity labelled tau interactomes in three neuronal expression systems. FDR, false discovery rate. Appendix Table 4 presents complete GO enrichment.

(**C**) Annotated interactome Network with mapped enrichment clusters for cytoskeletal regulation (FDR 1.5×10^{-22}), synapse association (FDR 8.12×10^{-48}), and synaptic vesicle cycle (FDR 1.25×10^{-21}). Tau is highlighted at the centre of the network.

(**D**, **E**) BioID2-identified tau interactors mapped onto process of (D) synaptic vesicle cycle and (E) post-synaptic receptor trafficking with a focus on AMPA receptor regulation. Additional key process/pathway components are included (grey).

To confirm the association between NSF and tau, subcellular localization of both endogenous NSF and tau was determined in cultured neurons by immunofluorescence confocal imaging. Imaging suggested partial signal overlap in somatic regions (**Fig 2.4A**) and in dendrite branches (**Fig 2.4Ai-iii**). NSF co-immunoprecipitated with tau (2N4R, 441 aa) from 293T cells (**SM Fig 2.3A**). Immunoprecipitated tau readily co-purified with transfected and endogenous (FLAG-)NSF (**SM Fig 2.3A**). Glutamate substitution of Threonine-205 (T205) – mimicking phosphorylation at T205, which we previously showed to inhibit interactions of tau [223] – did not affect the tau-NSF complex (**SM Fig 2.3A**). Tau readily co-purified with immunoprecipitated NSF from 293T cells (**SM Fig 2.3B**). Finally, NSF immunoprecipitated in a complex with tau from cortical lysates of ALZ17 mice expressing human tau (**Fig 2.4B-C**). To determine specific binding regions within tau, we generated various truncation and deletion variants of tau (**Fig 2.4D**). However, neither deletion of tau N-terminal, proline-rich region, C-terminal region, or deletion of microtubule-binding repeats reduced interaction with NSF (**Fig 2.4E**). Acknowledging this, absent from the variants was a truncation at both N-/C-terminals. Taken together, these results corroborate a complex of tau with exocytosis ATPase NSF in primary neurons, heterologous cells, and brain tissue, and indicate a potential multi-region binding mode.

To address whether tau-NSF interaction was direct, we isolated recombinant tau and NSF (**Appendix Fig S3A-C**) and measured complex affinity by microscale thermophoresis (MST), which determines dissociation constants (K_D) in solution [228]. Thermophoretic measurements confirmed a direct interaction (K_D = 146 $\pm$ 70 nM) (**Fig 2.4F**, **SM Fig 2.3C-D**), which is below antibody-tau interactions, yet stronger than reported tau-microtubule binding ($K_D \approx$ 1100 nM) [229]. To confirm specific binding, we performed MST with NSF and either heat-treated tau, albumin, or catalase, none of which facilitated binding (**Appendix Fig S3D-F**). Notably, purification, reassembly, and MST conditions were chosen to maintain NSF in its quaternary structure (see **Methods**) [226], indicating that tau binds the functional native ATPase hexamer directly.

We next investigated functional aspects of a direct tau-NSF interaction. The NSF homohexamer is toroidal with a central pore [226] and uses energy from ATP hydrolysis to minimise GluA2 endocytosis [219] and to drive cis-SNARE complex disassembly following vesicle-membrane fusion [226]. We measured NSF ATPase activity in the presence of tau under conditions that facilitate NSF activity and function. ATPase activity of NSF alone was similar to NSF with addition of a control peptide (TAT-Scramble) (**Fig 2.4G-H**, **SM Fig 2.3C-D**), consistent with previous reports [230]. Co-incubation with TAT-NSF, a NSF-inhibiting peptide [231], markedly reduced ATPase activity by ~35%. Notably, increasing concentrations of recombinant tau (8/16/24 nM) led to rate reductions by ~30-65% (**Fig 2.4G-H**, **SM Fig 2.3C-D**). These results show tau specific inhibition of NSF ATPase activity in a concentration-dependent manner. To confirm ATPase inhibition by tau was not attributable to protein crowding effects, NSF was incubated with heat-treated tau, albumin, or catalase without notable

ATPase activity changes (**Fig 2.4G-H**, **SM Fig 2.3C-F**, **Appendix Fig S4**). We generated recombinant tau variants analogous to variants used in co-immunoprecipitation (*see* **Fig 2.4D**) and tested their effect on NSF activity in vitro. While full-length tau significantly inhibited NSF, none of the deletion or truncation variants did (**SM Fig 2.3G**-**H**), despite the immunoprecipitation experiment showing that these tau variants all bind NSF (**Fig 2.4D**). This indicates that multiple regions of tau may bind NSF and contribute to the inhibitory effect of tau on NSF activity.

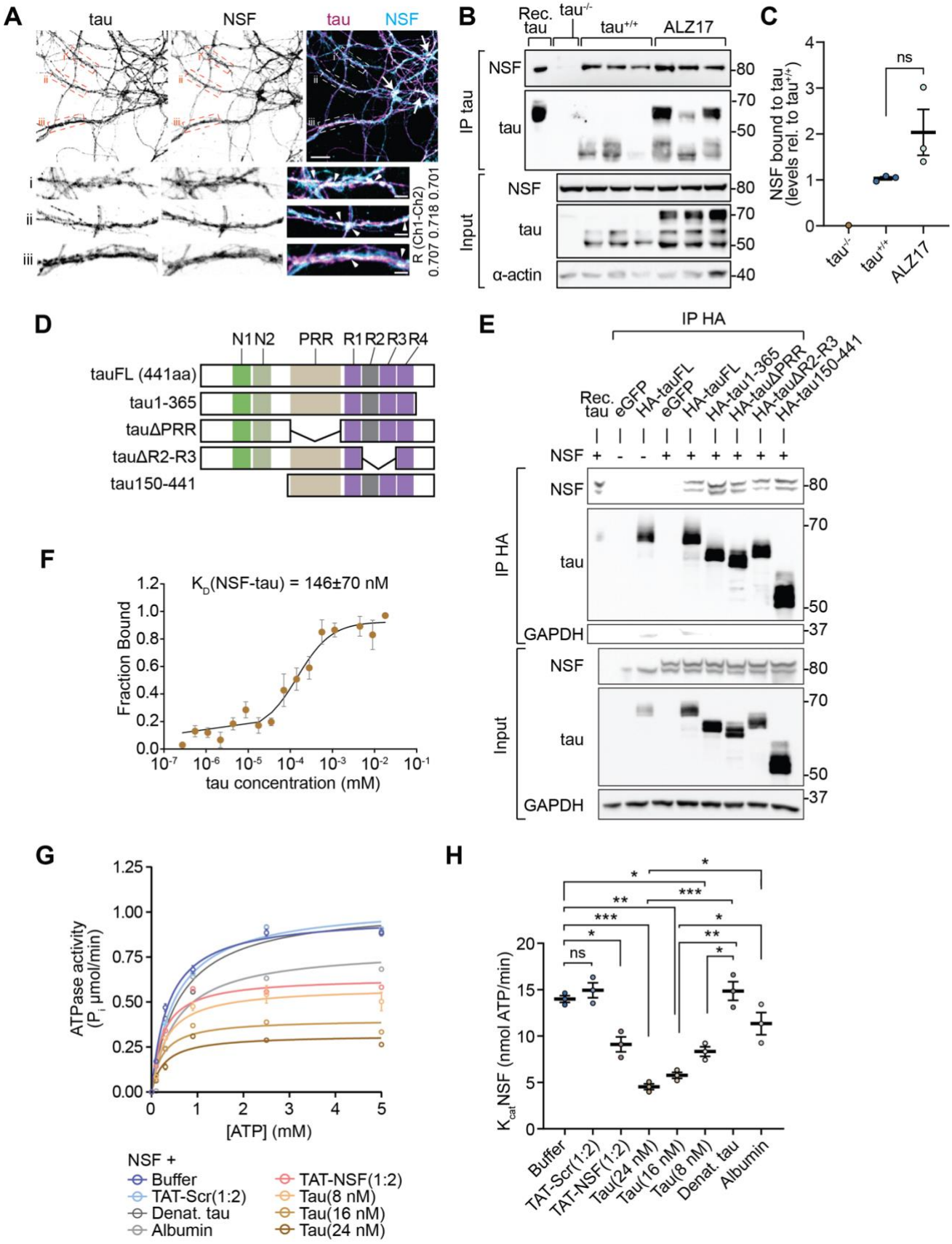
A
tau
NSF
tau
NSF
i
ii
iii
R (Ch1-Ch2)
0.707 0.718 0.701
B
Rec. tau
tau-/-
tau+/+
ALZ17
IP tau
NSF
tau
Input
NSF
tau
α-actin
80
70
50
80
70
50
40
C
NSF bound to tau
(levels rel. to tau+/+)
ns
tau-/-
tau+/+
ALZ17
D
N1 N2
PRR
R1 R2 R3 R4
tauFL (441aa)
tau1-365
tauΔPRR
tauΔR2-R3
tau150-441
E
IP HA
Rec. tau
eGFP
HA-tauFL
eGFP
HA-tauFL
HA-tau1-365
HA-tauΔPRR
HA-tauΔR2-R3
HA-tau150-441
NSF + - - + + + + + +
IP HA
NSF
tau
GAPDH
Input
NSF
tau
GAPDH
80
70
50
37
80
70
50
37
F
KD(NSF-tau) = 146±70 nM
Fraction Bound
tau concentration (mM)
G
ATPase activity
(Pi µmol/min)
[ATP] (mM)
NSF +
Buffer
TAT-Scr(1:2)
Denat. tau
Albumin
TAT-NSF(1:2)
Tau(8 nM)
Tau(16 nM)
Tau(24 nM)
H
Kcat NSF (nmol ATP/min)
ns
Buffer
TAT-Scr(1:2)
TAT-NSF(1:2)
Tau(24 nM)
Tau(16 nM)
Tau(8 nM)
Denat. tau
Albumin

Figure 2.4. ***Direct interaction with tau regulates activity of essential synaptic vesicular ATPase NSF***.

(**A**) Confocal immunofluorescence for endogenous tau and NSF in primary murine hippocampal neurons (DIV15). Colocalization of tau and NSF is apparent in perinuclear compartments (arrows) and neurites (insets i-iii). Scale bar, 25 µm. Inset of magnified neurite with partial overlap of tau and NSF signals (arrowheads). Scale bar, 3 µm. Co-distribution (R Ch1-Ch2) are indicated.

(**B-C**) Co-immunoprecipitation (Co-IP) of tau and NSF from mouse brain. (**B**) Endogenous and transgenic tau were immunoprecipitated from mouse brain lysates of $tau^{-/-}$, ALZ17tg or ALZ17non-tg mice using anti-tau antibody followed by immunoblot probed for NSF, tau and α-actin. Endogenous NSF was co-immunoprecipitated with transgenic and endogenous tau from ALZ17tg or ALZ17non-tg but not from tau-/- with. GAPDH, input loading control (n = 3 biological replicates). Recombinant tau and NSF served as controls. (**C**) Densitometric quantification of co-IP results in (B).

(**D-E**) Co-IP of HA-tagged tau with NSF from 293T cells. (**D**) Schematic of tau deletion and truncation constructs used for expression in 293T cells. (**E**) Co-IP of NSF with haemagglutinin (HA)-tagged truncated tau variants from cultured cells. HA-tagged tau variants and NSF were expressed in 293T cells followed by immunoprecipitation using HA antibody and immunoblot probed for NSF, tau and GAPDH. (n = 3 biological replicates).

(**F**) Microscale thermophoretic (MST) measurement of direct tau and NSF interaction. MST binding curve of recombinant hexameric NT-647-NHS-labelled NSF (27 pM) and recombinant tau (18 mM – 0.275 nM). Dissociation constant: $K_D = 146 \pm 70$ nM (sigmoidal curve fit, $R^2 = 0.844$). (n = 5 technical replicates).

(**G**) Inhibition of NSF ATPase activity with increasing concentrations of tau. NSF activity (70 nM) was assessed alone or in the presence of NSF-inhibiting peptide TAT-NSF or control TAT-Scramble peptides (140 nM); or co-incubated with recombinant tau protein (8 nM, 16 nM, 24 nM), or heat-denatured tau (dTau, 8 nM) or albumin (Alb, 16 nM). Data were fitted to Michaelis-Menten model to determine rate constants ($R^2 = 0.904$ - 0.994 for all conditions; n = 3 technical replicates).

(**H**) Rate constants derived from kinetic data in i. (n = 3 technical replicates) ATP hydrolysis is similar in NSF and NSF incubated with control peptide TAT-Scr, albumin, or denatured tau, yet lower with increasing concentrations of tau or after addition of NSF-inhibiting peptide TAT-NSF.

Data information: Values are means ± S.E.M (normalized to control). Adjusted p-values: ***p < 0.001, **p < 0.01, *p < 0.05, ns, not significant, ANOVA with Sidak's test.

Tau regulates the subcellular distribution of NSF and GluA1-containing AMPA receptors

NSF ATPase activity dissociates Protein interacting with C kinase-1 (PICK1) from AMPAR, stabilising membrane-bound receptors upon NMDA receptor (NMDAR) activation [141]. Thus, tau may affect AMPAR surface expression through inhibition of NSF. To interrogate AMPAR surface expression in the absence of tau, we determined levels of whole-cell surface GluA1 AMPAR by surface biotinylation in $tau^{+/+}$ and $tau^{-/-}$ neurons. To modulate surface GluA1 levels in dependence of neuronal activation and NMDAR signalling [209], neurons were incubated with MK801, a blocker of NMDAR calcium influx [232], and/or bicuculline (Bic), which reduces $GABA_A$-dependent hyperpolarisation and hence elevates baseline network excitation [233]. $Tau^{-/-}$ neurons showed significantly lower surface GluA1 levels in control, Bic- and MK801 + Bic treatment conditions compared with $tau^{+/+}$ cells (**Fig 2.5A**, **SM Fig 2.4A**). Surface GluA1 was comparable between $tau^{+/+}$ and $tau^{-/-}$ neurons when treated with MK801 (**Fig 2.5B, SM Fig 4B-C**), suggesting that NMDAR signalling is required for tau-dependent effects on whole-culture surface GluA1 AMPAR.

Subcellular localization of tau primarily to axons [151, 221] and to dendritic neurites [10] implies locale-specific regulation of NSF by tau. To address effects of tau on subcellular NSF localization and surface AMPAR, we confirmed tau expression status in hippocampal *tau*$^{+/+}$ and *tau*$^{-/-}$ neurons and then analysed NSF localization and surface GluA1 intensity in neurites of by confocal microscopy (**Fig 2.5C, SM Fig 2.4D**-**E**). Consistent with previous findings in cortical neurons [234], Bic-stimulation, chemically simulating neuronal excitation, in *tau*$^{+/+}$ and *tau*$^{-/-}$ neurons reduced neurite surface GluA1 expression (**SM Fig 2.4F**). Neurite NSF in *tau*$^{-/-}$ + Bic neurons was ~14% higher than in *tau*$^{+/+}$ + Bic (**SM Fig 2.4G**); whereas ~14% lower NSF was apparent in untreated *tau*$^{-/-}$ compared with *tau*$^{+/+}$ (**SM Fig 2.4G**). These results suggest that tau-deficiency in neurons results in neuritic accumulation of NSF upon neuronal activation.

We next addressed neurite surface GluA1 AMPARs under these conditions. To control for baseline NMDAR-dependent changes in surface GluA1, neurons were treated with MK801 [232] or vehicle, then neurite intensities of NSF and surface GluA1 were determined (**Fig 2.5C-E**). Consistent with MK801-induced lowering of neurite GluA1 levels [232, 235], neurite surface GluA1 was lower in all MK801-treated neurons compared to controls (**Fig 2.5C-D**). *Tau*$^{-/-}$ + MK801 surface GluA1 was ~28% lower than *tau*$^{+/+}$ + MK801 (**Fig 2.5C-D**). Control untreated *tau*$^{-/-}$ had ~14% lower neurite NSF than *tau*$^{+/+}$, and *tau*$^{-/-}$ + MK801 neurite NSF was ~13% lower than in *tau*$^{+/+}$ + MK801 (**Fig 2.5C**-**E**). To control for differentiation effects of *tau*$^{-/-}$ neurons upon isolation and plating, we expressed human tau (441 amino acid) in *tau*$^{-/-}$ neurons using AAV (**Figs 2.5C-E**, **SM Fig 2.4D**). Surface GluA1 of *tau*$^{-/-}$ + AAV^{tau} neurites was ~32% higher than of *tau*$^{-/-}$ (**Fig 2.5D**), resembling levels in *tau*$^{+/+}$ neurites. Thus, tau is required for maintaining neurite localization of NSF and surface GluA1 under NMDAR block. Taken together, the results support a functional tau-NSF interaction controlling activity and localization of NSF and AMPAR surface expression.

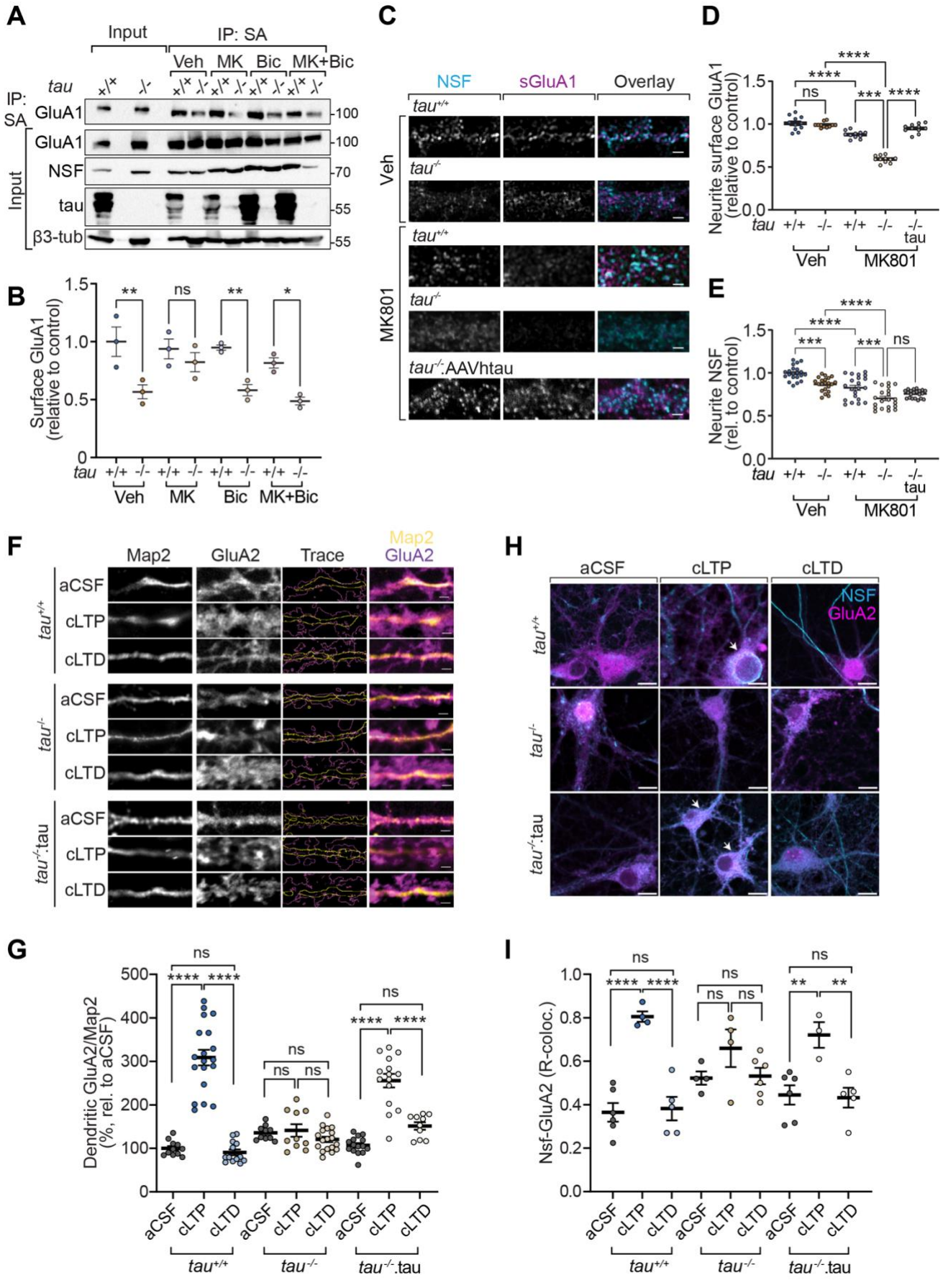
A
Input
IP: SA
Veh
MK
Bic
MK+Bic
tau
IP: SA
GluA1
Input
GluA1
NSF
tau
β3-tub
100
100
70
55
55
B
Surface GluA1 (relative to control)
tau
Veh
MK
Bic
MK+Bic
C
NSF
sGluA1
Overlay
Veh
MK801
tau+/+
tau-/-
tau-/-:AAVhtau
D
Neurite surface GluA1 (relative to control)
Veh
MK801
E
Neurite NSF (rel. to control)
F
Map2
GluA2
Trace
Map2 GluA2
aCSF
cLTP
cLTD
tau+/+
tau-/-
tau-/-:tau
G
Dendritic GluA2/Map2 (%, rel. to aCSF)
tau+/+
tau-/-
tau-/-.tau
H
aCSF
cLTP
cLTD
NSF GluA2
I
Nsf-GluA2 (R-coloc.)

Figure 2.5. ***Tau regulates NSF localization and GluA2 trafficking in chemically induced plasticity***.

(**A**) Impaired AMPA-type glutamate receptor surface expression in cultured *tau*$^{-/-}$ neurons. Cortical *tau*$^{+/+}$ or *tau*$^{-/-}$ neurons were surface biotinylated after incubation with non-competitive NMDAR antagonist MK-801 (50 µM, 3 min) and/or $GABA_AR$ antagonist bicuculline (30 µM, 10 min) at 37°C. Surface GluA1 levels were detected by immunoblot after with streptavidin (SA) enrichment. Input was probed for total cellular GluA1, NSF, tau and βIII-tubulin. (n = 3 biological replicates) Input and SA-enrichment from non-surface biotinylated neurons served as negative controls.

(**B**) Reduced neuronal surface GluA1 in *tau*$^{-/-}$ neurons. Quantification of *tau*$^{+/+}$ and *tau*$^{-/-}$ surface GluA1 upon treatment and SA-enrichment shown in (A).

(**C**) Cell surface GluA1 and total NSF immunostaining in primary mouse hippocampal neurons (DIV15). *Tau*$^{+/+}$, *tau*$^{-/-}$ neurons and *tau*$^{-/-}$ expressing human tau (*tau*$^{-/-}$.AAV^{tau}) were treated with either vehicle (Veh; DMSO) or MK-801 (50 µM) for 3 min. Representative confocal images of whole cell (left) and neurites (right) are shown (n = 3 biological replicates). NSF, surface GluA1 and cell nuclei (DAPI) were visualized. Scale bar, 25 µm.

(**D**-**E**) Quantification of neurite surface GluA1 and neurite NSF relative to *tau*$^{+/+}$ Veh control. Reduced surface GluA1 (D) and total NSF (n = 10-12 neurites from 3 biological replicates) (E) localized to neurites in *tau*$^{-/-}$ neurons treated with MK801 (n = 21-23 neurites from 3 biological replicates).

(**F**) Changes in secondary dendrite GluA2 expression in neurons (DIV18) upon cLTP/cLTD induction. *Tau*$^{-/-}$ neurons were transfected with tau at DIV12 (= *tau*$^{-/-}$.tau) or mock transfected (*tau*$^{-/-}$). Cells were stained for GluA2, dendritic marker Map2, and NSF at 2 h post-cLTP/cLTD induction or treatment with control artificial cerebrospinal fluid (aCSF). Dendritic GluA2 cluster analysis was based on GluA2-Map2 binary intensity map. Representative insets from n = 10-20 dendrites per condition from 2 mice per genotype. Scale bar, 3 µm.

(**G**) Quantification of GluA2 mean intensity relative to Map2 area and normalised to aCSF controls. Secondary dendrite GluA2 increased in tau-expressing (*tau*$^{+/+}$ and *tau*$^{-/-}$.tau) neurons upon cLTP induction. (n = 10-19 dendrites from 3 biological replicates).

(**H**) Representative immunostaining for whole-cell NSF and GluA2 in *tau*$^{+/+}$, *tau*$^{-/-}$ and tau-transfected *tau*$^{-/-}$ (*tau*$^{-/-}$.tau) neurons at 2 h post-cLTP/cLTD induction or treatment with control artificial cerebrospinal fluid (aCSF). (n = 3-6 biological replicates per condition with 10-20 cells each). Scale bar, 10 µm. Arrows indicate areas of marked co-distribution.

(**I**) Co-localisation analysis of NSF and GluA2 upon chemical LTP/LTD induction. Note significantly higher proportional co-distribution of NSF and GluA2 in tau-expressing (tau+/+ and *tau*$^{-/-}$.tau) cells upon cLTP induction. (n = 3-6 cells from 3 biological replicates).

Data information: Values are means ± S.E.M (normalized to control). Adjusted p-values: ****p < 0.0001, ***p < 0.001, **p < 0.01, *p < 0.05, ns, not significant, ANOVA with Sidak's test.

Chemical LTP induces Tau-NSF colocalization and GluA2 clustering in dendrites.

Surface stabilization of AMPARs is central to forms of synaptic plasticity induced by NMDAR signals underlying memory processes [148]. Increase or reduction of post-synaptic AMPAR levels contributes to two main forms of plasticity, long-term potentiation (LTP) or long-term depression (LTD), respectively [148]. Tau and NSF have independently been indirectly associated with synaptic plasticity [171, 220]. Yet, how the roles of tau and NSF may overlap is unclear. We therefore investigated NSF and AMPAR distribution under conditions of chemically induced LTP and LTD (cLTP, cLTD) in primary neurons with or without tau. Chemical induction of LTP/LTD, based on exposure of cultured neurons to modified artificial cerebrospinal fluid (aCSF), is an approach to investigate plasticity-linked synaptic

molecular changes [236, 237]. Inducing either cLTP or cLTD is activity-dependent, requiring small or large increases in intracellular calcium ($[Ca^{2+}]_i$) for cLTD or cLTP, respectively; moreover, high $[Ca^{2+}]_i$ initiates weakening of NSF-GluA2 binding and impairs AMPAR-trafficking [219, 238]. We validated cLTP and cLTD induction methods using live cell imaging of cellular calcium dynamics and surface GluA1 measurements. GcAMP6f live imaging [239] confirmed cellular calcium ($[Ca^{2+}]_i$) responses characteristic of LTP or LTD upon induction of cLTP or cLTD, respectively, as compared with aCSF alone (**Appendix Fig S5A**-**B**). Moreover, we quantified surface GluA1 levels relative to transfected GFP-GluA1 (total) in treated neurons (**Appendix Fig S5C**-**D**) [240]. GluA1 surface levels upon cLTD and cLTP were characteristic of long-term plasticity, and highest surface GluA1 expression coincided with cLTP as described previously [241]. These results corroborate our chemical plasticity protocol. Interestingly, cLTP induction resulted in an increase in partial tau-NSF signal overlap (**Appendix Fig S5E**).

Synaptic plasticity involves receptor trafficking [210], mediated by post-synaptic vesicle cycling and lateral diffusion of AMPARs in dendrites [209]. To determine impact of tau on plasticity-linked dendritic AMPAR-trafficking, we fixed YFP-expressing neurons following cLTP or cLTD and labelled GluA2, dendrite marker Map2, and NSF (**Fig 2.5F-G**). Due to heterogeneous localisation of synapses and spine morphology [242], we quantified GluA2 clustering proximal to dendritic marker Map2 within secondary dendrites (**Fig 5F**). Compared with control aCSF, dendritic GluA2 levels were significantly higher in cLTP-induced *tau*$^{+/+}$ – but not in *tau*$^{-/-}$ – neurons (**Fig 2.5G**). NSF-GluA2 co-localisation was significantly higher in cLTP-induced tau-competent neurons as compared under aCSF or cLTD conditions (**Fig 2.5H-I**). In summary, tau is required for GluA2 recruitment into dendritic clusters in a model of chemically-induced long-term potentiation, a process that coincides with recruitment of tau-NSF co-distribution.

Tau-dependent changes in NSF-regulated AMPAR expression impair fear conditioning and object recognition memory in mice

Direct association between tau and NSF, regulation of NSF activity by tau, and finally tau-dependent changes in plasticity-related recruitment of NSF and surface AMPARs, prompted us to investigate the role of the tau-NSF axis in memory function in mice, for which we employed two paradigms of associative learning, fear conditioning and object recognition (**Fig 2.6A, SM Fig 2.5A**). Mice were stratified into three groups (*tau*$^{+/+}$, and 2 groups of *tau*$^{-/-}$), followed by bilateral hippocampal AAV injection to deliver (i) expression and localization control (eGFP) in all groups, and (ii) human tau in one *tau*$^{-/-}$ group (*tau*$^{-/-}$.AAV^{tau}). Mice were cannulated into the hippocampus for peptide infusion. Sections and immunostaining verified expression of tau and/or EGFP, and cannula proximity to target CA1 neurons (**Fig 2.6B**). Mice were entrained with tone-foot shock association in the auditory cued fear conditioning (CFC) paradigm [243]. Infusion of cell-permeable Tat fusion peptides TAT-NSF or

TAT-Scramble (TAT-Scr) was administered after training, while under brief general anaesthesia (GA). GA control was included for potential anaesthesia-induced effects. Test trials were performed after 24 h and memory was evaluated based on freezing response (**Fig 2.6C**). TAT-NSF inhibited memory, indicated by low freezing response, in *tau*$^{+/+}$ and *tau*$^{-/-}$.AAV^{tau} significantly (**Fig 2.6C**). Memory was unimpaired in TAT-Scr and GA control *tau*$^{-/-}$ mice, as well as mostly unimpaired in *tau*$^{+/+}$ and *tau*$^{-/-}$.AAV^{tau} mice (**Fig 2.6C**). Within each experimental group, mice expressing tau showed consistently lower memory (i.e., less freezing behaviour) than *tau*$^{-/-}$ mice (**Fig 2.6C**), suggesting that the presence of tau in mouse brain limited the strength of conditioned stimulus association. Consistent with effects of tau and NSF inhibition in fear conditioning, object recognition (NOR) was impaired by TAT-NSF infusion in *tau*$^{+/+}$, *tau*$^{-/-}$, and *tau*$^{-/-}$.AAV^{tau} as compared with corresponding TAT-Scr-treated groups. Within TAT-NSF or TAT-Scr infused groups, tau-expressing mice (*tau*$^{+/+}$ and *tau*$^{-/-}$.AAV^{tau}) showed lower novel object preference as compared with tau negative (*tau*$^{-/-}$), indicating that presence of tau limits recognition memory (**Fig 2.6D**).

GluA1 receptors temporarily increase in post-synaptic densities (PSDs) during LTP formation and after CFC trials [210]. Mouse brain tissue after hippocampal TAT-NSF/-Scr peptide infusions was harvested immediately following NOR test trial and was pooled by group for biochemical analysis. Post-synaptic complexes associated with PSD-95, a major receptor-organizing scaffold of PSDs [244], were co-precipitated from hippocampus lysates to assess incorporation of GluA1/2 into PSD complexes (**SM Fig 2.5B**). GluA1/2 bound to Psd-95 was consistently lower in TAT-NSF treated hippocampal tissue (**SM Fig 2.5B**). Both GluA1 and GluA2 bound to PSD-95 was higher in the *tau*$^{+/+}$ and *tau*$^{-/-}$.AAVtau tissue as compared with *tau*$^{-/-}$ group infused with TAT-Scr (**SM Fig 2.5C**). This indicates that impact of tau-deficiency and NSF inhibition on memory performance are associated with changes of AMPAR incorporation into post-synaptic complexes. Taken together, memory task performance correlated with TAT-NSF infusion and tau expression. Furthermore, binding of GluA1 and GluA2 AMPARs into complexes with PSD-95 changed with NSF inhibition and tau expression.

Tau-dependent pathologic mechanisms of synaptic dysfunction, including tau-dependent impairment of synaptic plasticity [245], may target NSF. To address the impact of disease-associated, pathologic tau and of Aβ on NSF, we measured ATPase activity of NSF incubated with tau immunoprecipitated from brain lysates from mouse models with of frontotemporal dementia expressing pathogenic tauP301S (Tau58/2) or wildtype human tau (ALZ17) or from Aβ-expressing APP transgenic mice. Immunoprecipitated pathologic tau in Tau58/2 transgenic and human tau in ALZ17 lysates suppressed induced NSF activity significantly more than murine tau immunoprecipitated from *tau*$^{+/+}$ as compared with IgG controls (**Figs 2.6E**, **SM 2.5D**). Tau precipitated from APP transgenic APP23, tau-deficient APP23 (APP23.*tau*$^{-/-}$) and App-deficient *App*$^{-/-}$ lysates did not suppressed NSF activity further than tau from *tau*$^{+/+}$ (**SM Fig 2.5E**). Neither immunoprecipitated Aβ nor synthetic oligomerized

Aβ altered activity of NSF in vitro (**SM Fig 2.5F-I**). Samples from human neocortex IP-ed tau incubated in NSF ATPase assays. NSF incubated with tau precipitate from both MCI and AD was significantly lower in ATPase activity (**Fig 2.6F**). These results show inhibition of NSF activation by disease-associated human tau in mouse models and suggest that presence of Aβ does not induce tau to inhibit NSF nor does oligomerized Aβ alone.

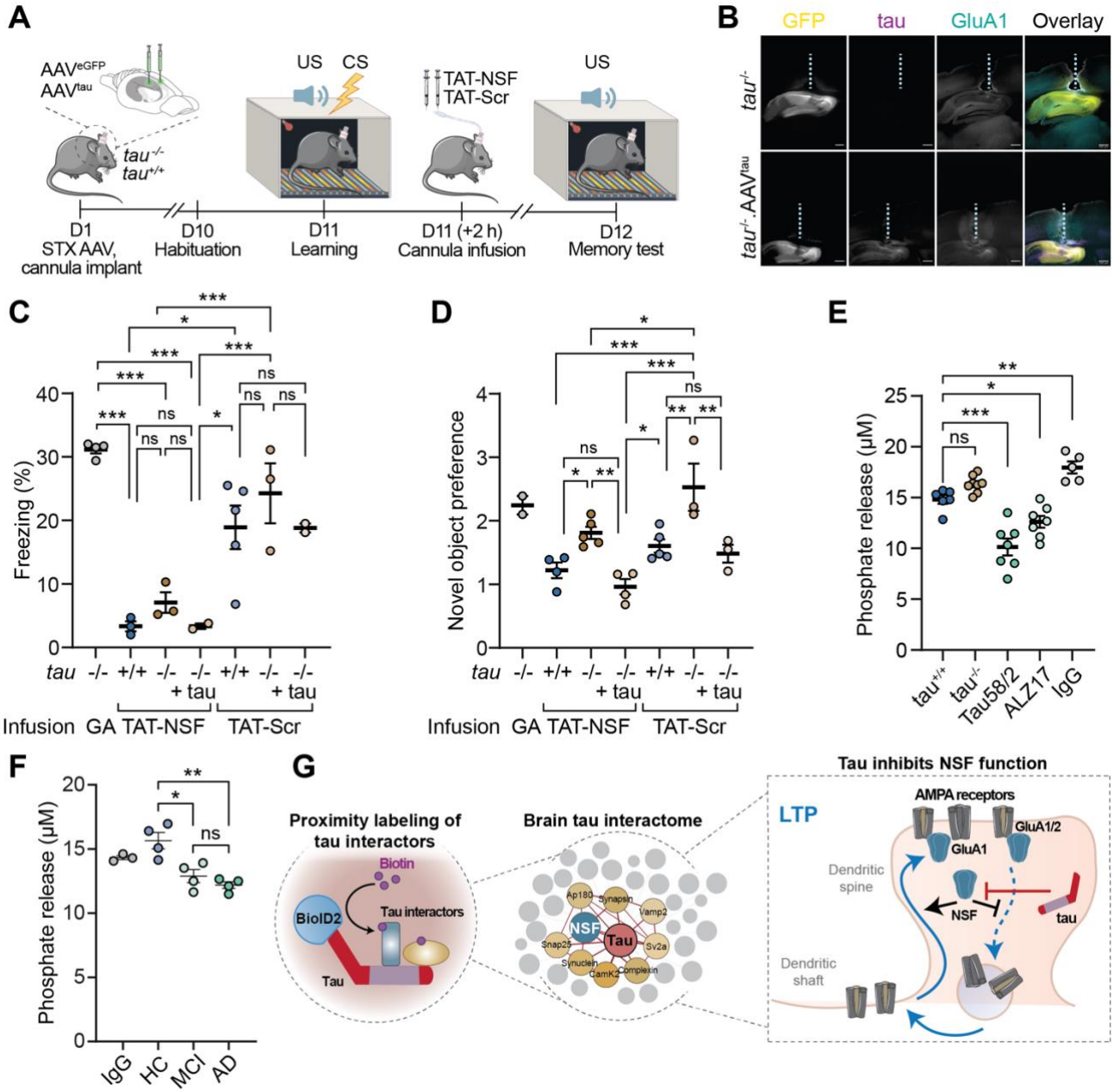

Figure 2.6. ***Tau limits NSF-dependent associative learning and mediates pathologic inhibition of NSF in tau-transgenic mouse models and in AD brain lysates***.

(**A**) Experimental schematic of contextual fear conditioning (CFC) paradigm. *Tau*$^{+/+}$ or *tau*$^{-/-}$ mice were stereotactically (STX) injected with AAV.syn-EGFP or co-injected with AAV.syn-EGFP and AAV.syn-hTau (= *tau*$^{-/-}$.AAV^{tau}) and implanted with bilateral hippocampal cannulas. TAT-NSF or scramble control peptide (TAT-Scr) was bilaterally infused after cued fear conditioning. Memory was tested 24 hours later.

(**B**) Examples of sagittal sections of *tau*$^{-/-}$ and AAV.syn-hTau-injected *tau*$^{-/-}$ (*tau*$^{-/-}$.AAV^{tau}) mice showing localized AAV-mediated expression of eGFP or tau and position of infusion cannulas ending in the hippocampus (dashed line). GluA1, immunolabelling for GluA1 AMPA receptor subunit. Scale bar, 50 µm.

(**C**) Cued fear conditioning memory in *tau*$^{+/+}$, *tau*$^{-/-}$ and *tau*$^{-/-}$.AAV^{tau} mice upon bilateral infusion of TAT-NSF or TAT-Scr. Due to infusion of Tat-fusion peptides occurring under brief isoflurane anaesthesia, a general anaesthesia (GA) control is included. Note that infusion of TAT-NSF lowers memory performance to comparable levels in *tau*$^{+/+}$, *tau*$^{-/-}$ and *tau*$^{-/-}$.AAV^{tau} mice. (n = 2-5 biological replicates)

(**D**) Novel object preference (fold preference over familiar object) in *tau*$^{+/+}$, *tau*$^{-/-}$ and *tau*$^{-/-}$.AAV^{tau} mice upon bilateral infusion of TAT-NSF or TAT-Scr (n = 2-5 biological replicates). Due to infusion of Tat-fusion peptides occurring under brief isoflurane anaesthesia, a general anaesthesia (GA) control is included (n = 2 for GA). Note that infusion of TAT-NSF lowers object discrimination to comparable levels in *tau*$^{+/+}$, *tau*$^{-/-}$ and *tau*$^{-/-}$.AAV^{tau} mice.

(**E**) ATPase assay of recombinant NSF upon incubation with tau coimmunoprecipitates (tau5) from cortical lysates of indicated genotypes, including from tau-transgenic mice (ALZ17, Tau58/2) (n = 5-8 biological replicates). IgG, control immunoprecipitate with non-specific IgG from *tau*$^{+/+}$ lysate.

(**F**) ATPase assay of recombinant NSF upon incubation with tau coimmunoprecipitates (tau5) from brain lysates of healthy controls (HC), mild cognitive impairment (MCI), and Alzheimer's disease (AD) (n = 3-4 biological replicates). IgG, control immunoprecipitate.

(**G**) Graphical schematic summarising BioID labelling and mechanism of tau interaction with NSF. Biotinylation proximity proteomics identified synaptic vesicle associated proteins within the tau protein interactome, including NSF ATPase. The presence of tau in dendrites inhibits NSF-dependent regulation of AMPARs during LTP, limiting performance of mice in CFC trials. In AD models, amyloid-β (Aβ) enhances inhibition of NSF primarily through tau.

Data information: Values are mean ± 95% confidence intervals. Adjusted p-values: ***p < 0.001, **p < 0.01, *p < 0.05, ns, not significant, ANOVA with Sidak's test.

In summary, this study provides a resource of neuronal tau interactomes in vivo and maps tau interactions onto synaptic processes. From there we define a role of the tau-NSF pathway in associative learning mediated by AMPAR trafficking and present NSF as a novel target of pathologic tau (**Fig 2.6G**).

Discussion

Experience-dependent molecular changes in synapses coincide with activation of pre- and post-synaptic neurons for the strengthening or weakening of neuronal connections, often during formation of a memory [148]. After activation of NMDARs, regulation of AMPAR composition and trafficking is critical in altering synaptic strength [141]. Receptor trafficking and neurotransmitter release are subject to the regulated cycling of synaptic vesicles and membrane protein/receptor binding partners [141]. While tau has previously been implicated in impairment of synaptic function under disease-associated conditions (e.g., when aberrantly phosphorylated or by pronounced mislocalisation) [155, 171], a physiologic role for tau in regulation of synaptic plasticity and key associated pathways remained elusive. To gain more insights into roles of tau in these processes, we mapped neuronal tau interactomes in vitro and in vivo by proximity labelling. Functional ontology analysis confirmed enriched associations with processes of cytoskeletal protein binding and synaptic vesicle cycling. We used imaging, co-IP, and microscale thermophoresis to corroborate a physical interaction between tau and a biotinylated tau interactor NSF. Using primary neurons and memory paradigms in mice, we determined a mechanistic link between tau, NSF ATPase activity, and AMPAR trafficking in encoding of associative memory. Pathologic tau from mouse models and human AD brain enhances inhibition of NSF. Thus, our study demonstrates that generating an extensive tau interactome can provide functional insights into the molecular control of associative learning and provide mechanistic targets of pathologic tau.

We report BioID of tau interactor candidate proteins in primary neurons and mouse brain. Semi-quantitative proteomics identified 260 unique proteins across expression in cortical mouse neurons, mouse cortex and hippocampus (P35), and *tau*$^{-/-}$ adult mouse hippocampus. 72 of 260 proteins (~28%) are previously identified potential tau interactors. Thus, 188 (~72%) new tau interacting proteins were identified in our study. While delivery of BioID2-tau expression by AAV permits expression in different neuronal systems, this approach may have limitations due to over-expression. Nevertheless, we detect a significant overlap between interactions defined in our study and by previous approaches [5, 11, 246]. As expected for a neuronal microtubule-associated protein, neuronal cytoskeleton-binding proteins were enriched in BioID tau interactomes. Interestingly, proteins participating in synaptic vesicle cycling were also enriched. Tau interactors mapped onto cytoskeletal organization, vesicle cycle, and post-synaptic processes complexes. Overall, we observed a high degree of overlap between interactomes from cultured neurons and interactomes in living brain, summarized into a physiologic network of tau interactors in live neurons. Compared with existing proteomic datasets of tau PPIs derived from traditional methods, BioID2 provided a unique overview of interactions, likely due to multiple factors including: (i) Samples are usually from lysates or fixed tissue, whereas BioID2 labelling takes place in situ [215, 216, 247], (ii) Tau PPIs are commonly investigated using models or specimens related to tau or neuropathology rather than

physiology [11, 248], (iii) Unlike many traditional PPI identification methods, BioID2 can label transient protein interactions [247]. Due to lack of competition and resulting vacant binding sites, episomally expressed tau in tau$^{-/-}$ neurons may localise to neurites more readily than in tau-competent neurons [221]. Despite this, BioID2 labelled more interactions of tau in tau$^{-/-}$ brains, indicating that lack of endogenous competition outweighs the effect of tau binding site sinks. This may, in part, reflect mobility of tau molecules within neurites and other subcellular compartments [225].

Synaptic vesicle cycle proteins, including receptor- and vesicle-associated ATPase NSF, formed a cluster within BioID-labelled tau interactomes. Neither occurrence nor biological significance of a direct tau-NSF PPI has previously been acknowledged. Physiologic tau and NSF interact in vitro, in cells, and in mouse brain. In primary neurons, tau and NSF colocalise in neurite extensions, suggesting localized functional complementarity. Conventional proteomics of fixed or lysed tissue using human AD and AD mouse model tissue report NSF in neurofibrillary tangles (NFTs) [11, 248]. However, these studies were limited to identification of NSF trapped as coaggregate. In contrast, we show that physiologic tau interacts with NSF to regulate NSF function. High binding affinity as determined by MST may explain coaggregation of NSF and tau in NFTs.

Regulation of NSF ATPase activity was mediated by direct binding of tau. Unlike soluble tau, heat-treated tau (95°C, 5 min) did not produce a thermophoretic binding curve nor inhibit NSF ATPase activity. Whether NSF interaction and regulation indeed requires conformational elements within soluble tau or whether recombinant tau used in this study is more heat-sensitive over tau derived from other preparation protocols, remains to be determined. Notably, secondary structures within tau are required for microtubule binding [190]. Comparable changes in catalytic rates and in binding by addition of tau suggest that, like TAT-NSF, tau may disrupt NSF hexamer assembly as a mechanism of functional inhibition [231]. Neurite NSF in tau$^{-/-}$ neurons is significantly elevated relative to tau$^{+/+}$ neurons. Tau-dependent NSF inhibition is likely connected to differences in neurite NSF localisation, based on hexamer disassembly and concomitant localization changes of NSF by binding with tau or upon TAT-NSF treatment. Notably, the ATPase-hydrolysis defective NSF(E329Q)-tagRFP variant showed lower hexamer stability [249] and a marked dispersion of NSF subunits from Golgi foci throughout the cell [250]. Interestingly, deletions of different regions in tau did not abolish binding to NSF in cells, yet reduced inhibition of NSF in isolated protein. Thus, multiple regions in tau may contribute differentially to binding and to inhibition of NSF hexamerization.

Surface GluA1 and colocalization of tau-NSF increase in wild-type neurons following cLTP. During early LTP, GluA1-rich AMPARs lateral diffusion into post-synaptic densities (PSDs) from extra-synaptic spaces is compensated by exocytosis of GluA2/3-rich AMPAR from endosomal pools [251]. Tau-competent neurons post-cLTP show high dendritic GluA2 intensity and neuronal NSF-GluA2 colocalization. NSF mediates replacement of GluA1-containing AMPARs in the PSD with GluA2-

containing AMPARs [210]. NSF maintains surface expression of AMPARs by displacing PICK1 from GluA2 in an ATP-dependent manner, allowing binding of scaffold protein GRIP1 to GluA2 [141]. A stable NSF-GluA2 interaction is required for encoding fear memory in the amygdala [252], and for mediating PKMζ-induced LTP/maintenance of contextual memory in the hippocampus [220]. Tau-deficient dendrites may have less localized and enhanced NSF activity, which maximise colocalization of NSF-GluA2 and impair efficient AMPAR-trafficking. Local tau limits NSF-GluA2 binding necessary for replacement of homomeric GluA1 AMPARs with GluA2-containing AMPARs seen in LTP. Thus, tau is required for integration and maintenance of GluA1/2 AMPARs within post-synapses by coordinating the local activity of NSF and GluA2 trafficking, particularly upon NMDAR engagement and LTP induction. Aβ in brain lysates lowers activation of NSF through tau. This mechanism may be involved in Aβ-induced LTP impairment of LTP expression [253]. Despite the potential implications for synaptic plasticity, our study focusses on AMPAR trafficking using chemically induced cellular models. The extent and nature of electrophysiologic changes impacted by tau and NSF such as AMPAR-mediated currents, synaptic strength, and excitability of neurons upon electrical induction of LTP or LTD (theta burst stimulation) remains to be determined.

We addressed the role of the tau-NSF-AMPAR axis in associative learning and resulting memory with two paradigms, object recognition and fear conditioning. For context-stimulus associations in CFC, plasticity at CA1 is induced and required [254]. During recall, context-fear associations were weaker in tau-competent- (i.e., *tau*$^{+/+}$ and *tau*$^{-/-}$.AAV^{tau}) and TAT-NSF-infused mice. While this alone does not implicate an NSF-mediated suppressive effect of tau on memory function, probe trials in tau-deficient conditions (i.e., *tau*$^{-/-}$) suggest that absence of tau results in derepressed memory recall even under conditions of NSF inhibition. NSF inhibition likely affects both pre- and post-synaptic functions of NSF, which is transmitter vesicle exocytosis and stabilization of AMPARs, respectively [231, 252]. Whether tau-NSF impacts on plasticity required at CA1 synapses during learning remains to be determined. Suppression of object recognition by NSF inhibition complements the findings in CFC by us and others [252]. Biochemical analysis of hippocampus after NOR showed lower abundance of PSD-95 complexes with GluA1 or 2 AMPAR subunits after NSF inhibition. Lower post-synaptic GluA integration would be consistent with impairments in NSF-dependent GluA2 diffusion kinetics, AMPAR recycling, and memory performance [209]. Thus, tau-dependent inhibition of NSF may reduce synaptic NSF-GluA2 interactions, hindering experience-dependent changes in post-synaptic AMPAR trafficking.

Pathogenic tau from brain lysates of mouse models for frontotemporal dementia (i.e., TAU58/2) and AD were able to suppress NSF activation. Though low sample number, our data with tau from human brain indicates that pathogenic tau in MCI and AD acquires inhibitory capacity towards NSF. Thus, inhibition of NSF downstream of pathogenic tau and concomitant dysregulation of AMPAR trafficking

may contribute to synaptic dysfunction in disease. Notably, neither oligomerized Aβ alone nor Aβ enriched from AD mouse models suppressed NSF activity, suggesting NSF inhibition may be a tau-specific pathomechanism in AD. Our results and others implicate tau in neuronal SNARE complex homeostasis [8]. SNARE protein vesicle trafficking is dysfunctional in necroptosis [255], a programmed form of neuroinflammatory cell death indicated in brain tissue from AD patients and from rodent models of AD [255-257]. However, whether tau and NSF are directly involved in necroptosis is unknown. While this is the first instance of a disease mechanism in neurodegenerative disorders implicating NSF dysregulation as a target of pathogenic tau, NSF has been associated with hereditary forms of epilepsy. Notably, human chromosome 17 region q21.31 harbours gene loci for both tau (MAPT) and NSF (NSF) [258]. Genome-wide association studies significantly link MAPT and NSF to general cognitive function [259]. Elevated synaptic NSF and AMPARs were linked to spontaneous spike wave formation in temporal lobe epilepsy [260]. Tau is required for hyperexcitability in mouse models of epilepsy and stroke [213]. It is an intriguing possibility that these effects of tau are at least in part mediated by inhibition of NSF and consequent imbalance of surface AMPARs.

Our results demonstrate that interactome mapping can deliver new functional insights into tau in neurobiology and disease (**Fig 2.6G**). Analysis of synaptic vesicle associated protein NSF revealed a physiologic mechanism of tau in AMPAR-trafficking and associative learning. Tau limits NSF-mediated surface expression of AMPARs during NMDAR engagement and upon LTP, with consequences during encoding of a contextual memory. This regulated encoding of normal memory may provide a candidate mechanistic link to the earliest stages of memory impairment seen in some neurodegenerative diseases.

Supplementary Figures

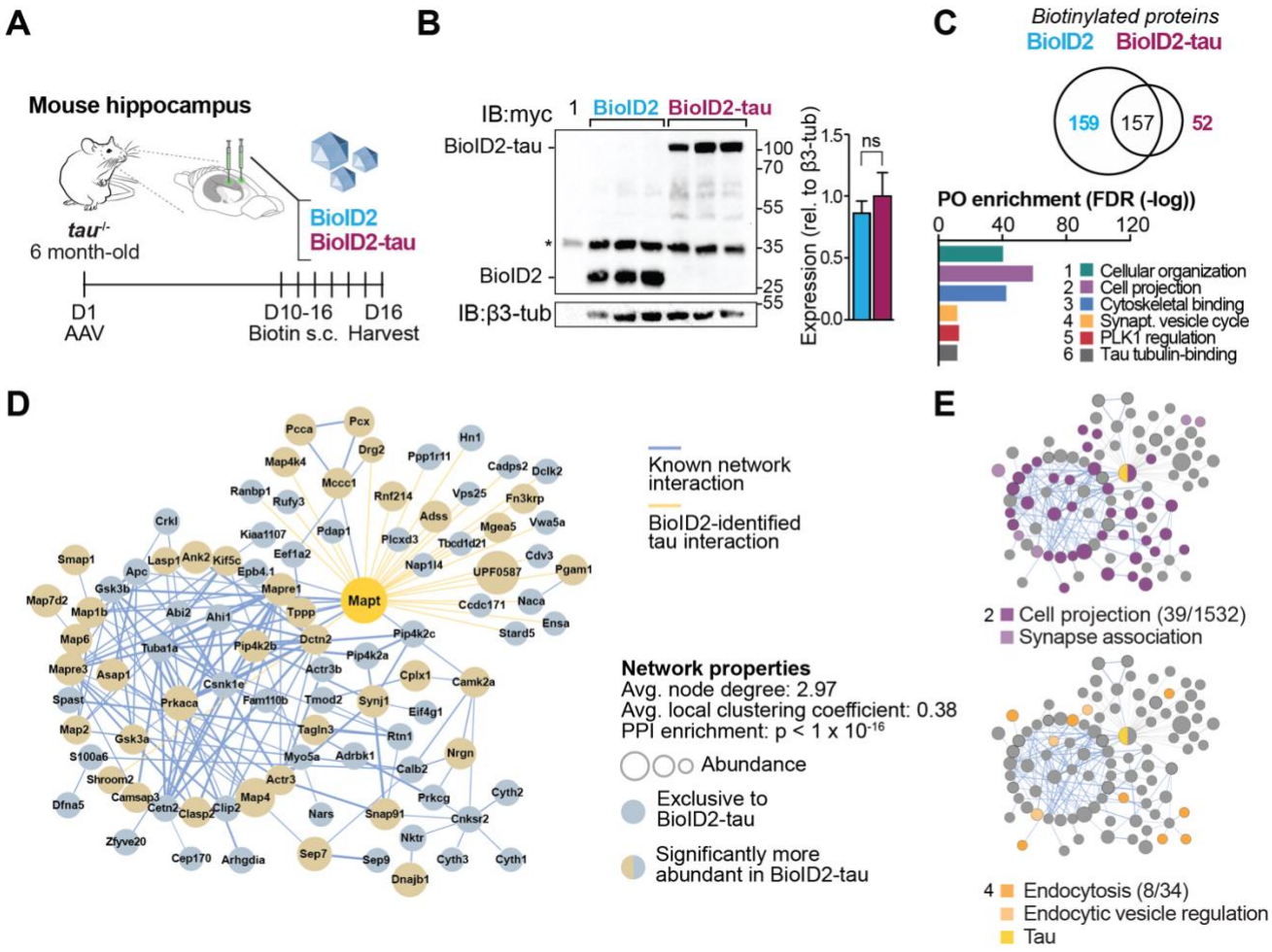

Supplementary Figure 2.1. ***Proximity labelled tau interactomes in adult mouse brain link cytoskeletal, synaptic, and synaptic vesicle-associated proteins***.

(**A**) Experimental schematic of neuronal interactome labelling in vivo in adult *tau*$^{-/-}$ (6 months).

(**B**) Immunoblot of hippocampal lysates from *tau*$^{-/-}$ mice expressing BioID2-tau or BioID2 control (n = 3 biological replicates) probed for myc-tagged BioID2 and BioID2-tau. Controls: lysates from (1) BioID2- or (2) BioID2-tau-expressing and (3) non-transduced mouse brain. Loading, glyceraldehyde-3-phosphate dehydrogenase (Gapdh). *, unspecific band. Relative quantification confirmed similar expression levels of BioID2 and BioID2-tau. Means ± S.E.M. ns, not significant (Student's t-test).

(**C**) Tau interactome in adult tau$^{-/-}$ mouse brain transduced to express BioID2-tau or BioID2 control (n = 6 biological replicates). Venn diagram shows overlapping and unique interacting proteins identified by biotinylation. Protein ontology (PO) enrichment (false discovery rate (FDR)) for highest ranking categories in 1 biological processes, 2 cell component, 3 molecular function, 4 KEGG pathway, 5 Reactome pathway, 6 PFAM protein domain are shown. Note most enriched functional annotation clusters: 2 cell projection and 4 endocytosis.

(**D**) Proximity labelled tau interactome network in adult *tau*$^{-/-}$ mouse brain (n = 6 biological replicates). Known functional associations and novel BioID2 identified interactions are integrated into network of significantly more abundant and exclusive interactors in BioID2-tau. Network properties and enrichment scores are listed (STRING v11.5). Novel association identified by BioID2 (yellow lines) are partially omitted for clarity.

(**E**) Functional ontology clusters mapped onto neuronal tau interactome network in (D) for cell component: cell projection and for KEGG: endocytosis. Additional associations with synaptic localization/function and synaptic vesicle regulation described in literature are mapped, respectively.

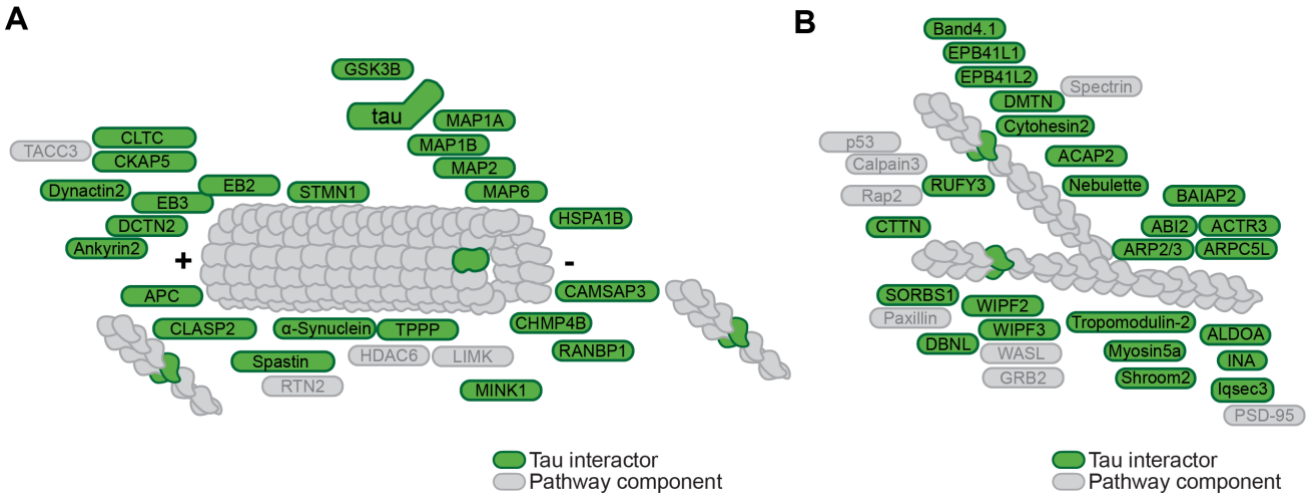

Supplementary Figure 2.2. ***Proximity ligation-identified tau interactors map onto microtubule and actin cytoskeleton and associated processes***.

(**A, B**) BioID2-identified tau interactors mapped onto cytoskeletal complexes and involving (**A**) microtubule and microtubule associated factors and (**B**) actin and actin-modulating factors. Additional key process/pathway/ complex components are included that were not identified by BioID2 are displayed.

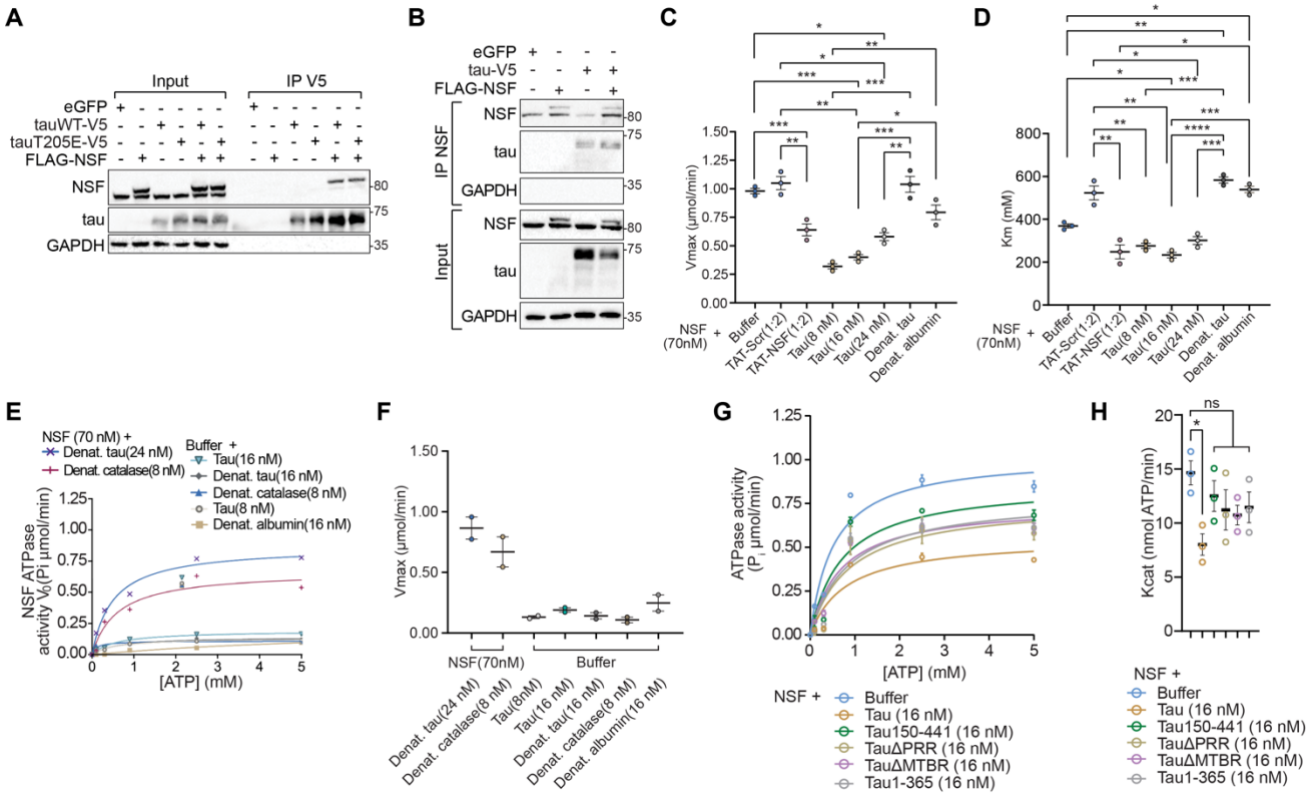

Supplementary Figure 2.3. ***Characteristics of tau interaction with and inhibition of synaptic ATPase NSF***.

(**A**) Co-immunoprecipitation (Co-IP) of tau and NSF. V5-tagged wildtype tau (tauWT) or tauT205E variant and FLAG-tagged NSF were expressed in heterologous 293T cells and immunoprecipitated from cell lysates using anti-V5 antibody. Immunoblots were probed with antibodies specific for tau and NSF. GAPDH, input loading control (n = 6 biol replicates). Quantification shows similar levels of NSF bound to tauWT and tauT205E (n = 6).

(**B**) Co-IP of NSF and tau. V5-tagged wildtype tau and FLAG-tagged NSF were expressed in heterologous 293T cells and immunoprecipitated from cell lysates using anti-NSF antibody. Immunoblots were probed with antibodies specific for tau and NSF. GAPDH, input loading control (n = 4 biological replicates).

(**C**) Co-incubation of recombinant human tau protein with NSF reduces maximal NSF ATPase rate of activity. See also Fig 2.4G-H. (n = 3 technical replicates)

(**D**) NSF affinity for ATP was lowest when co-incubated with soluble – but not heat-denatured – tau, and with TAT-NSF. (n = 3 technical replicates)

(**E**) Maximal ATPase activity of NSF remained high despite high concentrations of added heat-denatured tau (dTau, 24 nM) or albumin (dAlb, 8nM). Data were fitted with the Michaelis-Menten kinetic model to determine kinetic constants. (n = 2 technical replicates)

(**F**) Bar graph representation of maximal ATPase activity from E for k_{cat} and K_m values of NSF, see Appendix Fig S4. (n = 2 technical replicates)

(**G**) NSF ATPase activity in presence of full-length tau (16 nM) or indicated tau deletion or truncation variants (16 nM). Phosphate release from NSF activity (70 nM) was assessed alone or in the presence of recombinant tau protein (16 nM) or heat-denatured tau (dTau, 8 nM) or albumin (Alb, 16 nM). The design of recombinant tau variants is represented in Fig 4C. Data were fitted to Michaelis-Menten model to determine rate constants (R^2 = 0.842 - 0.933 for all conditions). (n = 3 technical replicates)

(**H**) Rate constants derived from kinetic data in G. (n = 3) ATP hydrolysis is not significantly lower in NSF incubated with tau truncation and deletion variants, while full-length tau incubation with NSF results in significantly lower ATPase activity. (n = 3 technical replicates).

Data information: Values are means ± S.E.M (normalized to control). Adjusted p-values: ****p < 0.0001, ***p < 0.001, **p < 0.01, *p < 0.05, ns, not significant, ANOVA with Sidak's test.

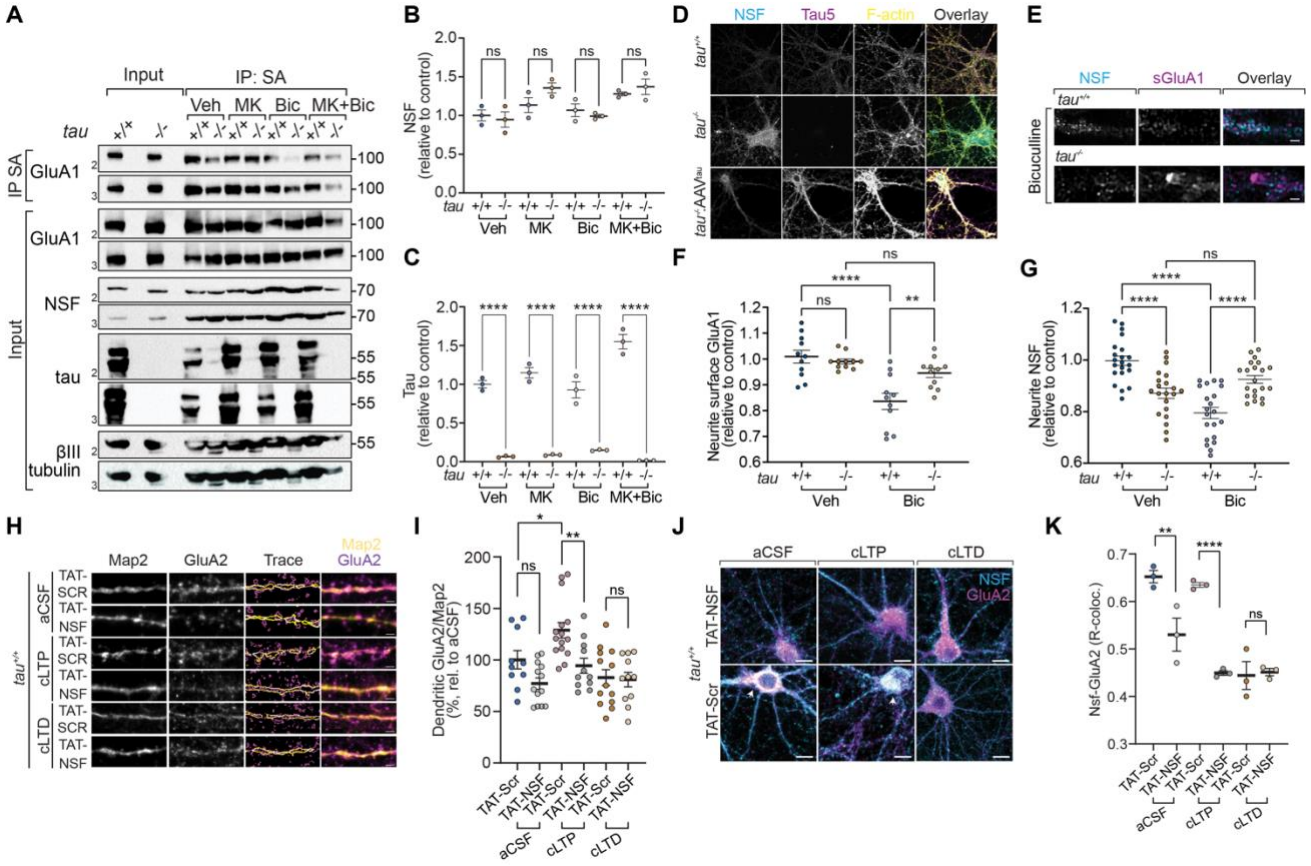

Supplementary Figure 2.4. ***Regulation of GluA surface and dendritic expression by tau and NSF***.

(**A**-**C**) Endogenous NSF expression remained stable in *tau*$^{+/+}$ and *tau*$^{-/-}$ cortical neurons across treatment conditions. See Fig 2.5A-B. (**A**) Biological replicate immunoblots used to quantify and compare surface GluA1 levels across MK801 (50 µM, 3 min) and/or bicuculline (30 mM, 10 min) treatments. Identical symbols beside immunoblots are from the same experiment. Surface proteins were enriched with streptavidin (SA) beads and resolved on SDS-PAGE for immunodetection of GluA1 levels. Input was loaded for detection of total cellular GluA1, NSF, tau, and βIII-tubulin. Input and SA-enrichment from non-surface biotinylated *tau*$^{+/+}$ or *tau*$^{-/-}$ neurons were included as negative controls. (**B-C**) Densitometric quantification of NSF and tau levels. (**B**) No statistically significant difference in endogenous NSF levels between conditions. (**C**) Endogenous tau expression confirmed in *tau*$^{+/+}$ neurons. (n = 3 biological replicates)

(**D**) Tau expression levels were consistent with reported genotypes and conditions at DIV15. Related to Fig 2.5C. *Tau*$^{+/+}$, *tau*$^{-/-}$ neurons and *tau*$^{-/-}$ neurons expressing human tau (*tau*$^{-/-}$.AAV^{tau}). Confocal images show immunofluorescent staining for NSF (cyan), tau (magenta), filamentous F-actin (yellow). Scale bar, 5 µm.

(**E**) Cell surface GluA1 and total NSF immunostaining in primary mouse hippocampal neurons (DIV15) treated with bicuculline (Bic, 30 µM, 10 min). Representative confocal images of *tau*$^{+/+}$ and *tau*$^{-/-}$ neurites are shown, from n = 2 mice per genotype. Cyan indicates NSF and magenta indicates surface GluA1. Scale bar, 3 µm.

(**F**) Reduced neurite surface GluA1 in Bic-treated *tau*$^{+/+}$, yet not *tau*$^{-/-}$ neurons. (n = 11 neurites from 3 biological replicates per condition).

(**G**) Lower neurite NSF in *tau*$^{-/-}$ compared to *tau*$^{+/+}$ of Veh controls. Higher levels of NSF in neurites of *tau*$^{-/-}$ compared to tau$^{+/+}$ neurons treated with bicuculline. (n = 21 neurites from 3 biological replicates per condition).

(**H**) Effect of NSF inhibition on dendritic GluA2 localization in cultured neurons upon chemically-induced LTP/LTD. *Tau*$^{+/+}$ primary neurons (DIV20) were treated with TAT-Scr control or NSF-inhibiting peptide TAT-NSF before induction of chemical long-term potentiation (cLTP) or chemical long-term depression (cLTD) models for 30 min. Cells were fixed 120 min post-cLTP/cLTD induction, and immunolabelled for Map2 and surface GluA2. Signal intensity threshold-based binary maps for surface GluA2 and Map2 traces were used to map signals of

surface GluA2 to dendritic shaft or proxy to synaptic localization. aCSF, artificial cerebrospinal fluid control solution. Scale bar, 3 µm.

(**I**) Quantification of dendritic GluA2 signals relative to binary Map2 signal map in primary neurons upon inhibition of NSF and induction of cLTP or cLTD. (n = 10-12 cells from 2 experiments)

(**J-K**) Effect of NSF inhibition on signal overlap of somatic NSF and GluA2 localization in cultured neurons upon chemically-induced LTP/LTD. *Tau*$^{+/+}$ primary neurons (DIV20) were treated with TAT-Scr control or NSF-inhibiting peptide TAT-NSF before induction of chemical long-term potentiation (cLTP) or chemical long-term depression (cLTD) models for X min. Cells were fixed 120 min post-cLTP/cLTD induction, and immunolabelled for NSF and GluA2. Somatic signals for NSF and GluA2 showed partial overlap in TAT-Scr-treated cells in aCSF and cLTP conditions. Scale bar, 10 µm. (**K**) Co-distribution (R-coloc.) of NSF and GluA2 signals in J. (n = 3 biological replicates)

Data information: Values are means ± S.E.M. Adjusted p-values: ****p < 0.0001, **p< 0.01, *p < 0.05, ns, not significant, ANOVA with Sidak's test.

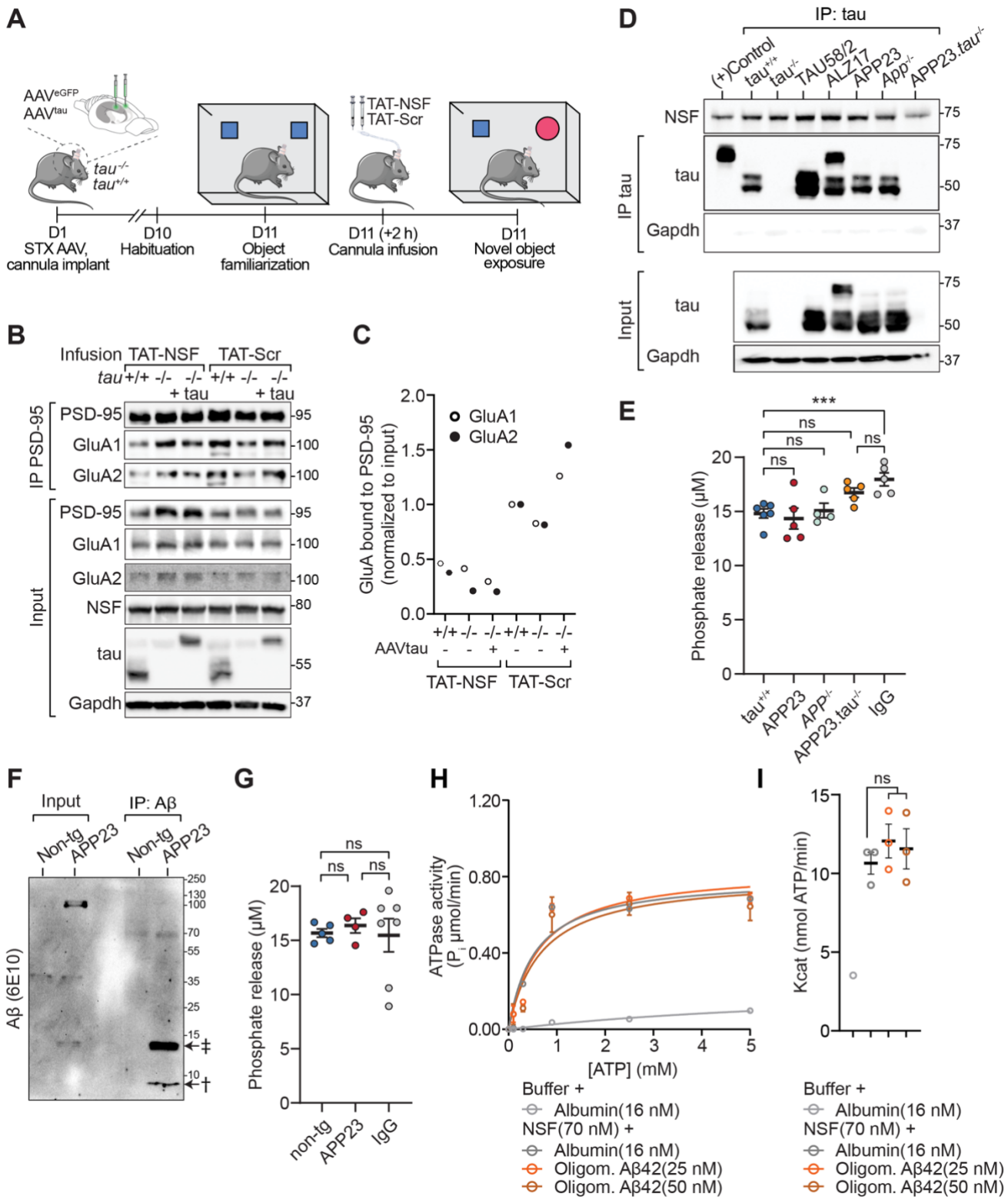

Supplementary Figure 2.5. ***PSD-95-GluA1/2 complexes in object recognition and inhibition of NSF ATPase activity by pathologic tau from mice and from human MCI and AD tissue***.

(**A**) Experimental schematic of novel object recognition tests. *Tau*$^{+/+}$ or *tau*$^{-/-}$ mice were stereotactically (STX) injected with AAV.syn-EGFP or co-injected with AAV.syn-EGFP and AAV.syn-hTau (= *tau*$^{-/-}$.AAV^{tau}) and implanted with bilateral hippocampal cannulas. TAT-NSF or scramble control peptide (TAT-Scr) was bilaterally infused after cued fear conditioning. Recognition memory was tested 6 hours later by exposure to a familiar and a novel object in the same test environment.

(**B**) Co-immunoprecipitation of GluA1 and GluA2 AMPAR subunits with PSD-95 from hippocampus of mice with indicated genotype and peptide/AAV treatment after object recognition paradigm. Immunoblots of co-immunoprecipitates of hippocampal lysates of $tau^{+/+}$, $tau^{-/-}$, or $tau^{-/-}$ mice upon AAV injection (+ tau), cannula implantation and object recognition testing. Immunoblots were probed for tau, NSF, PSD-95, GluA1, and GluA2. Gapdh, loading control. (n = 1).

(**C**) Densitometric quantification of synaptic GluA1 and GluA2 in co-precipitates with PSD-95 from B.

(**D**) Immunoblots of ATPase assay of recombinant NSF upon incubation with tau immunoprecipitated (tau5) from cortical lysates of indicated genotypes, including from *tau*$^{+/+}$, *tau*$^{-/-}$, P301S tau transgenic TAU58/2, wildtype tau transgenic ALZ17, APP-transgenic mice (APP23), APP knockout (*App*$^{-/-}$), and APP23 transgenic mice on tau knockout background (APP23.*tau*$^{-/-}$). Positive control for immunoblot ((+)Control) is recombinant tau and NSF.

(**E**) ATPase assay of recombinant NSF upon incubation with tau coimmunoprecipitates (tau5) from cortical lysates of indicated genotypes, including from tau-transgenic mice (ALZ17, Tau58/2) (n = 4-6 biological replicates). IgG, control immunoprecipitate with non-specific IgG from *tau*$^{+/+}$ lysate.

(**F**) Immunoblot of Immunoprecipitated Aβ (D54D2) from cortical lysates from APP-transgenic mice (APP23) and non-transgenic control (non-tg) was probed for Aβ (6E10). †, monomeric Aβ; ‡†, tri-/tetrameric Aβ.

(**G**) ATPase assay of recombinant NSF upon incubation with immunoprecipitated Aβ (D54D2) from cortical lysates from APP-transgenic mice (APP23) and non-transgenic control (non-tg) (n = 4-7 biological replicates). IgG, control immunoprecipitate with non-specific IgG from non-transgenic lysate. (**z**)

(**H**) ATPase assay of recombinant NSF upon incubation with oligomerised synthetic Aβ (n = 3 technical replicates). NSF (70 nM) ATPase activity in presence of albumin (16 nM) or oligomerized synthetic Aβ1-42 (25 or 50 nM) measured at indicated ATP concentrations. Data were fitted to Michaelis-Menten model to determine rate constants (R^2 = 0.886 - 0.972 for all conditions).

(**I**) Rate constants derived from ATPase activity in G. (n = 3 technical replicates) ATP hydrolysis is not significantly lower in NSF incubated with oligmerized synthetic Aβ1-42.

Data information: Values are means ± S.E.M. Adjusted p-values: ***p < 0.001, ns, not significant, ANOVA with Tukey's test.

Materials and Methods

Mice: C57BL/6J mice were purchased from ABR (Moss Vale, Australia). ALZ17 mice expressing non-mutant human tau in neurons and tau knock-out mouse strain ($tau^{-/-}$) were described previously [162, 261]. All mouse strains were maintained on a C57BL/6J background. All mice were housed (2-5 mice per cage) in the Macquarie University Central Animal Facility (CAF) or College of Medicine & Public Health Animal Facility (CMPHAF) of Flinders University. Animals were housed under standard conditions of temperature and humidity in a day/night cycle of 12/12 hours (light on at 6 am). All experimental subjects had normal health and immune status and were checked regularly at the animal research facility. Food and water were provided ad libitum. All procedures were conducted with a protocol approved by Macquarie University Animal Ethics Committee (AEC) or Flinders University Animal Welfare Committee in accordance with guidelines set forth by the Australian Code for the Care and Use of Animals for Scientific Purposes (NHMRC). Male and female mice were randomly assigned to each experimental condition and treatment, and all experiments were carried out between 2-7 pm.

For in vivo biotinylation experiments, C57BL/6J mice were injected with AAV vectors on postnatal day 0 (P0) and adult *tau*$^{-/-}$ mice underwent stereotaxic AAV injections at 6-months-old (mo). Adult (4-10 mo) $tau^{+/+}$ and *tau*$^{-/-}$ mice that underwent surgery for stereotaxic AAV injections and cannula implantation were individually caged following the procedure to avoid loss of implant due to conflict with littermates. Sample size estimations were based on previous studies [262] and subjects were stratified into experimental groups by genotype, AAV administration, and cannula infusion treatment.

Mice were genotyped by polymerase chain reaction (PCR) using isopropanol-precipitated DNA from tail biopsies as template. Oligonucleotide primers for genotyping transgenes and targeted alleles by PCR are described in the **Primer Table** below.

Primer Table

Construct	Forward primer (5'-3')	Reverse primer (5'-3')
Mouse ($tau^{-/-}$)	GCAATCACCTTCCCTCCATA	ATTCAACCCCCTCGAATTTT
pBSKS-tau	GGTCCTCGAGGCTGAGCCCCGCCAGGAG	CGTAGAATTCTCACAAACCCTGCTTGGCCAG
pAAV-mycBioID2	TCTGCGGTGGGCAGCGGATTCAAGAACCTGATCTGG	TAAGCTTGATATCGAATTTCACTTCTTCTCAGGCTGAAC

pAAV-mycBioID2-tau	TCTGCGGTGGGCAGCGGATTCAAGAACCTGATCTGG	TAAGCTTGATATCGAATTTCACAAACCCTGCTTGGCC
pHIS17-NSF	ACTTTAAGAAGGAGATATACAATGGCGGGCCGGAGCATGCAAG	ATGATGATGATGATGATGGTCAATCAAAATCAAGGGGGCTA
pHIS17-tau	ACTTTAAGAAGGAGATATACAATGGCTGAGCCCCGCCAGGAG	ATGATGATGATGATGATGCAAACCCTGCTTGGCCAGGGA

Primary mouse cultures: Cortical (CTX) and hippocampal (HC) neurons were dissociated from embryonic day 16.5 (E16.5) mouse brain of both sexes, using a standardized protocol [263]. Neurons were isolated from C57BL/6J *tau*$^{+/+}$ or *tau*$^{-/-}$ mouse embryos. For immunofluorescence imaging analyses, E16.5 neurons from CTX or HC were seeded at a density of 7.0 x 10^5 neurons onto 12 mm poly-D-lysine (P6407, Sigma, Merck, Sydney, AUS) coated glass coverslips. For BioID MS analyses, 4.0 x 10^6 CTX neurons were seeded onto 100 mm dishes. For surface biotinylation western blotting procedures, 2.5 x 10^6 CTX neurons were seeded onto 60 mm dishes. All neuron cultures were grown in Neurobasal Medium (21103049, Gibco, ThermoFisher, MA, USA) supplemented with 2% (v/v) B27 (17504044, Gibco, ThermoFisher) and 0.25% (v/v) GlutaMAX (35050079, Gibco, ThermoFisher). To minimise cross-contamination with cell lines, primary neurons were kept in a separate humidified incubator at 37°C and 5% CO2. Neurons were periodically monitored to confirm regular neurite outgrowth, morphology, and for absence of endogenous contaminants. Fixed tau$^{-/-}$ neurons and/or lysates from each experimental batch were immunostained to confirm the absence of tau protein expression.

Cell line: Human embryonic kidney 293T/17 [HEK 293T/17] (CRL3216, ATCC, VA, USA) cells between passage numbers 5-15 were cultured in Dulbecco's Modified Eagle Medium (DMEM) (11965092, Gibco, ThermoFisher) supplemented with 10% (v/v) foetal bovine serum (FBS) (SH30084.04HI, HyClone, UT, USA), 1x Penicillin-Streptomycin (15140148, Gibco, ThermoFisher), and 1x GlutaMAX (35050079, Gibco, ThermoFisher). Cells were kept in a humidified incubator at 37°C and 5% CO_2 and checked daily to monitor growth rate, confluence, morphology, and potential contamination.

Bacterial strains: For plasmid transfection in mammalian cells, constructs were amplified in E. coli Max Efficiency DH5a Competent cells (18258012, Invitrogen, ThermoFisher, MA, USA). AAV vectors were propagated in E. coli OneShot Stbl3 (C737303, Invitrogen, ThermoFisher) to avoid recombination events. Bacterial expression of recombinant proteins was induced in E. coli BL21(DE3)pLysS (C602003, Invitrogen, ThermoFisher). Colonies from all strains were grown using

LB broth with agar (L3147, Miller, Sigma, Merck, Sydney, AUS) and clones expanded with LB broth (L3522, Miller; Sigma, Merck).

Recombinant adeno-associated virus production: Packaging of AAV vectors was performed as described [213, 222, 223]. In brief, for packaging of AAV particles, HEK293T (CRL3216, ATCC) were seeded in DMEM (11965092, Gibco, ThermoFisher) supplemented with 10% (v/v) FBS (SH30084.04HI, HyClone) at 70-80% confluence. Culture medium was changed to Iscove's Modified Dulbecco's Medium (IMDM) (I3390, Sigma, Merck, Sydney, AUS) with 5% FBS 3 hours prior to transfection. Cells were transfected with viral genome-containing plasmid, pFdelta6 as helper plasmid and systemic neurotropic AAV-PHP.B plasmid containing rep and cap sequences using polyethyleneimine-Max (PEI) (23966-1, Polysciences, Taipei, Taiwan) as a transfection reagent. Cells and supernatant (SN) were harvested 72 hours post transfection. SN was clarified by adding 40% PEG8000/2.5 M NaCl (V3011, Promega, WI, USA) to a final concentration of 8% PEG8000/0.5 M NaCl and incubated at 4°C for at least 2 hours. Clarified SN was centrifuged at 2000g for 30 mins. Combined precipitate from clarified SN and cell pellet was treated with sodium deoxycholate (0.5% final concentration) and benzonase (~500 U) (E1014, Merck-Millipore, Sydney, AUS) at 37°C for 40 mins. After addition of NaCl, incubation at 56°C for 40 mins and freeze-thaw, the solution was centrifuged for 30 min at 5000g at 4°C. SNs were purified using iodixanol gradient by ultracentrifugation (475,900g, 2 h, 18°C). AAV particles were concentrated and exchanged into PBS in an Amicon 100 kDa 15 ml concentrator (UFC910008, Merck, Sydney, AUS) at 5000g at 4°C. Titres were determined by quantitative polymerase chain reaction (qPCR). AAV titres were: AAV-PHP.B-syn1-mycBioID2 (1.83×10^{14} viral genomes per ml (vg/ml)), AAV-PHP.B-syn1-mycBioID2hTau (1.10×10^{14} vg/ml), AAV-PHP.B-syn1-eGFP (8.97×10^{13} vg/ml), AAV-syn1-GCaMP6f (1.1×10^{12}), and AAV-syn1-hTauWT (1.7×10^{13}). After determining AAV genomic titres, aliquots were stored at -80°C.

Stereotaxic viral delivery and cannula implantation: For targeted HC and CTX injections of AAV-eGFP ± AAV-hTauWT and infusion of TAT-fused peptide solutions, *tau*$^{+/+}$ and *tau*$^{-/-}$ mice were anaesthetized by intraperitoneal (i.p.) injection of ketamine (100 mg.kg^{-1}, Imalgene 500, Merial, GA, USA) and xylazine (12 mg.kg^{-1}, Rompun, Bayer, Leverkusen, Germany). Mice were placed into a stereotaxic apparatus (Kopf Instruments) with mouse adaptor and lateral ear bars. With the aid of a microinjector (MicroSyringe Pump Controller, WPI, Coherent Scientific, SA, AUS), AAV injections were administered at one site each bilaterally, targeting the CA1 region of HC with the following coordinates: AP -1.9, L ± 1.9, DV -1.6 [264]. As an approximate indicator of TAT-peptide spread after infusion, all mice were administered 200 nL undiluted AAV-eGFP per site (n = 11). All *tau*$^{+/+}$ mice (n = 4) and some *tau*$^{-/-}$ mice (n = 4) received an additional 100 nL PBS per site, while the remaining *tau*$^{-/-}$ mice (n = 3) received an additional 100 nL undiluted AAV-hTauWT per site. Bilateral stainless steel guide cannulas (P1 Technologies, VA, USA) were implanted at coordinates AP -1.9, L ± 1.9, DV -0.6

to target the HC. Guides were secured with surgical superglue (TRM00728, 3M Vetbond, VIC, AUS) and dental cement (56972, 3M Vetbond, VIC, AUS). Animals were allowed to recover in individual cages for 9 days, and upon confirming a bodyweight similar to pre-surgery recordings, mice proceeded to behavioural testing. Minimal tissue damage and correct guide cannula placement were confirmed by immunostaining and fluorescence imaging (**Fig 2.6B**).

Memory testing and cannula infusion: Mice were habituated to an 18 x 18 x 30 cm fear conditioning chamber (Coulbourn Instruments, MA, USA) for 4 min on the tenth day from surgery. On the day after habituation, mice were trained by placing them into the chamber for 7.5 min, during which three foot-shocks (US; 0.8 mA, 1 s) were paired with a tone (CS); intervals between pairings were 1 min. The first CS-US pairing occurred 3 min after entry into the chamber. Mice were tested by returning them to the training context for 5 min, where three tones were presented without shocks. Memory was evaluated by quantifying time spent freezing (>250 msec) relative to testing time.

The novel object recognition (NOR) memory task in mice consisted of a habituation phase, a 2-object familiarisation, and a testing phase in a 45 x 45 x 45 cm NOR chamber [53]. During familiarisation, mice were exposed to two equally spaced identical objects (water-filled cell culture flasks) until both objects were explored for 20 sec or for a maximum of 10 min leger [53]. After 6 h, one object in the chamber was replaced by a 100 ml water-filled Schott bottle and mice were re-exposed to the NOR chamber for 10 min. The task was guided and completed using real-time recording and analyses done in real-time. Memory was evaluated by quantifying object exploration time ratios in the testing phase relative to the familiarisation phase.

At 1.5 h after training, all mice were temporarily anaesthetised (5-7 min) by inhalation of isoflurane (5% induction, 1.5% maintenance). The internal cannula tip protruded 1 mm beyond the guide cannula and was inserted bilaterally to infuse 500 nL (per site) of 8 μM Tat-Nsf or TAT-Scramble. To control for potential effects of isoflurane inhalation, memory was evaluated for one additional anaesthetised but non-cannulated mouse**.**

Mouse brain cryo-preservation: From each experimental condition, right hemispheres from P35 mice and cannula implanted mice were fixed in 4% paraformaldehyde (PFA) (P6148, Merck) at 4°C overnight and subsequently immersion-fixed in each of 10%, 20%, and 30% sucrose (S5-500, ThermoFisher, MA, USA) PBS solutions (rotation, 12h, 4°C). Hemispheres were embedded in Tissue-Tek (4583, Sakura, emgrid, SA, Australia) and stored at -80°C until histological sectioning and staining.

Histological sections and staining: Brain sections were stained as previously described with some modifications [265]. Frozen right hemispheres of mouse brain were cryo-sectioned (15 μm) and dried

on slides in (1 h, 37°C). Tissue was permeabilized in PBS with 0.01% Triton X-100 (10789704001, Sigma, MI, USA) for 5 min at RT followed by blocking in PBS with 3% goat blocking serum for 45 min. Tissue sections were incubated with primary antibodies (1 h, RT), thrice washed with PBS, and incubated with secondary antibody conjugated to a fluorophore (1/500; 1 h, RT) to visualise proteins of interest. DNA was stained with DAPI (1/1000) and biotinylated proteins were detected using SA-Cy3 (1/1000).

BS3 assay: Bis(sulphosuccinimidyl)suberate (BS3; 21586, ThermoFisher) is a membrane-impermeable, homo-bifunctional N-hydroxysuccinimide ester (NHS ester) with a 1.14 nm spacer arm that forms stable amide bonds with primary amines at pH 7-9. BS3 selectively crosslinks extracellular-facing cell surface proteins to form aggregates of high molecular mass while intracellular proteins retain their normal molecular mass. A protocol for isolating cytosolic protein was adapted and modified [262]. Hippocampi were rapidly dissected from euthanised mouse brain and chopped into ~150 μm^3 pieces using fine scissors to maximise accessible tissue surface area. To isolate cytosolic protein, pooled samples were added to 2 mM BS3 (~1/3 of sample) diluted in 500 µl aCSF (pH ~7.4, 120 mM NaCl, 2.5 mM KCl, 1.25 mM NaH_2PO_4, 26 mM $NaHCO_3$, 1.3 mM $MgSO_4$, 2.5 mM $CaCl_2$, 10 mM glucose) or added to aCSF (~1/3 of sample). Remaining fraction was allocated for immunoprecipitation by Psd95. Tissue in aCSF was incubated at 4°C with rotation for 30 min, after which the unreacted esters were quenched by incubation with added tris(hydroxymethyl)aminomethane (TRIS) (Tris) (10 mM) (93362, Sigma) and glycine (50 mM) (410225, Sigma) (10 min with rotation, 4°C). Samples were gently spun to clear and replace the quenching buffer supernatant. This was repeated two more times and final resuspension was in 400 µl RIPA buffer (50 mM Tris pH 8.0, 150 mM NaCl, 5 mM ethylenediaminetetraacetic acid (EDTA), 1% Nonidet-P40, 0.1% sodium dodecyl sulphate (SDS), 0.5% sodium deoxycholate, 1 mM sodium vanadate (Na_3VO_4), 10 mM sodium fluoride (NaF), 0.1% glycerophosphate, 1 mM sodium pyrophosphate (NaPP), 1x Complete Mini protease inhibitor (Roche Applied Science, Sydney, Australia)). Tissue was hand-homogenised and sonicated (8 s, 20% amplitude) before centrifugation (13,000g, 2 min, 4°C). Protein concentration of supernatant fractions was measured by BCA and aliquots stored at -80°C. SDS-PAGE and western blot were used to compare total and intracellular pools of GluA1 and GluA2.

Immunoprecipitation: Immunoprecipitation was performed from cell or tissue lysates as previously described [10]. Briefly, cells and tissue were lysed in modified RIPA buffer (no SDS) on ice and lysates cleared by centrifugation (10,000g, 10 min, 4°C). Protein concentration was determined by BCA assay and 500 µg of protein lysate was incubated with 1 µl of primary antibody for 3 h with rotation at 4°C and additional 1 h with 30 µl buffer-equilibrated Protein G magnetic beads (70024S, CST, Arundel, Australia). Incubation was followed by three washes in modified RIPA, resuspended in 40 µl of loading

buffer (50 mM Tris-HCl pH 6.8, 2% SDS, 5% β-mercaptoethanol, 0.01% bromophenol blue, 6% glycerol) and incubated at 95°C for 5 min. The SN was separated from the beads using a magnetic rack and 5 µl was used for input sample lanes.

Immunoblotting: Western blotting was performed as previously described [223]. Briefly, samples were separated by 8% SDS-PAGE and following protein transfer, membranes were blocked with 5% skim milk powder in Tris-buffered saline with 0.1% Tween-20 (TBS-T) before probing with primary and secondary antibodies (1 h each, RT). Visualising blots was performed as described previously [266]. Bands were visualised by chemiluminescence using Luminata Crescendo Western HRP Substrate (WBLUR0500, Millipore, Merck, Sydney, AUS) on a digital imaging system (Chemidoc XRS+; Bio-Rad, Sydney, Australia). Densitometric quantification of Western blot results was performed using Fiji [267].

Biotinylated protein enrichment in mouse brain lysates: 500 nL of undiluted AAV-mycBioID2 or AAV-mycBioID2hTau were injected at 2 sites each bilaterally into the telencephalon of cryo-anaesthetized post-natal day 0 (P0) C57BL/6J mice (n = 14 per group) as described [223]. From P28, a subcutaneous (s.c.) injection of biotin solution (24 $mg.kg^{-1}$) was administered for 7 consecutive days. For AAV expression of BioID2 constructs in adult hippocampus, *tau*$^{-/-}$ mice were anesthetized by i.p. injection of ketamine (100 $mg.kg^{-1}$) and xylazine (12 $mg.kg^{-1}$) and placed on a stereotaxic frame. Injections of 200 nL diluted AAV solution (100 nL AAV + 100 nL PBS) were administered at two sites each bilaterally, targeting the hippocampus with the following coordinates: AP -2, L ± 2, DV -2.1, and AP -3.6, L ± 2.5, DV -2.1 [264]. After 9 days of recovery in their home cages, tau$^{-/-}$ mice received 7 consecutive days of s.c. biotin injections (24 $mg.kg^{-1}$).

Sham AAV (vehicle) and sham biotin (vehicle) injections were additionally performed for P35 mice and adult tau$^{-/-}$ mice (n = 2 each). On day 7 of s.c. biotin injections, all mice were deeply anaesthetised by i.p. injection of ketamine (100 $mg.kg^{-1}$) and xylene (12 $mg.kg^{-1}$) before transcardial perfusion with PBS (pH 7.4). Per AAV condition, cortical and hippocampal tissue from each P35 mouse hemisphere was dissected and combined, while each bilateral hippocampus from tau$^{-/-}$ mice was combined. Dissected brain tissue was flash-frozen in liquid nitrogen before storing at -80°C for immunoblotting and mass spectrometric (MS) analyses.

Homogenisation of biotinylated mouse brain tissue: Protein lysate from brain tissue was isolated as described [216]. Briefly, dissected CTX and HC tissue was homogenised (~15 repetitive triturations) in 300 µl of Buffer-A (50 mM HEPES pH 7.5 (7365-45-9, Sigma, Merck); 150 mM NaCl; 4 µg/1 ml Leupeptin (78435, ThermoFisher), 4 µg/1 ml PepstatinA (78435, ThermoFisher); 1 mM EDTA (E6758, Merck) in 2 mM PMSF (52332, Sigma, Merck)) followed by addition of 300 µl Buffer-B (50 mM HEPES pH 7.5; 150 mM NaCl; 1 mM EDTA, 2% Triton X-100 (10789704001, Sigma); 0.4%

SDS (436143, Merck); 2% deoxycholate (D6750, Merck,)) on ice using a Dounce homogeniser (Heidolph-Instruments, Schwabach, Germany). Samples were sonicated (2 x 10 s, 20% amplitude) and the SN cleared from a preliminary centrifugation (15,000g, 15 min, 4°C) was ultra-centrifuged (65,000g, 30 min, 4°C) to remove remaining insoluble particles and SDS was added to a final concentration of 1%. Protein concentrations were recorded and aliquots containing 40 µg protein per sample were reserved for WB. Remaining lysates were adjusted to 2.5 mg protein per sample and stored at -80°C until preparation for MS.

Biotinylation in primary cortical mouse neurons: At 14 days in vitro (DIV14), cells were infected with AAV-mycBioID2 (n = 3) or AAV-mycBioID2-hTau (n = 3). At DIV21, the culture medium was enriched with biotin (B4639, Sigma, Merck) to a final concentration of 50 µM for 30 h and washed twice with phosphate-buffered saline (PBS). For immunofluorescence imaging, neurons on coverslips were fixed in 4% PFA (15 min, RT) and stored at 4°C after three PBS washes. For MS, neurons in 100 mm dishes were lysed in 400 µl RIPA buffer and after rotation at 4°C for 30 mins, centrifuged (16,000g, 10 min, 4°C) to retrieve the SN. Protein concentration was determined using BCA (23225, ThermoFisher). Lysate volumes were adjusted to 1.5 mg protein per sample and stored at -80°C until biotinylated protein enrichment.

Biotinylated protein enrichment from brain and neuron lysates: Precipitation and trypsin digest of protein lysate samples were performed as previously described [215, 268]. Briefly, three volumes of methanol and one volume each of chloroform and water were added to each sample, vortexed and centrifuged (15,000g, 2 min), creating a disc-like protein pellet at the hydrophilic-hydrophobic solvent interface. Upon removal of solvents, three volumes of methanol were used to resuspend the protein pellet before centrifugation (15,000g, 2 min), and then removed to air-dry the remaining pellet (15 mins, RT). Protein from each sample was resuspended in 200 µl buffer (4 M urea, 0.1% ProteaseMAX surfactant buffer (V2072, Promega), 50 mM NH_4HCO_3) and following a brief sonication pulse, DL-dithiothreitol (DTT) (10197777001, Sigma, Merck) was added to a 5 mM final concentration and samples were incubated in a Thermos-mixer (800 rpm; 1 h, 55°C). Iodoacetamide (I6125, Sigma, Merck) was added to a final 10 mM concentration and re-incubated (800 rpm, 20 min, in the dark). Trypsin buffer containing NH_4HCO_3 (150 µl, 50 mM), ProteaseMAX (2.5 µl, 1% in 50 mM NH_4HCO_3), and 1:100 (w_{enz}/w_{prot}) trypsin (V5111, Promega, WI, USA) was added to each sample and incubated (300 rpm, 4 h, 37°C). Trifluoroacetic acid (TFA) (302013, Merck) was added to 0.1% final concentration to inhibit trypsin, then samples were centrifuged (20,000g, 20 min) and the SN transferred for desalting to solid-phase extraction tC18 cartridges (WAT036810, Waters, MA, USA) as described previously [269]. Briefly, cartridges were sequentially washed with 3 ml acetonitrile (271004, Sigma, Merck), 3 ml 0.5% acetic acid (695092, Merck) in 50% acetonitrile, and 3 ml 0.1% TFA in dH_2O. After adding the peptide samples, cartridges were washed with 3 ml 0.1% TFA in dH_2O,

followed by 250 µl 0.5% acetic acid in dH_2O. Peptides were eluted with a solution of 1 ml 0.5% acetic acid in 80% acetonitrile and dried overnight in a vacuum concentrator. A modified biotinylated peptide-enrichment protocol was used [268] whereby peptides were resuspended in a 250 µl dissolution buffer (0.05% SDS in PBS) with an added 55 µl equilibrated neutravidin (NA) magnetic bead slurry (09-981-155, GE, ThermoFisher, MA, USA) and incubated at RT on a rotator for 2 h. NA-bound peptides were immobilised by magnet and washed sequentially with 1.5 ml PBS, and 1.5 ml PBS with an increasing acetonitrile gradient (2.5%, 5%, 10% acetonitrile), rotating for 5 min at each wash step. Bead-bound peptides were resuspended in 250 µl dissociation buffer (0.2% TFA, 0.1% formic acid, 80% acetonitrile) and incubated (rotating, 15 min) before magnet immobilisation and collection of 'SN1'. To maximise peptide recovery, beads were resuspended and re-incubated in 250 µl dissociation buffer under heat (700 rpm, 5 min, 95°C), followed by collection and addition of SN2 to SN1. Eluates were dried under vacuum and resuspended to 0.5 µg/µl of 0.2% heptafluorobutyric acid (HFBA) (524311, Supelco, Merck) with 1% formic acid (F0507, Sigma, Merck) for MS analysis.

Mass spectrometry: Mass spectrometry was performed as described previously [215]. Peptide samples sourced from primary neurons and mouse brain were run (3 µg injected per run) and captured on a C18 cartridge (Acclaim PepMap 100, 5 µm 100 Å, Thermo Scientific Dionex, Waltham, USA) using a Q Exactive Orbitrap (ThermoFisher) before switching to a capillary column (~20 cm) containing C18 reverse phase packing (Reprosil-Pur, 1.9 µm, 200 Å, Dr Maisch GmbH, Ammerbuch-Entringen, Germany), and eluted with 40 min gradient of buffer A (H_2O:CH_3CN of 98:2 with 0.1% formic acid) to buffer B (H_2O:CH_3CN of 20:80 with 0.1% formic acid) at 200 nL/min. The mass spectrometer was set to positive ion mode. Peak lists were generated using MASCOT Distiller (Matrix Science, London, UK) and searched using the MASCOT search engine (v2.6.2, Matrix Science). Peak lists were matched to amino acid sequences from the SwissProt database (downloaded 10-8-19; Mammalia taxonomy, 66946 entries) and the Peptide Prophet algorithm [270] assigned identity to peptides with FDR = 1.6% and to proteins with FDR = 0.4%. Each protein was considered identified when assigned 1 unique peptide with a peptide score >38. All identified biotinylated proteins for background and experimental conditions are listed in **Appendix Tables 3-11**.

Network generation and analysis: Biotinylated protein lists from myc-BioID2 and myc-BioID2-hTau primary neuron and mouse brain samples were scrutinised using adapted and modified criteria [216], with more stringent and customised cut-offs. Biotinylated protein abundance was inferred from its assigned spectral count (SC), summated from the replicates of each condition. Relative abundance was expressed as SC fold change (SCFD) of a biotinylated protein in the myc-BioID2-hTau list relative to the myc-BioID2 list. Proteins constituting the tau interactome fulfilled at least one of the following criteria: (1) any statistically significant increase in SCFD, (2) SCFD ≥4; if exclusively identified in myc-BioID2-hTau samples, (3i) SC ≥2 (primary neurons) or (3ii) SC ≥4 (mouse brain). Functional protein-

protein interaction networks and protein ontology were generated using STRING (v11.0) database annotations for the entire human proteome. Interactomes and network properties were visually represented using CytoScape (v3.7.2).

Surface biotinylation of whole neuronal GluA1: Enrichment of surface biotinylated proteins was performed using a modified protocol [262] (see **Fig 2.5A**-**E**; **SM Fig 2.4A**-**G**). On DIV15, MK801 (50 mM) or vehicle (20 µl ddH_2O) was added to 60 mm dishes of primary neurons and re-incubated for 4 min (37°C, 5% CO_2). Cells were washed once each with PBS and artificial cerebrospinal fluid (aCSF; 150 mM NaCl, 2 mM $CaCl_2$, 5 mM KCl, 10 mM HEPES (pH 7.4), and 30 mM glucose in ddH_2O) before re-incubation in 3 ml pre-heated aCSF containing bicuculline (30 mM) (0130, Tocris, Vic, AUS) or vehicle (25 ml ddH_2O) for 10 min. Neurons were washed twice in PBS and re-incubated in 3 ml pre-heated aCSF for 30 mins at 37°C and 5% CO_2 before transferring onto ice and washing once each with ice cold aCSF and PBS. On ice, neurons were incubated with 3 ml PBS containing 0.1 mg/ml NHS-SS-Biotin (21331, Pierce, ThermoFisher) per dish for 30 min. Unreacted NHS esters of the biotinylation reagent were quenched using two 5 min incubations in 3 ml ice-cold quenching buffer (0.1 mM $CaCl_2$, 1 mM $MgCl_2$, 25 mM Tris·Base (pH 8), 20 mM glycine in PBS) per dish on ice. Neurons were finally re-incubated in 3 ml aCSF for 30 mins at 37°C/5% CO_2 prior to three PBS washes and harvesting with lysis buffer (LysB; 1x protease inhibitor tablet (per 10 ml buffer), 50 mM sodium fluoride (NaF), 10 mM tetrasodium pyrophosphate ($Na_4P_2O_7$), 1% Tergitol (NP40, Sigma, Merck), 0.5% sodium deoxycholate (NaDOC), 0.02% SDS, 1 mM sodium orthovanadate (Na_3VO_4) in PBS). Homogenates were centrifuged to remove debris (16000g, 30 min, 4°C) and supernatant (SN) protein concentrations determined by BCA (23225, ThermoFisher). Biotin-labelled surface proteins per sample were concentrated by incubating 80% of each sample SN on a rotator at 4°C with 30 µl LysB-equilibrated neutravidin magnetic beads (09-981-155, GE, ThermoFisher) for 3 h. Immobilised beads were washed three times in LysB with rotation at 4°C for 5 min each time. Biotinylated protein-enriched samples were immobilised and isolated following 5 min incubation in 2X Laemmli buffer (95°C, 700 rpm). Protein from the remaining 20% SN was denatured in final 2X Laemmli buffer and served as reference for relative signal intensity attained from the enriched samples. Sample proteins were resolved by 1D SDS PAGE and immunoblotting targeted AMPA receptor subunit GluA1, NSF, tau, and βIII tubulin. Densitometric quantification of GluA1 from NA-IP was expressed relative to total lysate GluA1 and normalised to vehicle-treated $tau^{+/+}$.

Sub-neuronal localisation of NSF and surface GluA1: Primary hippocampal mouse neurons from $tau^{+/+}$ and $tau^{-/-}$ mice were harvested and dissociated from E16.5 embryos as previously described [263] and seeded at a density of 7.0 x 10^5 on 12 mm coverslips (n = 2-3 per condition). On DIV15, MK801 (50 mM) (0924, Tocris, Vic, AUS) or vehicle (20 ml ddH_2O) was added to cell cultures and re-incubated for 4 min. Cells were washed once with PBS and once with extracellular solution (ECS; 10

mM HEPES (pH 7.4), 150 mM NaCl, 2 mM $CaCl_2$, 5 mM KCl, 30 mM glucose) before re-incubation in 1 ml pre-heated ECS containing bicuculline (30 mM) or vehicle (25 ml ddH_2O) for 10 min. Neurons were washed twice in PBS and re-incubated in 1 ml pre-heated ECS for 30 mins prior to three ice cold PBS washes and fixation with 4% paraformaldehyde (PFA). Permeabilization procedures were performed at RT using a modified method described previously [262]. All antibodies, dyes, and molecular probes used in all fluorescence imaging procedures were diluted in 3% goat blocking buffer (gBB) (3% goat serum; Vector Laboratories, Sydney, Australia). For surface GluA1 staining, membrane surface proteins were blocked with gBB for 20 min followed by incubation with anti-N-terminal GluA1 mouse antibody (1/200; 30 min, RT). Prior to intracellular protein or total receptor immunostaining, cells were washed three times with PBS, permeabilised with 0.1% Triton-X (10789704001, Sigma) in PBS for 3 min and washed twice more with PBS before incubation with gBB (45 min, RT). Surface GluA1 stained neurons were incubated with rabbit antibody for Nsf (1/500, 1 h), whereas neurons for total GluA1 quantification were incubated with rabbit antibody for Nsf (1/500) and mouse antibody for GluA1 (1/500) for 1 hour. Following three PBS washes, all samples were incubated for 1 hour at RT with fluorophore-conjugated secondary antibodies (1/500) and DAPI (1/1000). After three more PBS washes, coverslips were transferred onto glass microscope slides with mounting medium.

Transduction of primary neurons: Primary hippocampal mouse neurons grown on PDL-coated 12 mm coverslips were transduced on DIV7. Using a modified protocol [271], rAAVs (AAV-YFP, AAV-hTau, AAV-GcAMP6f) were added to achieve a multiplicity of infection (MOI) of 1. Eighty percent of the culture medium was replaced with NB (21103049, Gibco, ThermoFisher) medium containing 10^7 viral particles. Two days post-transduction (2DPT), NB (21103049, Gibco, ThermoFisher) was replaced with original culture medium and neurons were re-incubated.

Transfection of primary neurons: Expression plasmids pCI-SEP-GluA1 (#24000, Addgene) or pCMV-hTauV5-DEST were used for transfection of primary neurons on 12 mm coverslips with Lipofectamine 3000 Reagent (L3000015, Invitrogen, ThermoFisher). Briefly, for each well, 0.5 ug plasmid DNA was mixed with 25 ul Lipofectamine 3000 and 25 ul P3000 in 0.5 ml NB (21103049, Gibco, ThermoFisher) and incubated for 15 mins at RT. Eighty percent of growth medium was replaced with DNA-lipid complex mixture and added to neurons. After incubation for 3 h, neurons were aspirated and re-incubated with the original culture medium.

TAT-NSF and SNARE proteins in neuron cLTP/cLTD: Primary hippocampal neurons on 12 mm coverslips were induced using modified chemical LTP or LTD induction protocols [236, 237]. For cLTP, neuron culture medium was replaced with modified artificial cerebrospinal fluid (aCSF) (cLTP; 20 min with 20 mM HEPES pH 7.4, 125 mM NaCl, 25 mM $NaHCO_3$, 1.25 mM NaH_2PO_4, 1 mM $MgCl_2$, 2.5 mM KCl, 6 mM $CaCl_2$, 10 mM glucose, 30 µM bicuculline; 10 min with added final 150 µM glycine,

10 mM sucrose). For cLTD, neuron culture medium was replaced with aCSF (cLTD; 20 min with 20 mM HEPES pH 7.4, 130 mM NaCl, 25 mM $NaHCO_3$, 1.25 mM NaH_2PO_4, 2 mM $MgCl_2$, 5 mM KCl, 3 mM $CaCl_2$, 10 mM glucose; 10 min with added final 100 µM NMDA (0114/50, Tocris), 20 mM sucrose). For the control condition, neuron culture medium was replaced with aCSF (20 min with 20 mM HEPES pH 7.4, 127.5 mM NaCl, 25 mM $NaHCO_3$, 1.25 mM NaH_2PO_4, 1.5 mM $MgCl_2$, 3.75 mM KCl, 4.5 mM $CaCl_2$, 10 mM glucose; 10 min with added final, 10 mM sucrose). Following incubation with either treatment, solutions were replaced with original culture medium and incubated for 90 min. Neurons were then washed with PBS and fixed in 4% PFA. For inhibition of NSF during cLTP/cLTD induction, modfidie aCSF solutions were supplemented with either 1 mM TAT-NSF700 (AS-62238, AnaSpec) or 1 mM TAT-NSF700SCR (AS-62209, AnaSpec).

Live neuron calcium imaging and analysis: Neural activity causes rapid changes in free intracellular calcium [141]. To measure the effects of cLTP and cLTD solutions on intracellular calcium levels, we used live cell imaging of primary mouse hippocampal neurons (DIV15) with AAV-mediated expression of protein calcium sensor GcAMP6f [239]. Neurons were imaged on coverslips in an incubation chamber using confocal microscope ConfoCor – LSM 510 (ZEISS, Oberkochen, Germany), equipped with an inverted Axiovert 200M 10x/0.4 NA air objective. Cells were scanned using a 488-nm argon ion laser with 800 x 800 µm field of view at a rate of 1 frame/s. Approximately 100 neurons were imaged in aCSF for ~45 s (n = 6) and again after 20 min incubation with aCSF to induce cLTP, cLTD, or unmodified aCSF (control) for ~55 s (n = 2 per condition). Images were background subtracted using a global uniformly applied threshold minimum.

Relative fluorescence responses (Df/f0) were quantified by dividing the fluorescence intensity value from all in-frame pixels at each second during treatment (~55 s = 55 values) by the average background fluorescence value (aCSF pre-treatment mean intensity across 45 s incubation) [239].

Immunostaining primary cortical mouse neuron coverslips: Neurons were washed with PBS and fixed in 4% PFA (15 min, RT), then washed thrice with PBS and stored at 4°C until staining procedures. Prior to intracellular protein or total receptor immunostaining, cells were permeabilised with 0.1% Triton-X (10789704001, Sigma) in PBS for 3 min and washed twice more with PBS before blocking off-target binding by incubation with goat blocking buffer (gBB; 45 min, RT). Neurons were blocked with goat blocking buffer (gBB) (3% goat serum; Vector Laboratories) and all antibodies and dyes were diluted for immunostaining in gBB. For surface GluA1 staining, membrane surface proteins were blocked with gBB for 20 min followed by incubation with anti-N-terminal GluA1 mouse antibody (1/200; 30 min, RT).

Neurons were incubated for 1 h at RT with primary antibodies for the following epitopes: myc proto-oncogene protein (MYC; 1/1500; 986565, Invitrogen), humanised tau isoform 2N4R (tau13; 1/2000;

ab19030, abcam, MA, USA), total N-terminal region of glutamate ionotropic receptor subunit 1 (GluA1; 1/500; MAB2263, Merck-Millipore), N-ethylmaleimide-sensitive fusion protein (NSF; 1/500; 3924S, CST), total glutamate ionotropic receptor subunit 2 (GluA2; 1/400; SAB4501295, Merck), microtubule-associated protein 2 (Map2; 1/750; ab5392, abcam), post-synaptic density protein 95 (Psd95; 1/400; ab12093, abcam), endogenous mouse tau and humanised tau (tau5; 1/500; MAB361, Sigma), extracellular signal-regulated kinase 1 (Erk1; 1/500; PLA0235, Sigma), synaptosomal-associated protein 25 (Snap25; 1/1000; ab66066, abcam), and vesicle-associated membrane protein 2 (Vamp2; 1/500; 13508, CST).

Neurons were then washed three times with PBS and incubated with secondary antibodies and/or dyes for 1 h at RT. At 1/500 dilutions, the secondary fluorophore-conjugated antibodies used were: donkey anti-mouse Alexa-488 (A32766, ThermoFisher) and Alexa-594 (A32744, ThermoFisher), donkey anti-rabbit Alexa-350 (10039, ThermoFisher) and Alexa-405 (A48257, ThermoFisher), goat anti-chicken Alexa-647 (A32933; ThermoFisher), and donkey anti-goat (A11058, ThermoFisher). Filamentous actin was labelled with Alexa-488 phalloidin (1/1000; A12379, ThermoFisher). DNA was stained with 6-diamidino-2-phenylindole (DAPI; 1/1000; 62248, ThermoFisher), and biotinylated proteins were labelled with streptavidin-Cy3 (SA-Cy3; 1/500; S6402, Merck). After three final PBS washes, coverslips were transferred onto glass microscope slides with Fluoromount-G mounting medium (0100-01, SouthernBiotech).

Immunofluorescence imaging: All epifluorescence imaging of immunofluorescent-stained cells (**Fig 2.1D**) and histological sections (**Fig 2.2C**, **Appendix Fig S1A**-**B**) was performed using a BX51 bright field/epifluorescence microscope (UplanFL N lenses [∞/0.17/FN26.5]: 10x/0.3, 40x/0.75, Olympus, Tokyo, Japan) equipped with a DP80 colour camera (Olympus) operating through cellSens software (Olympus).

Confocal imaging of immunofluorescent-stained neurons was performed using two inverted confocal microscopes: (i) LSM 880 (ZEISS) with a 100X oil objective (aPlan-Apochromat 100X/1.46 oil, ZEISS) operating through ZEN (ZEISS) software (**Figs 2.4A**; **2.5C**,**F**,**H**; **SM Fig 2.4E,H,J**) and (ii) FV 3000RS IX83 (Olympus) imaged with a 100X oil objective (UAPON 100X oil, 1.49 NA, Olympus) with high-sensitivity spectral detectors (TruSpectral Detection, Olympus), operating through cellSens (Olympus) software (**SM Fig 2.4D**; **Appendix Fig S5C**,**F**).

Immunofluorescence imaging analyses: Image analyses were performed using Fiji [267] without prior knowledge of the performed experimental manipulation. Channel intensities were quantified from images with arbitrarily set and uniformly applied global thresholds.

To measure the spatial overlap of fluorescence signals from two channels, co-localisation analyses were performed for tau-NSF (**Fig 2.4A**) and NSF-GluA2 (**Fig 2.5H**; **SM Fig** 2.**4J**) using Fiji [267, 272].

To quantify relative neurite expression of NSF and surface GluA1 (**Fig 2.5C**-**E**; **SM Fig** 2.**4E**-**G**), whole neurons and neurites were first traced manually [273]. Within regions of interest, signal contribution in each channel was determined (% total of pixel^2) for NSF and surface GluA1 (normalised for total GluA1). Subcellular localisation of each signal was quantified by expressing neurite/neuron signal.

To quantify dendritic GluA2 in cLTP/cLTD (**Fig 2.5F**-**G**; **SM Fig 2.4H-I**), confocal image stacks (~3 µm z-axis) were first projected into a single two-dimensional plane. As an indicator of general activity and responsiveness to external stimuli, only neurons expressing YFP were used in the analyses – the AAV-mediated expression of YFP is under transcriptional control of the promoter of c-Fos, an immediate early gene. A region of secondary dendrite (dendrite after 2nd branching from somatic extension) spanning ~20 µm in length was cropped (n = 10-19 per genotype, per condition) and the dendritic GluA2 signal was manually traced [274]. To capture and quantify both punctate and distributed GluA2 expression in dendrites, total signal intensity from manual traces was expressed relative to area occupied by the corresponding Map2 signal. This tracing captured GluA2-containing AMPARs in both spinous process and extra-synaptic regions of secondary dendrites [275, 276].

Plasmid constructs: For biotinylation experiments, human MAPT gene encoding full length wild-type tau (hTauWT-FL, 441 amino acids) was cloned into the EcoRI (R3101S, New England Biolabs (NEB), MA, USA) site of plasmid myc-BioID2-MCS (#74223, AddGene) and amplified in DH5a Competent cells (Invitrogen, 18258012, ThermoFisher). Constructs for generation of AAV particles included – and were based on – pAAV-hsyn1-eGFP-WPRE (#58867, AddGene). The eGFP coding sequence was replaced with hTauWT-FL, myc-BioID2, and myc-BioID2-hTauWT-FL coding sequences at the BamHI (R3136S, NEB) site. AAV vectors were propagated in OneShot Stbl3 (C737303, Invitrogen, ThermoFisher) to avoid recombination events. For immunoprecipitation experiments, NSF was expressed from plasmid pcDNA3-FLAG-NSF (#74924, AddGene) and hTauWT-FL was expressed from pcDNA3.1-HA-hTauWT [223]. For immunoprecipitation and neuronal cLTP/cLTD experiments, the coding sequences for hTauWT-FL and hTauT205A were cloned into the SacI (R3156S, NEB) site of pcDNA3.2/V5-DEST (12489019, Invitrogen, ThermoFisher). For tau-NSF interaction mapping, tau variants (tauD236, tauD305, tauD368, tauWT-FL) were tagged with FLAG by cloning into the EcoRI site of pFLAG-c1 (provided by Dr Arne Ittner). For recombinant protein expression, the coding sequences for hTauWT-FL and NSF (744 amino acids) were each cloned into the NdeI (R0111S, NEB) and EcoRI sites of pHis17-MinD (provided by Dr Arne Ittner). For relative surface GluA1 expression in neuronal cLTP/cLTD, SEP-GluA1 was expressed from plasmid pCI-SEP-GluR1 (#24000, AddGene). Oligonucleotide primers for PCR-based generation of plasmid constructs are listed in **Primers** table. All ligation reactions were carried out using HiFi Assembly 2X Master Mix

(E2621S, NEB) and all PCR reactions using Q5 High Fidelity 2X Master Mix (M0492S, NEB). All constructs were verified by sequencing.

HEK293T cell transfection and cell lysis: HEK293T cells (CLR-3216, ATCC) were maintained in DMEM (11965092, Gibco, ThermoFisher) supplemented with 10% FBS (v/v), 1% penicillin/streptomycin (v/v), and 2 mM L-glutamine at 37°C, 5% CO_2, and 55% humidity. Cells were seeded on 60 mm plates (1.0 x 10^6 cells) 24 h before transfection and media was replaced 1.5 h prior to transfection. Plasmid DNA was transfected using polyethylenimine (PEI; 23966, Polysciences) at 80% confluency. Four micrograms of plasmid DNA and 12 µl of PEI were added to saline to a final volume of 420 µl. DNA was allowed to incubate for 15 mins and then added dropwise to each cell culture plate.

Recombinant protein production: Tau (full-length, truncated, internal deletion) and NSF were purified as done previously [5, 223] as 6xHis-fusion proteins from E. coli BL21(DE3)pLysS (C2527H, NEB) using His GraviTrap columns (11-0036-89, GE, ThermoFisher) followed by concentration and buffer exchange using ultrafiltration spin columns (15,000 molecular weight cut-off, UFC9003, Merck). Tau and NSF were suspended in either MST-compatible buffer (125 mM sodium phosphate pH 8.0, 150 mM NaCl, 1 mM EDTA, 1 mM ATP, 1 mM DTT, 10% glycerol) or ATPase assay-compatible buffer (50 mM TrisCl pH 8.0, 150 mM NaCl, 1 mM EDTA, 1 mM DTT, 10% glycerol).

Microscale thermophoresis: Microscale thermophoretic interaction measurements were done as previously described [223]. Fluorescent dye labelling of recombinant protein NSF was carried out as per manufacturer instructions (MO-L011, RED-NHS 2nd Generation, NanoTemper, Vic, AUS). Briefly, 50 µl of 600 µM dye solution was added to 450 µl of 20 µM hexameric NSF protein solution and incubated for 30 min in the dark at RT. Excess dye from the labelled NSF solution was removed using an equilibrated gravity flow column included in the labelling kit before a final elution in MST buffer modified to accommodate hexameric NSF protein structural and functional integrity (125 mM sodium phosphate pH 8.0, 150 mM NaCl, 1 mM EDTA, 1 mM ATP, 1 mM DTT, 10% glycerol) to final concentration 20 µM NSF [226].

For the MST interaction, recombinant tau protein in the same buffer was added to NSF solution and used for a 16-step serial dilution (1:1, vol:vol) with a final volume of 20 µl. Concentration of labelled NSF remained constant at 27 pM while tau concentration ranged from 18 mM to 0.275 nM. At the maximum concentration of unlabelled tau protein, all NSF binding sites were saturated (tau-NSF complex).

MST experiments were carried out using a Monolith NT.115 (NanoTemper, Munich, Germany). Experiments were performed at medium MST power at 25°C and LED power was set to 20%. MST

traces of normalised fluorescence were fitted to a one-site binding model to extract the K_D value from characteristic sigmoid concentration-response curve.

ATPase assay: The ATPase activity of 35 nM and 70 nM (hexameric) NSF under various conditions was quantified by measuring the amount of generated phosphate (Pi) from ATP hydrolysis using ATPase Assay Kit (ab270551, abcam) as per manufacturer instructions. Reactions were performed at 37°C for 30, 60, or 120 min, with ATP (0, 0.1, 0.3, 0.9, 2.5, 5 mM), and stable end-point signals were measured by a change in absorbance of PiColourLock (superior malachite green dye provided in the kit) in the presence of phosphomolybdate complexes using a spectrophotometer (640 nm wavelength). To test for Pi contaminants and intrinsic ATP hydrolytic activity, assay constituents (protein solutions, buffer, dH_2O, ATP) were first incubated with or without 1 mM ATP. All recombinant protein buffers were phosphate-free. Values for kinetic constants k_{cat}, V_{max}, and K_m were obtained by fitting data with the Michaelis-Menten kinetic model ($y = V_{max}(S)/(K_m + [S])$). Aβ preparation ($A\beta_{1-42}$; Bachem) for ATPase assays was prepared and pre-aggregated at a concentration of 100 µM as described [223]. To perform ATPase assay immunoprecipitated proteins, brain lysate was prepared in a mild lysis buffer (Tris pH 7.4 50 mM, NaCl 150 mM, EDTA 0.5 mM, Tween-20 0.5%, sodium deoxycholate 0.5%, SDS 0.1%, cOmplete protease tablet (Roche)), filtered through a 25-gauge needle, and centrifuged (10,000g, 15 min, 4°C). Supernatant lysate containing 400 µg protein was incubated with IgG antibody, or antibodies targeting tau protein (tau5; 1/500; ab80579; abcam) or amyloid-beta peptide (b-amyloid; 1/500; 8243; CST) (3 h, rotating, 4°C; ~350ul), followed by Protein-G beads (20 µL (NEB)) equilibrated with mild lysis buffer (1 h, rotating, 4°C). After three washes and resuspension in 210 µL ATPase assay-compatible buffer (Tris pH 7.4 20 mM, NaCl 150 mM, Tween-20 0.1%, $MgCl_2$ 2.5 mM, ATP 1 mM), recombinant NSF hexamer was added (5 nM) and solution was allowed to incubate (1 h, RT). Generated phosphate was determined by ATPase assays and the presence of NSF and tau by immunoblot with antibodies targeting tau (1/2000; 46687; CST) and amyloid-beta peptide (1/10,000; A1474; Sigma).

Statistics: Statistical analyses were performed using Prism (v8.2.0) (GraphPad). Overall inter-sample condition comparison of protein SC medians was performed using the non-parametric Mann-Whitney test. Inter-group multiple SC comparisons of individual biotinylated protein were performed using Fisher's Exact Test. Statistical significance was set at $p< 0.05$ (*), $p< 0.01$ (**), $p< 0.001$ (***), $p< 0.0001$ (****), and no significance (n.s.). Details on individual test parameters are provided in figure legends.

CHAPTER THREE

TAU-ASSOCIATED PROTEIN-PROTEIN INTERACTION NETWORKS IN NEURONAL ENSEMBLES OF MEMORY

This chapter is based on a manuscript currently in preparation.

Author contributions:

Author	*Research design (%)*	*Data collection and analysis (%)*	*Writing and editing (%)*
Prikas, E	47	80	92
Poljak, A	3	10	3
Ittner, A	50	10	5
Total	**100**	**100**	**100**

Table of abbreviations

Abbreviation	Meaning
IEG	Immediate early gene
PPI	Protein-protein interaction
BioID	Biotin identification
MiniTid	MiniTurboID
rAAV	Recombinant adeno-associated virus
RAM	Robust Activity Marking
d2tTA	Destabilised tetracycline transactivator
TRE	Tetracycline-transactivator response element
Dox	Doxycycline
MWM	Morris Water Maze
EC	Encoding-Consolidation
RRc	Retrieval-Reconsolidation
ECRRc	Encoding-Consolidation-Retrieval-Reconsolidation
pSyn1	Neuronal human *Synapsin-1* minimal promoter
SA	Streptavidin
rSoWP	Relative sum of weighted performance
RM	AAV.RAM-MiniTid
RMT	AAV.RAM-MnTid-tau
SM	AAV.Syn1-MnTid
SMT	AAV.Syn1-MnTid-tau
NCC	Non-cue controls
PO	Protein ontology
POI	Proteins of interest

Introduction

Memory refers to the cognitive processes of encoding, storing, retaining, and retrieving sensory information from previous events and experiences [277]. Memories are a consequence of learning, which may be explicit (declarative, conscious), or implicit (non-declarative, unconscious) [278]. Explicit memories can be processed sensory information with specific attached meaning (sematic)

and/or with a specific spatiotemporal component (episodic) [279]. Implicit memories include the unconscious learning and retrieval of procedures (e.g., tying shoelaces), unconscious associations (e.g., name of an individual and a particular scent), and priming, whereby exposure to one stimulus affects one's response to a subsequent target stimulus, (e.g., faster recognition of target word 'referee' following priming word 'football' rather than 'cupboard') [280-282]. In either case, memory processes often involve environmental stimuli causing internal psychophysical changes with enduring and latent features [28, 283, 284]. Memory function is crucial for living organisms capable of learning because it permits contextualisation of current and future events by referencing previous events. The retention and retrieval of relevant information can be evolutionarily adaptive when applied to make decisions or taking actions that prolong survival, reproductive success, and flourishing [285].

Despite these characterisations of memory, there is a lack of answers to seemingly fundamental questions about where memories are stored and how memories are maintained and retrieved. This suggests that our knowledge of molecular mechanisms underlying memory processes must be incomplete.

Our current understanding of memory is conceptually linked to the engram: the physicochemical changes in a neuronal network that constitute a memory trace, based on Hebbian principles of learning [28, 98]. The memory trace, or engram, is formed by a set of neurons that are activated and modified while learning about an event, location or fact (integrated external and interoceptive sensory stimuli), and reactivated upon re-exposure to the same experience, leading to a change in behaviour [286]. While cells recruited to the engram undergo changes in excitability and synaptic plasticity [287-289], underlying molecular adaptations ensuring the formation and enduring existence of an engram cell ensemble remain largely unknown.

The formation of engrams is preceded by neural circuit plasticity and experience-dependent gene transcription [290, 291]. Engram technologies exploit this knowledge with transgenic model organisms and viral vectors engineered to competitively bind promoters of endogenous neuronal activity markers: immediate early genes (IEGs) such as *Fos* and *Arc* [292, 293]. Tetracycline-responsive control systems allow targeted cell labelling during specific phases of learning or testing paradigms [294, 295]. Viral vectors allow expression of fluorescent protein activity markers alongside light-sensitive ion channels (LSICs) [296]. Cell surface expression of LSICs during learning in context A allows for later optogenetic manipulation of cell activity in novel context B, to induce a behaviour consistent with (false) memory recall, e.g., fear response (freezing) following a tone that was previously associated with a foot shock in context A [293, 297]. This suggests that an electrochemical association between some specific subset of hippocampal neurons partially underlies the elicitation of an observable behaviour (here, freezing).

Despite the success of optogenetic technologies in identifying engram cell ensembles, investigations have primarily focused on implicit associative memory using contextual/cued fear conditioning paradigms [298, 299]. Reactivating engram cell ensemble sequences to emulate more complex implicit procedural memories or explicit episodic memories with spatiotemporal components pose a bigger challenge. Moreover, the proportional changes in distributed brain-wide activity that represent features of longer-term memories (e.g., hippocampus-dependent neocortical rearrangements) are not easily recapitulated by optogenetic manipulations [300, 301]. Another limitation is that learning-induced changes in brain regions associated with memory involve integration of multiple sensory stimuli [302]. Direct light stimulation to activate those memory regions bypasses a relevant, yet unanswered question in memory research: What are the mechanisms that select neurons to ultimately be recruited to the engram? Answering this question requires a higher resolution approach that links electrochemical activity of engram-recruited cells to molecular interactions that underlie changes within these cells.

The ability to tag, activate, inhibit, and modify neurons has made it possible to address underlying cellular and molecular mechanisms of engram cell ensembles. While it is necessary to investigate biological mechanisms required for memory processes, we must further determine how the processed information from these experiences is integrated and maintained discretely and discriminably until retrieval and beyond. Many studies report a link between both formation and retrieval of memory and enhanced synaptic connectivity [303-305]. Initial changes to synaptic structures of communicating neurons are immediate responses to activity that require dynamic, often transient protein-protein interactions (PPIs) [306, 307]. Proteins associated with synaptic vesicles, actin-binding proteins, and glutamate receptors are recruited from nearby synapses [308-311]. These synaptic changes influence the probability of downstream longer-term processes such as protein synthesis- and gene expression [312, 313]. Hence, a targeted focus on PPIs may reveal, in further detail, how preliminary, dynamic, plasticity-associated interactions shape more stable and prolonged changes in cells and cell states. Much progress has been made in delineating timescales across which molecular mechanisms linked to learning and memory do or do not require protein synthesis or differential gene expression, yet the search for how and where memories are stored continues.

Global methods of characterising engram cells rely on activity-dependent changes in transcriptomic and epigenomic signatures [314]. While engram labelling may occur in physiologically relevant conditions, preserving the native expression profile and minimising RNA transcript degradation during processing and preparation of samples are critical but remain challenging [315, 316]. Fluorescence labelling for later isolation and single-cell RNA sequencing using single IEG promoters may bias the number and type of engram cell populations [317, 318]. This is because different ensembles using different IEGs and different functional circuitry may coexist within the same engram, or multiple non-

overlapping cell populations under different IEG control are activated by the same stimulus [317, 318]. The misrepresentation of engram cell identities can be mitigated by using multiple promoters and labelling probes, or by using a synthetic IEG promoter with binding elements for multiple IEG-associated transcription factors [319]. Another methodological limitation of IEG promoter-driven fluorescent protein labelling is the inability to distinguish activity-dependent 'experience' cells (background) from activity-dependent 'memory' cells [320]. Missing from the current literature is an approach able to discriminate memory-dependent from experience-dependent molecular events using extensive and appropriate control conditions. Labelling active cells in control mice that are subjected to memory-independent 'versions' of the same behaviour tests as experimental mice would provide a comparable experience between cohorts whilst generating background data to subtract from the experimental condition read-outs. This gap in approach suggests a gap in knowledge in the interrogation of RNAseq data, optogenetic manipulations of cell-cell interactions, and protein-protein interaction identification methods.

The literature dedicated to understanding molecular mechanisms that underlie memory processes focuses heavily on activity-dependent gene expression [314, 321]. Yet only protein interactions (protein-protein, protein-DNA, protein-RNA) mediate and regulate all critical processes linked to learning and memory function – from dynamic synaptic interactions to protein synthesis and transcription [148, 210, 211]. An experimental approach relying on a phenomenon as ubiquitous as protein interactions to investigate and understand memory processes *in vivo* must focus on specific and localised interactions in relevant cells in mouse brain during and/or after performing memory tasks, with appropriate controls for protein- and task-specificity.

I previously mapped tau protein interactions in cultured neurons and in living mouse brain tissue using BioID2 (**Fig 2.1**), [214, 216]. These proteins included cytoskeletal regulation factors, synaptic and vesicle cycle factors, and relevant functional interactions that had not previously been investigated. The tau interaction networks revealed pre- and postsynapse localising NSF and associated synaptic vesicle proteins as tau interactor candidate in mouse brain at steady state. Whether this reflects the tau interactome of a smaller subset of neurons is unknown, yet NSF may be a target of tau in engram neurons [322]. Upon targeted investigation, tau-NSF interactions reduced NSF ATPase activity and reduced the stability of AMPARs at synapses in culture models of synaptic plasticity (**Fig 2.5**). Furthermore, the tau-NSF interaction is important for fear conditioning and object recognition memory, whereby the compromised test performance of tau-positive mice resembled that of mice infused with an NSF inhibitor (**Fig. 2.6**). Whether these or other functional tau interactions specifically occur in engram cells and mediate functions that support learning and memory remains unclear.

Tau may engage in specific interactions in the engram. The dynamic gene regulatory networks of engram cells, from recruitment to reactivation at recall may affect engram tau localisation and

interactions [323]. Activity-dependent IEG expression following initial engram recruitment leads to the transcription of genes associated with ongoing activation and neuronal excitability [324]. During later phases of memory consolidation and retrieval, gene transcripts are enriched with synaptic receptors and channels, and new synapses form [323, 325]. Changes in gene expression may result in specific proteomes and subsequently permitting specific protein interactions. Therefore, defined protein interaction networks may be linked to engram cell ensemble states that reflect specific phases of the learning and memory process.

Tau interactions may mediate the function of a cell ensemble that supports learning and memory of a specific behavioural task. The role of tau in neurons that form engrams, or cellular traces of memory, in the brain has not been explored. I hypothesised that neuronal tau protein interactions, including within memory engram cells, were critical for both neuronal function and within a connected circuit associated with learning and memory processes.

To this end, I further characterised the role of tau in memory by investigating how tau interactions are affected during different phases of spatial memory. I developed a strategy for engram-specific proximity labelling of tau interactors in mouse brain during spatial learning and memory. Key tau interactions specific to engram states were identified, which differed from the general tau interaction profile during memory processes or at rest. Selected state-specific network proteins were confirmed as bona fide tau interactors, suggesting a significant link between tau function and mechanisms underlying learning and memory. These experiments together provide the first engram-specific tau interactomes from behaving mice and link physiologic events across multiple layers of system analysis, from molecular interactions to complex animal behaviour.

Results

Activity-dependent expression of MiniTurboID-tau for labelling interactions during spatial learning and memory

The first aim was to establish a method for labelling tau protein-protein interactions (PPIs) in the hippocampus of behaving mice. This required a feasible experimental strategy for labelling PPIs in cells active during a spatial memory task and discriminating them from spatial task-independent labelled PPIs. The biotin identification (BioID) technique was used previously to label transient and stable PPIs in neurons and mouse brain [214, 216]. Biotinylation enzyme MiniTurboID (from here, MiniTid) is a truncated genetic mutant of E. coli *BirA*, which reduces potential steric interference relative to the larger BioID2 used in chapter 2 [326]. Due to the truncation and a substitution of 14 amino acids in its primary sequence, MiniTid has high biotinylation efficiency and very low background labelling [326]. To identify tau-specific interactions, I cloned this modified bacterial biotin ligase with a FLAG identification tag 'FLAG-MiniTurboID' fused to the N-terminus of tau (MiniTid-tau). Preliminary tests showed that biotinylated proteins were detected in cells expressing MiniTid within 60 min of incubation in biotin-enriched medium (**SM Fig 3.1A**) but has been reported in as little as 10 min [326]. The enhanced catalytic efficiency, low background labelling, and the limited packaging capacity of recombinant adeno-associated virus (rAAV) made MiniTid the most suitable enzyme for labelling dynamic and temporally specific interactions that underlie memory processes.

To restrict MiniTid expression – and hence, biotinylation – to active neuronal ensembles, we used the Robust Activity Marking (RAM) system that can be packaged in rAAV vectors [319]. The system is based on an engineered promoter containing DNA motifs for binding of activity marker c-Fos, a transcription factor that is critical for neural circuit function and plasticity, as well as the binding motif of neuronal activity-dependent gene *Npas4*, for enhanced specificity and sensitivity [319, 327]. The synthetic RAM promoter (pRAM) has low reporter gene expression during basal conditions and exhibits strong and sensitive activity-dependent expression in neurons [319]. A second feature of the RAM system is that pRAM drives expression of a destabilised tetracycline transactivator (d2tTA), which minimises an otherwise accumulating stable tTA from binding to the tTA-responsive element (TRE) outside of the experimental testing window (**Fig 3.1A**) [319]. For enhanced temporal control of effector gene transcription, d2tTA binds TRE in the absence of doxycycline (Dox-Off), upstream of the fusion protein MiniTid-tau DNA sequence (**Fig 3.1A**). Combining the RAM system with proximity labelling proteomics allows for temporal control of activity-dependent expression and labelling in the presence of biotin.

For localised MiniTid expression with and without tau (MiniTid(+/-tau)) and recovery from surgery, I performed bilateral hippocampal rAAV injections by stereotactic surgery (day 3) and necessarily

allowed mice 7 days to recover (**Fig 3.1B**). To eliminate tau binding competition between endogenous and episomally expressed MiniTid-tau, *tau* knock-out mice (*tau*$^{-/-}$) mice were used. To induce spatial learning and memory, mice underwent the Morris Water Maze (MWM) task [328]. To minimise expression of the fusion protein in active neurons not associated with MWM (during recovery from surgery), mice were placed on doxycycline from two days prior to surgery (day 1) until two days prior to MWM (day 9) (**Fig 3.1B**). This allowed for accumulation to – and depletion from – an effective steady state level of systemic doxycycline respectively, prior to MWM. To ensure efficient spatial learning and to promote proximity-labelling in task-dependent neurons, mice were habituated to the MWM ~12 h prior to the first biotin injection (day 10) (**Fig 3.1B**). For proximity labelling from MWM day 1 (day 11), subcutaneous biotin injections in some mice began on day 10. Mice were allocated to one of three biotin injection schedules and to one of two sacrifice time points across days 10-16 of the experiment, in a total of three groups (**Fig 3.1B**). These combinations were chosen in accordance with the phases of spatial learning and memory being interrogated. Labelling was largely restricted to the hippocampus because this brain region is necessary for spatial learning and memory [329]. Limiting MiniTid-tau expression and labelling to hippocampal cells active during spatial learning and memory (**Fig 3.1C**; *left*, *red nodes*) maximised the proportion of biotinylated (labelled) proteins that were recovered from these cells, for identification by mass spectrometry (**Fig 3.1C**; *centre-right*). The resulting lists of protein identities served as inputs for the functional association PPI database STRING [330] (**Fig 3.1C**; *far right*). The purpose for using this database was to generate a network interaction overview for further detailed analysis of the tau interactor candidates.

This overview described three key elements of the experimental strategy towards generating tau engram interactomes: (i) activity-dependent expression and (ii) tau-specific labelling during (iii) one of three phases of spatial learning and memory in mice. The next two figures are targeted to expression and labelling of MiniTid constructs (**Fig 3.2**) and to inducing spatial learning and memory in mice during the MWM task (**Fig 3.3**).

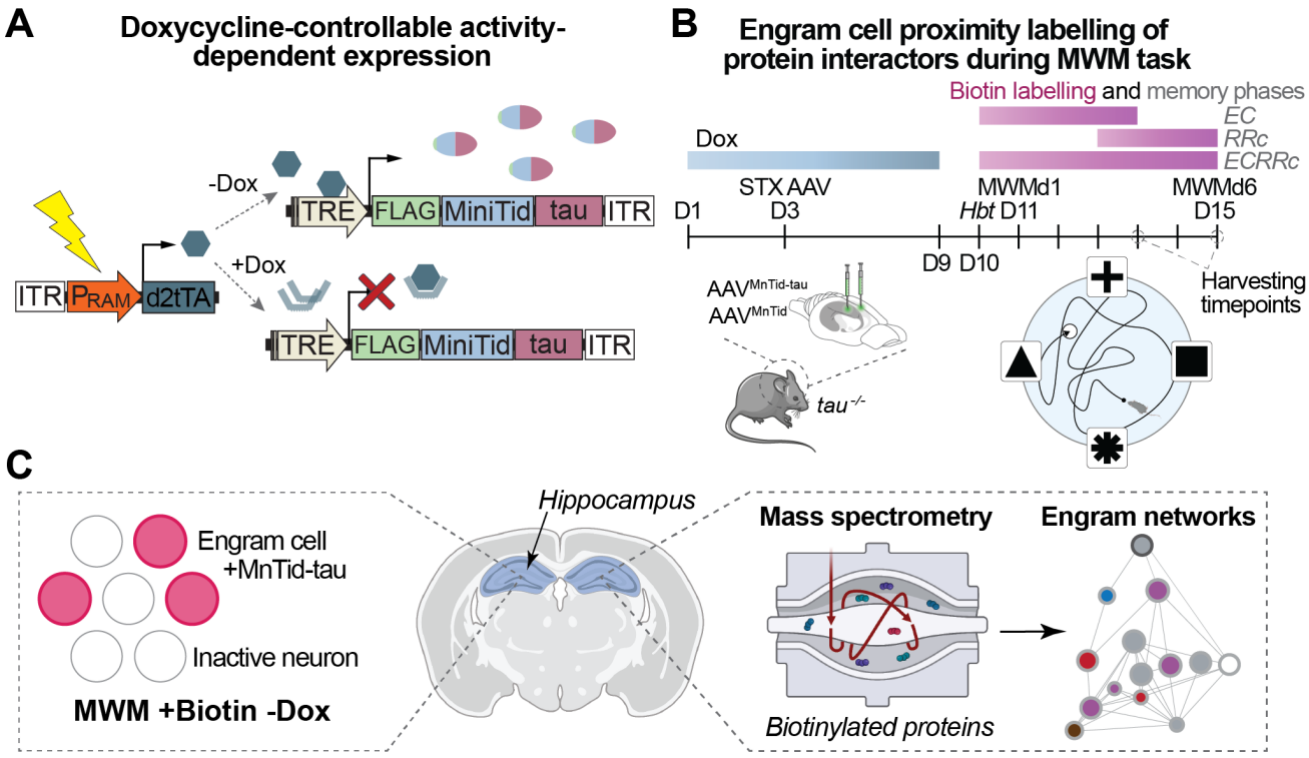

Figure 3.1. ***Theoretical and experimental strategy for proximity labelling of tau interactors in active engram cells***.

(**A**) Expression of MiniTurboID-tau in active neurons, under control of doxycycline. Schematic of Dox-OFF system with RAM promoter (pRAM) driving expression of destabilised tet transactivator (d2tTA). Binding of d2tTA to promoter tet-transactivator response element (TRE) is inhibited by doxycycline (+Dox), where removal (-Dox) allows transcription of fusion protein FLAG-MiniTurboID-tau (MiniTid-tau).

(**B**) Experimental schematic overview for spatial task-dependent proximity labelling. Tau knock-out (*tau*$^{-/-}$) mice on doxycycline chow were stereotactically (STX) injected with AAV.MiniTid(+/-tau). Mouse chow containing doxycycline was replaced with normal chow two days prior to commencing the Morris Water Maze (MWM) task to allow expression of MiniTid(+/-tau). Depending on the interrogated memory phase, mice were harvested on MWM days 4 or 6 after subcutaneous biotin injections on day 10 to MWMd4 (encoding-consolidation, EC), MWMd3-6 (retrieval-reconsolidation, RRc), or day 10 to MWMd6 (learning-consolidation-retrieval, ECRRc).

(**C**) Model showing theoretical neuronal and engram cell states. Tau interactor labelling in hippocampus (blue shaded area) during MWM is constrained to active neurons in the absence of doxycycline and in the presence of biotin (*red node*). Labelled proteins identified by mass spectrometry are used to generate networks based of functional associations in the STRING interaction database [330].

To label proteins in mouse brain during the MWM task, mice were assigned to one of four rAAV conditions (**Fig 3.2A**). These differed by whether tau was fused to the MiniTid labelling enzyme and by the promoter controlling the expression of the labelling protein (**Fig 3.2A**). Mice in the experimental group expressed MiniTid-tau under the control of pRAM for tau-specific labelling in activity-dependent cells during the MWM task (**Fig 3.2A-B**). The first control condition was to have mice expressing MiniTid, also under pRAM control, for non-specific activity-dependent labelling during MWM (**Fig 3.2A-B**). The second and third rAAV controls were mice expressing labelling proteins MiniTid-tau or MiniTid driven by neuronal human *Synapsin-1* minimal promoter (pSyn1) [331]. In the pSyn1 groups, the labelling proteins began expressing in neurons upon removal of Dox from the mouse feeding

schedule, regardless of the behavioural task (**Fig 3.2A**-**B**). Comparison of MiniTid-tau labelled proteins under control of pRAM versus pSyn1 separated tau interactions in active cells from tau interactions under 'basal' conditions. A Venn diagram and table were used to visualise and summarise the conditions under which cellular proteins were differentially labelled in each rAAV group (**Fig 3.2C**). Lists of proteins labelled under these four conditions formed the basis for later inter-group comparisons and background subtraction in generating tau engram interactomes. Therefore, a crucial next step was to confirm the expression and labelling functionality of these rAAV constructs.

Immunoblot of hippocampal (HC) lysates confirmed the expression of MiniTid-tau and the absence of endogenous tau in *tau*$^{-/-}$ mice (**Fig 3.2D**-**E**). FLAG signals indicated the expression of MiniTid with or without tau (FLAG-MiniTid-tau, FLAG-MiniTid). The strength of FLAG signals confirmed comparable expression of pRAM-FLAG-MiniTid-tau throughout MWMd1-6 (**Fig 3.2D**). In a second attempt to confirm expression, the FLAG signal was slightly stronger on MWMd6 relative to MWMd2 in both pRAM- and pSyn1-driven MiniTid-tau expression (**Fig 3.2E**). Similarly, the FLAG signal appeared slightly stronger at 7 days off doxycycline relative to 4 days, in HC of pRAM-MiniTid mice (**Fig 3.2F**). I next analysed the effect of localised HC injections of AAV.RAM-MiniTid-tau and AAV.RAM-MiniTid on biotinylation levels in the HC relative to the cortex (CTX). Two streptavidin (SA) blots were used to compare the HC and CTX of 10 mice and despite 500% the initial mass of protein lysate in the CTX samples, the SA-HRP signal from the HC lysates appeared consistently stronger across MWd1-6 (**Fig 3.2G**-**H**). Therefore, localised expression of functional labelling enzymes MiniTid-tau and MiniTid, and not just elevated circulating biotin, led to a localised increase in protein biotinylation (**Fig 3.2G**-**H**).

Immunostaining and imaging of endogenous IEG activity markers suggest that different features of a memory are associated with engram cell ensembles, distributed across multiple brain regions [300, 332]. In the dentate gyrus, engrams represent the contextual component (conditioned stimulus) of a fear-associated memory [292, 300]. This, in part, includes a crucial spatial component, which is necessary for contextual memory formation [333, 334]. In successful contextual memory retrieval, neurons activated during learning are reactivated [300, 335]. Synthetic activity-dependent labelling systems significantly overlap with endogenous hippocampal IEG expression following multiple exposures to the same context, but not to different contexts [297, 319, 336]. The overlap supports a link between a specific engram cell ensemble and a specific context, and for the role of hippocampal neurons in context memory. To visualise activity-dependent expression and biotinylation following a spatial memory task, HC from mice expressing MiniTid or MiniTid-tau following MWMd6 were labelled for FLAG tag with an antibody and for incorporated biotin with SA (**Fig 3.2I**). A consistent FLAG signal confirmed comparable levels of pRAM- and pSyn1-driven MiniTid-tau and MiniTid expression (**Fig 3.2I**, *column **1***). The FLAG signal was detected in all rAAV groups (**Fig 3.2I**, *column **1***), despite previous reports of potential MiniTid instability and of relatively sparse engram activation in the

dentate gyrus during the MWM task [326, 337]. Signals for FLAG overlapped with SA in the dentate gyrus, and *Cornu ammonis* 1/2 (CA1, CA2) in all rAAV groups (**Fig 3.2I**, *column **5***). The non-overlapping regions of FLAG and SA indicate interactor labelling (**Fig 3.2I**, *column **5***). Together, these histological analyses indicate that both activity-dependent and constitutive expression of MiniTid constructs can label proteins in the HC of behaving mice.

Taken together, these results support the first successful application of an activity-dependent gene expression system together with proximity labelling proteomics. Labelling occurred within the time frames relevant to characterise the spatial engram. Furthermore, labelling was localised to cells in the HC activated during the MWM spatial memory task.

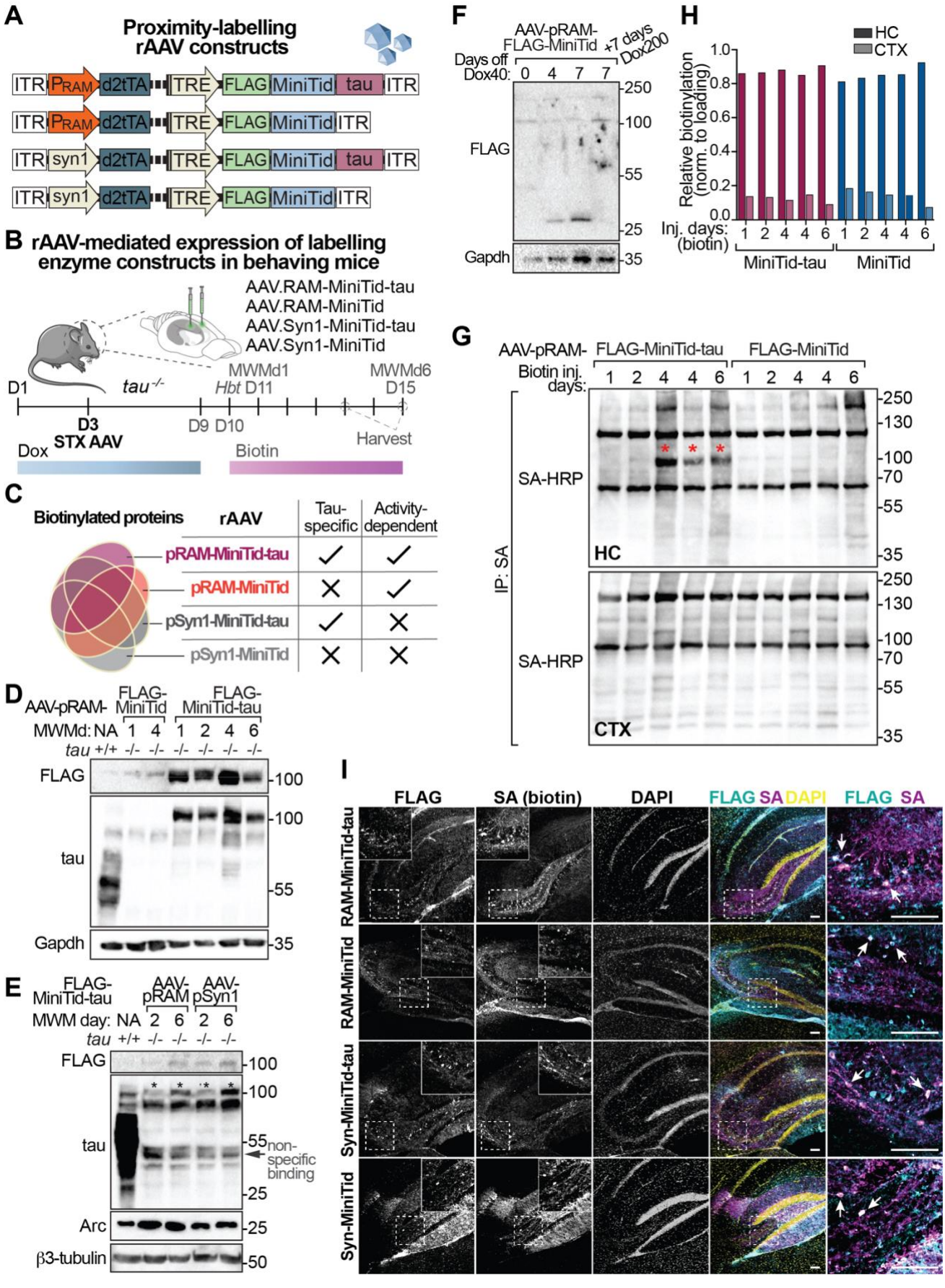
A
Proximity-labelling rAAV constructs
ITR PRAM d2tTA TRE FLAG MiniTid tau ITR
ITR PRAM d2tTA TRE FLAG MiniTid ITR
ITR syn1 d2tTA TRE FLAG MiniTid tau ITR
ITR syn1 d2tTA TRE FLAG MiniTid ITR
B rAAV-mediated expression of labelling enzyme constructs in behaving mice
AAV.RAM-MiniTid-tau
AAV.RAM-MiniTid
AAV.Syn1-MiniTid-tau
AAV.Syn1-MiniTid
D1
tau -/-
MWMd1
Hbt D11
MWMd6
D15
D3
STX AAV
D9 D10
Harvest
Dox
Biotin
C
Biotinylated proteins
rAAV
Tau-specific
Activity-dependent
pRAM-MiniTid-tau
pRAM-MiniTid
pSyn1-MiniTid-tau
pSyn1-MiniTid
D
AAV-pRAM-
FLAG-MiniTid
FLAG-MiniTid-tau
MWMd: NA 1 4 1 2 4 6
tau +/+ -/- -/- -/- -/- -/- -/-
FLAG
tau
Gapdh
100
100
55
35
E
FLAG-MiniTid-tau
AAV-pRAM
AAV-pSyn1
MWM day: NA 2 6 2 6
tau +/+ -/- -/- -/- -/-
FLAG
tau
Arc
β3-tubulin
100
100
55
non-specific binding
25
25
50
F
AAV-pRAM-FLAG-MiniTid
+7 days Dox200
Days off Dox40: 0 4 7 7
FLAG
Gapdh
250
100
55
25
35
H
HC
CTX
Relative biotinylation (norm. to loading)
1.0
0.8
0.6
0.4
0.2
0.0
Inj. days: (biotin) 1 2 4 4 6 1 2 4 4 6
MiniTid-tau
MiniTid
G
AAV-pRAM-
FLAG-MiniTid-tau
FLAG-MiniTid
Biotin inj. days: 1 2 4 4 6 1 2 4 4 6
IP: SA
SA-HRP
HC
SA-HRP
CTX
250
130
100
70
55
35
I
FLAG
SA (biotin)
DAPI
FLAG SA DAPI
FLAG SA
RAM-MiniTid-tau
RAM-MiniTid
Syn-MiniTid-tau
Syn-MiniTid

Figure 3.2. ***Temporally controlled and activity-dependent expression for proximity labelling in mouse spatial memory.***

(**A**) Adeno-associated virus (AAV) constructs for the activity and/or neuron-specific expression of MiniTurboID-tau or MiniTurboID control. RAM – robust activity marker; d2tTA – destabilised tet transactivator; TRE – tet-transactivator response element; Syn-1 – synapsin-1 minimal promoter; WPRE – Woodchuck Hepatitis Virus Post-transcriptional Regulatory Element; ITR – inverted terminal repeat.

(**B**) Experimental schematic emphasising the hippocampal injection of rAAV constructs in *tau*$^{-/-}$ mice on day 3. Expression of labelling constructs MiniTid-tau and MiniTid was supressed by doxycycline until two days prior to commencing the MWM task.

(**C**) Venn diagram and table comparing features of rAAV constructs for biotinylating proteins in behaving mice. Labelling is either neuronal and activity-dependent (pRAM) or neuronal (Syn1) and either tau-specific or non-specific (+/-tau). Labelling is most conditional for AAV.pRAM-MiniTid-tau, being both activity-dependent and tau-specific.

(**D**-**F**) Immunoblots of mouse brain lysates showing expression of MiniTid-tau and MiniTid at multiple experimental time points. (**D**) Immunoblot of hippocampal lysates from *tau*$^{-/-}$ mice harvested at MWM days 1/2/4/6. Expression of MiniTid-tau was detected by anti-tau antibody staining. Loading, glyceraldehyde-3-phosphate dehydrogenase (Gapdh). (**E**) Immunoblot of hippocampal lysates from *tau*$^{-/-}$ mice harvested at MWM days 2 and 6. The expression of MiniTid-tau was detected by staining with anti-FLAG and anti-tau antibodies. Asterisks (*) indicate detection of tau, indicating fusion protein expression on the anti-tau immunoblot. Loading, activity-regulated cytoskeleton-associated protein (Arc); beta-3 tubulin. (**F**) Immunoblot of hippocampal lysates from *tau*$^{-/-}$ mice harvested at 0-, 4-, and 7-days following doxycycline (Dox40) removal from the diet and following 7 days of Dox reintroduction (Dox200). The expression of MiniTid was detected by staining with and anti-FLAG antibody. Loading, Gapdh.

(**G**-**H**) Precipitation of biotin-labelled proteins from 200 µg hippocampus (HC) protein per lane and 1000 µg cortex (CTX) protein per lane of mice following 2/4/6 days of biotin injections. Biotinylated proteins in brain lysates of mice expressing MiniTid(+/-tau) were precipitated using streptavidin (SA) and detected using HRP-conjugated SA (SA-HRP). Asterisks (*) indicate fusion protein self-biotinylation. (**H**) Densitometric quantification of SA-precipitation results in (G).

(**I**) Confocal immunofluorescence images of sagittal mouse hippocampal sections. Hippocampal slices were immunostained for MiniTurboID(+/-tau) (FLAG), for incorporated biotin (streptavidin, SA), and for cell nuclei (DAPI). Representative samples from n = 3 biological replicates. Insets of magnified hippocampus with partial overlap of FLAG and SA signals (arrowheads). Scale bars, 200 µm.

Inducing efficient spatial learning and memory for proximity labelling during the MWM task

Hippocampal CA1/CA3 place cells form spatial maps (internal representations of space) that activate when an animal visits place fields (i.e., a specific location in the environment) [92, 338]. During a virtual navigation task, high *Fos*-responsive CA1 neurons encode accurate spatial maps [339]. In a MWM task, targeted inhibition of Fos-positive neurons activated during MWMd1 impaired performance on MWMd2 [337]. Therefore, to induce spatial learning and memory, mice were trained to find a hidden platform using distal cue navigation in the MWM [328]. Acclimation to the water and to climbing the platform kept the task timeline to six days and improved task performance metrics on days 1-4 compared to non-habituated mice (**SM Fig 3.2A**). Days of subcutaneous biotin injections were based on four phases of spatial learning and memory linked to MWM performance (**Fig 3.3A**) [340, 341]. For biotinylation of interactors during encoding and consolidation (EC), mice assigned to

this group were administered with daily biotin injections until harvest point MWMd4, beginning one day prior to MWMd1 (**Fig 3.3A**). For biotinylation of interactors during retrieval and reconsolidation (RRc), mice assigned to this group were administered biotin on MWMd3-6 (**Fig 3.3B**). For biotinylation of interactors across all four phases of spatial learning and memory, (ECRRc), mice assigned to this group were injected with biotin for seven days ending on MWMd6 (**Fig 3.2B**). Based on previous measures of pRAM-driven fluorescent reporter gene expression after fear conditioning, HCs were dissected 1.5 hours after the last MWM trial to maximise the preservation of labelled proteins [319].

The reasoning for the memory phase categorisations is based on well-established performance improvement trajectories of mice across multiple days of performing the MWM [328]. On the initial day of MWM training, mice have no relevant spatial memory to draw from to complete the task, and so retrieval is absent. On day 1, mice can only be encoding and consolidating MWM-associated spatial memories. While this continues throughout all 6 days of MWM, the amount of new information encoded (and thus consolidated) is arguably at maximum on day 1 and at minimum by day 6. As performance improves through training, task-relevant memories accumulate, making retrieval (and reconsolidation) more desirable to efficiently complete the MWM task. So, while memories are destabilised each time they are retrieved and modified by encoding prior to being (re)consolidated, encoding and consolidation are likely highest on MWMd1, whereas retrieval and reconsolidation predominate by MWMd6.

I aimed to identify proteins that were representative of interactions in neurons linked to successful spatial learning and memory. To ensure this link between interactors and learning/memory, I quantified the task performance metric of 'latency to platform' that acted as a cut-off for collection and pooling of HC for further processing [342]. Because of ongoing MWM experiments (increasing *n* numbers), the cut-off could not be based on rank order of performance. Comparing linear regression slopes was inadequate due to low goodness of fit values (R^2) from to day-to-day variability in individual performing mice. Instead, to measure improvement over 4 or 6 days while still accounting for performance on any single day, average daily latency to platform from 4 trials was weighted and summed for each half of the 4-day or 6-day MWM experiment (Sum of Weighted Performance, SoWP; **Fig 3.3B**). The second half performance was expressed relative to the first half (relative SoWP, rSoWP; **Fig 3.3B**). For mice harvested at timepoint MWMd4, the minimum necessary improvement was 15% (rSoWP > 15%), while for the MWMd6 timepoint, the cut-off was a 30% improvement (rSoWP > 30%) (**Fig 3.3B**). Mice above the cut-off were categorised as 'high performers' whereas those below the cut-off were 'low performers'. In total, ~18% (n = 24) of all mice (n = 135) were deemed to be 'low performers' (**SM Fig 3.3B**) and either excluded from further analyses or pooled with 'non-cue controls' as 'non-learners' in network comparisons. All non-cue controls incidentally also failed to reach the cut-off, supporting an appropriately set arbitrary cut-off and confirming the reliance

on distal cues for navigating to the hidden platform (**SM Fig 3.3B**) [342]. Approximately 80% of 'low performer' mice employed non-spatial strategies such as excessive thigmotaxis or floating. Therefore, this performance quantification and cut-off was more stringent than traditional subjective approaches to eliminating outliers in the MWM task. Performance in the MWMd1-4/6, measured by latency to platform, is shown for all mice combined and is overlayed by performance of the four constitutive cohorts, separated by rAAV condition (**Fig 3.3C**). To minimise the potential effect of extinction on spatial memory, and subsequently on memory-independent labelling, probe trials were not conducted [342, 343]. There was no measurable difference in performance between rAAV groups (**Fig 3.3C-D**), so the potential differences in biotinylated protein lists were attributed to the bait protein tau and not to different performance outcomes.

Some hippocampal cells respond to experiences independently from engram cells that activate to encode components of experience [99]. Therefore, limiting the range of experience and maximising learning would preferentially activate neurons involved in memory. Together, the strategies of habituation and confirming high performance in the MWM task were aimed towards maximising recovery of proteins labelled in memory-activated cells but not experience-activated cells. This maximisation of protein labelling in spatial learning/memory-associated neurons set the stage for isolating and identifying tau interactor candidates from engram cells.

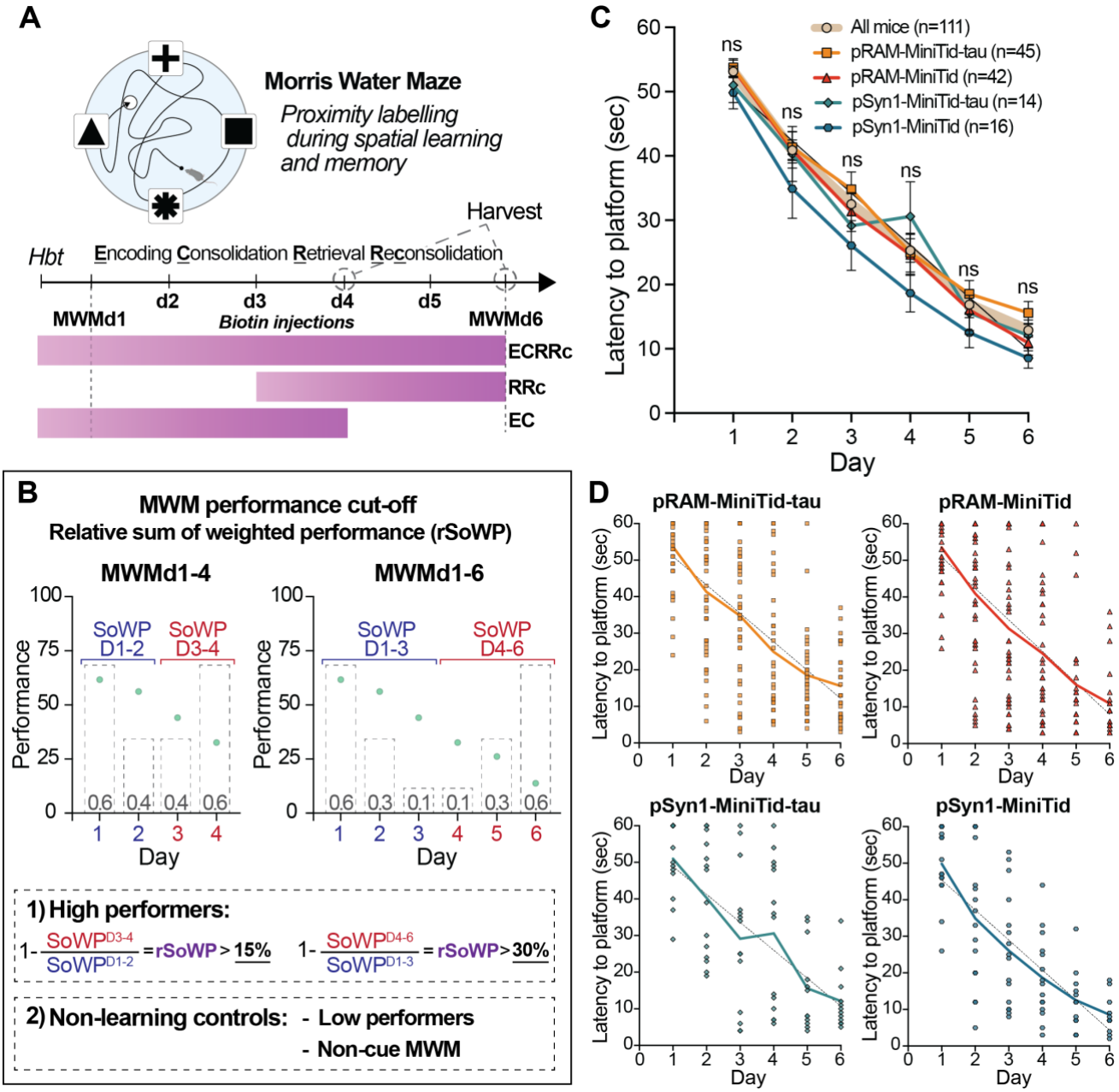

Figure 3.3. ***Habituation and performance cut-offs ensured robust spatial learning and memory in the MWM task.*** Biotinylation in memory-associated cells is maximised when the source of task-dependent cell activity is high performing mice.

(**A**) Daily subcutaneous biotin injections corresponding to spatial memory phases. For proximity labelling during all spatial memory phases (ECRRc), mice were injected for 7 days until MWMd6. For labelling during retrieval and reconsolidation (RRc), mice were injected on MWMd3-6. For encoding and consolidation (EC), mice were injected for 5 days until MWMd4. Habituation (Hbt) of mice to water and the platform on day 10 aided early learning (see **SM Fig 3.2A**). Mice were harvested on their allocated final day of the MWM (d4 or d6).

(**B**) Performance cut-offs for mice performing in the MWM task over 4 or 6 days. The mean performance value was weighted for each day and summed into a value representing the first and second half of either 4 or 6 days of MWM (sum of weighted performance, SoWP). Initial and final days were weighted highest (0.6) while the central days were weighted lowest (MWMd1-4: 0.4 on MWMd2-3; MWMd1-6: 0.1 for MWMd3-4). Performance in the second half was expressed as a percentage of performance in the first half (relative SoWP, rSoWP). High performers were mice with over 15% improvement across MWMd1-4, and mice with over 30% improvement

across MWMd1-6. Low performers and non-cue spatial learning controls were grouped into 'non-learning controls'. Their performance is shown in **SM Fig 3.2B**.

(**C**) MWM learning over 4-6 days of all four experimental groups combined (circle-beige line) and separated into four groups. Performance is measured as latency to platform (LP) [342]. No significant between-group differences in daily average LP. Day 1 (p = 0.646 - >0.999, ns), Day 2 (p = 0.664 - >0.999, ns), Day 3 (p = 0.352 - >0.999, ns), Day 4 (p = 0.531 - >0.999, ns), Day 5 (p = 0.903 - >0.999, ns), Day 6 (p = 0.319 - >0.999, ns). Values on graph are means +/-SEM error bars. Ns, not significant, ANOVA with post-hoc test with Sidak's multiple comparisons adjustment.

(**D**) MWM learning over 4-6 days of four experimental groups from (**C**), separated into four graphs with individual values. pRAM-MiniTid-tau (slope = -8.121, R^2 = 0.451, 234 values from n = 45 mice), pRAM-MiniTid (slope = -7.792, R^2 = 0.446, 205 values from n = 42 mice), pSyn1-MiniTid-tau (slope = -7.629, R^2 = 0.428, 80 values from n = 14 mice), pSyn1-MiniTid (slope = -8.205, R^2 = 0.535, 86 values from n = 16 mice).

Optimization of procedures for robust labelling and identification of engram cell-specific tau interactors

Conditional expression of the MiniTid enzyme in sparse populations of hippocampal neurons yielded immunoblots signals that varied in strength (**Fig 3.2D**-**F**). The inconsistent detection of signals indicating MiniTid expression have also been attributed partial enzyme instability, due to deletion of the N-domain during engineering [326]. Conditional expression of the partly unstable MiniTid enzyme in sparse populations of hippocampal neurons yielded immunoblots signals that varied in strength (**Fig 3.2D**-**F**) [326]. This had the consequential effect of limiting total biotinylation and hence, limiting the amount of recoverable biotinylated protein in proteomic analyses (see **Appx Tables 12,16**). One solution, employed with some success, was to increase the absolute starting protein by pooling samples prior to enriching them for biotinylated proteins. While the experimental methods served to maximise activity-dependent tau-specific labelling, precipitation necessarily yielded results that suggested biotinylation of both endogenous and episomal origin, indicated by consistent visible bands across all samples on SA blots and from mass spectrometry (MS) based protein lists, independent of condition (**Fig 3.2G**; **Appx Table 12**). The predominant source of endogenously biotinylated proteins in cells is carboxylation reactions associated with metabolism in mitochondria [344-346]. Since identification of proteins by MS depends on within-sample relative protein abundance, the aim was to reduce endogenously biotinylated proteins from samples for MS analysis. This was achieved by isolating and removing intact mitochondria from tissue (whole cell) prior to enrichment of the remaining cytosolic fraction [347]. Successful fractionation was confirmed by SA blot, whereby the SA signal was consistently higher in whole cell and mitochondrial fractions relative to the cytosolic fraction (**SM Fig 3.3A**-**B**). In support of this, the proportion of representative sample MS peptide lists with mitochondrial origin were tissue (48.4%), cytosolic fraction (17.2%), and mitochondrial fraction (83.3%) (**SM Fig 3.3C**; **Appx Tables 12-14**). Together these results suggested that there was a significant initial contribution of endogenously biotinylated proteins in biochemical and proteomic samples; and that attempts to reduce mitochondrial proteins from cytosolic fractions were successful.

The strategy for removing mitochondria from samples prior to proteomic analysis was adopted for the final ~25% of processed samples that contributed to the results presented in this chapter.

Proximity-dependent labelling proteomics in state-specific spatial memory engram neurons.

After successfully labelling proteins in the HC of mice during the MWM task, the next aim was to produce three tau engram interactomes representing phases of spatial learning and memory. To achieve this, proteins isolated from mouse HC following MWM were identified by mass spectrometry (MS) and used to generate three functional association networks according to STRING [330].

For engram-state dependent and tau-specific labelling, mice were injected with AAV.RAM-MnTid-tau (from here, RMT). These mice were allocated to groups by memory phases (Encoding-Consolidation-Retrieval-Reconsolidation) including EC (MWMd1-4), RRc (MWMd3-6), and ECRRc (MWMd1-6), based on days of biotin injections and sacrifice. Labelled proteins were isolated and identified by MS, creating three key experimental groups (i) RMT-EC, (ii) RMT-RRc, and (iii) RMT-ECRRc with three corresponding lists of potential tau engram interactors. These lists were compared to rAAV control lists for each memory phase: (i) AAV.RAM-MiniTid (RM) for tau-independent labelling, (ii) AAV.Syn1-MnTid-tau (SMT) for activity-independent labelling, and (iii) AAV.Syn1-MnTid (SM) for tau- and activity-independent labelling. Crucially, an additional list of proteins labelled in non-cue controls (NCC), pooled from all four rAAV conditions, most closely represented interactions in task-independent but experience-sensitive HC cells [320]. Proteins in the experimental lists were deemed redundant if they co-occurred in any control list of that memory phase. Although arbitrarily set relative abundance cut-offs can adequately address experimental aims [322, 348], this higher stringency maximised the probability that proteins in each list were indeed associated to an engram state-dependent tau function.

Physiologic state functions of the tau protein extend beyond regulating axonal transport and microtubule assembly [184]. These include the translocation of tau into dendritic spines of activated synapses, suggesting a potential role for tau in synaptic plasticity [149]. Previously, Dox-inducible expression of short hairpin RNA targeting tau in HC of adult C57 wild-type mice modestly impaired performance in the MWM and associated with reduced spine density [164]. To investigate tau-mediated interactions in spatial encoding-consolidation, four groups of mice (RMT-EC, RM-EC, SMT-EC, RMT-EC) together labelled 119 unique proteins from 976 total biotinylated peptides during MWMd1-4 (**Appx Tables 15,16**). The NCC control group contained 46 unique proteins from 294 total peptides and was included in subtraction from all experimental lists (**Appx Table 24**). Following subtraction of 38 proteins that overlapped with the rAAV controls and NCC controls, 62 proteins were exclusive to pRAM-MiniTid-tau (RMT-EC) (**Fig 3.4A**, Venn diagram). These were mapped onto a functional network representing tau interactions in spatial encoding and consolidation engram cells

(PPI enrichment: $P = 4.0 \times 10^{-15}$, average node degree = 2.87, clustering coefficient = 0.353; **Fig 3.4A**). A protein ontology (PO) analysis of the finalised RMT-EC network showed enrichment of processes relating to glutamate receptor signalling and calcium ion-regulated exocytosis (**Fig 3.4C**, **Appx Table 17**). Proteins localising to the postsynaptic density and the perinuclear region were also enriched (**Fig 3.4C**, **Appx Table 17**). A PO analysis of proteins exclusive to pooled background controls showed most enrichment in processes of SNARE complex assembly and axonal regulation, and functions linked to MAP kinase signalling and purine metabolism (**Appx Table 16**). The only protein labelled in both networks was protein phosphatase calcineurin (subunit Ppp3ca), which is a confirmed tau interactor in mouse brain [349]. Among the network interactors separated by one degree from tau were an NMDA receptor subunit (Grin2b), calcium/calmodulin-dependent kinase 2 (Camk2a/b), and synaptosome-associated protein 91 (Snap91). Spatial learning in the MWM does not occur without postsynaptic NMDA receptor activation at CA1 synapses or without activation of Camk2a, a synaptic kinase that is also critical for various forms of plasticity underlying learning and memory [350-352]. Hippocampal CA1 synapses of mice lacking the endocytosis regulator Snap91 (*AP180*$^{-/-}$) have impaired neurotransmission, a process that is regulated by Snap91 alongside vesicle-associated proteins such as network protein Vamp3 [353]. Endophilin-A1 (Sh3gl2) was identified in the RMT-EC network, a regulator of synaptic membrane curvature dynamics and endocytosis [354]. Within the cluster of vesicle-associated proteins, I also note the confirmed tau binding partner Nsf. *Tau*-deficient neurons mislocalise neurite Nsf, whereas the tau binding to Nsf reduces Nsf activity and impairs both contextual fear and object recognition memories, as described in chapter 2 [355]. Other tau binding candidates included spine density regulating protein cortactin (Cttn) [356] and p21 activated protein kinase 2 (Pak2) that links Rho GTPases to cytoskeleton organisation and nuclear signalling [357]. While not statistically enriched with nuclear proteins, the RMT-EC network was populated with nuclear-localising and nucleic acid-binding proteins, including: the DNA methylation-sensing transcription modulator linked to Rett syndrome, MeCP2 [358], the transcription regulator protein Set which inhibits CREB-binding protein from facilitating activity-dependent transcription during learning [359-361], and RNA processing and stabilizing proteins Hnrnpm, Cmtr1, Papd4, and Ddx46. Physiologic stimulation of primary neurons induces DNA double-strand breaks (DSBs) [362]. Following trace or contextual fear conditioning, mice accumulate histone markers of DNA damage in the hippocampus and elsewhere [363, 364]. In both cell and animal models, DSBs were causally linked to downstream upregulated IEG expression, including *Fos Arc*, and *Npas4* [362-364]. Identifying a sizeable number of nucleic acid-associated proteins is consistent with reported tau functions in binding and stabilising genomic DNA, and nuclear and cytoplasmic RNA [365-367]. This targeted approach for labelling engram interactions highlighted central factors implicated in learning (Grin2b, Camk2a) while mapping tau associations that, taken together, support multiple tau functions in various subcellular locations of EC engram cells.

The potential role of tau in physiologic memory retrieval and/or reconsolidation is unknown. In mouse models of early Alzheimer's Disease, one report linked impaired memory retrieval to reduced dendritic spine density in dentate gyrus engram neurons [368]. I hypothesised that labelling tau interactions in RRc engram cells would begin to describe tau functions during these memory phases. From proteins labelled during MWMd3-6, lists from RMT-RRc, RM-RRc, SMT-RRc, and RMT-RRc were combined, totalling 141 unique proteins from 659 total biotinylated peptides. After subtraction of 27 proteins co-occurring in control lists, 51 proteins found exclusively in RMT-RRc (**Fig 3.4B**, Venn diagram) were mapped onto a tau interactome (PPI enrichment: $P = 1.0 \times 10^{-3}$; average node degree = 1.29, clustering coefficient = 0.395; **Fig 3.4B**). The finalised RMT-RRc network was enriched with proteins linked to G-protein-coupled receptor signalling and coding region instability determinant (CRD)-mediated mRNA stabilization processes, and clathrin-coated pits and presynapse sub-compartments (**Fig 3.D**, **Appx Table 20**). Among the identified proteins was protein LIN-7 homolog C (Lin7c), a PDZ domain-containing protein that localises to postsynaptic densities and interacts with multiple receptors and channels [369]. The interactome contained different proteins involved in vesicle processing such as component of Adaptor Protein 2 (Ap2m1) and an endocytosis-regulating phosphatase, synaptojanin-1 (Synj1) [370]. Tau is a confirmed substrate for another interactome protein, casein kinase 1 (Csnk1g1/3). Compared to RMT-EC, the RMT-RRc interactome had notably more proteins associated with G-protein signalling (Gnat1/2, Gnas) and fewer transcription factors. Putative tau binding partners in RMT-RRc indicate that tau engaged with phosphatase proteins in an intracellular environment with different associated protein ontology.

At the time of thesis submission, the tau interactome of mice assigned to the entire MWM spatial learning and memory paradigm (ECRRc) was incomplete but has been included as part of **SM Fig 3.4**. Beyond this paragraph, the remaining text will focus on networks in **Fig 3.4**. The combination of proteins labelled by RMT-ECRRc, RM-ECRRc, SMT-ECRRc, and RMT-ECRRc amounted to 185 proteins from a total of 1283 biotinylated peptides. Following subtraction of 41 overlapping background proteins, 34 proteins were unique to RMT-ECRRc (**SM Fig 3.4A**, Venn diagram). These were mapped onto a functional association network to represent tau interactions in neurons associated with spatiotemporal processing (PPI enrichment: P = 0.051, average node degree = 0.706, clustering coefficient = 0.475; **Fig 3.4A**). Protein ontology enrichment was limited relative to networks in Fig 3.4, but included proteins associated with neuron development and the compartment of neuron projections (**SM Fig 3.4B**, **Appx Table 23**).

Investigating engram state-specific tau interactomes from the MWM task revealed tau interactor candidates exclusive to engram cells that are encoding, retrieving, and/or consolidating spatial memory information. Except for tau and Ppp3ca, proteins in each network were exclusive to each network (**SM Fig 3.4C**). Upon comparing engram state-specific interactomes, significant differences

were evident in the enriched ontological sub-domains. In the encoding-consolidation engram state (MWMd1-4), putative tau interactors were predominately associated with long-term potentiation and the postsynapse (**Appx Table 17**). Interactors from the retrieval-reconsolidation engram state (MWMd3-6) were associated with GPCR signalling and subcellular protein localisation (**Appx Table 20**). The marked heterogeneity in enriched molecular functions and cell localisation between engram states suggests that tau interactions may differ depending on the spatial engram state. With this as a conceptual starting point, I attempted to confirm the formation of complexes between tau and putative tau interactors in a cultured cell model.

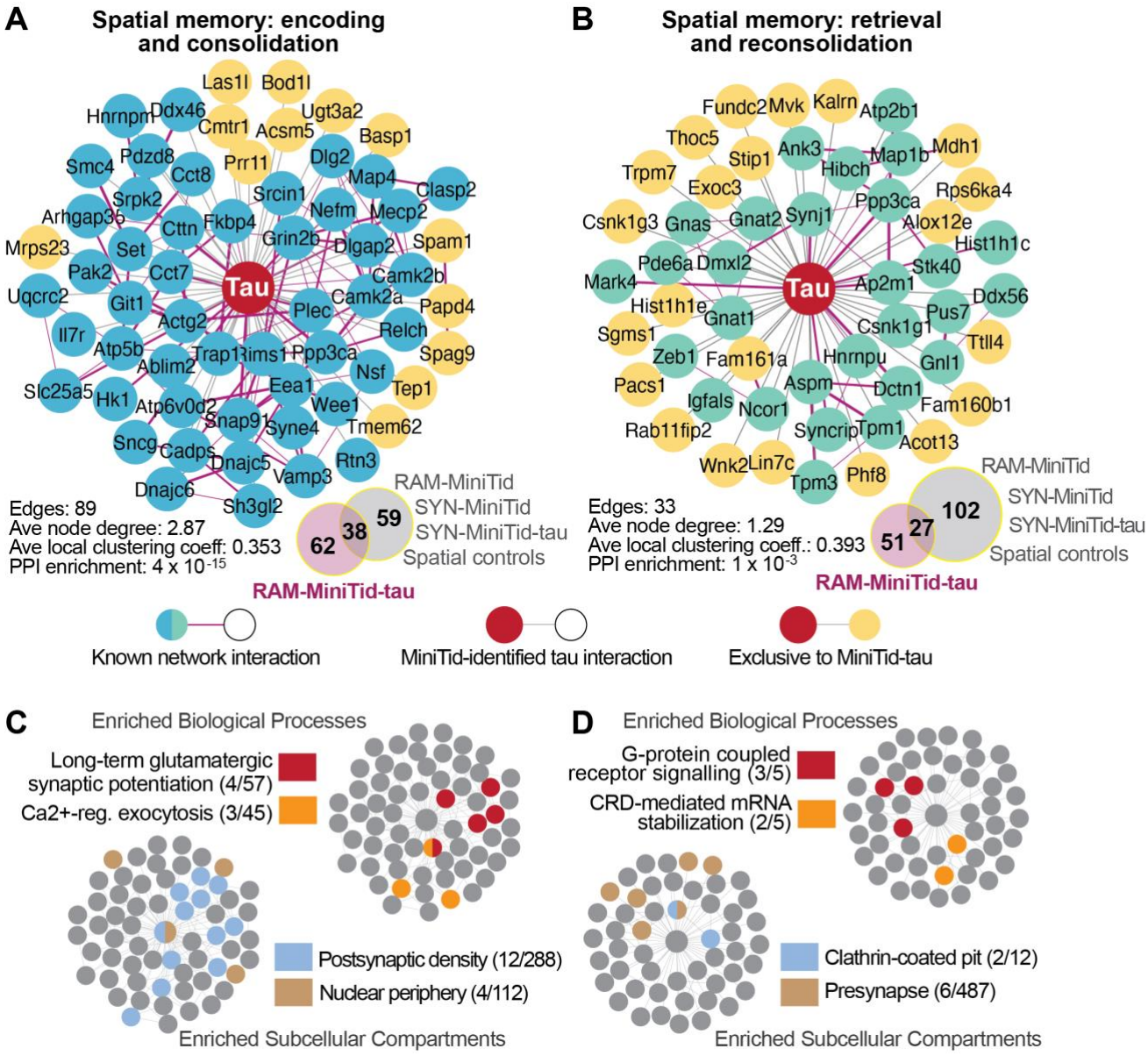

Figure 3.4: ***Tau interactomes in spatial learning and memory engrams***. Interactions of tau, labelled in mouse brain during the Morris Water Maze (MWM) task. Experimental group mice were transduced to express MiniTurboID-tau under activity-dependent control (RAM promoter, pRAM). Two interactomes at two phases of spatial memory were generated by harvesting mice at two MWM time points: day 4 (encoding-consolidation, EC) and final day 6 (retrieval-reconsolidation, RRc).

(**A**) Tau protein-protein interaction (PPI) network in mouse hippocampus during spatial memory EC (n = 12 biological replicates). Network of exclusive interactors with network properties (STRING v11.5). Venn diagram shows unique proteins (network nodes) and overlapping proteins from experimental group AAV.RAM-MiniTid-tau compared to four additional groups (consolidated lists from 3 x rAAV groups and spatial learning controls, n = 12 biological replicates). Spatial control mice performed the MWM without cues (non-learning) during activity-dependent expression of either MiniTid or MiniTid-tau.

(**B**) Tau protein-protein interaction (PPI) network in mouse hippocampus during spatial memory RRc (n = 8 biological replicates). Venn diagram shows unique proteins (network nodes) and overlapping proteins by comparing group experimental group to background controls (3 x rAAV groups and learning controls, combined n = 12 biological replicates).

(**C**) Protein ontology enrichment summary for high-ranking categories from network in (**A**) based on STRING 'Strength' calculation. Strength scores and false discovery rates associated with the presented gene counts are shown in **Appendix Table 17**.

(**D**) Protein ontology enrichment summary for high-ranking categories from network in (**B**) based on STRING 'Strength' calculation. Strength scores and false discovery rates associated with the presented gene counts are shown in **Appendix Table 20**.

Five engram state-specific interaction candidates form complexes with tau

Network associations of tau in engram cells depended on the engram state associated with phases of memory E-C-R-Rc. Interactions of tau may mediate engram-specific factors that are involved in state-specific functions. If these factors relate to different functions underlying memory phase processing, an expansion of the core tau interactomes would shed further light on the suggested role of tau in memory encoding, storage, and/or retrieval. With the aim of generating integrated protein networks using multiple fusion proteins, putative tau engram interactors were fused to MiniTid and screened, by coimmunoprecipitation, for formation of stable interaction complexes with tau.

To consider the scope of their functional relevance, a subset of tau interactor candidates from across the three engram networks became proteins of interest (POIs). The rationale for this selection was to remain agnostic about the potential specific role of tau in engram interactions and to represent an approximately equal distribution of candidates from each phase of spatial memory (E-C-R-Rc) and candidate protein functions across ontological domains (**Appx Table 25**). Hence, the following POIs were selected and fused to MiniTid: Ap2m1 (RRc), Csnk1g1 (RRc), Csnk1g3 (RRc), Camk2a (EC), Cttn (EC), Lin7c (RRc), Mecp2 (EC), Pak2 (EC), Ppp3ca (RRc), Set (EC), Sh3gl2 (EC), and Vamp3 (EC).

Expression blots confirmed the stability, and biotinylation blots confirmed and functionality, of each fusion protein transfected in 293T cells (**Fig 3.3A**). In cases of multiple clones (Lin7c, Csnk1g3), SA-HRP signal pattern similarity between clones and difference between MiniTid-POIs supported that these fusion proteins mediated targeted non-random biotinylation of the cellular proteome (**Fig 3.5A**). Soluble MiniTid did not copurify with immunoprecipitated tau (**Fig 3.5B**-**C**), hence potential tau-POI interactions were likely mediated by the bait portion of each fusion protein. Five MiniTid-POIs

coimmunoprecipitated with tau, suggesting that these proteins formed stable complexes with tau in cell culture (**Fig 3.5B**-**C**).

The first bait protein confirmed to interact with tau was Mecp2 (**Fig 3.5B**, *left***, 3C**, *right*). Mecp2 was identified in the spatial learning tau interactome (RMT-EC, **Fig 3.4A**). Like tau, Mecp2 is considered to be an intrinsically disordered protein (IDP) [371, 372]. It binds methylated DNA and histones and acts as a methylation-dependent modulator of transcription [373]. Spontaneous and familial mutations in the Mecp2 gene can affect epigenetically regulated gene expression as described in Rett syndrome, a neurodevelopmental disorder affecting cognitive ability [374]. In healthy behaving mice, Mecp2-mediated splicing events induced by spatial learning are necessary for successful memory consolidation, which corroborates the identification of Mecp2 in RMT-EC (**Fig 3.4A**) [375].

The next confirmed tau binding partner was Lin7c (**Fig 3.5B**-**C**, *right*), a mammalian homolog of a PDZ domain containing protein first identified in tight junctions of polarized *Caenorhabditis elegans* vulval cells [369, 376]. In neurons, the heterotrimeric complex of Lin2/7/10 localises proteins to cell-cell junctions through β-catenin [377]. Dendritic shaft-spine translocation of β-catenin is activity dependent and may be mediated by Lin7, consistent with identification of Lin7c in RMT-RRc (**Fig 3.4B**) [378].

Coimmunoprecipitation confirmed that labelled Camk2a in RMT-EC (**Fig 3.4A**) represented a bona fide tau engram interaction (**Fig 3.5C**, *left*). Camk2a is a critical serine/threonine kinase that moves between synapses and the nucleus during synaptic plasticity, including LTP and spatial learning [352, 379]. Tau-Camk2a complexes have previously been described in biochemical assays and isolated from cell culture and AD model mouse tissue, but not in a physiologic memory-dependent context [248, 380, 381].

A subunit of phosphatase calcineurin (Ppp3ca) labelled in RMT-EC and EMT-RRc (**Fig 3.4A**-**B**) was confirmed to interact with tau in cells (**Fig 3.5C**, *left*). Calcineurin is a confirmed tau interactor in mouse brain, and is competitively inhibited by calmodulin-calcineurin interactions [349]. Calcineurin also regulates endocytosis and cytoskeletal remodelling in neurons [382, 383]. Previously confirmed tau interactions such as with calcineurin corroborate and help to validate novel PPI approaches and may provide clues on the molecular state of tau during labelling, including phosphorylation and localisation.

Finally, endophilin-A1 (Sh3gl2) coimmunoprecipitated with tau (**Fig 3.5C**, *centre*), originally identified in engram samples from RMT-EC (**Fig 3.4A**). Sh3gl2 is a regulator of membrane curvature dynamics [354]. It localises in dendritic spines of CA1 neurons and is necessary for long-term potentiation of spatial and contextual memory [384]. Little is known about how tau and Sh3gl2 may interact, but clues may lie in Sh3gl2 localisation and function.

Due to the proximity-dependence of biotin labelling, the remaining MiniTid-POIs may still interact with tau, but in a transient manner [247]. And the coimmunoprecipitation results do not discount non-precipitated proteins from being transiently interacting partners with tau. Despite this, the confirmed baits together do support that tau differentially engages with engram cell effectors throughout different subcellular compartments, including in the pre- and postsynapse, nucleus, and plasma membrane.

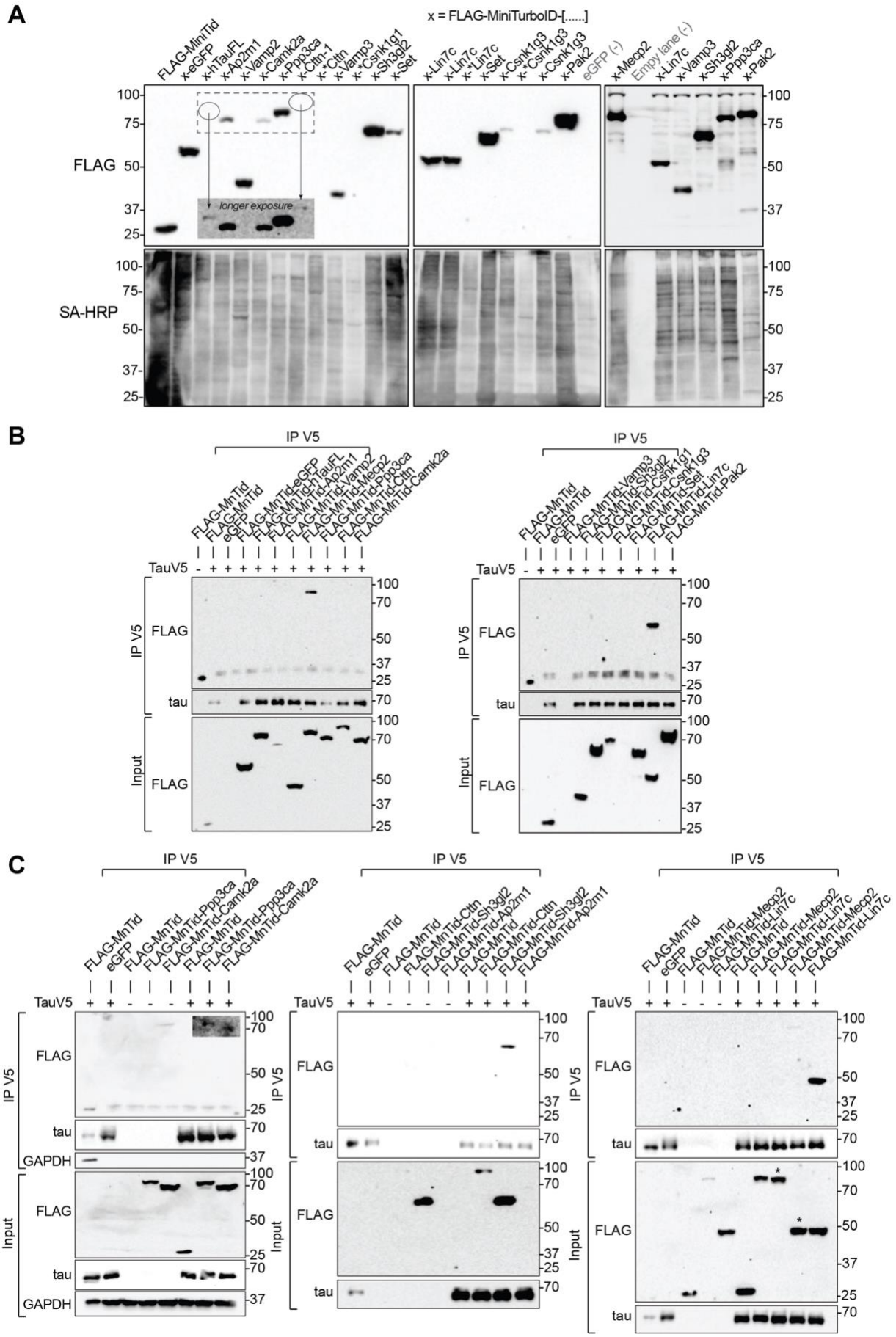
A
x = FLAG-MiniTurboID-[.....]
FLAG-MiniTid
x-eGFP
x-hTauFL
x-Ap2m1
x-Vamp2
x-Camk2a
x-Ppp3ca
x-Cttn-1
x-Cttn
x-Vamp3
x-Csnk1g1
x-Sh3gl2
x-Set
x-Lin7c
x-Lin7c
x-Lin7c
x-Set
x-Csnk1g3
x-Csnk1g3
x-Csnk1g3
x-Pak2
eGFP (-)
x-Mecp2
Empty lane (-)
x-Lin7c
x-Vamp3
x-Sh3gl2
x-Ppp3ca
x-Pak2
FLAG
SA-HRP
longer exposure
100
75
50
37
25
B
IP V5
FLAG-MnTid
FLAG-MnTid
eGFP
FLAG-MnTid-eGFP
FLAG-MnTid-hTauFL
FLAG-MnTid-Ap2m1
FLAG-MnTid-Vamp2
FLAG-MnTid-Mecp2
FLAG-MnTid-Ppp3ca
FLAG-MnTid-Cttn
FLAG-MnTid-Camk2a
FLAG-MnTid-Vamp3
FLAG-MnTid-Sh3gl2
FLAG-MnTid-Csnk1g1
FLAG-MnTid-Csnk1g3
FLAG-MnTid-Csnk1g3
FLAG-MnTid-Set
FLAG-MnTid-Lin7c
FLAG-MnTid-Pak2
TauV5
IP V5
FLAG
tau
Input
FLAG
C
IP V5
FLAG-MnTid
eGFP
FLAG-MnTid
FLAG-MnTid-Ppp3ca
FLAG-MnTid-Camk2a
FLAG-MnTid
FLAG-MnTid-Ppp3ca
FLAG-MnTid-Camk2a
FLAG-MnTid
eGFP
FLAG-MnTid
FLAG-MnTid-Cttn
FLAG-MnTid-Sh3gl2
FLAG-MnTid-Ap2m1
FLAG-MnTid
FLAG-MnTid-Cttn
FLAG-MnTid-Sh3gl2
FLAG-MnTid-Ap2m1
FLAG-MnTid
eGFP
FLAG-MnTid
FLAG-MnTid-Mecp2
FLAG-MnTid-Lin7c
FLAG-MnTid
FLAG-MnTid-Mecp2
FLAG-MnTid-Lin7c
FLAG-MnTid-Mecp2
FLAG-MnTid-Lin7c
TauV5
IP V5
FLAG
tau
GAPDH
Input
FLAG
tau
GAPDH

Figure 3.5. ***A subset of functional MiniTurboID fusion proteins are confirmed as tau protein interactors***.

(**A**) Immunoblots of 293T showing expression (*top row*) and biotinylation (*bottom row*) from FLAG-tagged MiniTid constructs fused to proteins of interest (MiniTid-POIs). Expression of MiniTid-POIs was detected by anti-FLAG antibody staining. Biotinylated proteins from cell lysates were detected using streptavidin (SA) conjugated to HRP (SA-HRP). Expression of – and biotinylation by – at least one clone of each MiniTid-POI was detected.

(**B**-**C**) Co-immunoprecipitation (Co-IP) of V5-tagged tau and MiniTid-POIs from cultured cells. V5-tagged tau and MiniTid-POIs were co-expressed in 293T cells followed by immunoprecipitation using V5 antibody and immunoblot probed with antibodies for FLAG, tau, and for loading, GAPDH. (**B**) FLAG-MiniTid fused to MeCP2 (*left*) and to Lin7c (*right*) co-immunoprecipitated with tau. (**C**) FLAG-MiniTid fused to Ppp3ca (*left*), CamK2a (*left*), Sh3gl2 (*centre*), MeCP2 (*right*), and Lin7c (*right*) co-immunoprecipitated with tau. *Left:* Inset, longer exposure. *Right:* Asterisks (*), reversed order of two marked lanes.

Bioinformatic analyses of theoretically expanded tau engram interactomes.

When comparing the STRING statistics of tau interactomes RMT-EC to RMT-RRc, the in-built analyses highlighted differences in the enriched ontological sub-domains (**Fig 3.4**). This suggested that engram state-specific properties were ‘captured’ by labelling tau interactions throughout phases of spatial learning and memory. A subset of state-dependent network factors was confirmed to interact with tau (**Fig 3.5**). These five POIs (Camk2a, Mecp2, Lin7c, Ppp3ca, Sh3gl2) were fused to MiniTid as baits, with the future aim of manually expanding the core tau network, generating true degrees of separation between nodes (as opposed to starting with a list of apparently direct tau interactors and mapping these onto a network of STRING-predicted associations). For instance, since Camk2a and Mecp2 were identified in the EC network, the MiniTid-Camk2a and MiniTid-Mecp2 interactomes will be generated under the same conditions (i.e., biotinylation during MWMd1-4). These interaction networks will expand from Camk2a and Mecp2 nodes based in the initial ‘core’ tau interactome. This strategy would approach a more accurate representation of edge-node relationships.

Despite the state-specificity in identifying the POIs, learning makes memories transiently labile [385]. As representations are constantly being updated, thus, so too is the retrieved and reconsolidated memory content [385]. To simulate a physiologically plausible relationship between the six proteins from across ECRRc, they were combined into a single list. Tau is central to these six proteins because (i) it is the only protein confirmed to interact with the other five (ii) in multiple phases of developing spatial memory.

Starting with these six proteins, a hybrid network of 26 nodes was created using STRING [330]. This contextualised the interactions within a larger set of interrelated proteins to better understand how tau and binding partners might coordinate to support dynamic engram state functions. While a simulation and analysis like this is novel, results are based on text-mined prior knowledge of functional associations [386], from a focused starting list of proteins. Five nodes were integrated immediately, while incorporation of Sh3gl2 demanded three network expansions, taking the network from 6 to 26

nodes with 141 edges (average nodal degree = 10.8, **Appx Table 26**). Among the nodes introduced by the expansion were two more proteins identified in the RMT-EC interactome, Camk2b and Grin2b (**Fig 3.4A**). To attribute the high nodal degree to the starting six nodes, the engram network statistics were compared to ten unbiased tau networks of equal size (from 6 to 26 nodes) (**Appx Table 27**). The average local clustering coefficient, a measure of nodal neighbourhood connectivity was highly variable (**Appx Table 27**) [387]. Despite all networks sharing tau as an input protein, the expanded engram interactome had the highest average nodal degree (10.8) compared to the unbiased tau network controls (6.8 – 9.2, **Appx Table 27**). Replacing tau with a control protein in the hybrid engram network reduced the average nodal degree (-16%, 9.08 from 10.8) and had mixed effects on the unbiased networks, with the highest average nodal degree value equalling that of the engram network (10.8) (**Appx Table 27**). Upon closer inspection, the expansion from that random list had captured Mecp2. When ranking proteins in the hybrid engram network by edges, Mecp2 and Creb1 ranked equal first (17 edges), followed by Camk2a (13), tau (11), Ppp3ca (11), Lin7c (7), and Sh3gl2 (3) (range 17-3, **Appx Table 26)**. This network analysis confirmed that the engram network had highly associated nodes because of the identity of the starting six nodes.

To support PO analyses, I noted central nervous system functions of the six engram proteins and illustrated their localisation in neurons (**Fig 3.6A**). The approach to building out the links between the engram proteins involved scanning for directly or indirectly shared but targeted pathways that were consistent with an active engram state environment (e.g., stimulation or plasticity, but not apoptosis or inflammation). A cluster of five nodes in the hybrid engram network was associated to both gene expression and plasticity at synapses, and indirectly linked tau, Camk2a/b, and/or Ppp3ca to Mecp2 (**Fig 3.6Bi**; **Appx Table 28**). A literature search guided by this approach supports a link between Camk2a and Mecp2: Camk2a phosphorylates nuclear Mecp2 in activity dependent *Bdnf* transcription [388]. This link can be applied in the opposite direction, whereby Mecp2 activity upregulates expression of Camk2a and of overlapping cluster nodes Grin1 and Grin2b (**Fig 3.6Bi**) [389]. The possible role for tau in this interplay of proteins in the nucleus currently remains unclear. Despite the coverage of these large overlapping clusters, they excluded Lin7c and Sh3gl2 (**Fig 3.6Bi**). Less well characterised proteins that appear less often in the literature are less likely to be text-mined and associated with a PO [390]. No specific PO linked tau to Lin7c in any meaningful or practical manner, i.e., most PO descriptions were vaguely named, with background gene counts of >1,000 (**Appx Table 28**). Network enrichment for response to stimulation and cell-cell communication indirectly co-associated tau and Lin7c respectively, again through five nodes that included Ppp3ca and Grin2b (**Fig 3.6Bii**). The rationale for pairing these POs containing confirmed engram binding partners was to represent a plausible sequence of molecular events that may take place in an ensemble of cells: activating stimulus and downstream signalling to cell-cell communication [391]. Shared node Ppp3ca is a signalling molecule that links the stimulus-dependent signalling cluster, including tau, with Lin7c

of the cell-cell communication cluster. In the final network, tau, Sh3gl2, and Ctnnb1 to link the larger cell projection morphogenesis cluster, by being co-associated to the smaller neurite projection extension cluster (**Fig 3.6iii**). Tau predominately localises to axons and has the well-defined function of regulating cargo transport and localising proteins [4], while Sh3gl2, labelled during spatial learning, is linked to dendritic spine growth in potentiating synapses [384]. While no explicit link between tau and Sh3gl2 has been reported to-date, tau and confirmed binding partner Sh3gl2 may interact with changing frequency, subject to localised demands in engram versus resting states.

The analysis presented some potential ways in which tau may functionally associate with five confirmed physical interaction partners. These insights helped to prepare for targeted mechanistic experiments in future.

A

Interactor localisation mapped over tau distribution (red)	Protein	Engram state	Canonical protein function
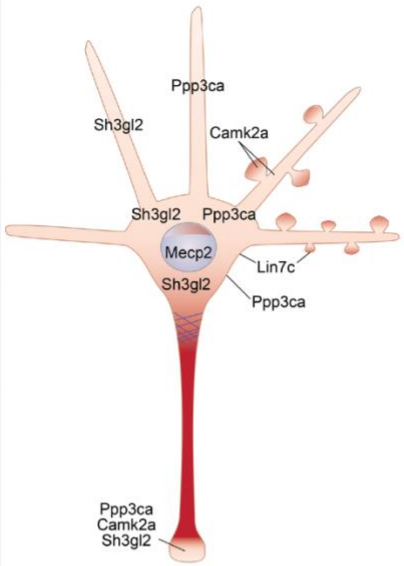	Tau	ECRRc	Microtubule-associated axonal transport.
	Camk2a	EC	Homododecameric kinase. NMDA receptor- and SV-associated synaptic plasticity.
	Mecp2	EC	Methylated DNA binding for transcriptional regulation, including genes influencing cognition.
	Sh3gl2	EC	Membrane curving for synaptic vesicle endocytosis.
	Ppp3ca	RRc	Heterotrimeric phosphatase. Akt, MAPK, NF-kB signalling in growth, transcription, metabolism.
	Lin7c	RRc	Trimer complex (2-7-10), PDZ domain. Cell adhesion regulation; integral membrane protein trafficking.

B

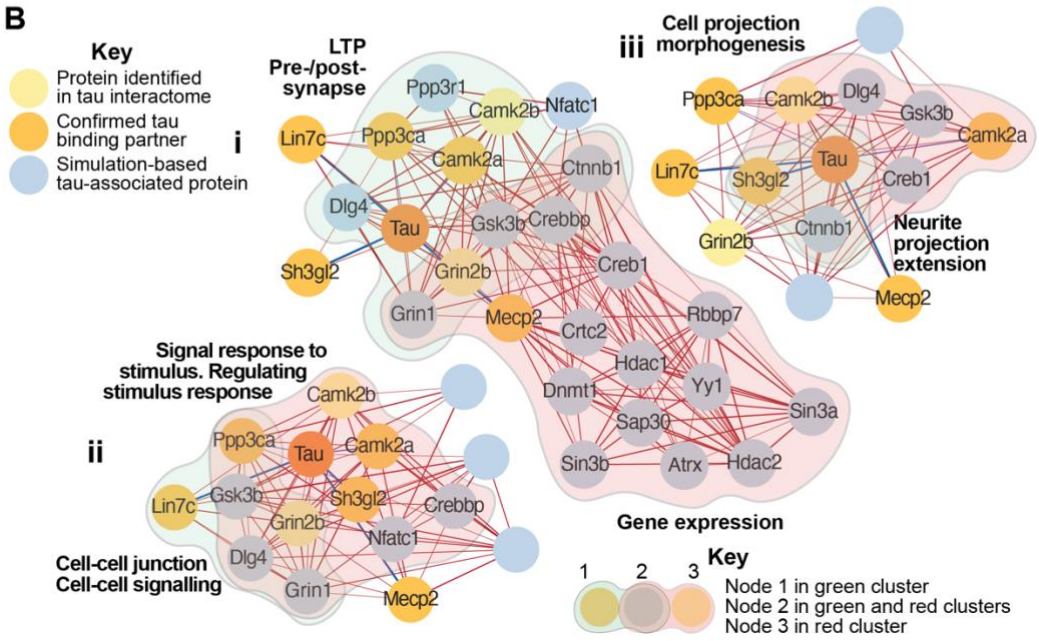

Figure 3.6. ***Tau interactions in expanded engram networks***.

(**A**) Summary table of tau and confirmed interactors illustrating simplified subcellular distribution patterns in neurons and a brief note on known functions according to UniProt [392].

(**B**) Confirmed tau engram interactors were mapped onto functionally associated proteins. Opaque green and red overlays correspond to adjacent protein ontology labels. Associations between tau, confirmed interactors (orange) and EC or RRc engram hits (yellow) are STRING-based (red edges). Nodes introduced by STRING are in blue. (**i**) Hybrid tau interactome of 6 engram proteins of interest with 20 additional nodes by STRING. Network and overlay shows how protein ontology can reveal synaptic proteins important in long-term potentiation (LTP) that are indirectly linked to effectors of gene expression (by reliance on red-green overlap). (**ii**) Strategy for finding common binding partners with less well characterised proteins (e.g., Lin7c) shown in a hybrid sub-network. Pairs of chosen ontologies are most meaningful when targeted, small, and rationally selected (functional complementarity or continuity between POs). (**iii**) Same as in (ii), linking smaller processes with larger ones.

Discussion

It is assumed that for learning to occur, a stimulating experience must result in enduring physical and functional changes [28, 335]. But is an enduring physical change necessary for an enduring functional change? Multiple physical states and molecular configurations may underlie a single enduring functional change that represents information currently described as a 'memory trace'. Hence, the content of a memory may be described in terms of an interplay between molecules, or molecular interactions. The synapse has been described as a dynamic molecular assembly with a morphologically labile structure [393, 394]. Contextual learning induces immediate increases in engram synapse weight [395], whereas engram spine density may reduce following learning, thought to be a selectively strengthening of remaining spines (a 'refinement') [396]. The maintenance and retrieval of spatial memory can be irreversibly impaired by inhibition of a single protein, PKM-zeta [397]. Hence, engram interactomes may contribute to a proteo-centric view of memory formation and to the nature of the engram.

Here, I established and optimized a strategy for labelling tau protein-protein interactions (PPIs) in mouse brain during learning and memory formation/retrieval. This was achieved by AAV-mediated delivery and expression of MiniTid-tau under control of a synthetic IEG-sensitive promoter. Mice injected with biotin performed the MWM task of spatial memory while tau interactions were being labelled in active mouse HC. Stringent performance cut-offs ensured that the labelled proteins were sourced from similarly high performing mice. Spatial learning controls labelled proteins that were experience- but not spatial memory task-dependent. Pan-neuronal expression of MiniTid-tau in some mice were additional controls for tau-specific yet activity-independent interactions. Using mass spectrometry, 324 total proteins were identified, 102 (~31%) of which were both tau-specific and memory task-dependent. These lists provided the nodal identities of two distinct tau engram interactomes and represented engram state-dependent tau interactions. A subset of these interactions was confirmed and further scrutinised with literature and by bioinformatics-based methods.

The choice of tau as bait for the labelling enzyme was partly influenced by a gap in knowledge between the identified role of tau in neurodegenerative memory loss [10, 155], and the relatively less well-described roles of tau in physiology. For example, if amyloid-beta and aberrant post-translational processing can promote synaptic relocalisation of axonal tau and impair memory [151], how might tau functions in non-disease states be implicated in memory mechanisms? I previously mapped tau protein interactions in live wild type and tau knock-out (*tau*$^{-/-}$) mouse brain and identified synaptic ATPase NSF as a potential tau binding partner [214, 216]. I found that tau-NSF interactions reduced memory performance in mice during fear conditioning and novel object recognition (**Fig 2.6, SM Fig 2.5**) [355]. After identifying this link between tau and physiological memory I hypothesised that this

and other functional tau interactions would be critical in engram cells that support learning and memory in the hippocampus.

Protein-protein interaction identifying methods often favour stable interactions or might be undirected. For example, affinity-purification-mass spectrometry biasing stable interactions, or BioID approaches mapping entire sub-compartments [398-400]. Global methods of characterising engram cells rely on regional or brain-wide activity-dependent changes in transcriptomic and epigenomic signatures [300, 314]. My experimental strategy for investigating protein interaction in learning and memory was to focus on tau, an individual protein less centrally implicated in cell activation than, for example, the NMDA receptor. An NMDA receptor subunit as bait would make distinguishing between memory- and experience-dependent activity challenging, because place cells and engram cells both activate when navigating space, and these cells share signalling pathways and molecular mechanisms (e.g., NMDA receptors are necessary for long-term maintenance of hippocampal place maps but are also central to learning) [401-403]. This targeted approach for labelling tau interactions during spatial learning/memory yielded engram state-dependent differences in the tau interaction profiles. Early learning phases of encoding and consolidation (EC) were dominated by glutamate signalling pathway factors and gene expression regulators (Camk2a/b, Grin2b, Mecp2, Set), whereas memory retrieval labelling included phosphatases and membrane-localising factors (Ppp3ca, Synj1, Lin7c) (**Fig 3.4**). This implies that tau interactions are as central to the state of engrams as is necessary for them to be representative of these dynamic states, and that this in turn allows one to discriminate between said states based on the tau interactomes themselves. Hence, comparing different interactomes from different spatial memory phases introduces a temporal specificity to the output data [404]. One potential reason for this ‘interactome capture’ is that cumulative labelling of transient and stable interactions coupled to activity-dependent expression is both targeted and sensitive [215, 247, 348]. Relating to this cumulative labelling of interactors across time, when comparing the EC and RRc interactomes to the ECRRc interactome (**SM Fig 3.4**), the tau interactors in the EC and RRc networks did not overlap with the ECRRc network. Due to the extended labelling period for generating the ECRRc interactome (6 days) compared to EC (4 days) and RRc (4 days), protein turnover in mouse brain sourced for the ECRRc network may have reduced the abundance of EC proteins. But this does not explain why RRc network proteins did not overlap with ECRRc network proteins. One factor contributing to this incongruence in network protein identities between networks may have been the much larger total number of control/background mice used for the ECRRc network, as there were many more shared ‘redundant’ proteins between the networks. Another reason may be technical: either the semi-quantitative method used by MS software, whereby confidence in assigning protein identities and abundance to peptide fragments is affected by the abundance of other peptide fragments in the sample. In considering these possibilities, the differences between EC or RRc and

ECRRc warrant additional experimental samples (n = ~5 per network), and possibly also more control samples.

This marked heterogeneity in enriched molecular functions and cell localisation between engram states suggests that tau differentially engages with protein in various roles and locales, depending on the spatial engram state. With this as a conceptual starting point, I attempted to confirm a subset of labelled proteins as tau binding partners (Camk2a, Mecp2, Ppp3ca, Lin7c, Sh3gl2; **Fig 3.5**). Interacting proteins were functionally diverse, suggesting that tau functions may be broader than previously thought. In turn, the molecular state of tau in specific engrams might be inferable from labelling well-characterised interactions, different to inferences from previously unknown interactions. For instance, during both encoding-consolidation and retrieval-reconsolidation (EC, RRc), calcineurin (subunit Ppp3ca) was labelled, which is a confirmed tau binding partner that influences the balance of phosphorylated and dephosphorylated tau, and tau metabolism in axons and at the synapse [349, 405, 406]. Therefore, a proportion of tau interactions during engram activity may take place when tau is localised to the synapse [407]. This information can then be leveraged for preliminary functional evaluations of novel tau interactions. Novel tau binding partner Lin7c was identified in the same interactome as Ppp3ca (RRc). In neurons, the heterotrimeric complex Lin2/7/10 localises proteins to gap junction plasma membranes through β-catenin [377], which was independently found to translocate from dendritic shafts to spines in an activity dependent manner [378]. This movement may be mediated by Lin7c, describing the conditions under which synapse-localised tau interacts with Lin7c [406]. Furthermore, Lin7 binds directly to NMDA receptor subunit NR2B, a protein in the EC interactome (Grin2b, **Fig 3.4A**), during microtubule transport in neurites, and localises to postsynaptic densities [369]. A potential role of tau in mediating localisation of Lin2/7/10 complex and glutamate receptors has not previously been interrogated but may contribute to activity-dependent changes underlying learning [408].

Understanding the link between tau and neuronal activity and excitation will be critical to definitively describing the role of tau, not just in disease, but also in active engrams. Learning-induced activity is sufficient to cause DNA double-strand breaks in mouse brain [363, 364]. Multiple lines of evidence present the contribution of tau to neural network dysfunction and excitotoxicity [10, 409], and the effect of excitation on tau, which can undergo activity-dependent translocation into synapses [149]. Different reports describe a protective role of tau when cells activate, by binding to and stabilizing both RNA and DNA in the cytoplasm and nucleus [365-367]. In line with this, I found multiple nucleic acid-associating proteins in both networks, from nuclear transcription factors (e.g., Mecp2, Set) to cytosolic mRNA-binding proteins (e.g., Hnrnpm, Hnrnpu, Syncrip). I confirmed an interaction between tau and the transcription modulating protein Mecp2, which appeared in the EC engram interactome. *Mecp2* mutations cause the cognitive deficits seen in Rett Syndrome [374], but is also linked to physiologic

memory formation through another tau interactor labelled in the same interactome, Cam2ka [388, 389]. If or how tau fits into this picture is currently unknown, however activity-dependent DNA damage may lead to elevated DNA-protective nuclear tau that interferes with the ability of Mecp2 to sense methylated DNA. Mecp2 is a major part of my ongoing investigations into functional interactions of tau and the memory engram.

I attempted to simulate a portion of my ongoing tau PPI investigations with a bioinformatic analysis. The purpose of the analysis was to simulate one way of engaging with an expanded tau interactome. While the analysis-based outcomes warrant further scrutiny, and then experimental validation, the analysis can provide a parallel hypothesis-generating framework to be confirmed by targeted approaches such as function-based experiments or complementary PPI methods such as proximity ligation assays. While I expanded a network from six starting nodes (tau and five confirmed tau interactors), the strategy for generating the network could have also been different. For example, expanding networks from six single independent nodes. While this is more consistent with the physical approach to generating and consolidating proximity labelling proteomic data, conclusions from such outputs often evade reliability. Combining six independently amplified datasets risks introducing entirely unrelated datapoints, which would be challenging to integrate regardless. Yet data management strategies upon gathering and consolidating such sizeable datasets is a valid consideration for any medium-throughput proximity labelling approach. In future, the addition of a secondary tau interactor mediated by a primary tau interactor will amplify the novelty of an already powerful strategy. Because of the capacity for extensive labelling using proximity labelling, it would be interesting to determine how many degrees of fusion proteins would fundamentally change our understanding of a mammalian interactome. Questions about how interactions mediate engram state-dependent learning and memory become entirely within reach to answer.

The activity-dependent labelling approach provides a basis for interrogating interactions in animal models of disease. Tau is implicated in a large subset of neurodegenerative diseases, including Alzheimer's Disease (AD), where tau pathology and cognitive decline correlate [410, 411]. Neurodegenerative disease and aberrant tau phosphorylation promote somatodendritic redistribution of axonal tau [151] and synaptic interactions of tau are linked to the role of tau in synaptic pathology [8]. Labelling tau interactions during redistribution could identify key mediators and facilitating factors. Furthermore, since both human AD and transgenic mouse models display aberrant activity and synchronicity of neuronal networks [412], activity-dependent target identification might deliver targets selectively in active cells. Since our understanding of AD aetiology is incomplete and lack effective treatments, the therapeutic value stemming from these insights could be significant.

The tau engram interactomes presented here together represent a significant and unique advance towards the molecular nature of a persistent and retrievable engram. Targeted activity-dependent

labelling reveals the interactions that support engram cell functions. Interrogating processes of memory at this level in behaving mice provides insights that have previously been unavailable.

Supplementary Figures

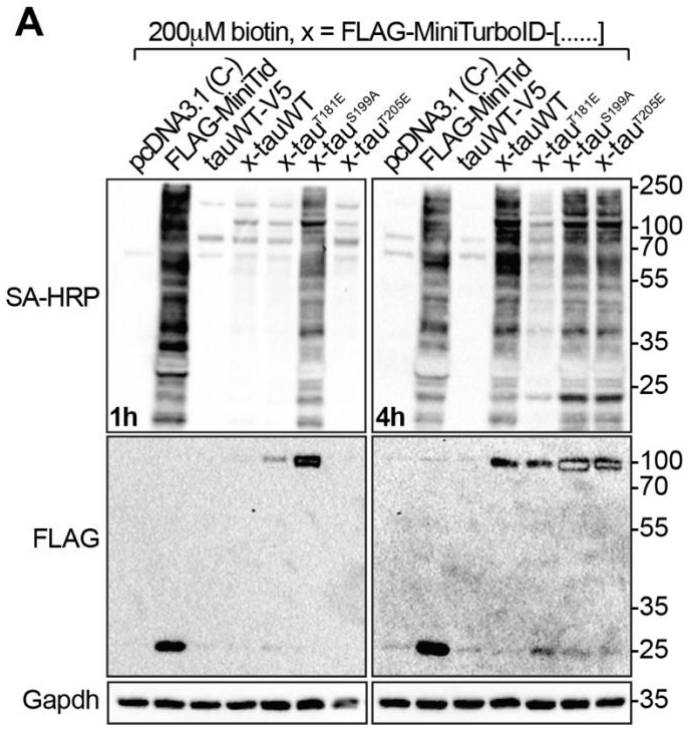

Supplementary Figure 3.1. ***Efficient biotinylation by MiniTurboID upon addition of biotin to cells***. (**A**) Comparison of enzyme activity between soluble MiniTurboID [326] and MiniTurboID fuse to one of four tau protein variants: tau wild type (WT), tauT181E, tauS199A, or tauT205E. At 48 h post-transfection, cells were incubated with media containing 200 μM biotin and harvested one or four hours later. Streptavidin-HRP (SA-HRP) signal denotes protein biotinylation and anti-FLAG signal indicates MiniTurboID expression in HEK 293T cell cytosol. Expression levels of tau variant bait protein strength varied more in cells incubated with biotin for 1 hour than 4 hours. Consistent Gapdh signal indicated equal protein loading.

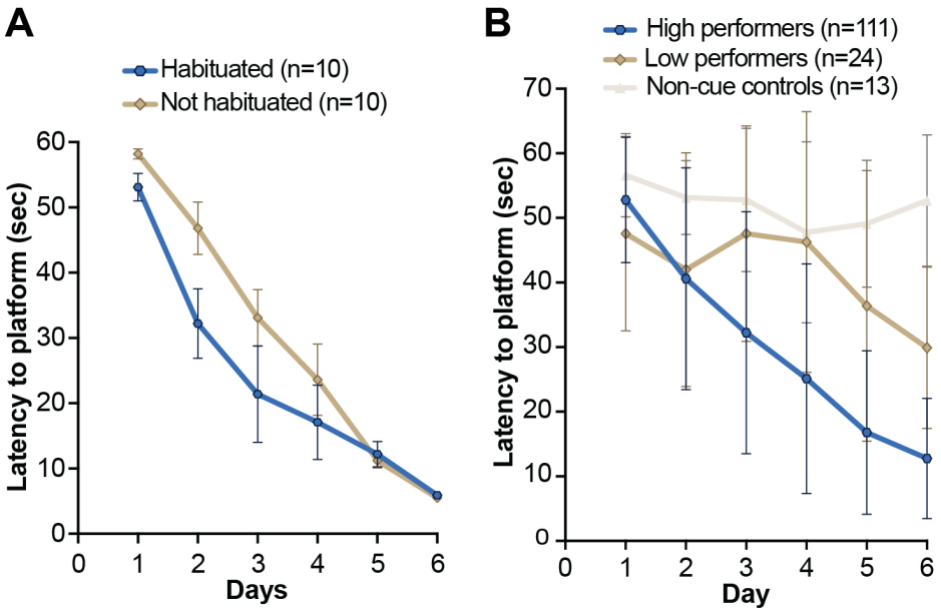

Supplementary Figure 3.2. ***Effects of habituation on performance in the MWM task and performance differences between learners and non-learners.***

(**A**) Habituated mice (blue line, hexagon) find the hidden platform slightly faster than non-habituated mice (beige line, diamond) over MWMd1-4 but not MWMd5-6. Performance in the MWM task measured as latency to platform [342].

(**B**) Latency to platform for mice separated by rSoWP (see **Fig 3.2B**) into high performers and low performers. The performance of non-cue controls is included for comparison.

Values on graph are means +/-SEM error bars.

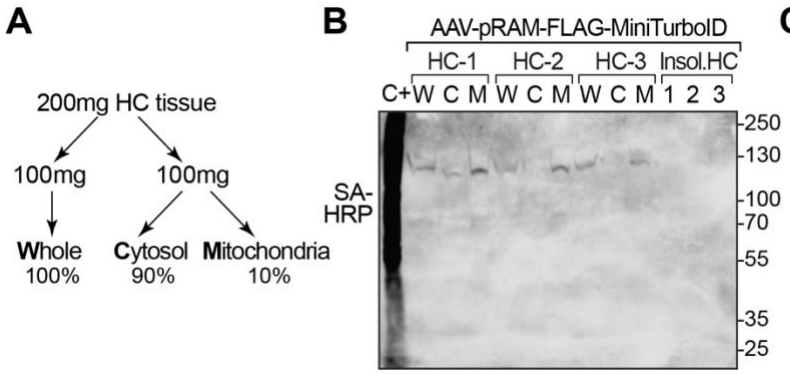

C

Mitochondrial peptides in fractionated samples

MS Sample	Peptide hits	Mitochondrial peptide proportion
Whole cell	161	48.4% (78)
Cytosolic fraction	58	17.2% (10)
Mitochondrial fraction	12	83.3% (10)

Supplementary Figure 3.3. ***Mitochondrial protein isolation reduced mitochondrial protein in cytosolic fraction for mass spectrometry analyses.***

(**A**) Flow diagram outlining the process of isolating cytosolic and mitochondrial fractions of samples from hippocampal tissue.

(**B**) Biotinylated proteins in hippocampal (HC-1/2/3) tissue from mice injected with AAV.RAM-MiniTid. Whole (W), cytosolic (C), and mitochondrial fractions were analysed for the presence of biotinylated protein, detected using HRP-conjugated streptavidin HRP (SA-HRP)

(**C**) Table summarises results from mass spectrometry (MS) analyses showing that cytosolic fractions contain the lowest proportion of mitochondrial peptides. The proportion and number of mitochondrial proteins in lists of identified biotinylated proteins from whole cell samples, a cytosolic fraction, and a mitochondrial fraction. This is a summary of Appendix Tables 12-14.

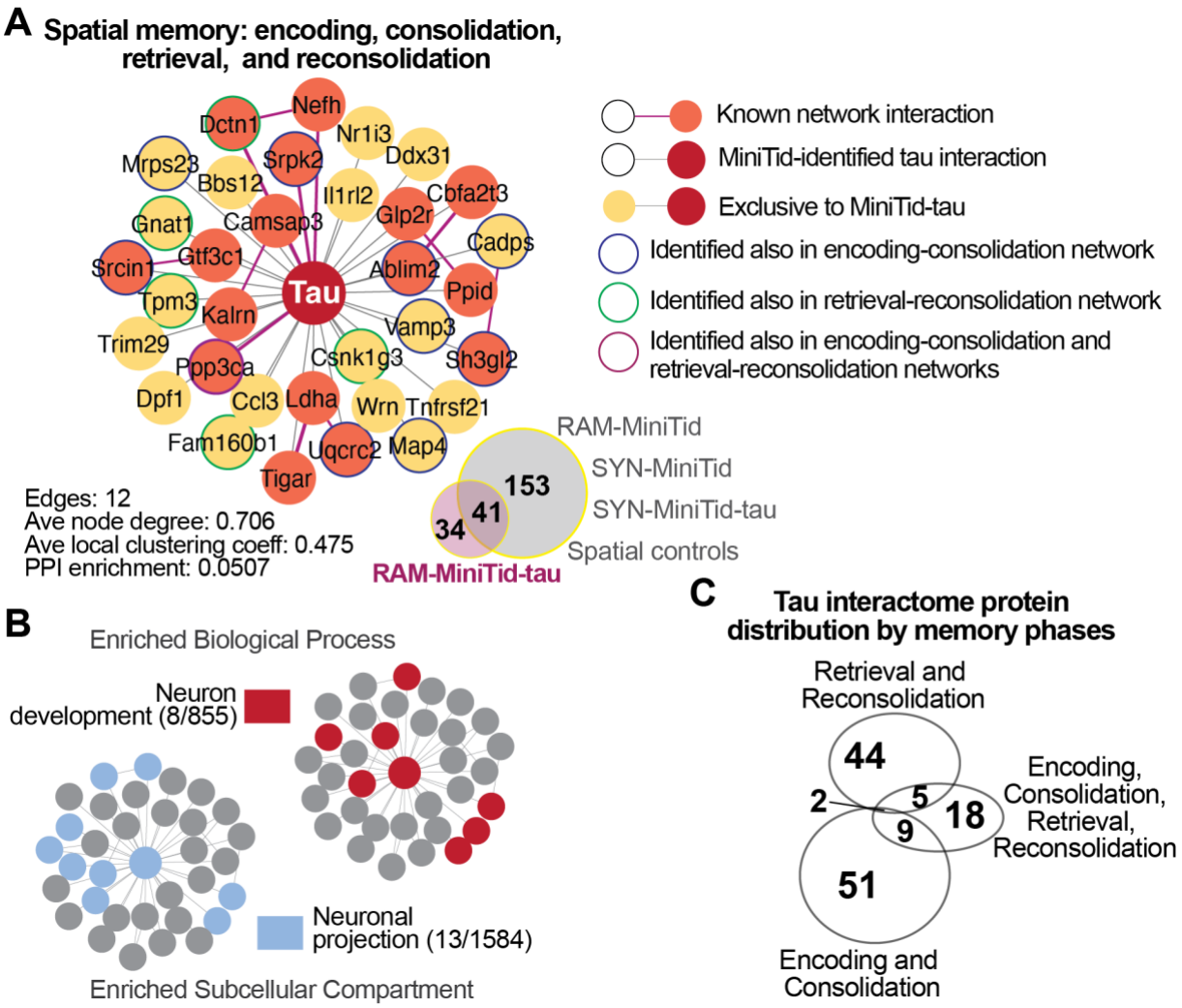

Supplementary Figure 3.4. ***Tau interactome in spatial learning and memory engram***. Interactions of tau, labelled in mouse brain during the Morris Water Maze (MWM) task. Experimental group mice were transduced to express MiniTurboID-tau under activity-dependent control (RAM promoter, pRAM). Tau interactome of spatial learning and memory was generated by harvesting mice on MWM final day 6 (encoding-consolidation-retrieval-reconsolidation, RRc).

(**A**) Tau protein-protein interaction (PPI) network in mouse hippocampus during spatial memory EC (n = 12 biological replicates). Network of exclusive interactors with network properties (STRING v11.5). Venn diagram shows unique proteins (network nodes) and overlapping proteins from experimental group AAV.RAM-MiniTid-tau compared to four additional groups (consolidated lists from 3 x rAAV groups and spatial learning controls, n = 22 biological replicates). Spatial control mice performed the MWM without cues (non-learning) during activity-dependent expression of either MiniTid or MiniTid-tau.

(**B**) Protein ontology enrichment for high-ranking categories from network in (**A**) based on STRING 'Strength' calculation. For strength score and false discovery rates, refer also to **Appendix Table 23**.

(**C**) Venn diagram summarising unique and overlapping proteins from the three tau interactomes.

Materials and Methods

Mice: C57BL/6J mice were purchased from ABR (Moss Vale, Australia). Tau knock-out mouse strain (*tau*$^{-/-}$) were described previously [162, 261]. All mouse strains were maintained on a C57BL/6J background. All mice were housed (2-5 mice per cage) in the College of Medicine & Public Health Animal Facility (CMPHAF) of Flinders University under standard conditions of temperature and humidity in a day/night cycle of 12/12 hours (light on at 6 am). All experimental subjects had normal health and immune status and were checked regularly at the animal research facility. Food and water were provided ad libitum. All procedures were conducted with a protocol approved by Flinders University Animal Welfare Committee in accordance with guidelines set forth by the Australian Code for the Care and Use of Animals for Scientific Purposes (NHMRC). Male and female mice were randomly assigned to each experimental condition and treatment, and all experiments were carried out between 2-7 pm.

For in vivo biotinylation experiments, adult (4-10 months old, mo) *tau*$^{+/+}$ and *tau*$^{-/-}$ mice underwent stereotaxic AAV injections at 6 mo. Sample size estimations were based on previous studies [262] and subjects were stratified into experimental groups by genotype, AAV administration, and cannula infusion treatment.

Mice were genotyped by polymerase chain reaction (PCR) using isopropanol-precipitated DNA from tail biopsies as template. Oligonucleotide primers for genotyping transgenes and targeted alleles by PCR are described in the **Primer Table** below.

Primer Table

Construct	(5'-3') Forward primer	(5'-3') Reverse primer
Mouse (tau$^{-/-}$)	GCAATCACCTTCCCTCCATA	ATTCAACCCCCTCGAATTTT
pBSKS-tau	GGTCCTCGAGGCTGAGCCCCGCCAGGAG	CGTAGAATTCTCACAAACCCTGCTTGGCCAG
pBSKS-Sh3gl2	TGGATCCCCCGGGCTGCAGGATGTCGGTGGCAGGGCTGAAG	TATCGATAAGCTTGATATCGCTAATGGGGCAGAGCAACCAG
pBSKS-Csnk1g1	TGGATCCCCCGGGCTGCAGGATGGACCATTCTAATAGGGAA	TATCGATAAGCTTGATATCGTCACTTGTGTCGCTGGGCTGT
pBSKS-Csnk1g3		

pBSKS-Lin7c	TGGATCCCCCGGGCTGCAGGATGG CGGCGCTGGGCGAACCT	TATCGATAAGCTTGATATCGTTAGGT CTGTTGTCTGCGTTTTG
pBSKS-Set	TGGATCCCCCGGGCTGCAGGATGTC TGCGCCGACGGCCAAAG	TATCGATAAGCTTGATATCGTTAGAT CTCACTCTCTTCCAGAATC
pBSKS-Ap2m1	TGGATCCCCCGGGCTGCAGGATGAT CGGAGGCTTATTCATC	TATCGATAAGCTTGATATCGCTAGCA GCGGGTTTCATAAAT
pCMV-Flag-MnTid-Ap2m1	CAGGGATCTCAGATCTCGATCGGAG GCTTATTCATC	GAGGCTCGAGAGGCCTTGCTAGCAG CGGGTTTCATAA
pCMV-Flag-MnTid-Ppp3ca	CAGGGATCTCAGATCTCGTCCGAGC CCAAGGCAATT	GAGGCTCGAGAGGCCTTGCTACTGA ATATTGCTGCTATTA
pCMV-Flag-MnTid-Csnk1g1	CAGGGATCTCAGATCTCGGTGGGAC CCAACTTCAGG	GAGGCTCGAGAGGCCTTGTCACTTG TGTCGCTGGGC
pCMV-Flag-MnTid-Csnk1g3	CAGGGATCTCAGATCTCGGAAAATA AAAAGAAAGACA	GAGGCTCGAGAGGCCTTGCTATTTG TGGCGCTGTAT
pCMV-Flag-MnTid-Cttn	CAGGGATCTCAGATCTCGTGGAAAG CCTCTGCAGGC	GAGGCTCGAGAGGCCTTGCTACTGC CGCAGCTCCAC
pCMV-Flag-MnTid-Pak2	CAGGGATCTCAGATCTCGTCTGATAA CGGAGAACTG	GAGGCTCGAGAGGCCTTGTTAACGG TTACTCTTCATT
pCMV-Flag-MnTid-Sh3gl2	CAGGGATCTCAGATCTCGTCGGTGG CAGGGCTGAAG	GAGGCTCGAGAGGCCTTGCTAATGG GGCAGAGCAAC
pCMV-Flag-MnTid-CamK2a	CAGGGATCTCAGATCTCGGCTACCA TCACCTGCACC	GAGGCTCGAGAGGCCTTGTCAATGG GGCAGGACGGA
pCMV-Flag-MnTid-Lin7c	CAGGGATCTCAGATCTCGGCGGCGC TGGGCGAACCT	GAGGCTCGAGAGGCCTTGTTAGGTC TGTTGTCTGCGT
pCMV-Flag-MnTid-MeCP2	CAGGGATCTCAGATCTCGGTAGCTG GGATGTTAGGG	GAGGCTCGAGAGGCCTTGTCAGCTA ACTCTCTCGGT

pCMV-Flag-MnTid-tau	CAGGGATCTCAGATCTCGGCTGAGCCCCGCCAGGA	AGAGGCTCGAGAGGCCTTGTCACAAACCCTGCTTGGCCA
pCMV-Flag-MnTid-eGFP	CAGGGATCTCAGATCTCGGTGAGCAAGGGCGAGGAGCTG	AGAGGCTCGAGAGGCCTTGCTACTTGTACAGCTCGTCCAT
pAAV-hSYN1-d2TTA-TRE	TTCTCTGGCCTAACTGGCCGAAGTGCAAGTGGGTTTTA	CGGGAAGCCATGGCTCCAGCGCAGATGGTCGCGCCCGT
pAAV-RAM-Flag-MnTid	TGAACCGTCAGATCGCCAGCCACCATGGATTACAAGG	ACTTATCCTTGAGAGACGTATCACTGCAGCTTTTCGGCAG
pAAV-RAM-Flag-MnTid-tau	TGAACCGTCAGATCGCCAGCCACCATGGATTACAAGG	TACTTATCCTTGAGAGACGTATCACAAACCCTGCTTGGCC

Cell line: Human embryonic kidney 293T/17 [HEK 293T/17] (CRL3216, ATCC, VA, USA) cells between passage numbers 5-15 were cultured in Dulbecco's Modified Eagle Medium (DMEM) (11965092, Gibco, ThermoFisher) supplemented with 10% (v/v) foetal bovine serum (FBS) (SH30084.04HI, HyClone, UT, USA), 1x Penicillin-Streptomycin (15140148, Gibco, ThermoFisher), and 1x GlutaMAX (35050079, Gibco, ThermoFisher). Cells were kept in a humidified incubator at 37°C and 5% CO_2 and checked daily to monitor growth rate, confluence, morphology, and potential contamination.

Bacterial strains: For plasmid transfection in mammalian cells, constructs were amplified in E. coli Max Efficiency DH5α Competent cells (18258012, Invitrogen, ThermoFisher, MA, USA). AAV vectors were propagated in E. coli OneShot Stbl3 (C737303, Invitrogen, ThermoFisher) to avoid recombination events. Colonies from both strains were grown using LB broth with agar (L3147, Miller, Sigma, Merck, Sydney, AUS) and clones expanded with LB broth (L3522, Miller; Sigma, Merck).

Recombinant adeno-associated virus production: Packaging of AAV vectors was performed as described [213, 222, 223]. In brief, for packaging of AAV particles, HEK293T (CRL3216, ATCC) were seeded in DMEM (11965092, Gibco, ThermoFisher) supplemented with 10% (v/v) FBS (SH30084.04HI, HyClone) at 70-80% confluence. Culture medium was changed to Iscove's Modified Dulbecco's Medium (IMDM) (I3390, Sigma, Merck, Sydney, AUS) with 5% FBS 3 hours prior to transfection. Cells were transfected with viral genome-containing plasmid, pFdelta6 as helper plasmid and systemic neurotropic AAV-PHP.B plasmid containing rep and cap sequences using polyethyleneimine-Max (PEI) (23966-1, Polysciences, Taipei, Taiwan) as a transfection reagent. Cells were harvested 72 hours post transfection and centrifuged at 1000g for 10 min at 4°C to pellet the

cells. The cells were resuspended in 10 mL PBS with 0.001% Pluronic F-68 (24040032, Gibco, ThermoFisher) and lysed by sonication (3 x 10 s, 30% amplitude). Following centrifugation at 3220g for 15 min at 4°C, benzonase (~500 U) (E1014, Merck-Millipore, Sydney, AUS) was added to the cleared supernatant (SN) and incubated at 37°C for 45 min. The viral suspension was centrifuged at 2415g for 10 min at 4°C. SNs were purified using iodixanol gradient by ultracentrifugation (200,000g, 2 h, 16°C). AAV particles were concentrated and exchanged into PBS in an Amicon 100 kDa 15 ml concentrator (UFC910008, Merck, Sydney, AUS) at 3000g at 4°C. Titres were determined by quantitative polymerase chain reaction (qPCR). AAV titres were: AAV-PHP.B-RAM-d2TTA-TRE-FlagMnTid (2.24 x 10^{13} viral genomes per ml (vg/ml)), AAV-PHP.B-hSyn1-d2TTA-TRE-FlagMnTid (1.32 x 10^{14} vg/ml), AAV-PHP.B-RAM-d2TTA-TRE-eGFP (9.69 x 10^{12} vg/ml), AAV-PHP.B-RAM-d2TTA-TRE-FlagMnTid-Tau (1.91 x 10^{13} vg/ml), AAV-PHP.B-hSyn1-d2TTA-TRE-FlagMnTid-Tau (6.42 x 10^{13} vg/ml). After determining AAV genomic titres, aliquots were stored at -80°C.

Stereotaxic viral delivery: For targeted hippocampal (HC) injections of rAAVs, $tau^{+/+}$ and $tau^{-/-}$ mice were anaesthetized by intraperitoneal (i.p.) injection of ketamine (100 $mg.kg^{-1}$, Imalgene 500, Merial, GA, USA) and xylazine (12 $mg.kg^{-1}$, Rompun, Bayer, Leverkusen, Germany). Mice were placed into a stereotaxic apparatus (Kopf Instruments) with mouse adaptor and lateral ear bars. With the aid of a microinjector (MicroSyringe Pump Controller, WPI, Coherent Scientific, SA, AUS), AAV injections were administered at one site each bilaterally, targeting the CA1 region of HC with the following coordinates: AP -1.9, L ± 1.9, DV -1.6 [264]. Animals were allowed to recover for 7 days, and upon confirming a bodyweight similar to pre-surgery recordings, mice proceeded to behavioural testing.

Memory testing: Spatial learning and memory was tested using the Morris Water maze (MWM) task [328, 413, 414]. A water tank for mouse MWM (144 cm diameter, 60 cm height) with white non-reflective interior surface was custom built and placed in a room with indirect lighting and filled with water (19-22°C) with diluted non-irritant white dye. Four distal cues, each with a different symbol, surrounded the tank at the four quadrants in perpendicular positions. In the target quadrant (Q4), a 12 cm diameter platform was submerged 1 cm below the water surface. For spatial memory control mice, all conditions were identical, except that the cues faced away from the inside of the tank. Videos were recorded on CCD camera and analysed using AnyMaze Software. For spatial memory acquisition, four trials of 60 seconds each were performed per day (= one session) for a total of six sessions. The starting position was randomized along the outer edge of the start quadrant for all trials. To measure task performance, recordings were analysed for latency to platform escape [50]. To exclude vision impairments, (acquisition of visually-cued controls) a marker above the platform was placed and mice performed 4 x 60 s trials on day one. Mice were gender and age-matched and tested at 3-8 months old. Mice that displayed continuous floating behaviour were excluded. Tracking of swim

paths was done using the AnyMaze software (Stölting). To exclude motor impaired mice, average swimming speed was determined.

Mouse brain cryo-preservation: From each experimental condition, right hemispheres from mice were fixed in 4% paraformaldehyde (PFA) (P6148, Merck) at 4°C overnight and subsequently immersion-fixed in each of 10%, 20%, and 30% sucrose (S5-500, ThermoFisher, MA, USA) PBS solutions (rotation, 12h, 4°C). Hemispheres were embedded in Tissue-Tek (4583, Sakura, emgrid, SA, Australia) and stored at -80°C until histological sectioning and staining.

Histological sections and staining: Brain sections were stained as previously described with some modifications [265]. Frozen right hemispheres of mouse brain were cryo-sectioned (15 µm) and dried on slides in (1 h, 37°C). Tissue was permeabilized in PBS with 0.01% Triton X-100 (10789704001, Sigma, MI, USA) for 5 min at RT followed by blocking in PBS with 3% goat blocking serum for 45 min. Tissue sections were incubated with primary antibodies (1 h, RT), thrice washed with PBS, and incubated with secondary antibody conjugated to a fluorophore (1/500; 1 h, RT) to visualise proteins of interest. Expression of MiniTurboID constructs were detected using mouse anti-FLAG (1/500, F1804, Sigma), DNA was stained with DAPI (1/1000) and biotinylated proteins were detected using SA-Cy3 (1/1000).

Immunoprecipitation: Immunoprecipitation was performed from cell or tissue lysates as previously described [10]. Briefly, cells and tissue were lysed in modified RIPA buffer (no SDS) on ice and lysates cleared by centrifugation (10,000g, 10 min, 4°C). Protein concentration was determined by BCA assay and 500 µg of protein lysate was incubated with 1 µl of primary antibody for 3 h with rotation at 4 °C and additional 1 h with 30 µl buffer-equilibrated Protein G magnetic beads (70024S, CST, Arundel, Australia). Incubation was followed by three washes in modified RIPA, resuspended in 40 µl of loading buffer (50 mM Tris-HCl pH 6.8, 2% SDS, 5% β-mercaptoethanol, 0.01% bromophenol blue, 6% glycerol) and incubated at 95°C for 5 min. The SN was separated from the beads using a magnetic rack and 5 µl was used for input sample lanes. Immunoprecipitation was performed with goat anti-V5 tag (1/500, 95038, abcam).

Immunoblotting: Western blotting was performed as previously described [223]. Briefly, samples were separated by 10% SDS-PAGE and following protein transfer, membranes were blocked with 5% skim milk powder in Tris-buffered saline with 0.1% Tween-20 (TBS-T) before probing with primary and secondary antibodies (1 h each, RT). Visualising blots was performed as described previously [266]. Bands were visualised by chemiluminescence using Clarity Western ECL Substrate (1705060, Bio-Rad, Sydney, AUS) on a digital imaging system (Chemidoc XRS+; Bio-Rad, Sydney, Australia). Densitometric quantification of Western blot results was performed using Fiji [267]. Expression of MiniTurboID constructs were detected using mouse anti-FLAG (1/500, F1804, Sigma). Tau expression was detected using mouse anti-tau (1/2000, 4019S, CST). Arc expression was detected

using rabbit anti-Arc (1/2000, 28916, CST). Gapdh expression was detected using mouse anti-GAPDH (1/2000, MAB374, Sigma). Biotinylated proteins were detected using streptavidin (SA) HRP (1/2000, 3999S, CST).

Biotinylated protein enrichment in mouse brain lysates: For AAV expression of MiniTurboID constructs in adult hippocampus, tau$^{-/-}$ mice were anesthetized by i.p. injection of ketamine (100 mg.kg^{-1}) and xylazine (12 mg.kg^{-1}) and placed on a stereotaxic frame. Injections of 300 nL undiluted AAV solution were administered at two sites each bilaterally, targeting the hippocampus with the following coordinates: AP -2, L ± 2, DV -2.1, and AP -3.6, L ± 2.5, DV -2.1 [264]. After 7 days of recovery in their home cages, mice received 4-7 consecutive days of s.c. biotin injections (24 mg.kg^{-1}).

Sham AAV (vehicle) and sham biotin (vehicle) injections were additionally performed for tau$^{-/-}$ mice (n = 2 each). 4-7 consecutive days of s.c. saline injections (3 mL.kg^{-1}). All mice were deeply anaesthetised by i.p. injection of ketamine (100 mg.kg^{-1}) and xylene (12 mg.kg^{-1}) before transcardial perfusion with PBS (pH 7.4). Per AAV condition, each bilateral HC from each mouse was combined. Dissected brain tissue was flash-frozen in liquid nitrogen before storing at -80°C for immunoblotting and mass spectrometric (MS) analyses.

Mitochondrial isolation and removal: Mitochondrial organelles were isolated as per manufacturer instructions (89801, ThermoFisher). Briefly, ~100 mg of hippocampal tissue was washed with sterile 1xPBS, spun down, and PBS was discarded. Tissue was cut into small pieces and hand homogenised (5 triturations) in 800µL of PBS. Tissue samples were centrifuged tissue at 1,000g for 3 minutes at 4°C and SN discarded. Pellets were suspended in 800µL of BSA/Reagent A Solution and vortexed at medium speed for 5 sec, then incubated on ice for 2 min. 10µL of Mitochondria Isolation Reagent B was added and vortexed at maximum speed for 5 sec. Samples were incubated of ice for 5 min with a 5 sec vortex mix at every minute, then 800µL of Mitochondria Isolation Reagent C was added. Tubes were inverted twice and centrifuged (700g, 10 min, 4°C) and the pellet stored as the control insoluble fraction. Transferred SN was centrifuged (3000g, 15 min, 4°C) and the SN (cytosolic fraction) was kept for methanol precipitation and further processing for either mass spectrometry or western blot. Mitochondrial pellet was kept as control for mass spectrometry and western blotting.

Homogenisation of biotinylated mouse brain tissue: Protein lysate from brain tissue was isolated as described [216]. Briefly, dissected HC tissue was homogenised (~15 repetitive triturations) in 300 µl of Buffer-A (50 mM HEPES pH 7.5 (7365-45-9, Sigma, Merck); 150 mM NaCl; 4 µg/1 ml Leupeptin (78435, ThermoFisher), 4 µg/1 ml PepstatinA (78435, ThermoFisher); 1 mM EDTA (E6758, Merck) in 2 mM PMSF (52332, Sigma, Merck)) followed by addition of 300 µl Buffer-B (50 mM HEPES pH 7.5; 150 mM NaCl; 1 mM EDTA, 2% Triton X-100 (10789704001, Sigma); 0.4% SDS (436143, Merck); 2% deoxycholate (D6750, Merck,)) on ice using a Dounce homogeniser (Heidolph-Instruments,

Schwabach, Germany). Samples were sonicated (2 x 10 s, 20% amplitude) and the SN cleared by centrifugation (20,000g, 30 min, 4°C) and SDS was added to a final concentration of 1%. Protein concentrations were recorded and aliquots containing 40 µg protein (expression) and/or 1000 µg proten (biotinylation) per sample were reserved for WB. Remaining lysates were adjusted to 2.5 mg protein per sample then 3 samples were pooled (7.5 mg total) and stored at -80°C until preparation for MS.

Biotinylated protein enrichment from brain lysates: Precipitation and trypsin digest of protein lysate samples were performed as previously described [215, 268]. Briefly, three volumes of methanol and one volume each of chloroform and water were added to each sample, vortexed and centrifuged (15,000g, 2 min), creating a disc-like protein pellet at the hydrophilic-hydrophobic solvent interface. Upon removal of solvents, three volumes of methanol were used to resuspend the protein pellet before centrifugation (15,000g, 2 min), and then removed to air-dry the remaining pellet (15 mins, RT). Protein from each sample was resuspended in 400 µl buffer (4 M urea, 0.1% ProteaseMAX surfactant buffer (V2072, Promega), 50 mM NH_4HCO_3) and following a brief sonication pulse, DL-dithiothreitol (DTT) (10197777001, Sigma, Merck) was added to a 5 mM final concentration and samples were incubated in a Thermos-mixer (800 rpm; 1 h, 55°C). Iodoacetamide (I6125, Sigma, Merck) was added to a final 10 mM concentration and re-incubated (800 rpm, 20 min, in the dark). Trypsin buffer containing NH_4HCO_3 (150 µl, 50 mM), ProteaseMAX (2.5 µl, 1% in 50 mM NH_4HCO_3), and 1:100 (w_{enz}/w_{prot}) trypsin (V5111, Promega, WI, USA) was added to each sample and incubated (700 rpm, 4 h, 37°C). Trifluoroacetic acid (TFA) (302013, Merck) was added to 0.1% final concentration to inhibit trypsin, then samples were centrifuged (20,000g, 20 min) and the SN transferred for desalting to solid-phase extraction tC18 cartridges (WAT036810, Waters, MA, USA) as described previously [269]. Briefly, cartridges were sequentially washed with 3 ml acetonitrile (271004, Sigma, Merck), 3 ml 0.5% acetic acid (695092, Merck) in 50% acetonitrile, and 3 ml 0.1% TFA in dH_2O. After adding the peptide samples, cartridges were washed with 3 ml 0.1% TFA in dH_2O, followed by 250 µl 0.5% acetic acid in dH_2O. Peptides were eluted with a solution of 1 ml 0.5% acetic acid in 80% acetonitrile and dried overnight in a vacuum concentrator. A modified biotinylated peptide-enrichment protocol was used [268] whereby peptides were resuspended in a 250 µl dissolution buffer (0.05% SDS in PBS) with an added 55 µl equilibrated neutravidin (NA) magnetic bead slurry (09-981-155, GE, ThermoFisher, MA, USA) and incubated at RT on a rotator for 2 h. NA-bound peptides were immobilised by magnet and washed sequentially with 1.5 ml PBS, and 1.5 ml PBS with an increasing acetonitrile gradient (2.5%, 5%, 10% acetonitrile), rotating for 5 min at each wash step. Bead-bound peptides were resuspended in 250 µl dissociation buffer (0.2% TFA, 0.1% formic acid, 80% acetonitrile) and incubated (rotating, 15 min) before magnet immobilisation and collection of 'SN1'. To maximise peptide recovery, beads were resuspended and re-incubated in 250 µl dissociation buffer under heat (700 rpm, 5 min, 95°C), followed by collection and addition of SN2 to SN1. Eluates were

dried under vacuum and resuspended to 0.5 µg/µl of 0.2% heptafluorobutyric acid (HFBA) (524311, Supelco, Merck) with 1% formic acid (F0507, Sigma, Merck) for MS analysis.

Mass spectrometry: Mass spectrometry was performed as described previously [215]. Peptide samples sourced from primary neurons and mouse brain were run (3 µg injected per run) and captured on a C18 cartridge (Acclaim PepMap 100, 5 µm 100 Å, Thermo Scientific Dionex, Waltham, USA) using a Q Exactive Orbitrap (ThermoFisher) before switching to a capillary column (~20 cm) containing C18 reverse phase packing (Reprosil-Pur, 1.9 µm, 200 Å, Dr Maisch GmbH, Ammerbuch-Entringen, Germany), and eluted with 40 min gradient of buffer A (H_2O:CH_3CN of 98:2 with 0.1% formic acid) to buffer B (H_2O:CH_3CN of 20:80 with 0.1% formic acid) at 200 nL/min. The mass spectrometer was set to positive ion mode. Peak lists were generated using MASCOT Distiller (Matrix Science, London, UK) and searched using the MASCOT search engine (v2.6.2, Matrix Science). Peak lists were matched to amino acid sequences from the SwissProt database (downloaded 10-8-19; Mammalia taxonomy, 66946 entries) and the Peptide Prophet algorithm [270] assigned identity to peptides with FDR = 1.6% and to proteins with FDR = 0.4%. Each protein was considered identified when assigned 1 unique peptide with a peptide score >38. All identified biotinylated proteins for background and experimental conditions are listed in **Appendix Tables 3-18**.

Network generation and analysis: Three biotinylated protein lists from AAV.RAM-MiniTurboID-tau (RMT), one representing each spatial memory phase encoding-consolidation (EC), retrieval-reconsolidation (RRc), and a combined group of memory (ECRRc), were generated from hippocampal mouse samples were scrutinised using maximally stringent cut-offs. All overlap identities of biotinylated proteins between RMT-EC/RRc/ECRRc and a combination of proteins identified, in each memory phase, for the control rAAV groups were removed (control rAAV groups: pAAV.RAM-MiniTurboID, AAV.Syn1-MiniTurboID-tau, and AAV.Syn1-MiniTurboID). Functional protein-protein interaction networks and protein ontology were generated using STRING (v11.5) database annotations for the entire human proteome. Interactomes and network properties were visually represented using CytoScape (v3.9.1).

Transfection of cell culture: Plasmid DNA was transfected using polyethylenimine (PEI; 23966, Polysciences) at 80% confluency. Four micrograms of plasmid DNA and 12 µL of PEI were added to saline to a final volume of 420 µL. DNA was allowed to incubate for 15 min and then added dropwise to each 60 mm cell-culture plate.

Immunofluorescence imaging: Confocal imaging of immunofluorescent-stained cells and tissue was performed using the inverted confocal microscope LSM 880 (ZEISS) with a 10X air objective (aPlan-Apochromat 10X/1.49, ZEISS) operating through ZEN (ZEISS) software.

Immunofluorescence imaging analyses: Image analyses were performed using Fiji [267] without prior knowledge of the performed experimental manipulation. Channel intensities were quantified from images with arbitrarily set and uniformly applied global thresholds.

Plasmid constructs: For biotinylation experiments, mouse genes Ap2m1, Csnk1g1, Csnk1g3, Sh3gl2, Set, Lin7c, Pak2, Ppp3ca, Camk2a, and Mecp2 were cloned into the EcoRI (R3101S, New England Biolabs (NEB), MA, USA) site of plasmid pBluescript SK (-). Then, human MAPT gene encoding full length wild-type tau (hTauWT-FL, 441 amino acids), eGFP (#58867, AddGene), Ap2m1, Csnk1g1, Csnk1g3, Sh3gl2, Set, Lin7c, Pak2, Ppp3ca, Camk2a, and Mecp2 were cloned into the EcoRI (R3101S, NEB, USA) site of plasmid FLAG-MiniTurboID-MCS (#124647, AddGene) and amplified in DH5a Competent cells (Invitrogen, 18258012, ThermoFisher). Constructs for generation of AAV particles included – and were based on – pAAV-pRAM-d2tTA-TRE-MCS-WPRE (#63931, AddGene). The WPRE sequence was replaced with FLAG-MiniTurboID, FLAG-MiniTurboID-tau at the AgeI-HF (R3552S, NEB) and SpeI (R3133S) sites. The pRAM sequence was replaced with pSyn1 from (#58867, AddGene) at the SpeI (R3133S) and EcoRI (R3101S, NEB, USA) sites. AAV vectors were propagated in OneShot Stbl3 (C737303, Invitrogen, ThermoFisher) to avoid recombination events. For immunoprecipitation experiments, hTauWT-FL was expressed from pcDNA3.2-DEST-hTauWT-V5 [223]. Oligonucleotide primers for PCR-based generation of plasmid constructs are listed in **Primers** table. All ligation reactions were carried out using HiFi Assembly 2X Master Mix (E2621S, NEB) and all PCR reactions using Q5 High Fidelity 2X Master Mix (M0492S, NEB). All constructs were verified by sequencing.

HEK293T cell transfection and cell lysis: HEK293T cells (CLR-3216, ATCC) were maintained in DMEM (11965092, Gibco, ThermoFisher) supplemented with 10% FBS (v/v), 1% penicillin/streptomycin (v/v), and 2 mM L-glutamine at 37°C, 5% CO_2, and 55% humidity. Cells were seeded on 6-well plates (3.0×10^5 cells) 36 h before transfection ant the culture media was replaced 2 hours before transfection. The plasmid DNA was transfected using polyethylenimine (PEI; 23966, Polysciences) when cells were at 75% confluency. Three micrograms of DNA and 9 µl of P.E.I. were added to saline to a final volume of 235 µl. DNA incubated for 10 mins and added dropwise to each well.

Statistics: All statistical analyses were performed using Prism (v9) (GraphPad). Inter-group comparisons were performed using ANOVA with post-hoc test with Sidak's multiple comparisons adjustment. Statistical significance was set at $p< 0.05$ (*), $p< 0.01$ (**), $p< 0.001$ (***), $p< 0.0001$ (****), and no significance (n.s.). Details on individual test parameters are provided in figure legends.

BIBLIOGRAPHY

1. Kandel, E.R. and J.H. Schwartz, *Molecular biology of learning: modulation of transmitter release.* Science, 1982. **218**(4571): p. 433-43.
2. Janning, D., et al., *Single-molecule tracking of tau reveals fast kiss-and-hop interaction with microtubules in living neurons.* Mol Biol Cell, 2014. **25**(22): p. 3541-51.
3. Hirokawa, N., et al., *Selective stabilization of tau in axons and microtubule-associated protein 2C in cell bodies and dendrites contributes to polarized localization of cytoskeletal proteins in mature neurons.* J Cell Biol, 1996. **132**(4): p. 667-79.
4. Dixit, R., et al., *Differential regulation of dynein and kinesin motor proteins by tau.* Science, 2008. **319**(5866): p. 1086-9.
5. Stefanoska, K., et al., *An N-terminal motif unique to primate tau enables differential protein-protein interactions.* J Biol Chem, 2018. **293**(10): p. 3710-3719.
6. Gauthier-Kemper, A., et al., *Annexins A2 and A6 interact with the extreme N terminus of tau and thereby contribute to tau's axonal localization.* J Biol Chem, 2018. **293**(21): p. 8065-8076.
7. Sharma, V.M., et al., *Tau impacts on growth-factor-stimulated actin remodeling.* J Cell Sci, 2007. **120**(Pt 5): p. 748-57.
8. Zhou, L., et al., *Tau association with synaptic vesicles causes presynaptic dysfunction.* Nat Commun, 2017. **8**: p. 15295.
9. Chabrier, M.A., et al., *Synergistic effects of amyloid-beta and wild-type human tau on dendritic spine loss in a floxed double transgenic model of Alzheimer's disease.* Neurobiol Dis, 2014. **64**: p. 107-17.
10. Ittner, L.M., et al., *Dendritic function of tau mediates amyloid-beta toxicity in Alzheimer's disease mouse models.* Cell, 2010. **142**(3): p. 387-97.
11. Hashimoto, S., et al., *Tau binding protein CAPON induces tau aggregation and neurodegeneration.* Nature communications, 2019. **10**(1): p. 2394.
12. Guyer, P., Horstmann, RP, *Idealism*, in *The Stanford Encyclopedia of Philosophy*. 2019: Stanford University.
13. Psillos, S., Curd, M, *The Routledge Companion to Philosophy of Science*. 2010, London: Routledge.
14. Tinbergen, N., *Ethology and stress diseases.* Science, 1974. **185**(4145): p. 20-7.
15. Araiba, S., *Current Diversification of Behaviorism.* Perspect Behav Sci, 2020. **43**(1): p. 157-175.
16. Hurford, J.R., *The evolution of the critical period for language acquisition.* Cognition, 1991. **40**(3): p. 159-201.
17. Mason, W.A. and S.P. Mendoza, *Generic aspects of primate attachments: parents, offspring and mates.* Psychoneuroendocrinology, 1998. **23**(8): p. 765-78.
18. Chomsky, N., *Review of Skinner's Verbal Behavior.* Language, 1959. **35**(1): p. 29-58.
19. Kandel, E., *Biology of the mind.* Newsweek, 2006. **147**(13): p. 47.
20. Tuic, *Tool use in chimpanzees*. 2018, OneKindPlanet.
21. Akhtar, A., *The flaws and human harms of animal experimentation.* Camb Q Healthc Ethics, 2015. **24**(4): p. 407-19.
22. Morgan, K., Tromborg CT, *Sources of stress in captivity.* Applied Animal Behaviour Science 2007. **102**: p. 262–302.
23. Macleod MR, O.C.T., Howells DW, Donnan GA, *Pooling of animal experimental data reveals influence of study design and publication bias.* Stroke, 2004(35): p. 1203-1208.
24. Tulving, E., *Episodic and semantic memor*, in *Organization of Memory*, E. ulving, Donaldson, W., Editor. 1972, Academic Press: New York. p. 381–403.
25. Clayton, N.S. and J.R. Krebs, *Memory in food-storing birds: from behaviour to brain.* Curr Opin Neurobiol, 1995. **5**(2): p. 149-54.
26. Dickinson, A., *Learning: the need for a hybrid theory.*, in *Science of Memory: Concepts*, H.L. Roediger, Dude, Y., Fitzpatrick, S.M., Editor. 2007, Oxford University Press: Oxford.

27. Jacobs, L.F., *The PROUST hypothesis: the embodiment of olfactory cognition.* Anim Cogn, 2023. **26**(1): p. 59-72.
28. Semon, R., *The mneme*. 1921, London: Allen, Unwin.
29. Moscovitch, *Science of Memory: Concepts,*, ed. Y. Roediger, Dudai, SM. 2007: Oxford Univ. Press.
30. Semon, R., *Mnemic Psychology* 1923: Allen & Unwin.
31. Lashley, K., *Brain Mechanisms and Intelligence: A Quantitative Study of Injuries to the Brain*, ed. D.B.o. Psychology. Vol. 1038. 1963: Dover Publications.
32. Hebb, D.O., *The Organization of Behavior: A Neuropsychological Theory*. 1949: Wiley.
33. Shatz, C.J., *The developing brain.* Sci Am, 1992. **267**(3): p. 60-7.
34. Knierim, J.J. and J.P. Neunuebel, *Tracking the flow of hippocampal computation: Pattern separation, pattern completion, and attractor dynamics.* Neurobiol Learn Mem, 2016. **129**: p. 38-49.
35. Zago, S., et al., *Bartolomeo Panizza and the discovery of the brain's visual center.* Arch Neurol, 2000. **57**(11): p. 1642-8.
36. Dronkers, N.F., et al., *Paul Broca's historic cases: high resolution MR imaging of the brains of Leborgne and Lelong.* Brain, 2007. **130**(Pt 5): p. 1432-41.
37. Gross, C., *Brain, vision, memory: tales in the history of neuroscience*. 1998, Cambridge, MA: MIT Press.
38. Abel, T. and K.M. Lattal, *Molecular mechanisms of memory acquisition, consolidation and retrieval.* Curr Opin Neurobiol, 2001. **11**(2): p. 180-7.
39. Camina, E. and F. Guell, *The Neuroanatomical, Neurophysiological and Psychological Basis of Memory: Current Models and Their Origins.* Front Pharmacol, 2017. **8**: p. 438.
40. Dickerson, B.C. and H. Eichenbaum, *The episodic memory system: neurocircuitry and disorders.* Neuropsychopharmacology, 2010. **35**(1): p. 86-104.
41. Binder, J.R. and R.H. Desai, *The neurobiology of semantic memory.* Trends Cogn Sci, 2011. **15**(11): p. 527-36.
42. Pilly, P.K. and S. Grossberg, *How do spatial learning and memory occur in the brain? Coordinated learning of entorhinal grid cells and hippocampal place cells.* J Cogn Neurosci, 2012. **24**(5): p. 1031-54.
43. Devitt, A.L., D.R. Addis, and D.L. Schacter, *Episodic and semantic content of memory and imagination: A multilevel analysis.* Mem Cognit, 2017. **45**(7): p. 1078-1094.
44. Clayton, N.S., L.H. Salwiczek, and A. Dickinson, *Episodic memory.* Curr Biol, 2007. **17**(6): p. R189-91.
45. McRae, K., Jones, M, *Semantic Memory*, in *The Oxford Handbook of Cognitive Psychology*, R. D, Editor. 2013, McRae, Ken; Jones, Michael: Ney York. p. 206-216.
46. Conway, M.A. and C.W. Pleydell-Pearce, *The construction of autobiographical memories in the self-memory system.* Psychol Rev, 2000. **107**(2): p. 261-88.
47. Ino, T., et al., *Brain activation during autobiographical memory retrieval with special reference to default mode network.* Open Neuroimag J, 2011. **5**: p. 14-23.
48. Mehta, M., *Spatial Memory in Humans*, in *Encyclopedia of Psychopharmacology*, I. P, Editor. 2010, Springer: Berlin, Heidelberg. p. 1262–1266,.
49. Wang, T., K. Schweizer, and X. Ren, *Executive Control in Learning: Evidence for the Dissociation of Rule Learning and Associative Learning.* Adv Cogn Psychol, 2019. **15**(1): p. 41-51.
50. Vorhees, C.V. and M.T. Williams, *Assessing spatial learning and memory in rodents.* ILAR J, 2014. **55**(2): p. 310-32.
51. Medina, J., *The biology of recognition memory*. 2008.
52. Manns, J.R., R.O. Hopkins, and L.R. Squire, *Semantic memory and the human hippocampus.* Neuron, 2003. **38**(1): p. 127-33.
53. Leger, M., et al., *Object recognition test in mice.* Nat Protoc, 2013. **8**(12): p. 2531-7.
54. Schacter, D.L., *Implicit expressions of memory in organic amnesia: learning of new facts and associations.* Hum Neurobiol, 1987. **6**(2): p. 107-18.

55. Ioannou, A., Anastassiou-Hadjicharalambous, X. , *Non-associative Learning*, in *Encyclopedia of Evolutionary Psychological Science*, T. Shackelford, Weekes-Shackelford, V., Editor. 2018, Springer.
56. Pearce, J.M. and M.E. Bouton, *Theories of associative learning in animals.* Annu Rev Psychol, 2001. **52**: p. 111-39.
57. Buccafusco, J., *Methods of Behavior Analysis in Neuroscience*. 2 ed, ed. B. JJ. 2009, Boca Raton: CRC Press/Taylor & Francis.
58. Willingham, D.B., M.J. Nissen, and P. Bullemer, *On the development of procedural knowledge.* J Exp Psychol Learn Mem Cogn, 1989. **15**(6): p. 1047-60.
59. Weingarten, E., et al., *From primed concepts to action: A meta-analysis of the behavioral effects of incidentally presented words.* Psychol Bull, 2016. **142**(5): p. 472-97.
60. Reisberg, D., *Cognition: Exploring the Science of the Mind*. 2007.
61. Kellman, P., *Perceptual learning*, in *Stevens' Handbook of Experimental Psychology, Learning, Motivation, and Emotion*, H.G. Pashler, R, Editor. 2002, Wiley: New York.
62. Shanks, D., *Concept Learning and Representation: Models*, in *International Encyclopedia of the Social & Behavioral Sciences*, P. Smelser, Baltes, NJ, Editor. 2001, Pergamon. p. 2491-2495.
63. Tyng, C.M., et al., *The Influences of Emotion on Learning and Memory.* Front Psychol, 2017. **8**: p. 1454.
64. Thompson, R.F. and J.J. Kim, *Memory systems in the brain and localization of a memory.* Proc Natl Acad Sci U S A, 1996. **93**(24): p. 13438-44.
65. Broadbent, N.J., et al., *Object recognition memory and the rodent hippocampus.* Learn Mem, 2010. **17**(1): p. 5-11.
66. Oh, J.P. and J.H. Han, *A critical role of hippocampus for formation of remote cued fear memory.* Mol Brain, 2020. **13**(1): p. 112.
67. Treves, A., Rollls, ET, *Computational constraints suggest the need for two distinct input systems to the hippocampal CA3 network.* Hippocampus, 1992. **2**: p. 189-199.
68. Gilbert, P., Kesner, RP., Lee, I., *Dissociating hippocampal subregions: A double dissociation between dentate gyrus and CA1.* Hippocampus, 2001. **11**(6): p. 626-636.
69. Vanderah, T., Gould, D, *Nolte's The Human Brain*. 2020, Elsevier.
70. Bear, M., Connors, B., Paradiso, MA., *Memory Circuits, Chapter 24*, in *Neuroscience: Exploring The Brain*. 2020. p. 975.
71. Witter, M.P., *The perforant path: projections from the entorhinal cortex to the dentate gyrus.* Prog Brain Res, 2007. **163**: p. 43-61.
72. Amaral, D.G. and M.P. Witter, *The three-dimensional organization of the hippocampal formation: a review of anatomical data.* Neuroscience, 1989. **31**(3): p. 571-91.
73. Chrobak, J.J., A. Lorincz, and G. Buzsaki, *Physiological patterns in the hippocampo-entorhinal cortex system.* Hippocampus, 2000. **10**(4): p. 457-65.
74. Ishizuka, N., J. Weber, and D.G. Amaral, *Organization of intrahippocampal projections originating from CA3 pyramidal cells in the rat.* J Comp Neurol, 1990. **295**(4): p. 580-623.
75. Kondo, H., P. Lavenex, and D.G. Amaral, *Intrinsic connections of the macaque monkey hippocampal formation: II. CA3 connections.* J Comp Neurol, 2009. **515**(3): p. 349-77.
76. Banks, S.J., et al., *fMRI of verbal and nonverbal memory processes in healthy and epileptogenic medial temporal lobes.* Epilepsy Behav, 2012. **25**(1): p. 42-9.
77. Rolls, E.T. and R.P. Kesner, *Pattern separation and pattern completion in the hippocampal system. Introduction to the Special Issue.* Neurobiol Learn Mem, 2016. **129**: p. 1-3.
78. Rolls, E.T., *A theory of hippocampal function in memory.* Hippocampus, 1996. **6**(6): p. 601-20.
79. Rolls, E.T., *A quantitative theory of the functions of the hippocampal CA3 network in memory.* Front Cell Neurosci, 2013. **7**: p. 98.
80. Rolls, E., Deco, D., *The Noisy Brain: Stochastic Dynamics as a Principle of Brain Function*. 2010, Oxford: Oxford University Press.
81. Clelland, C.D., et al., *A functional role for adult hippocampal neurogenesis in spatial pattern separation.* Science, 2009. **325**(5937): p. 210-3.

82. Scaplen, K., Agster, KL., Burwelll, RD. , *Anatomy of the Hippocampus and the Declarative Memory System*, in *Learning and Memory: A Comprehensive Reference*, J. Byrne, Menzel, R., Wixted, JT., Eichenbaum, H., Sara, SJ, Editor. 2017, Oliver Walter. p. 2600.
83. Wang, S.H. and R.G. Morris, *Hippocampal-neocortical interactions in memory formation, consolidation, and reconsolidation.* Annu Rev Psychol, 2010. **61**: p. 49-79, C1-4.
84. Rolls, E.T., *Pattern separation, completion, and categorisation in the hippocampus and neocortex.* Neurobiol Learn Mem, 2016. **129**: p. 4-28.
85. Hopfield, J.J., *Neural networks and physical systems with emergent collective computational abilities.* Proc Natl Acad Sci U S A, 1982. **79**(8): p. 2554-8.
86. Hainmueller, T. and M. Bartos, *Dentate gyrus circuits for encoding, retrieval and discrimination of episodic memories.* Nat Rev Neurosci, 2020. **21**(3): p. 153-168.
87. Eichenbaum, H., *A cortical-hippocampal system for declarative memory.* Nat Rev Neurosci, 2000. **1**(1): p. 41-50.
88. Hemond, P., et al., *Distinct classes of pyramidal cells exhibit mutually exclusive firing patterns in hippocampal area CA3b.* Hippocampus, 2008. **18**(4): p. 411-24.
89. Cherubini, E. and R. Miles, *The CA3 region of the hippocampus: how is it? What is it for? How does it do it?* Front Cell Neurosci, 2015. **9**: p. 19.
90. Rolls, E.T. and R.P. Kesner, *A computational theory of hippocampal function, and empirical tests of the theory.* Prog Neurobiol, 2006. **79**(1): p. 1-48.
91. Rolls, E., *Roles of long term potentiation and long term depression in neuronal network operations in the brain, in Cortical Plasticity*, ed. M. Fazeli, Collingridge, GL. 1996, Oxford: Bios.
92. O'Keefe, J.N., L., *The Hippocampus as a Cognitive Map*. 1978, Oxford, UK: Oxford University Press.
93. Moser, E.I., et al., *Grid cells and cortical representation.* Nat Rev Neurosci, 2014. **15**(7): p. 466-81.
94. Morgado-Bernal, I., *Learning and memory consolidation: Linking molecular and behavioral data.* Neuroscience, 2011. **176**: p. 12-9.
95. Brodal, P., *The Hippocampal Formation: Learning and Memory*, in *The Central Nervous System*. 2016.
96. Hartley, T., et al., *Space in the brain: how the hippocampal formation supports spatial cognition.* Philos Trans R Soc Lond B Biol Sci, 2014. **369**(1635): p. 20120510.
97. Preston, A.R. and H. Eichenbaum, *Interplay of hippocampus and prefrontal cortex in memory.* Curr Biol, 2013. **23**(17): p. R764-73.
98. Hebb, D.O., *The organization of behavior, a neuropsychological theory*. 1949, New York: Wiley.
99. Goode, T.D., et al., *An Integrated Index: Engrams, Place Cells, and Hippocampal Memory.* Neuron, 2020. **107**(5): p. 805-820.
100. Costandi, M., *Neuroplasticity*. 2016, Cambridge, Massachusetts: The MIT Press.
101. Kano, M. and K. Hashimoto, *Synapse elimination in the central nervous system.* Curr Opin Neurobiol, 2009. **19**(2): p. 154-61.
102. Goda, Y. and G.W. Davis, *Mechanisms of synapse assembly and disassembly.* Neuron, 2003. **40**(2): p. 243-64.
103. VanGuilder Starkey, H.D., et al., *Neuroglial expression of the MHCI pathway and PirB receptor is upregulated in the hippocampus with advanced aging.* J Mol Neurosci, 2012. **48**(1): p. 111-26.
104. Stevens, B., et al., *The classical complement cascade mediates CNS synapse elimination.* Cell, 2007. **131**(6): p. 1164-78.
105. Sudhof, T.C., *Towards an Understanding of Synapse Formation.* Neuron, 2018. **100**(2): p. 276-293.
106. Oh, W.C., et al., *De novo synaptogenesis induced by GABA in the developing mouse cortex.* Science, 2016. **353**(6303): p. 1037-1040.
107. Kempermann, G., H. Song, and F.H. Gage, *Neurogenesis in the Adult Hippocampus.* Cold Spring Harb Perspect Biol, 2015. **7**(9): p. a018812.

108. Lim, D.A. and A. Alvarez-Buylla, *The Adult Ventricular-Subventricular Zone (V-SVZ) and Olfactory Bulb (OB) Neurogenesis.* Cold Spring Harb Perspect Biol, 2016. **8**(5).
109. Jurkowski, M.P., et al., *Beyond the Hippocampus and the SVZ: Adult Neurogenesis Throughout the Brain.* Front Cell Neurosci, 2020. **14**: p. 576444.
110. Kee, N., et al., *Imaging activation of adult-generated granule cells in spatial memory.* Nat Protoc, 2007. **2**(12): p. 3033-44.
111. Snyder, J.S., N. Kee, and J.M. Wojtowicz, *Effects of adult neurogenesis on synaptic plasticity in the rat dentate gyrus.* J Neurophysiol, 2001. **85**(6): p. 2423-31.
112. Wilbrecht, L., et al., *Structural plasticity underlies experience-dependent functional plasticity of cortical circuits.* J Neurosci, 2010. **30**(14): p. 4927-32.
113. Grafman, J., *Conceptualizing functional neuroplasticity.* J Commun Disord, 2000. **33**(4): p. 345-55; quiz 355-6.
114. Sadato, N., et al., *Activation of the primary visual cortex by Braille reading in blind subjects.* Nature, 1996. **380**(6574): p. 526-8.
115. Pascual-Leone, A., J. Grafman, and M. Hallett, *Modulation of cortical motor output maps during development of implicit and explicit knowledge.* Science, 1994. **263**(5151): p. 1287-9.
116. Levin, H.S., et al., *Dyscalculia and dyslexia after right hemisphere injury in infancy.* Arch Neurol, 1996. **53**(1): p. 88-96.
117. Rosenich, E., et al., *Cognitive Reserve as an Emerging Concept in Stroke Recovery.* Neurorehabil Neural Repair, 2020. **34**(3): p. 187-199.
118. Gerrow, K. and A. Triller, *Synaptic stability and plasticity in a floating world.* Curr Opin Neurobiol, 2010. **20**(5): p. 631-9.
119. Magee, J.C. and C. Grienberger, *Synaptic Plasticity Forms and Functions.* Annu Rev Neurosci, 2020. **43**: p. 95-117.
120. J, B., *Synaptic Plasticity*, in *Neuroscience Online section 1 chapter 7*. 1997.
121. Pan, B. and R.S. Zucker, *A general model of synaptic transmission and short-term plasticity.* Neuron, 2009. **62**(4): p. 539-54.
122. Regehr, W.G., *Short-term presynaptic plasticity.* Cold Spring Harb Perspect Biol, 2012. **4**(7): p. a005702.
123. Debanne, D., et al., *Paired-pulse facilitation and depression at unitary synapses in rat hippocampus: quantal fluctuation affects subsequent release.* J Physiol, 1996. **491 (Pt 1)**(Pt 1): p. 163-76.
124. Bao, J.X., E.R. Kandel, and R.D. Hawkins, *Involvement of pre- and postsynaptic mechanisms in posttetanic potentiation at Aplysia synapses.* Science, 1997. **275**(5302): p. 969-73.
125. Kessels, H.W. and R. Malinow, *Synaptic AMPA receptor plasticity and behavior.* Neuron, 2009. **61**(3): p. 340-50.
126. Luscher, C. and R.C. Malenka, *NMDA receptor-dependent long-term potentiation and long-term depression (LTP/LTD).* Cold Spring Harb Perspect Biol, 2012. **4**(6).
127. Chistiakova, M., et al., *Heterosynaptic plasticity: multiple mechanisms and multiple roles.* Neuroscientist, 2014. **20**(5): p. 483-98.
128. Kang, H., et al., *An important role of neural activity-dependent CaMKIV signaling in the consolidation of long-term memory.* Cell, 2001. **106**(6): p. 771-83.
129. Lisman, J., et al., *Memory formation depends on both synapse-specific modifications of synaptic strength and cell-specific increases in excitability.* Nat Neurosci, 2018. **21**(3): p. 309-314.
130. Lisman, J., R. Yasuda, and S. Raghavachari, *Mechanisms of CaMKII action in long-term potentiation.* Nat Rev Neurosci, 2012. **13**(3): p. 169-82.
131. Cooper, L.N. and M.F. Bear, *The BCM theory of synapse modification at 30: interaction of theory with experiment.* Nat Rev Neurosci, 2012. **13**(11): p. 798-810.
132. Moscovitch, M., et al., *Episodic Memory and Beyond: The Hippocampus and Neocortex in Transformation.* Annu Rev Psychol, 2016. **67**: p. 105-34.
133. Buzsaki, G., *Hippocampal sharp wave-ripple: A cognitive biomarker for episodic memory and planning.* Hippocampus, 2015. **25**(10): p. 1073-188.
134. Dan, Y. and M.M. Poo, *Spike timing-dependent plasticity: from synapse to perception.* Physiol Rev, 2006. **86**(3): p. 1033-48.

135. Barrett, K., Barman, SM., Boitano S., Brooks HL., *Ganong's Review of Medical Physiology*. 2012: McGraw Hill.
136. Skeberdis, V.A., et al., *mGluR1-mediated potentiation of NMDA receptors involves a rise in intracellular calcium and activation of protein kinase C.* Neuropharmacology, 2001. **40**(7): p. 856-65.
137. Ambrosini, A., et al., *Metabotropic glutamate receptors negatively coupled to adenylate cyclase inhibit N-methyl-D-aspartate receptor activity and prevent neurotoxicity in mesencephalic neurons in vitro.* Mol Pharmacol, 1995. **47**(5): p. 1057-64.
138. Kandel, E.R., Y. Dudai, and M.R. Mayford, *The molecular and systems biology of memory.* Cell, 2014. **157**(1): p. 163-86.
139. Park, M., *AMPA Receptor Trafficking for Postsynaptic Potentiation.* Frontiers in cellular neuroscience, 2018. **12**: p. 361.
140. Kwapis, J.L. and F.J. Helmstetter, *Does PKM(zeta) maintain memory?* Brain Res Bull, 2014. **105**: p. 36-45.
141. Diering, G.H. and R.L. Huganir, *The AMPA Receptor Code of Synaptic Plasticity.* Neuron, 2018. **100**(2): p. 314-329.
142. Hanger, D.P., D. Goniotaki, and W. Noble, *Synaptic Localisation of Tau.* Adv Exp Med Biol, 2019. **1184**: p. 105-112.
143. Oblak, A.L., et al., *Model organism development and evaluation for late-onset Alzheimer's disease: MODEL-AD.* Alzheimers Dement (N Y), 2020. **6**(1): p. e12110.
144. Preuss, C., et al., *A novel systems biology approach to evaluate mouse models of late-onset Alzheimer's disease.* Mol Neurodegener, 2020. **15**(1): p. 67.
145. Guo, T., W. Noble, and D.P. Hanger, *Roles of tau protein in health and disease.* Acta Neuropathol, 2017. **133**(5): p. 665-704.
146. Chen, Y., A.K.Y. Fu, and N.Y. Ip, *Synaptic dysfunction in Alzheimer's disease: Mechanisms and therapeutic strategies.* Pharmacol Ther, 2019. **195**: p. 186-198.
147. Forner, S., et al., *Synaptic Impairment in Alzheimer's Disease: A Dysregulated Symphony.* Trends in neurosciences, 2017. **40**(6): p. 347-357.
148. Huganir, R.L. and R.A. Nicoll, *AMPARs and synaptic plasticity: the last 25 years.* Neuron, 2013. **80**(3): p. 704-17.
149. Frandemiche, M.L., et al., *Activity-dependent tau protein translocation to excitatory synapse is disrupted by exposure to amyloid-beta oligomers.* The Journal of neuroscience : the official journal of the Society for Neuroscience, 2014. **34**(17): p. 6084-97.
150. Stern, J.L., et al., *Single-molecule imaging of Tau dynamics on the microtubule surface.* Methods Cell Biol, 2017. **141**: p. 135-154.
151. Ittner, A. and L.M. Ittner, *Dendritic Tau in Alzheimer's Disease.* Neuron, 2018. **99**(1): p. 13-27.
152. Zempel, H. and E.M. Mandelkow, *Tau missorting and spastin-induced microtubule disruption in neurodegeneration: Alzheimer Disease and Hereditary Spastic Paraplegia.* Mol Neurodegener, 2015. **10**: p. 68.
153. Hoover, B.R., et al., *Tau mislocalization to dendritic spines mediates synaptic dysfunction independently of neurodegeneration.* Neuron, 2010. **68**(6): p. 1067-81.
154. Tracy, T.E. and L. Gan, *Tau-mediated synaptic and neuronal dysfunction in neurodegenerative disease.* Current opinion in neurobiology, 2018. **51**: p. 134-138.
155. Tracy, T.E. and L. Gan, *Tau-mediated synaptic and neuronal dysfunction in neurodegenerative disease.* Curr Opin Neurobiol, 2018. **51**: p. 134-138.
156. McInnes, J., et al., *Synaptogyrin-3 Mediates Presynaptic Dysfunction Induced by Tau.* Neuron, 2018. **97**(4): p. 823-835 e8.
157. Moreno, H., et al., *Tau pathology-mediated presynaptic dysfunction.* Neuroscience, 2016. **325**: p. 30-8.
158. Xia, D., C. Li, and J. Gotz, *Pseudophosphorylation of Tau at distinct epitopes or the presence of the P301L mutation targets the microtubule-associated protein Tau to dendritic spines.* Biochim Biophys Acta, 2015. **1852**(5): p. 913-24.
159. Zhao, X., et al., *Caspase-2 cleavage of tau reversibly impairs memory.* Nat Med, 2016. **22**(11): p. 1268-1276.
160. Kovacs, G.G., *Tauopathies.* Handb Clin Neurol, 2017. **145**: p. 355-368.

161. van Hummel, A., et al., *No Overt Deficits in Aged Tau-Deficient C57Bl/6.Mapttm1(EGFP)Kit GFP Knockin Mice.* PLoS One, 2016. **11**(10): p. e0163236.
162. Tan, D.C.S., et al., *Generation of a New Tau Knockout (tauDeltaex1) Line Using CRISPR/Cas9 Genome Editing in Mice.* J Alzheimers Dis, 2018. **62**(2): p. 571-578.
163. Denk, F. and R. Wade-Martins, *Knock-out and transgenic mouse models of tauopathies.* Neurobiol Aging, 2009. **30**(1): p. 1-13.
164. Velazquez, R., et al., *Acute tau knockdown in the hippocampus of adult mice causes learning and memory deficits.* Aging Cell, 2018. **17**(4): p. e12775.
165. Biundo, F., et al., *A role for tau in learning, memory and synaptic plasticity.* Sci Rep, 2018. **8**(1): p. 3184.
166. Goncalves, R.A., et al., *Behavioral Abnormalities in Knockout and Humanized Tau Mice.* Front Endocrinol (Lausanne), 2020. **11**: p. 124.
167. Ahmed, T., et al., *Cognition and hippocampal synaptic plasticity in mice with a homozygous tau deletion.* Neurobiol Aging, 2014. **35**(11): p. 2474-2478.
168. Kimura, T., et al., *Microtubule-associated protein tau is essential for long-term depression in the hippocampus.* Philosophical transactions of the Royal Society of London Series B, Biological sciences, 2014. **369**(1633): p. 20130144.
169. Marciniak, E., et al., *Tau deletion promotes brain insulin resistance.* J Exp Med, 2017. **214**(8): p. 2257-2269.
170. Suzuki, M. and T. Kimura, *Microtubule-associated tau contributes to intra-dendritic trafficking of AMPA receptors in multiple ways.* Neuroscience letters, 2017. **653**: p. 276-282.
171. Regan, P., et al., *Tau phosphorylation at serine 396 residue is required for hippocampal LTD.* The Journal of neuroscience : the official journal of the Society for Neuroscience, 2015. **35**(12): p. 4804-12.
172. Goedert, M., et al., *Multiple isoforms of human microtubule-associated protein tau: sequences and localization in neurofibrillary tangles of Alzheimer's disease.* Neuron, 1989. **3**(4): p. 519-26.
173. Goedert, M., M.G. Spillantini, and R.A. Crowther, *Cloning of a big tau microtubule-associated protein characteristic of the peripheral nervous system.* Proc Natl Acad Sci U S A, 1992. **89**(5): p. 1983-7.
174. Liu, C. and J. Gotz, *Profiling murine tau with 0N, 1N and 2N isoform-specific antibodies in brain and peripheral organs reveals distinct subcellular localization, with the 1N isoform being enriched in the nucleus.* PloS one, 2013. **8**(12): p. e84849.
175. Gao, Y.L., et al., *Tau in neurodegenerative disease.* Ann Transl Med, 2018. **6**(10): p. 175.
176. Alonso Adel, C., et al., *Promotion of hyperphosphorylation by frontotemporal dementia tau mutations.* J Biol Chem, 2004. **279**(33): p. 34873-81.
177. Bullmann, T., et al., *Expression of embryonic tau protein isoforms persist during adult neurogenesis in the hippocampus.* Hippocampus, 2007. **17**(2): p. 98-102.
178. Spillantini, M.G. and M. Goedert, *Tau protein pathology in neurodegenerative diseases.* Trends Neurosci, 1998. **21**(10): p. 428-33.
179. Li, K., M.C. Arikan, and A. Andreadis, *Modulation of the membrane-binding domain of tau protein: splicing regulation of exon 2.* Brain Res Mol Brain Res, 2003. **116**(1-2): p. 94-105.
180. Gerke, V., C.E. Creutz, and S.E. Moss, *Annexins: linking Ca2+ signalling to membrane dynamics.* Nat Rev Mol Cell Biol, 2005. **6**(6): p. 449-61.
181. Spittaels, K., et al., *Glycogen synthase kinase-3beta phosphorylates protein tau and rescues the axonopathy in the central nervous system of human four-repeat tau transgenic mice.* J Biol Chem, 2000. **275**(52): p. 41340-9.
182. Jaworski, T., E. Banach-Kasper, and K. Gralec, *GSK-3beta at the Intersection of Neuronal Plasticity and Neurodegeneration.* Neural Plast, 2019. **2019**: p. 4209475.
183. Morris, M., et al., *The many faces of tau.* Neuron, 2011. **70**(3): p. 410-26.
184. Brandt, R., N.I. Trushina, and L. Bakota, *Much More Than a Cytoskeletal Protein: Physiological and Pathological Functions of the Non-microtubule Binding Region of Tau.* Front Neurol, 2020. **11**: p. 590059.
185. Brandt, R., J. Leger, and G. Lee, *Interaction of tau with the neural plasma membrane mediated by tau's amino-terminal projection domain.* J Cell Biol, 1995. **131**(5): p. 1327-40.

186. Kempf, M., et al., *Tau binds to the distal axon early in development of polarity in a microtubule- and microfilament-dependent manner.* J Neurosci, 1996. **16**(18): p. 5583-92.
187. Conde, C. and A. Caceres, *Microtubule assembly, organization and dynamics in axons and dendrites.* Nat Rev Neurosci, 2009. **10**(5): p. 319-32.
188. Kadavath, H., et al., *Tau stabilizes microtubules by binding at the interface between tubulin heterodimers.* Proc Natl Acad Sci U S A, 2015. **112**(24): p. 7501-6.
189. Kolarova, M., et al., *Structure and pathology of tau protein in Alzheimer disease.* Int J Alzheimers Dis, 2012. **2012**: p. 731526.
190. Kellogg, E.H., et al., *Near-atomic model of microtubule-tau interactions.* Science, 2018. **360**(6394): p. 1242-1246.
191. Rosenberg, H.F., *Cytokines and fibrocyte differentiation -- altering the balance: an interview with Dr. Darrell Pilling. Interview by Helene F. Rosenberg.* J Leukoc Biol, 2008. **83**(6): p. 1334-5.
192. Rice, L.M., E.A. Montabana, and D.A. Agard, *The lattice as allosteric effector: structural studies of alphabeta- and gamma-tubulin clarify the role of GTP in microtubule assembly.* Proc Natl Acad Sci U S A, 2008. **105**(14): p. 5378-83.
193. Wang, H.W. and E. Nogales, *Nucleotide-dependent bending flexibility of tubulin regulates microtubule assembly.* Nature, 2005. **435**(7044): p. 911-5.
194. Buey, R.M., J.F. Diaz, and J.M. Andreu, *The nucleotide switch of tubulin and microtubule assembly: a polymerization-driven structural change.* Biochemistry, 2006. **45**(19): p. 5933-8.
195. Baas, P.W., et al., *Stability properties of neuronal microtubules.* Cytoskeleton (Hoboken), 2016. **73**(9): p. 442-60.
196. Baas, P.W. and M.M. Black, *Individual microtubules in the axon consist of domains that differ in both composition and stability.* J Cell Biol, 1990. **111**(2): p. 495-509.
197. Qiang, L., et al., *Tau Does Not Stabilize Axonal Microtubules but Rather Enables Them to Have Long Labile Domains.* Curr Biol, 2018. **28**(13): p. 2181-2189 e4.
198. Dyson, H.J. and P.E. Wright, *Intrinsically unstructured proteins and their functions.* Nat Rev Mol Cell Biol, 2005. **6**(3): p. 197-208.
199. Uversky, V.N., *Intrinsic disorder in proteins associated with neurodegenerative diseases.* Front Biosci (Landmark Ed), 2009. **14**(14): p. 5188-238.
200. Meszaros, B., et al., *Molecular principles of the interactions of disordered proteins.* J Mol Biol, 2007. **372**(2): p. 549-61.
201. Tompa, P., *The interplay between structure and function in intrinsically unstructured proteins.* FEBS Lett, 2005. **579**(15): p. 3346-54.
202. Xie, H., et al., *Functional anthology of intrinsic disorder. 1. Biological processes and functions of proteins with long disordered regions.* J Proteome Res, 2007. **6**(5): p. 1882-98.
203. Follis, A.V., et al., *Structural rationale for the coupled binding and unfolding of the c-Myc oncoprotein by small molecules.* Chem Biol, 2008. **15**(11): p. 1149-55.
204. Oldfield, C.J., et al., *Flexible nets: disorder and induced fit in the associations of p53 and 14-3-3 with their partners.* BMC Genomics, 2008. **9 Suppl 1**(Suppl 1): p. S1.
205. Oldfield, C.J., et al., *Coupled folding and binding with alpha-helix-forming molecular recognition elements.* Biochemistry, 2005. **44**(37): p. 12454-70.
206. Ballatore, C., V.M. Lee, and J.Q. Trojanowski, *Tau-mediated neurodegeneration in Alzheimer's disease and related disorders.* Nat Rev Neurosci, 2007. **8**(9): p. 663-72.
207. Chang, C.W., E. Shao, and L. Mucke, *Tau: Enabler of diverse brain disorders and target of rapidly evolving therapeutic strategies.* Science, 2021. **371**(6532).
208. Palop, J.J. and L. Mucke, *Network abnormalities and interneuron dysfunction in Alzheimer disease.* Nat Rev Neurosci, 2016. **17**(12): p. 777-792.
209. Penn, A.C., et al., *Hippocampal LTP and contextual learning require surface diffusion of AMPA receptors.* Nature, 2017. **549**(7672): p. 384-388.
210. Hanley, J.G., *The Regulation of AMPA Receptor Endocytosis by Dynamic Protein-Protein Interactions.* Frontiers in cellular neuroscience, 2018. **12**: p. 362.
211. Gonzalez-Lozano, M.A., et al., *Stitching the synapse: Cross-linking mass spectrometry into resolving synaptic protein interactions.* Sci Adv, 2020. **6**(8): p. eaax5783.

212. Prikas, E., et al., *Interaction between the guanylate kinase domain of PSD-95 and the proline-rich region and microtubule binding repeats 2 and 3 of tau.* Biochem Cell Biol, 2021. **99**(5): p. 606-616.
213. Bi, M., et al., *Tau exacerbates excitotoxic brain damage in an animal model of stroke.* Nat Commun, 2017. **8**(1): p. 473.
214. Kim, D.I., et al., *An improved smaller biotin ligase for BioID proximity labeling.* Mol Biol Cell, 2016. **27**(8): p. 1188-96.
215. Prikas, E., A. Poljak, and A. Ittner, *Mapping p38alpha mitogen-activated protein kinase signaling by proximity-dependent labeling.* Protein Sci, 2020. **29**(5): p. 1196-1210.
216. Uezu, A., et al., *Identification of an elaborate complex mediating postsynaptic inhibition.* Science, 2016. **353**(6304): p. 1123-9.
217. Cheerathodi, M.R. and D.G. Meckes, Jr., *BioID Combined with Mass Spectrometry to Study Herpesvirus Protein-Protein Interaction Networks.* Methods Mol Biol, 2020. **2060**: p. 327-341.
218. Bareja, A., et al., *The proximity-labeling technique BioID identifies sorting nexin 6 as a member of the insulin-like growth factor 1 (IGF1)-IGF1 receptor pathway.* J Biol Chem, 2018. **293**(17): p. 6449-6459.
219. Hanley, J.G., *NSF binds calcium to regulate its interaction with AMPA receptor subunit GluR2.* Journal of neurochemistry, 2007. **101**(6): p. 1644-50.
220. Migues, P.V., et al., *The maintenance of long-term memory in the hippocampus depends on the interaction between N-ethylmaleimide-sensitive factor and GluA2.* Hippocampus, 2014. **24**(9): p. 1112-9.
221. Iwata, M., et al., *Regulatory mechanisms for the axonal localization of tau protein in neurons.* Mol Biol Cell, 2019. **30**(19): p. 2441-2457.
222. Ittner, A., et al., *Reduction of advanced tau-mediated memory deficits by the MAP kinase p38gamma.* Acta Neuropathol, 2020. **140**(3): p. 279-294.
223. Ittner, A., et al., *Site-specific phosphorylation of tau inhibits amyloid-beta toxicity in Alzheimer's mice.* Science, 2016. **354**(6314): p. 904-908.
224. Roux, K.J., et al., *A promiscuous biotin ligase fusion protein identifies proximal and interacting proteins in mammalian cells.* J Cell Biol, 2012. **196**(6): p. 801-10.
225. Trushina, N.I., et al., *The Evolution of Tau Phosphorylation and Interactions.* Front Aging Neurosci, 2019. **11**: p. 256.
226. Zhao, M., et al., *Mechanistic insights into the recycling machine of the SNARE complex.* Nature, 2015. **518**(7537): p. 61-7.
227. Haucke, V., E. Neher, and S.J. Sigrist, *Protein scaffolds in the coupling of synaptic exocytosis and endocytosis.* Nature reviews Neuroscience, 2011. **12**(3): p. 127-38.
228. Wienken, C.J., et al., *Protein-binding assays in biological liquids using microscale thermophoresis.* Nature communications, 2010. **1**: p. 100.
229. Ackmann, M., H. Wiech, and E. Mandelkow, *Nonsaturable binding indicates clustering of tau on the microtubule surface in a paired helical filament-like conformation.* The Journal of biological chemistry, 2000. **275**(39): p. 30335-43.
230. Belluzzi, E., et al., *LRRK2 phosphorylates pre-synaptic N-ethylmaleimide sensitive fusion (NSF) protein enhancing its ATPase activity and SNARE complex disassembling rate.* Molecular neurodegeneration, 2016. **11**: p. 1.
231. Morrell, C.N., K. Matsushita, and C.J. Lowenstein, *A novel inhibitor of N-ethylmaleimide-sensitive factor decreases leukocyte trafficking and peritonitis.* The Journal of pharmacology and experimental therapeutics, 2005. **314**(1): p. 155-61.
232. Lu, W., et al., *Activation of synaptic NMDA receptors induces membrane insertion of new AMPA receptors and LTP in cultured hippocampal neurons.* Neuron, 2001. **29**(1): p. 243-54.
233. Johnston, G.A., *Advantages of an antagonist: bicuculline and other GABA antagonists.* Br J Pharmacol, 2013. **169**(2): p. 328-36.
234. Wang, Q., et al., *Neuropilin-2/PlexinA3 Receptors Associate with GluA1 and Mediate Sema3F-Dependent Homeostatic Scaling in Cortical Neurons.* Neuron, 2017. **96**(5): p. 1084-1098.e7.

235. Nabavi, S., et al., *Metabotropic NMDA receptor function is required for NMDA receptor-dependent long-term depression.* Proceedings of the National Academy of Sciences of the United States of America, 2013. **110**(10): p. 4027-32.
236. Franchini, L., et al., *Linking NMDA Receptor Synaptic Retention to Synaptic Plasticity and Cognition.* iScience, 2019. **19**: p. 927-939.
237. Heitz, F.D., et al., *The memory gene KIBRA is a bidirectional regulator of synaptic and structural plasticity in the adult brain.* Neurobiol Learn Mem, 2016. **135**: p. 100-114.
238. Malenka, R.C. and M.F. Bear, *LTP and LTD: an embarrassment of riches.* Neuron, 2004. **44**(1): p. 5-21.
239. Akerboom, J., et al., *Optimization of a GCaMP calcium indicator for neural activity imaging.* The Journal of neuroscience : the official journal of the Society for Neuroscience, 2012. **32**(40): p. 13819-40.
240. Hussain, N.K., et al., *Regulation of AMPA receptor subunit GluA1 surface expression by PAK3 phosphorylation.* Proc Natl Acad Sci U S A, 2015. **112**(43): p. E5883-90.
241. Davies, G., et al., *Study of 300,486 individuals identifies 148 independent genetic loci influencing general cognitive function.* Nat Commun, 2018. **9**(1): p. 2098.
242. Fekete, A., et al., *Underpinning heterogeneity in synaptic transmission by presynaptic ensembles of distinct morphological modules.* Nat Commun, 2019. **10**(1): p. 826.
243. Rosen, J.B., *The neurobiology of conditioned and unconditioned fear: a neurobehavioral system analysis of the amygdala.* Behavioral and cognitive neuroscience reviews, 2004. **3**(1): p. 23-41.
244. Sheng, M. and E. Kim, *The postsynaptic organization of synapses.* Cold Spring Harb Perspect Biol, 2011. **3**(12).
245. Sydow, A., et al., *Tau-induced defects in synaptic plasticity, learning, and memory are reversible in transgenic mice after switching off the toxic Tau mutant.* J Neurosci, 2011. **31**(7): p. 2511-25.
246. Tracy, T.E., et al., *Tau interactome maps synaptic and mitochondrial processes associated with neurodegeneration.* Cell, 2022. **185**(4): p. 712-728 e14.
247. Roux, K.J., et al., *BioID: A Screen for Protein-Protein Interactions.* Curr Protoc Protein Sci, 2018. **91**: p. 19 23 1-19 23 15.
248. Drummond, E., et al., *Phosphorylated tau interactome in the human Alzheimer's disease brain.* Brain, 2020. **143**(9): p. 2803-2817.
249. Zhao, C., E.C. Smith, and S.W. Whiteheart, *Requirements for the catalytic cycle of the N-ethylmaleimide-Sensitive Factor (NSF).* Biochim Biophys Acta, 2012. **1823**(1): p. 159-71.
250. Dalal, S., et al., *Distinct roles for the AAA ATPases NSF and p97 in the secretory pathway.* Mol Biol Cell, 2004. **15**(2): p. 637-48.
251. Herring, B.E. and R.A. Nicoll, *Long-Term Potentiation: From CaMKII to AMPA Receptor Trafficking.* Annu Rev Physiol, 2016. **78**: p. 351-65.
252. Joels, G. and R. Lamprecht, *Interaction between N-ethylmaleimide-sensitive factor and GluR2 is essential for fear memory formation in lateral amygdala.* The Journal of neuroscience : the official journal of the Society for Neuroscience, 2010. **30**(47): p. 15981-6.
253. Li, S., et al., *Soluble Abeta oligomers inhibit long-term potentiation through a mechanism involving excessive activation of extrasynaptic NR2B-containing NMDA receptors.* J Neurosci, 2011. **31**(18): p. 6627-38.
254. Gruart, A., M.D. Munoz, and J.M. Delgado-Garcia, *Involvement of the CA3-CA1 synapse in the acquisition of associative learning in behaving mice.* J Neurosci, 2006. **26**(4): p. 1077-87.
255. Yu, Z., et al., *Necroptosis: A Novel Pathway in Neuroinflammation.* Front Pharmacol, 2021. **12**: p. 701564.
256. Koper MJ, v.S.E., Ospitalieri S, Vandenberghe R, Vandenbulcke M, von Arnim C, Tousseyn T, Rechwald J, Rabe S, Staufenbiel M, Balusu S, De Strooper B, Rudolf Thal D, *Alzheimer's disease-related necroptotic pathology: An*

exclusive presence of the necrosome in granulovacuolar

degeneration inclusions in human and transgenicmouse brains. Alzheimer's & Dementia, 2020. **16**: p. e042460.

257. Caccamo, A., et al., *Necroptosis activation in Alzheimer's disease.* Nat Neurosci, 2017. **20**(9): p. 1236-1246.
258. Yates, A.D., et al., *Ensembl 2020.* Nucleic Acids Res, 2020. **48**(D1): p. D682-D688.
259. Savage, J.E., et al., *Genome-wide association meta-analysis in 269,867 individuals identifies new genetic and functional links to intelligence.* Nat Genet, 2018. **50**(7): p. 912-919.
260. Herold, C., et al., *ATPase N-ethylmaleimide-sensitive Fusion Protein: A Novel Key Player for Causing Spontaneous Network Excitation in Human Temporal Lobe Epilepsy.* Neuroscience, 2018. **371**: p. 371-383.
261. Probst, A., et al., *Axonopathy and amyotrophy in mice transgenic for human four-repeat tau protein.* Acta Neuropathol, 2000. **99**(5): p. 469-81.
262. Zhang, J., et al., *The AAA+ ATPase Thorase regulates AMPA receptor-dependent synaptic plasticity and behavior.* Cell, 2011. **145**(2): p. 284-99.
263. Fath, T., et al., *Primary support cultures of hippocampal and substantia nigra neurons.* Nat Protoc, 2009. **4**(1): p. 78-85.
264. Lein, E.S., et al., *Genome-wide atlas of gene expression in the adult mouse brain.* Nature, 2007. **445**(7124): p. 168-76.
265. Ittner, A.A., et al., *The nucleotide exchange factor SIL1 is required for glucose-stimulated insulin secretion from mouse pancreatic beta cells in vivo.* Diabetologia, 2014. **57**(7): p. 1410-9.
266. Stefanoska, K., et al., *Neuronal MAP kinase p38alpha inhibits c-Jun N-terminal kinase to modulate anxiety-related behaviour.* Sci Rep, 2018. **8**(1): p. 14296.
267. Schindelin, J., et al., *Fiji: an open-source platform for biological-image analysis.* Nat Methods, 2012. **9**(7): p. 676-82.
268. Schiapparelli, L.M., et al., *Direct detection of biotinylated proteins by mass spectrometry.* J Proteome Res, 2014. **13**(9): p. 3966-78.
269. Villen, J. and S.P. Gygi, *The SCX/IMAC enrichment approach for global phosphorylation analysis by mass spectrometry.* Nat Protoc, 2008. **3**(10): p. 1630-8.
270. Keller, A., et al., *Empirical statistical model to estimate the accuracy of peptide identifications made by MS/MS and database search.* Anal Chem, 2002. **74**(20): p. 5383-92.
271. Jin, L., et al., *High-efficiency transduction and specific expression of ChR2opt for optogenetic manipulation of primary cortical neurons mediated by recombinant adeno-associated viruses.* J Biotechnol, 2016. **233**: p. 171-80.
272. Dunn, K.W., M.M. Kamocka, and J.H. McDonald, *A practical guide to evaluating colocalization in biological microscopy.* Am J Physiol Cell Physiol, 2011. **300**(4): p. C723-42.
273. Meijering, E., *Neuron tracing in perspective.* Cytometry Part A : the journal of the International Society for Analytical Cytology, 2010. **77**(7): p. 693-704.
274. Mancuso, J.J., et al., *Methods of dendritic spine detection: from Golgi to high-resolution optical imaging.* Neuroscience, 2013. **251**: p. 129-40.
275. Parajuli, L.K., et al., *Geometry and the Organizational Principle of Spine Synapses along a Dendrite.* eNeuro, 2020. **7**(6).
276. Maynard, S.A. and A. Triller, *Inhibitory Receptor Diffusion Dynamics.* Frontiers in molecular neuroscience, 2019. **12**: p. 313.
277. Sherwood, L., *Human Physiology: From Cells to Systems*. 2015: Cengage Learning.
278. Graf, P. and D.L. Schacter, *Implicit and explicit memory for new associations in normal and amnesic subjects.* J Exp Psychol Learn Mem Cogn, 1985. **11**(3): p. 501-18.
279. Tulving, E., *Organization of Memory: Episodic and semantic memory*. 1972.
280. Tulving, E. and D.L. Schacter, *Priming and human memory systems.* Science, 1990. **247**(4940): p. 301-6.
281. Malmberg, K.J., J.G.W. Raaijmakers, and R.M. Shiffrin, *50 years of research sparked by Atkinson and Shiffrin (1968).* Mem Cognit, 2019. **47**(4): p. 561-574.
282. Foerde, K., B.J. Knowlton, and R.A. Poldrack, *Modulation of competing memory systems by distraction.* Proc Natl Acad Sci U S A, 2006. **103**(31): p. 11778-83.
283. Zlotnik, G. and A. Vansintjan, *Memory: An Extended Definition.* Front Psychol, 2019. **10**: p. 2523.
284. Klein, S.B., *What memory is.* Wiley Interdiscip Rev Cogn Sci, 2015. **6**(1): p. 1-38.

285. Nairne, J.S., J.N. Pandeirada, and S.R. Thompson, *Adaptive memory: the comparative value of survival processing.* Psychol Sci, 2008. **19**(2): p. 176-80.
286. Josselyn, S.A. and S. Tonegawa, *Memory engrams: Recalling the past and imagining the future.* Science, 2020. **367**(6473).
287. Whitaker, L.R. and B.T. Hope, *Chasing the addicted engram: identifying functional alterations in Fos-expressing neuronal ensembles that mediate drug-related learned behavior.* Learn Mem, 2018. **25**(9): p. 455-460.
288. Josselyn, S.A. and P.W. Frankland, *Memory Allocation: Mechanisms and Function.* Annu Rev Neurosci, 2018. **41**: p. 389-413.
289. Han, J.H., et al., *Neuronal competition and selection during memory formation.* Science, 2007. **316**(5823): p. 457-60.
290. Guzowski, J.F., *Insights into immediate-early gene function in hippocampal memory consolidation using antisense oligonucleotide and fluorescent imaging approaches.* Hippocampus, 2002. **12**(1): p. 86-104.
291. Johansen, J.P., et al., *Molecular mechanisms of fear learning and memory.* Cell, 2011. **147**(3): p. 509-24.
292. Denny, C.A., et al., *Hippocampal memory traces are differentially modulated by experience, time, and adult neurogenesis.* Neuron, 2014. **83**(1): p. 189-201.
293. Tanaka, K.Z., et al., *Cortical representations are reinstated by the hippocampus during memory retrieval.* Neuron, 2014. **84**(2): p. 347-54.
294. Shockett, P.E. and D.G. Schatz, *Diverse strategies for tetracycline-regulated inducible gene expression.* Proc Natl Acad Sci U S A, 1996. **93**(11): p. 5173-6.
295. Reijmers, L.G., et al., *Localization of a stable neural correlate of associative memory.* Science, 2007. **317**(5842): p. 1230-3.
296. Liu, X., et al., *Optogenetic stimulation of a hippocampal engram activates fear memory recall.* Nature, 2012. **484**(7394): p. 381-5.
297. Garner, A.R., et al., *Generation of a synthetic memory trace.* Science, 2012. **335**(6075): p. 1513-6.
298. Lee, C., et al., *Light Up the Brain: The Application of Optogenetics in Cell-Type Specific Dissection of Mouse Brain Circuits.* Front Neural Circuits, 2020. **14**: p. 18.
299. Borgomaneri, S., et al., *Memories are not written in stone: Re-writing fear memories by means of non-invasive brain stimulation and optogenetic manipulations.* Neurosci Biobehav Rev, 2021. **127**: p. 334-352.
300. Roy, D.S., et al., *Brain-wide mapping reveals that engrams for a single memory are distributed across multiple brain regions.* Nat Commun, 2022. **13**(1): p. 1799.
301. Squire, L.R., et al., *Memory consolidation.* Cold Spring Harb Perspect Biol, 2015. **7**(8): p. a021766.
302. Rothschild, G., *The transformation of multi-sensory experiences into memories during sleep.* Neurobiol Learn Mem, 2019. **160**: p. 58-66.
303. Frank, A.C., et al., *Hotspots of dendritic spine turnover facilitate clustered spine addition and learning and memory.* Nat Commun, 2018. **9**(1): p. 422.
304. Lamprecht, R., et al., *Fear conditioning drives profilin into amygdala dendritic spines.* Nat Neurosci, 2006. **9**(4): p. 481-3.
305. Lai, C.S., T.F. Franke, and W.B. Gan, *Opposite effects of fear conditioning and extinction on dendritic spine remodelling.* Nature, 2012. **483**(7387): p. 87-91.
306. Urban, N.T., et al., *STED nanoscopy of actin dynamics in synapses deep inside living brain slices.* Biophys J, 2011. **101**(5): p. 1277-84.
307. Schmid, E.M. and H.T. McMahon, *Integrating molecular and network biology to decode endocytosis.* Nature, 2007. **448**(7156): p. 883-8.
308. Bosch, M., et al., *Structural and molecular remodeling of dendritic spine substructures during long-term potentiation.* Neuron, 2014. **82**(2): p. 444-59.
309. Darcy, K.J., et al., *Constitutive sharing of recycling synaptic vesicles between presynaptic boutons.* Nat Neurosci, 2006. **9**(3): p. 315-21.

310. Dobie, F.A. and A.M. Craig, *Inhibitory synapse dynamics: coordinated presynaptic and postsynaptic mobility and the major contribution of recycled vesicles to new synapse formation.* J Neurosci, 2011. **31**(29): p. 10481-93.
311. Bury, L.A. and S.L. Sabo, *Coordinated trafficking of synaptic vesicle and active zone proteins prior to synapse formation.* Neural Dev, 2011. **6**: p. 24.
312. Clifton, N.E., et al., *Regulation and Function of Activity-Dependent Homer in Synaptic Plasticity.* Mol Neuropsychiatry, 2019. **5**(3): p. 147-161.
313. Vickers, C.A. and D.J. Wyllie, *Late-phase, protein synthesis-dependent long-term potentiation in hippocampal CA1 pyramidal neurones with destabilized microtubule networks.* Br J Pharmacol, 2007. **151**(7): p. 1071-7.
314. Fuentes-Ramos, M., M. Alaiz-Noya, and A. Barco, *Transcriptome and epigenome analysis of engram cells: Next-generation sequencing technologies in memory research.* Neurosci Biobehav Rev, 2021. **127**: p. 865-875.
315. Chen, G., B. Ning, and T. Shi, *Single-Cell RNA-Seq Technologies and Related Computational Data Analysis.* Front Genet, 2019. **10**: p. 317.
316. Nguyen, Q.H., et al., *Experimental Considerations for Single-Cell RNA Sequencing Approaches.* Front Cell Dev Biol, 2018. **6**: p. 108.
317. Jaeger, B.N., et al., *A novel environment-evoked transcriptional signature predicts reactivity in single dentate granule neurons.* Nat Commun, 2018. **9**(1): p. 3084.
318. Sun, X., et al., *Functionally Distinct Neuronal Ensembles within the Memory Engram.* Cell, 2020. **181**(2): p. 410-423 e17.
319. Sorensen, A.T., et al., *A robust activity marking system for exploring active neuronal ensembles.* Elife, 2016. **5**.
320. Hrvatin, S., et al., *Single-cell analysis of experience-dependent transcriptomic states in the mouse visual cortex.* Nat Neurosci, 2018. **21**(1): p. 120-129.
321. Gil-Marti, B., Barredo, C.G., Pina-Flores, S., Trejo, J.L., Turiegano, E., Martin, F.A., *The elusive transcriptional memory trace*. Vol. 1. 2022: Oxford Open Neuroscience.
322. Prikas, E., et al., *Tau target identification reveals NSF-dependent effects on AMPA receptor trafficking and memory formation.* EMBO J, 2022. **41**(18): p. e10242.
323. Marco, A., et al., *Mapping the epigenomic and transcriptomic interplay during memory formation and recall in the hippocampal engram ensemble.* Nat Neurosci, 2020. **23**(12): p. 1606-1617.
324. Yiu, A.P., et al., *Neurons are recruited to a memory trace based on relative neuronal excitability immediately before training.* Neuron, 2014. **83**(3): p. 722-35.
325. Rao-Ruiz, P., et al., *Engram-specific transcriptome profiling of contextual memory consolidation.* Nat Commun, 2019. **10**(1): p. 2232.
326. Branon, T.C., et al., *Efficient proximity labeling in living cells and organisms with TurboID.* Nat Biotechnol, 2018. **36**(9): p. 880-887.
327. Fu, J., et al., *Essential Functions of the Transcription Factor Npas4 in Neural Circuit Development, Plasticity, and Diseases.* Front Neurosci, 2020. **14**: p. 603373.
328. Vorhees, C.V. and M.T. Williams, *Morris water maze: procedures for assessing spatial and related forms of learning and memory.* Nat Protoc, 2006. **1**(2): p. 848-58.
329. Guzowski, J.F., et al., *Experience-dependent gene expression in the rat hippocampus after spatial learning: a comparison of the immediate-early genes Arc, c-fos, and zif268.* J Neurosci, 2001. **21**(14): p. 5089-98.
330. Szklarczyk, D., et al., *The STRING database in 2017: quality-controlled protein-protein association networks, made broadly accessible.* Nucleic Acids Res, 2017. **45**(D1): p. D362-D368.
331. Kugler, S., E. Kilic, and M. Bahr, *Human synapsin 1 gene promoter confers highly neuron-specific long-term transgene expression from an adenoviral vector in the adult rat brain depending on the transduced area.* Gene Ther, 2003. **10**(4): p. 337-47.
332. Vetere, G., et al., *Chemogenetic Interrogation of a Brain-wide Fear Memory Network in Mice.* Neuron, 2017. **94**(2): p. 363-374 e4.
333. Miller, A.M., et al., *Cues, context, and long-term memory: the role of the retrosplenial cortex in spatial cognition.* Front Hum Neurosci, 2014. **8**: p. 586.

334. Galvez-Marquez, D.K., et al., *Spatial contextual recognition memory updating is modulated by dopamine release in the dorsal hippocampus from the locus coeruleus.* Proc Natl Acad Sci U S A, 2022. **119**(49): p. e2208254119.
335. Tonegawa, S., et al., *Memory engram storage and retrieval.* Curr Opin Neurobiol, 2015. **35**: p. 101-9.
336. Ramirez, S., et al., *Creating a false memory in the hippocampus.* Science, 2013. **341**(6144): p. 387-91.
337. Lamothe-Molina, P.J., et al., *DeltaFosB accumulation in hippocampal granule cells drives cFos pattern separation during spatial learning.* Nat Commun, 2022. **13**(1): p. 6376.
338. Tolman, E.C., *Cognitive maps in rats and men.* Psychol Rev, 1948. **55**(4): p. 189-208.
339. Pettit, N.L., et al., *Fos ensembles encode and shape stable spatial maps in the hippocampus.* Nature, 2022. **609**(7926): p. 327-334.
340. Othman, M.Z., Z. Hassan, and A.T. Che Has, *Morris water maze: a versatile and pertinent tool for assessing spatial learning and memory.* Exp Anim, 2022. **71**(3): p. 264-280.
341. Zheng, C., et al., *Hippocampal place cell sequences differ during correct and error trials in a spatial memory task.* Nat Commun, 2021. **12**(1): p. 3373.
342. Vorhees, C.V. and M.T. Williams, *Morris water maze: procedures for assessing spatial and related forms of learning and memory.* Nature protocols, 2006. **1**(2): p. 848-58.
343. Goodman, J. and M.G. Packard, *The Memory System Engaged During Acquisition Determines the Effectiveness of Different Extinction Protocols.* Front Behav Neurosci, 2015. **9**: p. 314.
344. Sghaier, R., et al., *Biotin attenuation of oxidative stress, mitochondrial dysfunction, lipid metabolism alteration and 7beta-hydroxycholesterol-induced cell death in 158N murine oligodendrocytes.* Free Radic Res, 2019. **53**(5): p. 535-561.
345. Ochoa-Ruiz, E., et al., *Biotin deprivation impairs mitochondrial structure and function and has implications for inherited metabolic disorders.* Mol Genet Metab, 2015. **116**(3): p. 204-14.
346. Depeint, F., et al., *Mitochondrial function and toxicity: role of B vitamins on the one-carbon transfer pathways.* Chem Biol Interact, 2006. **163**(1-2): p. 113-32.
347. Zhang, Q., et al., *Circulating mitochondrial DAMPs cause inflammatory responses to injury.* Nature, 2010. **464**(7285): p. 104-7.
348. Spence, E.F., et al., *In vivo proximity proteomics of nascent synapses reveals a novel regulator of cytoskeleton-mediated synaptic maturation.* Nat Commun, 2019. **10**(1): p. 386.
349. Yu, D.Y., et al., *Tau binds both subunits of calcineurin, and binding is impaired by calmodulin.* Biochim Biophys Acta, 2008. **1783**(12): p. 2255-61.
350. Silva, A.J., et al., *Impaired spatial learning in alpha-calcium-calmodulin kinase II mutant mice.* Science, 1992. **257**(5067): p. 206-11.
351. Tsien, J.Z., P.T. Huerta, and S. Tonegawa, *The essential role of hippocampal CA1 NMDA receptor-dependent synaptic plasticity in spatial memory.* Cell, 1996. **87**(7): p. 1327-38.
352. Chang, J.Y., et al., *Mechanisms of Ca(2+)/calmodulin-dependent kinase II activation in single dendritic spines.* Nat Commun, 2019. **10**(1): p. 2784.
353. Koo, S.J., et al., *Vesicular Synaptobrevin/VAMP2 Levels Guarded by AP180 Control Efficient Neurotransmission.* Neuron, 2015. **88**(2): p. 330-44.
354. Ambroso, M.R., B.G. Hegde, and R. Langen, *Endophilin A1 induces different membrane shapes using a conformational switch that is regulated by phosphorylation.* Proc Natl Acad Sci U S A, 2014. **111**(19): p. 6982-7.
355. Prikas, E., Paric, E., Asih, PR., Stefanoska, K., Stefen, H., Fath, T., Poljak, A., Ittner, A., *Tau target identification reveals NSF-dependent effects on AMPA receptor trafficking and memory formation.* EMBO Journal, 2022.
356. Chen, Y.K. and Y.P. Hsueh, *Cortactin-binding protein 2 modulates the mobility of cortactin and regulates dendritic spine formation and maintenance.* J Neurosci, 2012. **32**(3): p. 1043-55.
357. Phee, H., et al., *Pak2 is required for actin cytoskeleton remodeling, TCR signaling, and normal thymocyte development and maturation.* Elife, 2014. **3**: p. e02270.
358. Li, C.H., et al., *MeCP2 links heterochromatin condensates and neurodevelopmental disease.* Nature, 2020. **586**(7829): p. 440-444.

359. Seo, S.B., et al., *Regulation of histone acetylation and transcription by INHAT, a human cellular complex containing the set oncoprotein.* Cell, 2001. **104**(1): p. 119-30.
360. Ortega-Martinez, S., *A new perspective on the role of the CREB family of transcription factors in memory consolidation via adult hippocampal neurogenesis.* Front Mol Neurosci, 2015. **8**: p. 46.
361. Merz, K., S. Herold, and D.C. Lie, *CREB in adult neurogenesis--master and partner in the development of adult-born neurons?* Eur J Neurosci, 2011. **33**(6): p. 1078-86.
362. Madabhushi, R., et al., *Activity-Induced DNA Breaks Govern the Expression of Neuronal Early-Response Genes.* Cell, 2015. **161**(7): p. 1592-605.
363. Boutros, S.W., et al., *Common cancer treatments targeting DNA double strand breaks affect long-term memory and relate to immediate early gene expression in a sex-dependent manner.* Oncotarget, 2022. **13**: p. 198-213.
364. Li, X., et al., *The DNA Repair-Associated Protein Gadd45gamma Regulates the Temporal Coding of Immediate Early Gene Expression within the Prelimbic Prefrontal Cortex and Is Required for the Consolidation of Associative Fear Memory.* J Neurosci, 2019. **39**(6): p. 970-983.
365. Sultan, A., et al., *Nuclear tau, a key player in neuronal DNA protection.* J Biol Chem, 2011. **286**(6): p. 4566-75.
366. Violet, M., et al., *A major role for Tau in neuronal DNA and RNA protection in vivo under physiological and hyperthermic conditions.* Front Cell Neurosci, 2014. **8**: p. 84.
367. Bou Samra, E., et al., *A role for Tau protein in maintaining ribosomal DNA stability and cytidine deaminase-deficient cell survival.* Nat Commun, 2017. **8**(1): p. 693.
368. Roy, D.S., et al., *Memory retrieval by activating engram cells in mouse models of early Alzheimer's disease.* Nature, 2016. **531**(7595): p. 508-12.
369. Jo, K., et al., *Characterization of MALS/Velis-1, -2, and -3: a family of mammalian LIN-7 homologs enriched at brain synapses in association with the postsynaptic density-95/NMDA receptor postsynaptic complex.* J Neurosci, 1999. **19**(11): p. 4189-99.
370. Montesinos, M.L., et al., *Recycling and EH domain proteins at the synapse.* Brain Res Brain Res Rev, 2005. **49**(2): p. 416-28.
371. Stelzl, L.S., et al., *Global Structure of the Intrinsically Disordered Protein Tau Emerges from Its Local Structure.* JACS Au, 2022. **2**(3): p. 673-686.
372. Hite, K.C., A.A. Kalashnikova, and J.C. Hansen, *Coil-to-helix transitions in intrinsically disordered methyl CpG binding protein 2 and its isolated domains.* Protein Sci, 2012. **21**(4): p. 531-8.
373. Lee, W., et al., *MeCP2 regulates gene expression through recognition of H3K27me3.* Nat Commun, 2020. **11**(1): p. 3140.
374. Wan, M., et al., *Rett syndrome and beyond: recurrent spontaneous and familial MECP2 mutations at CpG hotspots.* Am J Hum Genet, 1999. **65**(6): p. 1520-9.
375. Brito, D.V.C., et al., *MeCP2 gates spatial learning-induced alternative splicing events in the mouse hippocampus.* Mol Brain, 2020. **13**(1): p. 156.
376. Simske, J.S., et al., *LET-23 receptor localization by the cell junction protein LIN-7 during C. elegans vulval induction.* Cell, 1996. **85**(2): p. 195-204.
377. Perego, C., et al., *Mammalian LIN-7 PDZ proteins associate with beta-catenin at the cell-cell junctions of epithelia and neurons.* EMBO J, 2000. **19**(15): p. 3978-89.
378. Murase, S., E. Mosser, and E.M. Schuman, *Depolarization drives beta-Catenin into neuronal spines promoting changes in synaptic structure and function.* Neuron, 2002. **35**(1): p. 91-105.
379. Shioda, N., et al., *Nuclear Translocation of Calcium/Calmodulin-dependent Protein Kinase IIdelta3 Promoted by Protein Phosphatase-1 Enhances Brain-derived Neurotrophic Factor Expression in Dopaminergic Neurons.* J Biol Chem, 2015. **290**(35): p. 21663-75.
380. Litersky, J.M., et al., *Tau protein is phosphorylated by cyclic AMP-dependent protein kinase and calcium/calmodulin-dependent protein kinase II within its microtubule-binding domains at Ser-262 and Ser-356.* Biochem J, 1996. **316 (Pt 2)**(Pt 2): p. 655-60.
381. Virdee, K., et al., *Phosphorylation of human microtubule-associated protein tau by protein kinases of the AGC subfamily.* FEBS Lett, 2007. **581**(14): p. 2657-62.

382. Wu, X.S., et al., *Calcineurin is universally involved in vesicle endocytosis at neuronal and nonneuronal secretory cells.* Cell Rep, 2014. **7**(4): p. 982-8.
383. Kayyali, U.S., et al., *Cytoskeletal changes in the brains of mice lacking calcineurin A alpha.* J Neurochem, 1997. **68**(4): p. 1668-78.
384. Yang, Y., et al., *Endophilin A1 Promotes Actin Polymerization in Dendritic Spines Required for Synaptic Potentiation.* Front Mol Neurosci, 2018. **11**: p. 177.
385. Lee, J.L.C., K. Nader, and D. Schiller, *An Update on Memory Reconsolidation Updating.* Trends Cogn Sci, 2017. **21**(7): p. 531-545.
386. Botelho, J., et al., *Network Protein Interaction in Parkinson's Disease and Periodontitis Interplay: A Preliminary Bioinformatic Analysis.* Genes (Basel), 2020. **11**(11).
387. Holland, E., Leinhardt, A., *Transitivity in structural models of small groups.* Comparative Group Studies, 1971. **2**(2): p. 101-124.
388. Zhou, Z., et al., *Brain-specific phosphorylation of MeCP2 regulates activity-dependent Bdnf transcription, dendritic growth, and spine maturation.* Neuron, 2006. **52**(2): p. 255-69.
389. Lee, L.C., et al., *Association of CaMK2A and MeCP2 signaling pathways with cognitive ability in adolescents.* Mol Brain, 2021. **14**(1): p. 152.
390. Cowie, J., Wilks, Y., *Information Extraction*. 1996.
391. Ghandour, K., et al., *Orchestrated ensemble activities constitute a hippocampal memory engram.* Nat Commun, 2019. **10**(1): p. 2637.
392. UniProt, C., *UniProt: the Universal Protein Knowledgebase in 2023.* Nucleic Acids Res, 2023. **51**(D1): p. D523-D531.
393. Choquet, D. and A. Triller, *The dynamic synapse.* Neuron, 2013. **80**(3): p. 691-703.
394. Ziv, N.E. and A. Fisher-Lavie, *Presynaptic and postsynaptic scaffolds: dynamics fast and slow.* Neuroscientist, 2014. **20**(5): p. 439-52.
395. Ryan, T.J., et al., *Memory. Engram cells retain memory under retrograde amnesia.* Science, 2015. **348**(6238): p. 1007-13.
396. Sanders, J., et al., *Elimination of dendritic spines with long-term memory is specific to active circuits.* J Neurosci, 2012. **32**(36): p. 12570-8.
397. Sacktor, T.C., *PKMzeta, LTP maintenance, and the dynamic molecular biology of memory storage.* Prog Brain Res, 2008. **169**: p. 27-40.
398. Free, R.B., L.A. Hazelwood, and D.R. Sibley, *Identifying novel protein-protein interactions using co-immunoprecipitation and mass spectroscopy.* Curr Protoc Neurosci, 2009. **Chapter 5**: p. Unit 5 28.
399. Hayes, S., et al., *Studying protein-protein interactions: progress, pitfalls and solutions.* Biochem Soc Trans, 2016. **44**(4): p. 994-1004.
400. Go, C.D., et al., *A proximity-dependent biotinylation map of a human cell.* Nature, 2021. **595**(7865): p. 120-124.
401. Kentros, C., et al., *Abolition of long-term stability of new hippocampal place cell maps by NMDA receptor blockade.* Science, 1998. **280**(5372): p. 2121-6.
402. Whitlock, J.R., et al., *Learning induces long-term potentiation in the hippocampus.* Science, 2006. **313**(5790): p. 1093-7.
403. Ge, Y., et al., *Hippocampal long-term depression is required for the consolidation of spatial memory.* Proc Natl Acad Sci U S A, 2010. **107**(38): p. 16697-702.
404. Nelson, T.J., P.S. Backlund, Jr., and D.L. Alkon, *Hippocampal protein-protein interactions in spatial memory.* Hippocampus, 2004. **14**(1): p. 46-57.
405. Karch, C.M., A.T. Jeng, and A.M. Goate, *Calcium phosphatase calcineurin influences tau metabolism.* Neurobiol Aging, 2013. **34**(2): p. 374-86.
406. Liu, C., et al., *Co-immunoprecipitation with Tau Isoform-specific Antibodies Reveals Distinct Protein Interactions and Highlights a Putative Role for 2N Tau in Disease.* J Biol Chem, 2016. **291**(15): p. 8173-88.
407. Sallaberry, C.A., et al., *Tau and Membranes: Interactions That Promote Folding and Condensation.* Front Cell Dev Biol, 2021. **9**: p. 725241.
408. Li, F. and J.Z. Tsien, *Memory and the NMDA receptors.* N Engl J Med, 2009. **361**(3): p. 302-3.

409. Roberson, E.D., et al., *Amyloid-beta/Fyn-induced synaptic, network, and cognitive impairments depend on tau levels in multiple mouse models of Alzheimer's disease.* J Neurosci, 2011. **31**(2): p. 700-11.
410. Brier, M.R., et al., *Tau and Abeta imaging, CSF measures, and cognition in Alzheimer's disease.* Sci Transl Med, 2016. **8**(338): p. 338ra66.
411. Tort-Merino, A., et al., *Tau Protein is Associated with Longitudinal Memory Decline in Cognitively Healthy Subjects with Normal Alzheimer's Disease Cerebrospinal Fluid Biomarker Levels.* J Alzheimers Dis, 2019. **70**(1): p. 211-225.
412. D'Amelio, M. and P.M. Rossini, *Brain excitability and connectivity of neuronal assemblies in Alzheimer's disease: from animal models to human findings.* Prog Neurobiol, 2012. **99**(1): p. 42-60.
413. Ittner, A., et al., *Site-specific phosphorylation of tau inhibits amyloid-beta toxicity in Alzheimer's mice.* Science, 2016. **354**(6314): p. 904-908.
414. Tan, D., et al., *Generation of a New Tau Knockout (tau Δex1) Line Using CRISPR/Cas9 Genome Editing in Mice.* 2018. **62**(2): p. 571-578.

APPENDICES

[Provided separately due limitations in document size conversions]